Reliability assessment of an offshore wind turbine jacket with active learning approaches

Chao Ren

THÈSE

Pour obtenir le diplôme de doctorat

Spécialité Génie Mécanique

Préparée au sein de L'Institut National des Sciences Appliquées de Rouen Normandie

Reliability assessment of an offshore wind turbine jacket with active learning approaches

Présentée et soutenue par

Chao REN

Thèse soutenue publiquement le 13/04/2022
devant le jury composé de

M. Rodolphe LE RICHE	Directeur de recherche, École des Mines Saint Étienne, France	Rapporteur
M. Jean-Marc BOURINET	Maître de conférences HDR, SIGMA Clermont, France	Rapporteur
M. John Dalsgaard SØRENSEN	Professeur, Aalborg University, Danemark	Examinateur
Mme Nathalie BARTOLI	Maître de recherche HDR, ONERA, France	Examinatrice
M. Abdul-Hamid SOUBRA	Professeur, Université de Nantes, France	Examinateur
M. Eduardo SOUZA DE CURSI	Professeur, INSA Rouen Normandie, France	Directeur de thèse
M. Didier LEMOSSE	Maître de conférences HDR, INSA Rouen Normandie, France	Codirecteur de thèse
M. Younes AOUES	Maître de conférences, INSA Rouen Normandie, France	Encadrant de thèse

Thèse encadrée par M. Younes AOUES, M. Didier LEMOSSE et M. Eduardo SOUZA DE CURSI, LMN (EA 3828).

Acknowledgements

Three years ago, I decided to leave my hometown and embark on a new journey in a strange city. Today, I have finally reached the end of this journey. During this time, I have encountered so many difficulties and things. Thanks to your company and encouragement, I have been able to go this far.

First of all, I would like to thank my supervisors Younes AOUES, Didier LEOMSSE, Eduardo SOUZA DE CURSI for their guidance and encouragements. At the beginning, they guided me patiently. Later, when I had new ideas of my research, they always encouraged me and provided some useful advice. They gave me more freedom, which enhanced my ability to do independent research. Without their help and encouragement, I would not be where I am today. Also, I thank the reporters (Rodolphe LE RICHE and Jean-Marc BOURINET) for their careful reading and correcting my thesis and the examiners (John Dalsgaard SØRENSEN, Nathalie BARTOLI, Abdul-Hamid SOUBRA, Emmanuel ARDILLON) for accepting to be part of the jury .

In addition, I would like to thank my colleagues and friends. As an older colleague, Wilson Javier VELOZ PARRA helped me a lot when I started my research. Our communication and discussions have inspired me in my later research. Also, his optimistic attitude and humour made work and life in the laboratory much more enjoyable. Moreover, as my friends, Linlin JIA, Ruiping YANG, Jing ZHANG, Zhenhang WU and Ce ZHANG have brought me a lot of joy and unforgettable memories during this period. They listened to my complaints and worries when I was in difficulty and lonely. Thank they also for travelling with me through many countries. The scenery and the dishes that I have tasted have been even better by their company and sharing.

Furthermore, thank my family members for their support over the years, especially my mother and sister! My mother has always supported her son in pursuing his dreams and sticking to his beliefs. My sister has always been the first to wish me well and remind me to be happy on my birthday... All these things made me feel warm when I was in a foreign country.

Finally, I am grateful for the bad things, the pain and the COVID-19. They did not beat me down and they just made me stronger and better. Thanks also to the boy who made a brave decision over three years ago. Now, this journey is coming to an end. Another journey will start soon and I'm already eager to try!

Abstract

This dissertation aims to develop an approach for efficient and accurate reliability assessment of offshore wind turbine jacket. The offshore wind turbine jacket is subject to various uncertainties. The reliability analysis of the jacket foundation is generally performed using traditional approximation approaches (e.g.FORM/SORM) or Monte Carlo simulations. These approaches are either inaccurate or time-consuming and are not suitable for complex and computationally expensive simulation such as those required for offshore wind turbine jacket.

The first part of this dissertation aims to choose the accurate and efficient approach for the offshore load simulation. Firstly, three load simulation approaches used for dynamic analysis of offshore wind turbines (OWTs) structures are compared. The first one is the uncoupled method, the second is the sequentially coupled approach and the third one is the fully integrated (coupled) approach. Secondly, the influence of the jacket modeling techniques is investigated and two numerical models of the jacket are developed. One is with pure beam element (Beam model), while the second is with more advanced modeling by using super-element (Super-element model). For the comparison of load simulation approaches, the results show that the simulation results of the sequential approach are mostly in good agreement with those of the fully coupled approach. The uncoupled approach may lead to large errors in the extreme responses of dynamic analysis. Furthermore, for the comparison between the two jacket models, it is found that the responses of super-element jacket model are different from those of the beam model, especially in the jacket displacements.

The second part of this dissertation aims to evaluate the structural reliability of the jacket. Thus, two approaches are proposed for the component reliability assessment based on ensemble surrogate models with active learning approaches. The efficiency and accuracy of the proposed approaches are demonstrated by 4 representative examples and the beam jacket model. Finally, for the system reliability assessment, a new composite learning approach is proposed for the active learning Kriging approach with U function named AK-SYSm-U. The active learning Kriging approaches with H learning function are also adapted for the system reliability analysis. The efficiency and accuracy of the developed system approaches are also demonstrated by two numerical examples and the super-element jacket model. The results of the component reliability analysis show that the proposed ensemble surrogate models with active learning approaches can be effective in evaluating the reliability of high dimension and rare event problems with less computational cost than the single kriging surrogate model with active learning approaches (e.g AK-MCS). Moreover, the system reliability analysis results show that the proposed composite learning function for system reliability analysis is more robust and the developed active learning approaches with H learning function can efficiently and accurately estimate the failure probability of the system.

Keywords: Offshore wind turbine jacket, Offshore load simulation, Super-element, Finite element analysis, Reliability assessment, Active learning approaches, System reliability assessment.

General Introduction

There is no doubt that renewable energy is currently the most promising form of energy. Wind energy in general and recently offshore wind energy, in particular, have become more and more important in the renewable energy market. For offshore wind turbines, substructures and foundations account for a significant part of costs. Conventional monopile and tripod foundations are mainly used for shallow water of 20-40m. Jacket support structures have become the main support structures in the deep water (50-100m). Like most offshore structures, the jacket support structures withstand the complex loads of harsh environmental conditions, which may lead to fatigue, structural failure, and occasionally, even critical accidents. In particular, the increase of extreme weather conditions (typhoon, tsunami...) in last decades requires jacket support structures with a high-reliability index. Therefore, reliability assessment and reliability-based design optimization of jacket structures have become important research fields. However, there are many uncertainties in the design of a jacket structure: (1) the natural randomness of environmental factors such as wind, waves, and currents. (2) the uncertainties of the physical models due to the aero-hydro-sevro flexible structural simulation. (3) the analytical and numerical structural analysis. (3) fluctuation in material strength and dimensions. All these uncertainties make the reliability assessment of the jacket structures indispensable.

For the loading acting on the offshore wind turbine foundation, it is generally simulated using aero-hydro-sevro tools such as FAST and HAWC2, which is often based on three approaches. The first is the uncoupled simulation, the second is the sequentially coupled approach and the third is the fully coupled approach. The sequential approach is widely used in industry, due to intellectual properties and confidential issues between the foundation designer and the wind turbine manufacturer. The fully coupled approaches and the uncoupled approaches are commonly found in academic researches and studies. However, to the best of our knowledge, the accuracy and efficiency of these three approaches are not compared and studied. Moreover, the jacket support structures are generally modeled with pure beam elements to accelerate load simulation. Such simplification can lead to inaccuracies in the generated results, as the local joint flexibility of the jacket is lost. The influence of the jacket modeling techniques on the loading has not yet been investigated.

As for the reliability assessment approaches, the first-order and second order reliability methods are two representative approximation methods. They focus on finding a single most probable failure point and provide a good balance between accuracy and computational cost. The approximation approaches cannot meet the accuracy requirement for highly nonlinear problems. Compared to these approximation approaches, Monte Carlo simulation is a very robust approach for reliability assessment. The main shortcoming of MCS is that it requires a large number of samples and is time-consuming for many real engineering problems. Although some variance reduction techniques have been developed such as Importance Sampling (IS), Subset Simulation (SS) and Directional Simulation (DS), the computational cost remain still high and impractical for rare event problem. In the last two decades, the surrogate-assisted reliability analysis has become increasingly important. The basic idea is to replace the performance function by constructing a surrogate model, also called meta-model. Furthermore, the strategy for constructing a surrogate model can generally be classified into two types (1) "one shot" (non-adaptive) and (2) active learning approaches (adaptive). The "one shot" method requires generating all sample points

in advance and performing the reliability analysis by using the validated surrogate model. On the other hand, active learning methods select one or several sample points at each iteration to construct the surrogate model, which is updated at each iteration efficiently until the convergence. Therefore, the active learning approaches are normally more efficient than "one shot" approaches, which are also our interest.

In this thesis, one focus is on the load simulation approaches and the jacket modeling techniques. The influence of different load simulation approaches and jacket model on the loading is investigated. On the other hand, the active learning approaches are proposed for the jacket reliability assessment. Two active learning approaches based on ensemble surrogate model with local goodness measurement are developed for the component reliability analysis. Also, a new composite learning function is proposed for the system reliability analysis with Kriging method and U learning function. The active learning Kriging approaches with H learning function is also adapted for the system reliability analysis. The layout of this thesis is as follows:

Chapter 1 presents the recent development of wind energy and the overview of design tools of wind turbine components. The development of the renewable energy and wind energy is listed in section 1.2. The modern offshore wind turbine components and offshore wind turbine foundations are given section 1.3. Section 1.4 presents the offshore wind turbine foundation design, the major loads, design standards and some typical wind turbine simulation tools. The reliability assessment approaches are summarized in section 1.5. Conclusions are presented in section 1.6.

Chapter 2 investigates the influence of different load simulation approaches and jacket models on the responses. Section 2.2 presents the basic parameter of the 5MW wind turbine model of NREL and the offshore wind turbine jacket foundation, which are used for the following study. The basic theories of the load simulation approach and modeling techniques are given in section 2.3. The results of the influences of the load simulation approaches are given section 2.4. Section 2.5 presents the influences of different jacket models. Some conclusions and recommendations are section 2.6.

Chapter 3 shows the proposed ensemble surrogate models with active learning approaches. Section 3.2 lists some typical surrogate models and the basic assumption of the surrogate models. Section 3.3 had summarized the previous ensemble surrogate model methods and their limitations. The details of the proposed ensemble surrogate model with local good measurement are given in the section 3.4. The examples and application of the proposed approaches are shown in section 3.5. Conclusions and discussions presents in section 3.6.

Chapter 4 presents the proposed composite learning function and the adaption of Kriging with H learning function for system reliability analysis. Some typical learning functions for Kriging methods are summarized in section 4.2. Section 4.3 presents some typical active learning Kriging approaches for the system reliability analysis. Section 4.4 presents the problem of AK-SYS and AK-SYSi and a new

composite learning function. The adaption of Kriging with H learning function for system reliability analysis is presented in the section 4.5. Some examples and numerical application are given in section 4.6. The application on the offshore wind turbine jacket model is given in section 4.7.

Chapter 5 presents the general conclusion of this thesis and some perspectives for future works.

Contents

List of Publications

During this Ph.D., the following research works have been published:
Peer-reviewed journal papers

Chao REN, Younes AOUES, Didier LEMOSSE and Eduardo SOUZA DE CURSI. Comparative study of load simulation approaches used for the dynamic analysis on an offshore wind turbine jacket with different modeling techniques. **Engineering Structures**, 2021.

Chao REN, Younes AOUES, Didier LEMOSSE and Eduardo SOUZA DE CURSI. Ensemble of surrogates combining Kriging and Artificial Neural Networks for reliability analysis with local goodness measurement. **Structural safety**, 2022.

Peer-reviewed international conference papers

Chao REN, Younes AOUES, Didier LEMOSSE and Eduardo SOUZA DE CURSI. Structural Reliability Assessment of Offshore Wind Turbine Jacket Considering Corrosion Degradation. **14th World Congress in Computational Mechanics and ECCOMAS Congress**, 2020.

Chao REN, Younes AOUES, Didier LEMOSSE and Eduardo SOUZA DE CURSI. Global Sensitivity Analysis of Offshore Wind Turbine Jacket. **International Symposium on Uncertainty Quantification and Stochastic Modeling**, 2020.

List of Figures

List of Tables

List of Algorithms

List of Abbreviations

ALK: Active Learning Kriging
ANN: Artificial Neural Network
BS: Best Surrogate
BEM: Blade Element Momentum
CB: Craig-Bampton reduction
CAE: Computer-aided engineering
CRA: Component Reliability Analysis
CDF: Cumulative Distribution Function
CSP: Concentrating Solar Power
CAGR: Compound Annual Growth Rate
DS: Directional Simulation
DLC: Design Load Case
DoF: Degrees of Freedom
DoE: Design of Experiment
e.g.: exempli gratia
EOG: Extreme Operating Gust
EWM: Extreme Wind speed Model
EDC: Extreme Direction Change
ETM: Extreme Turbulence Model
ECM: Extreme Current Model
EFF: Expected Feasibility Function
FD: Foundation Designer
FEA: Finite Element Analysis
FAST: Fatigue, Aerodynamic, Structure and Turbulence code
FORM: First Order Reliability Method
FOWTs: Floating Offshore Wind Turbines
GWEC: Global Wind Energy Council
GSA: Global Sensitivity Analysis
GBFs: Gravity base foundations
HAWT: Horizontal-Axis Wind Turbine

HAWC2: Horizontal-Axis Wind Turbine Code-Second generation
IS: Importance Sampling
IEA: International Energy Agency
IEC: International Electrotechnical Commission
IRENA: International Renewable Energy Agency
LS: Line Sampling
LCOE: Levelized Cost Of Energy
LOO: Leave-One-Out
LHS: Latin Hypercube Sampling
LWAS: Local Weighted Average Surrogate
LBS: Local Best Surrogate
ML: Machine learning
MTW: Wind turbine manufacturer
MBS: Multi-body System
MCS: Monte Carlo Simulation
MLP: Multilayer Perceptron
MPFP: Most Probable Failure Point
MCMC: Markov Chain Monte Carlo
NREL: National Renewable Energy Laboratory
NTM: Normal Turbulence Model
NWP: Normal Wind Profile
OWT: Offshore Wind Turbine
OC4: Code Comparison Collaboration Continuation
PCE: Polynomial Chaos Expansion
PDF: Probability Density Function
RBDO: Reliability-Based Design Optimization
SS: Subset Simulation
SRA: System Reliability Analysis
SCF: Stress Concentration Factor
RNA: Rotor Nacelle Assembly
RSM: Response Surface Method
RWH: Reduced Wave Height
ReLU: Rectified Linear Unit
SVM: Support Vector Machine
SORM: Second Order Reliability Method
TLP: Tension-Leg Platform
VAWT: Vertical-Axis Wind Turbine
WAS: Weighted Average Surrogate

Part I

Introduction

Chapter 1

Wind turbine foundation design and Reliability assessment

Contents

1.1 Scope of this thesis

As the most promising sustainable energy source, wind energy is one of the best approaches to achieve carbon neutrality. Over the past decade, wind energy capacity has increase rapidly. The levelized cost of onshore wind energy have fallen to the competitiveness level compared to the conventional energies. However, the cost of offshore wind energy is still high, due to the costs associated with transport, installation, and maintenance. Compared with onshore wind energy, the offshore wind energy can provide higher and more stable wind speeds, which can also reduce the impact on the human activities. In order to promote the use of offshore wind energy, many national and regional policies have been made. More and more offshore wind farms are being built and planned.

In offshore wind energy, offshore wind turbine foundations account for a significant part of the costs. The offshore foundations are used to support the wind turbine and ensure the proper operation of the wind turbine. Offshore wind foundations can be categorized into bottom-fixed or floating offshore wind turbines. The choice of foundation depends on the seabed conditions and water depth. But compared with bottom-fixed offshore wind turbines, the technology and industry chain for floating wind turbines are not yet mature. In the foreseeable future, bottom-fixed turbines will be the mainstay of offshore wind farms. For the bottom-fixed offshore wind turbines, there are several types of the offshore wind turbine foundations such as monopile and jacket. The monopiles account currently for 80% of offshore wind turbine foundations and are mostly installed in shallow water. As the water depth of offshore wind turbines installations increases, jacket structures have become the main support for offshore wind turbines. Like most offshore structures, offshore jacket foundations are subject to complex loads and various uncertainties. To ensure the operation of the offshore wind turbine, higher reliability is required for the offshore foundations, especially with the increase in extreme weather conditions (typhoons, tsunamis, etc.). Therefore, the reliability analysis of offshore wind turbine foundations has become vital.

To assess the reliability of the offshore wind turbine jacket, uncertainty quantification and reliability analysis approaches are crucial. The offshore wind load simulation is often based on the numerical tools such as FAST and HAWC2. In this thesis, one of our focus is on the uncertainties arising from the numerical simulation of offshore wind turbine jacket. On the other hand, the reliability assessment of the offshore wind turbine jacket is normally based on Monte Carlo simulations, which is always time-consuming. An efficient and accurate approach to evaluate reliability of the offshore jacket foundation is also our concern.

1.2 Renewable energy and Wind energy development

Over the last decades, the renewable energy has got an impressive development. The cost of electricity generated from renewable energy keeps going down in recent years, more electricity is generated from renewable energy. According to the International Renewable Energy Agency (IRENA), the cost of the most renewable energy have seen a significant decline in the last decade. Table.1.1 presents the total installed cost, levelized cost of electricity and capacity factor in 2010 and 2020. The cost of wind and solar energy have an important decrease. The total installed cost of the solar photovoltaic (PV), concentrating solar power (CSP), offshore wind and onshore wind decrease, respectively, by 81%, 50%, 32% and 31%. Concerning the levelized cost of electricity, the cost in solar PV, CSP, offshore wind and onshore wind have also dropped by 85%,68%, 48% and 56% respectively. In particular, onshore wind and solar PV have become the less costly sources of electricity than the cheapest fossil fuel fired power generation. The solar and wind energies have been two main pillars of the renewable energies, specially the wind energies. The levelized cost of electricity of onshore wind have decreased to 0.039 $/kWh. The related cost of the offshore wind have also dropped to 0.084 $/kWh. Compared with solar energy, wind energy has much potential to exploited.

Table 1.1 – Total installed cost, levelized cost of electricity and capacity factor in 2010 and 2020 [Agency, 2021]

Renewable energy	Total installed costs ($/kW)			levelized cost of electricity ($/kWh)			Capacity factor (%)		
	2010	2020	Percent change	2010	2020	Percent change	2010	2020	Percent change
Bioenergy	2619	2543	-3%	0.076	0.076	0%	72	70	-2%
Geothermal	2620	4468	71%	0.049	0.071	45%	87	83	-5%
Hydropower	1269	1870	47%	0.038	0.044	18%	44	46	4%
Solar PV	4731	883	-81%	0.381	0.057	-85%	14	16	17%
CSP	9095	4581	-50%	0.340	0.108	-68%	30	42	40%
Onshore wind	1971	1355	-31%	0.089	0.039	-56%	27	36	31%
Offshore wind	4706	3185	-32%	0.162	0.084	-48%	38	40	6%

Up to 2020, more and more wind turbines have been installed over the world, as shown in Fig.1.1. The total installed wind capacity of the world has increased from about 200 GW to more than 700 GW. Compared with other regions, Asia has seen a significant increase of installed wind capacity. According to the data from Global Wind Energy Council (GWEC), 2020 saw global new wind power installations surpass 90 GW including onshore and offshore wind as shown in Fig.1.2. New installations in the onshore wind market reached 86.9 GW and the offshore wind market reached 6.1 GW. Need to be mentioned, China takes a lead in global wind power development. The word's top five markets in 2020 for new installation were China, the US, Brazil, Netherlands and Germany.

IIn addition, GWEC also predicts the global wind energy market with the average compound annual

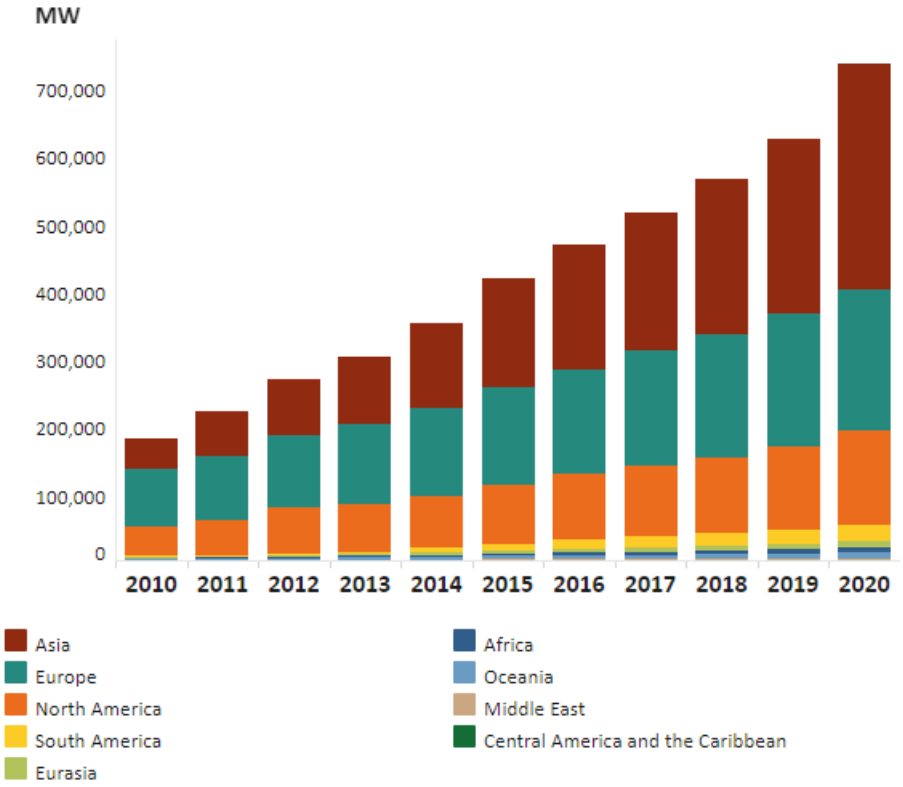

0.

Figure 1.1 – Global and regional installed wind capacity [Agency, 2021]

growth rate (CAGR) of 4% from 2020 to 2025 as shown in Fig.1.3. The outlook is based on input from regional, wind associations, government targets, available project information and input from industry experts and GWEC members. As we can see from Fig.1.3, the CAGR for onshore wind in the next five year is only around 0.3%. However, the CAGR for offshore wind in the next five year is up to 31.5%. New installations are likely to quadruple by 2025 from 6.1 GW in 2020. In total, more than 70 GW offshore wind capacity is expected to be added worldwide in 2021-2025. The positive outlook of offshore wind market is supported by many reasons. Some important reasons are summarized by GWEC as follows: (1) the sharp drop of offshore wind levelized cost of energy (LCOE), (2) increased offshore wind targets in Europe, the United States and key markets in Asia such as China and South Korea, (3) the expected commercialization and industrialization of floating wind, and (4) offshore wind's unique role in facilitating cross industry cooperation and accelerating the global energy transition from fossil fuel to renewable energy.

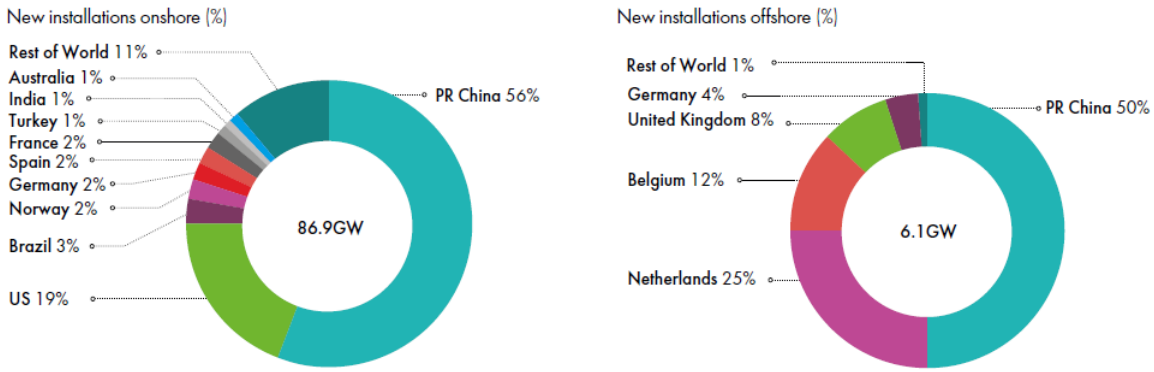

Figure 1.2 – New installed wind capacity of 2020 [Council, 2021]

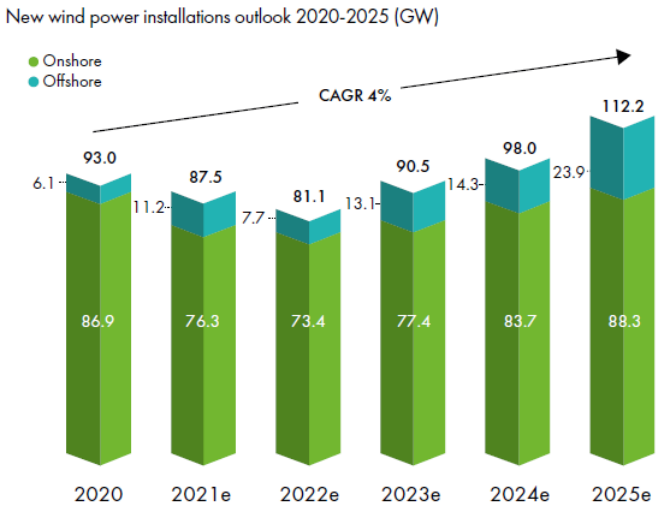

Figure 1.3 – New wind power installation outlook of 2020-2025 [Council, 2021]

1.3 Offshore wind turbines

Nowadays, the wind energy have mainly been classified into onshore and offshore wind energy. Compared to onshore wind energy, there is more space and more stable and high wind speed for offshore wind energy. More and more offshore wind turbines are currently under construction or planned. Onshore and offshore wind turbine both have the same principal subsystems of wind turbine. The key difference between of the onshore and offshore wind is that the offshore wind requires special substructures and foundations to support the wind turbines. In this section, a brief introduction and development of the modern wind turbine and offshore wind turbine foundation are given.

1.3.1 Wind turbine components

For the wind turbine, the most commercialized design for wind turbine is the three-bladed horizontal-axis wind turbine (HAWT) because of its efficiency and balance in economic, technology and manufacturing aspects. The modern three-bladed HAWT offers normally an overall efficient around 40-50 % [Secretariat, 2020] which is much higher than other turbine design like two-bladed HAWT or vertical-axis wind turbine (VAWT). In addition, the HAWT can be often classified by the rotor type (upwind/downwind), the site characteristic (onshore/offshore), the number of blades (three blades/two blades), the type of drive-train (direct-drive/gearbox), the generator type (fixed speed/variable speed) and the gird connectivity (connected/stand-alone). A sketch of an offshore upwind HWAT is illustrated in Fig.1.4.

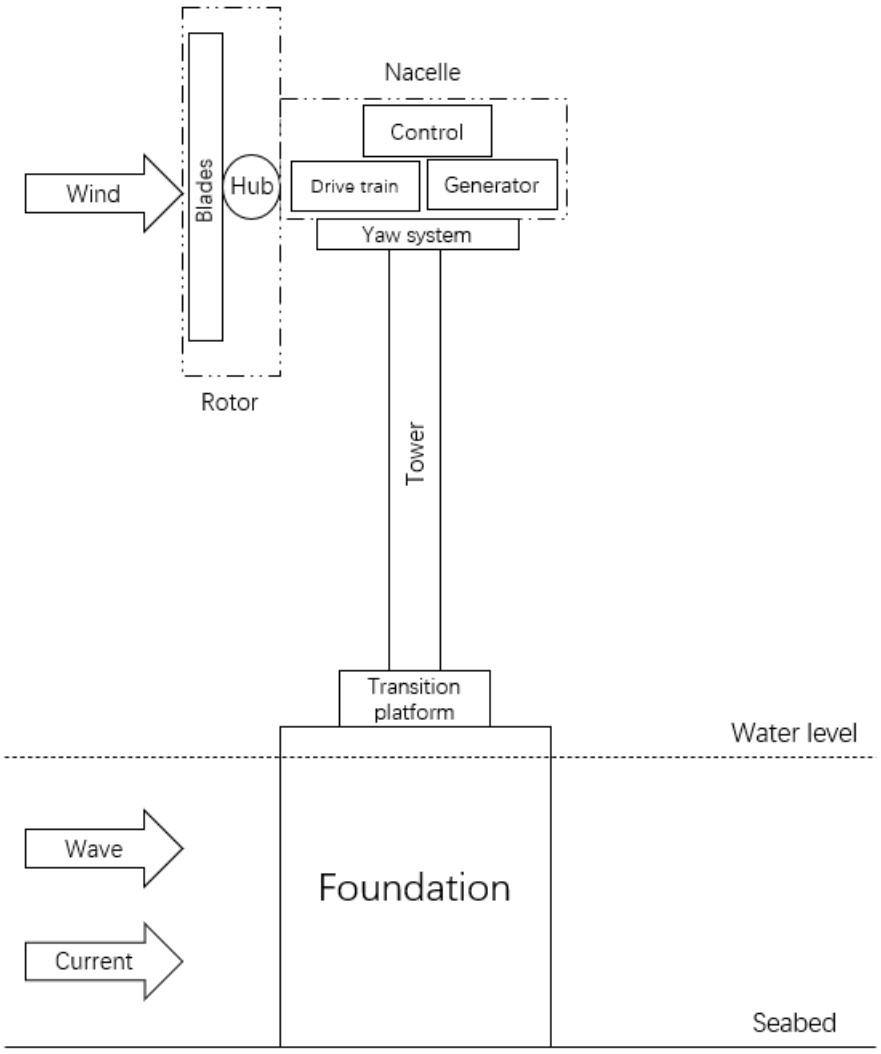

Figure 1.4 – Principal subsystems of a typical offshore horizontal-axis wind turbine

Rotor

The rotor is the rotating part of a turbine. It consists of (mostly) three blades and the central part that the blades are attached to the hub. The rotor connects to the generator, either directly (if it's a direct drive turbine) or through a shaft and a series of gears(a gearbox) that speed up the rotation and allow for a physically smaller generator. The rotor is often considered as the most important component from the performance of wind turbine.

Blades

Most turbines have three blades, which are made mostly of fibreglass. Turbine blades vary in size, but a typical modern land-based wind turbine has blades of over 52 meters. The largest turbine is GE's Haliade-X offshore wind turbine, with blades 107 meters long. The trend is to make them larger (for more power), lighter, and stronger. The blades have the form of an airfoil (same as the wings of an airplane) to be aerodynamic. When wind flows across the blade, the air pressure on one side of the blade decreases. The difference in air pressure across the two sides of the blade creates both lift and drag. The force of the lift is stronger than the drag and this causes the rotor to spin.

Hub

The turbine hub is part of the rotor. The function of the hub is to hold the blades and make it possible for them to rotate with respect to the rest of the turbine body. The hub is also connected to the turbine's main shaft. Depending on turbine size and design (constant or variable speed), the turbine rotor and hub assembly rotates at a rate of 10 to 25 revolutions per minute (rpm) [Morris, 2011].

Nacelle

The nacelle is housing on top of the tower that accommodates all the components that need to be on a turbine top. It contains mainly the drive-train, generator, and brake. The nacelle housing can protect the main turbine components from the undesirable weather such as rain or snow. For large wind turbine, the nacelle is designed to be large enough for personnel to check or repair the wind turbine components inside the nacelle. Fig.1.5 shows the main turbine components in nacelle.

Drive-train

The drive-train includes the rotating parts namely shafts, bearings, brakes and commonly a gearbox. Without or with the gearbox, that can classify the turbines into the gearbox model and the direct-drive model. Direct-drive turbines simplify nacelle systems and can increase efficiency and reliability by avoiding gearbox issues. They work by connecting the rotor directly to the generator to generate

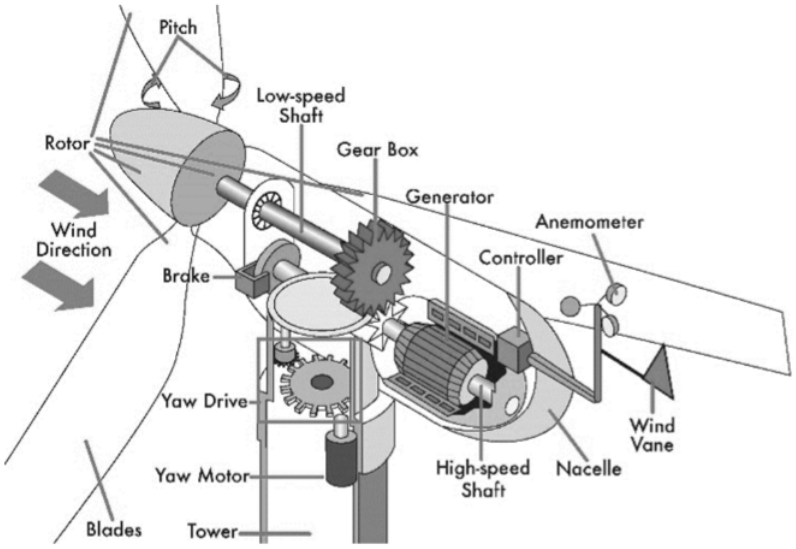

Figure 1.5 – Wind turbine nacelle [Lombardi et al., 2017]

electricity. Gearbox turbine converts the low-speed, high-torque rotation of the turbine's rotor to the high-speed,low-torque rotation of the generator.

Generator

The generator is the component that converts the mechanical energy of the rotor, harnessed from wind to electrical energy. Some generators are driven by gearboxes and others are direct-drives where the rotor attaches directly to the generator. At the commercial production level, all electricity generation is in the three-phase alternative current. In general, the choice of generator, therefore, is synchronous or asynchronous (induction) generator. Nevertheless, the generator associated with wind turbines, thus far, is the induction generator because a synchronous generator must turn at a tightly controlled constant speed (to maintain a constant frequency).

Yaw system

The yaw drive rotates the nacelle on upwind turbines to keep them facing the wind when wind direction changes. The yaw motors power the yaw drive to make this happen. Downwind turbines don't require a yaw drive because the wind manually blows the rotor away from it. However, as wind turbine get larger, the yaw system for downwind turbine will also be considered.

Tower

Made from tubular steel, the tower supports the structure of the turbine. Towers usually come in three sections and are assembled on-site. The tower in most modern turbines is round tubular steel of a diameter of 3–4 m, with a height of 75–110 m, depending on the size of the turbine and its location. The rule of thumb for a turbine tower is that it has the same height as the diameter of the circle its blades make when rotating. Because wind speed increases with height, taller towers enable turbines to capture more energy and generate more electricity.

Transition platform

The transition platform is normally made up out of a steel pipe construction, which is directly connected to the foundation. It is secured to the foundation by the use of a bolted or grouted connection. Also, the transition platform connects the wind turbines with the foundation and provides means to correct any misalignment of the foundation that may occurred during installation. It protects the foundation from corrosion and holds essential components including ladders and boat landing systems, which enables wind turbine technicians and others to access it as required.

Foundations

The wind turbine's foundation must have capacity to keep the wind turbine stable and upright even for the extreme load conditions. In the case of onshore wind turbine, the foundation is under the ground for the onshore turbines and it cannot be seen because it is covered by soil. It is a large and heavy structured block of concrete that must hold the whole turbine and the forces that affect it. For offshore wind turbines, the structures of the foundation is more complex and involves greater technical challenges [Jiang, 2021]. The offshore wind turbine foundation should endure both the impact of surging waves and the extreme weather conditions. More detailed discussion of the offshore wind turbine foundation is in the following subsection.

1.3.2 Offshore wind turbine foundations

For an offshore wind turbine, there are two main categories of the foundations: bottom-fixed and floating wind turbines. The choice of foundation type depends highly on the seabed conditions, water depth and estimated costs. In this subsection, a brief overview is provided here.

Bottom-fixed offshore wind turbines

The current offshore wind energy market is dominated by the bottom-fixed offshore wind turbines. Several types of bottom-fixed foundation are used in the offshore wind as shown in Fig.1.6. They are respectively gravity based, suction bucket, monopile, tripod and jacket structures. Among them, gravity

based, monopile and jacket structure foundations are more popular for the bottom-fixed offshore wind turbine. A brief introduction of these bottom-fixed foundations is given in the following:

Gravity base foundations (GBFs): The gravity base foundation is primarily designed according their self-weight, which must be sufficient to resist extreme overturning moments, leaving support structures standing upright on the seabed. The weights of GBFs range from 1500 to 4500 tonnes [Thomsen, 2014]. Therefore, gravity base foundations (GBFs) are usually made of concrete. They use their self weights to resist overturning moments and are appropriate for the clay, sandy soil and rock seabed conditions [Wu et al., 2019]. Normally, GBFs are used in water depths less than 10 m.

Monopile foundations: The monopile foundation has the simplest form as it consists of one single steel tube pile. Typical monopile OWTs have a diameter of 3–8 m and are considered economic for water depths of 20–40 m, and the development of monopiles of larger diameters and lengths is ongoing [Hermans and Peeringa, 2016]. The monopiles are widely used for offshore wind turbine foundations, due to its ease of manufacture, low cost, and manageable construction.

Jacket foundations: The jacket foundations are space frame structures welded from steel tubular members, which is usually fabricated in advance by welding on land. The jacket is normally transported to site and piled into the seabed [Wu et al., 2019]. Jacket foundations are relatively economical in terms of steel consumption, but storage, logistics, and installation can be expensive, substantially raising the overall cost [Thomsen, 2014]. Despite storage and logistics challenges, jacket-supported OWTs are competitive for intermediate water depths (50–90m).

Floating offshore wind turbines

Floating offshore wind turbines (FOWTs) are designed with with several dynamic characteristics to withstand various offshore load conditions [Wisatesajja et al., 2019]. Like floating oil and gas platforms, FOWTs rely on mooring and anchoring systems to fulfill their station-keeping purposes in deep water [Micallef and Rezaeiha, 2021]. Three types of FOWTs have been developed as both commercial and prototype systems including spar-buoy, spar-submersible, and tension-leg platforms as shown in Fig. 1.7.

The spar-buoy floating offshore wind turbine is supported by a simple cylindrical shape spar with ballast at the bottom of the platform to ensure that it floats and stays upright with a center of gravity below the center of buoyancy. The spar-buoy FOWTs are with good hydrostatic stability and small waterplane ares, which are suitable for operation in deep water and harsh environmental conditions. As shown in Fig. 1.7, the lower parts of the structure are heavy and the upper parts are usually lighter, thereby raising the center of buoyancy. These platforms require deep water as the draft of the platform is higher than or equal to the hub height above mean sea level. This ensures stability and reduces heave motion

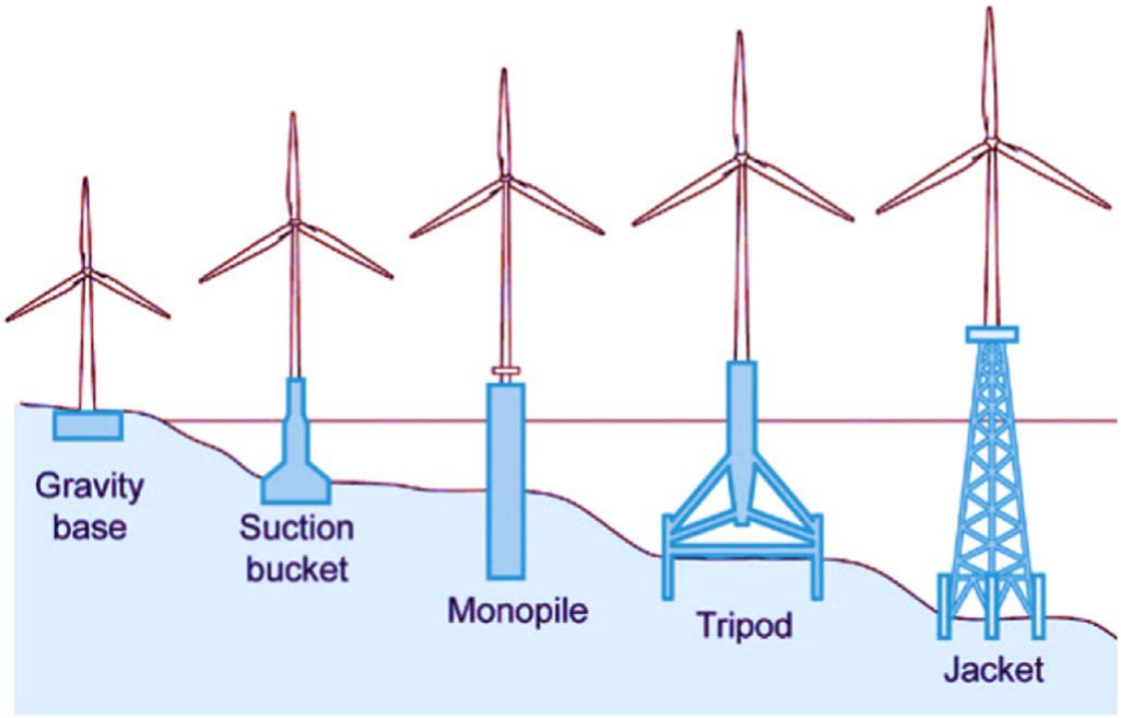

Figure 1.6 – Bottom-fixed offshore wind turbines [Moulas et al., 2017]

[Wisatesajja et al., 2019].

A semi-submersible FOWT is normally composed of three columns that are at distance from and connected to each other, which is simple to install. The wind turbine is mounted on one of the columnar tubes, or mounted at the geometric center of the platform, and supported by bracing members. The columnar tubes act as ballast to provide stability in the water. Compared with a single-column spar, a semi-submersible has more hydrodynamic stability and more structural stiffness to resist wave loads, due to the increase waterplane area. [Liu et al., 2016]

The tension-leg platform (TLP) is a semi-floating structure and vertically moored compliant platform, where the stability is created by the tension of the mooring lines anchored to the seabed. Many TLP floating offshore wind turbine concepts have been proposed in past [Sclavounos et al., 2010, Bachynski and Moan, 2012, Kausche et al., 2018, Uzunoglu and Soares, 2020], which are smaller and lighter due to the low draft and tension stability. However compared with spar and semi-submersible FOWTs, TLP structures are less commercialized due to the complexities in anchoring systems and installation process [Jiang, 2021].

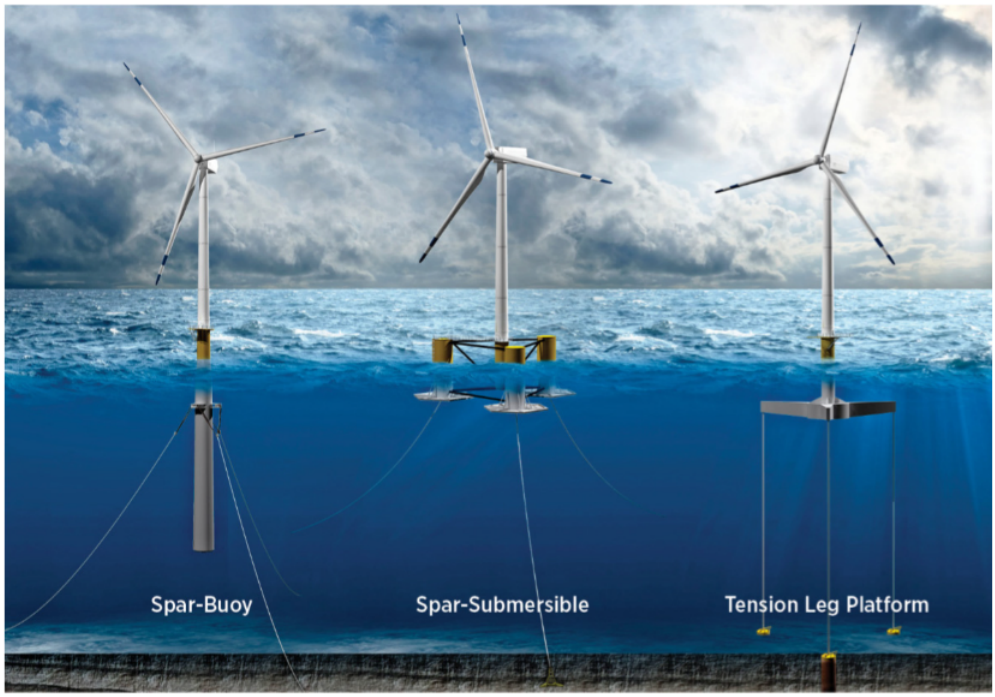

Figure 1.7 – Floating offshore wind turbines [Freeman et al., 2016]

1.4 Offshore wind turbine foundation design

In this section, the modern wind turbine foundation design process and tools are briefly introduced. The design of offshore foundation structures are much complex, which consider different load sources, wind and wave conditions. Thus, at first, the typical design cycle of the offshore wind turbine foundation is introduced and the basic dynamic theory of the OWT foundation is briefly discussed. Also, the major loads of offshore wind turbine are introduced. The typical design standard and design load conditions are also given. Finally, some useful and typical tools used for offshore wind turbine simulation are briefly discussed.

1.4.1 Basic dynamic theory of offshore wind turbine foundations

The equation of motion of the complete OWT model can be expressed as:

$$\mathrm{M}\ddot{u} + \mathrm{C}\dot{u} + \mathrm{K}u = f \tag{1.1}$$

where M is the mass matrix of the complete OWT model, C is the damping matrix and K is the stiffness matrix. f is the external load consisting of wind and wave loads and u is the response of OWT model. However, the offshore wind turbine is much complex and too large to be simulated or measured with

detailed modeling. Hence, the substructuring (super-element) methods are widely used in the offshore wind turbine simulations. The substructuring (super-element) approach can be summarized as follows [De Valk, 2013, Van der Valk, 2014, Voormeeren et al., 2014]:(1).Divide the complete structure into different substructures (2).Define a reduction matrix for every substructures that retains the interface degree of freedom (DoF) (3).Assemble the substructures to construct the complete reduced model by assembling the interfaces DoF of the different substructures.

Therefore, the equations of the complete OWT model can be rewritten for two substructures. The foundation is one substructure, denoted by f, the rest can be considered as the other substructure including tower, the RNA and the remaining parts, denoted by r. The equations can be expressed as:

$$\mathrm{M}^r \ddot{u}^r + \mathrm{C}^r \dot{u}^r + \mathrm{K}^r u^r = f^r + g^r \tag{1.2}$$

$$\mathrm{M}^f \ddot{u}^f + \mathrm{C}^f \dot{u}^f + \mathrm{K}^f u^f = f^f + g^f \tag{1.3}$$

where g^f and g^r are the internal loads of the two substructures. g^f and g^r should be equal of amplitude and opposite direction due to the equilibrium condition. Also, the displacements of the interface between the two substructures should be same, following the compatibility conditions. The interfaces loads (g^f) from the foundation designer are usually as input for the wind turbine designer, which reads:

$$g^f = \mathrm{M}^f \ddot{u}^f + \mathrm{C}^f \dot{u}^f + \mathrm{K}^f u^f - f^f \tag{1.4}$$

To get the interface loads, various approaches [Guyan, 1965, Craig Jr and Bampton, 1968, van der Valk and Rixen, 2014] can be used. More details of these approaches can be found in the following sections. Furthermore, to simplify the following discussion, the Eq.1.2 can be rewritten in the frequency domain, which is given by:

$$\left(-\omega^2 \mathrm{M}^f + j\omega \mathrm{C}^f + \mathrm{K}^f\right) u^f = f^f + g^f \tag{1.5}$$

In addition, for the OWT foundation simulation, two analysis methods are generally used. One is the dynamic analysis and the other is the quasi-static analysis. The dynamic analysis is to solve the responses of the foundation structure with a dynamic force, where the displacement (u_d) is the exactly the same as u^f:

$$u_d = u^f = \left(-\omega^2 \mathrm{M}^{(f)} + j\omega \mathrm{C}^{(f)} + \mathrm{K}^{(f)}\right)^{-1} \left(f^{(f)} + g^{(f)}\right) \tag{1.6}$$

The quasi-static analysis neglects the inertia and damping forces. The displacement (u_{qs}) of foundation can be approximated as:

$$u_{qs} = \mathrm{K}^{(f)-1} \left(f^{(f)} + g^{(f)}\right) \tag{1.7}$$

The accuracy of the quasi-static responses will depend on the first eigenfrequency ω^1 of the foundation and the excitation frequency of the external loads. If the ω^1 is higher than the highest excitation

frequency of the external loads, the quasi-static analysis can provide an accurate result [De Valk, 2013]. In addition, the above theory formulation are all based on the force controlled approaches and the displacement controlled approaches can be found in the references [De Valk, 2013, Van der Valk, 2014].

1.4.2 Design cycle for offshore wind turbine foundations

Generally, the offshore wind turbine design can be classified into two main substructures: the rotor-nacelle-assembly (RNA) and its support structure. The wind turbine manufacturer (WTM) is responsible for the detailed design of the RNA and the tower, modeling the aerodynamics and turbine controller. The foundation designer (FD) is response for the design of the offshore foundation, perform the soil modeling and determine the specific site wave loads acting on the foundation. For the offshore wind turbine foundation design, many different type of loading and control actions should be considered, such as:

(1). Aero-elastic coupling, i.e. the coupling of structural deformation and aerodynamic loads
(2). Rotational effects of the rotor
(3). The wind turbine's controller dynamics
(4). Hydrodynamic loads
(5). Soil-structure interaction
(6). ...

The foundation design can seen as a calculation cycle and several iterations are required before a satisfactory design is finished as shown in Fig.1.8. In addition, the wind climate, wave conditions, water depth and soil properties for the wind farm are needed before the foundation design process. If all these parameters are known, the typical foundation design cycle can be summarized as follows [Van der Valk, 2014]:

(1). The FD propose an initial foundation design considering the wind and wave conditions, soil properties, and water depth. The FD communicates the initial design and the wave loads with the WTM.
(2). The WTM integrates the foundation design structure within the aero-elastic model, as a result the aero-elastic model contains all the components of the OWT.
(3). The WTM performs the simulations of the full set of design load cases and check whether the current tower meets the design criteria.
(4). The loads or displacements at the interface between the tower and the foundation structures are extracted and passed to FD.
(5). The extracted loads or displacements with the synchronized wave loads are applied on the detailed foundation model. The FD should run a number of simulations on the detailed foundation to check whether the foundation design meet design criteria. If the current design cannot fulfills the design code or is too conservative, a new design loop starts.

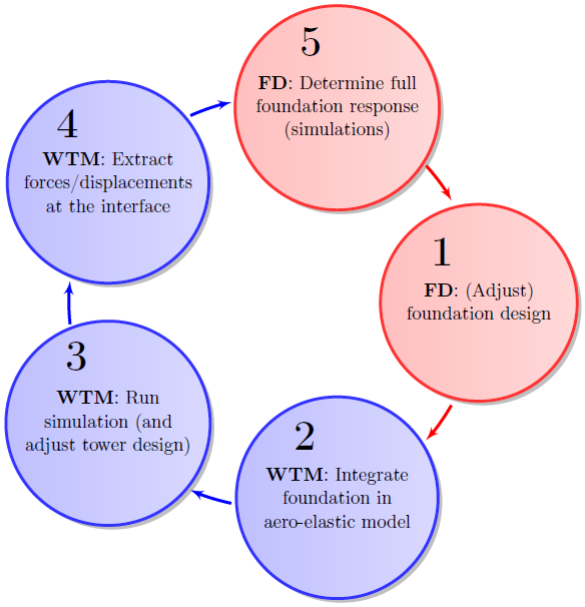

Figure 1.8 – Schematic overview of the design cycle of an OWT foundation [Van der Valk, 2014]

1.4.3 Major loads of offshore wind turbines

For the offshore wind foundation design or reliability assessment, the offshore wind turbine load calculations are vital. The offshore wind foundation are generally exposed to complex and variable loads. Fig.1.9 illustrates the various loads acting on the jacket support structures. Based on this figure, the details of the loading on the bottom-fixed foundations are given in the following.

Inertia load

The inertia or gravity load is significant source of load, which is mainly due to the mass of RNA and the foundation structure. As the wind turbine get larger today, the effect's of the inertia load is no doubt an important factor in offshore wind turbine foundation design. Also, the inertia load can greatly influence the buckling and modal frequencies limit states of offshore wind turbine.

Aerodynamic loads

The aerodynamic loads are always the primary loads for the wind turbine, which cannot be neglected. The aerodynamic loads come from wind load acting on the wind turbine blades and are transferred to top of wind tower from rotor. Typically, the aerodynamic loads transferred from rotor will be decomposed through the load matrix defined in turbine's axis for example thrust force and moment. Traditionally, the computational fluid dynamic tools can be used for the aerodynamic load simulation

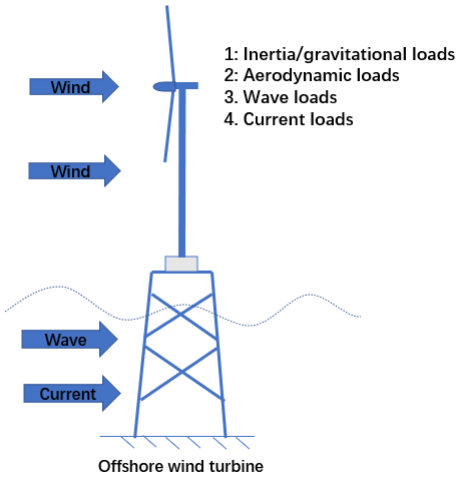

Figure 1.9 – Schematic overview of loading of offshore jacket structure

but needs an important computational efforts. As an alternative, the wind turbine aerodynamic calculations are widely based on one approximated approach-blade element momentum (BEM) theory. In this approximated approach, firstly, the aerodynamic interactions between the blades are neglected and secondly the forces are only determined by the lift and drag coefficients. A brief introduction of the BEM theory is given here. The wind turbine blades are considered as a finite number of elements. The axial force δT and torque δQ from the actuator disc and stream tube as shown in Fig.1.10 can be calculated by applying the momentum theory:

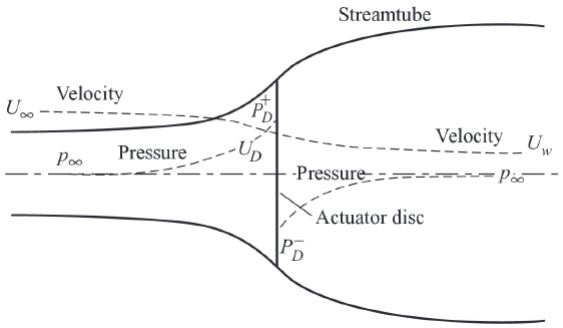

Figure 1.10 – Actuator disc and stream tube concept in [Burton et al., 2011]

$$\begin{aligned} \delta T &= 2\pi r \delta r \rho U_\infty (1-a) 2a U_\infty \\ \delta Q &= 2\pi r \delta r \rho U_\infty (1-a) 2a' r^2 \Omega \end{aligned} \tag{1.8}$$

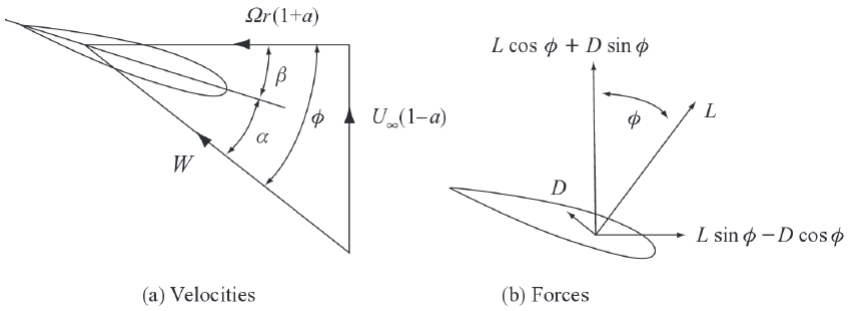

Figure 1.11 – Blade element approach [Burton et al., 2011] where D and L stand for the drag and lift forces

where U_∞ is the inflow wind speed and ρ is the air density, a and a' are the axial and tangential flow induction factors, r and ω are respectively the blade element radius and rotational speed. The quantities δT and torque δQ can be calculated in application of the blade element theory on a geometrical analysis as shown Fig.1.11, which is given by:

$$\begin{aligned} \delta T &= \frac{1}{2}\rho W^2 B c \left(C_l \cos\phi + C_d \sin\phi\right) \delta r \\ \delta Q &= \frac{1}{2}\rho W^2 B c r \left(C_l \sin\phi + C_d \cos\phi\right) \delta r \end{aligned} \tag{1.9}$$

where c is the profile chord and C_l and C_d are the lift and drag coefficients of the blade element,W is the resultant relative velocity at the blade, B is the number of blades. Combining the momentum (Eq.1.8) and blade element theories (Eq.1.9) together, two equations of equilibrium are then obtained:

$$\begin{aligned} \frac{W^2}{U_\infty^2} B \frac{c}{R} \left(C_l \cos\phi + C_d \sin\phi\right) &= 8\pi a(1-a)\mu \\ \frac{W^2}{U_\infty^2} B \frac{c}{R} \left(C_l \sin\phi + C_d \cos\phi\right) &= 8\pi\lambda\mu^2 a'(1-a) \end{aligned} \tag{1.10}$$

where $\mu = r/R$ and λ is the tip speed ratio. Once the equilibrium is reached and the parameters in Eq.1.10 are determined, the axial forces and torque can be calculated by integrating the differential quantities over the blades length. For more details of the BEM theories, readers can find the references [Burton et al., 2011, Ingram, 2011].

Wave loads

The wave loads is part of the hydrodynamic loads. Waves can induce a significant force on an offshore support structure. An accurate estimation of the wave load is very important for the offshore wind turbine foundation design or reliability assessment. Morrison's equation are normally used for the wave-induced drag and inertia forces, which is given by:

$$F = \rho V \dot{u} + \rho C_m V(\dot{u} - \dot{v}) + \frac{1}{2}\rho C_d A(u - v)|u - v| \tag{1.11}$$

where ρ is the sea water density, C_m and C_d are respectively the inertia and drag coefficients, A and V are respectively the cross sectional area of the structure body and the volume of the body, u and $\dot{u}$ are the flow velocity and acceleration, v and $\dot{v}$ are the body velocity and acceleration. Normally, the Morrison's equation is considered under the assumption of fixed structure where $v = 0$ and $\dot{v} = 0$. Need to be mentioned that the choice of wave theory is also important, which depends on the ocean site characteristics such as water depth, wave height and wave period. Two spectra methods are widely used to represent the wave information. One is the "Pierson-Moskwitz" proposed by [Pierson Jr and Moskowitz, 1964] and the other is the "Jonswap" proposed by [Hasselmann et al., 1973].

Current loads

The current load is also part of hydrodynamic loads. Current accounts for the movement of water. The movement caused by current can also induce a drag acting on the offshore foundation. The current velocity is can be estimated using an exponential profile [IEC, 2009] as follows:

$$u_c(z) = u_{\mathrm{MSL}} \left(\frac{d+z}{d} \right)^{\frac{1}{7}} \tag{1.12}$$

where u_{MSL} is the current velocity at mean sea level, d is the depth of water and z is the reference depth.

1.4.4 Wind turbine design process

In reality, the loads acting on the wind turbine are stochastic and cannot predicted. Therefore, in the wind turbine design process, a wind turbine requires to withstand different design load cases under different load conditions. The design conditions can be mainly classified into two categories: normal condition and extreme condition, which can normally cover all the realistic wind conditions. In the normal condition, the wind turbine requires to generate the electricity safely and resist the fatigue load. In the extreme conditions, the wind turbine should withstand the ultimate loads without significant damage. A various load cases are defined in the design standards. In section, a brief introduction are given about the design standard, design wind condition, and design load cases.

Design standard

The design standard suggest specific requirements for wind turbine under different load assumptions, which gives a target for wind turbine design process and need to be considered early. The standards, norm, and codes have been established by countries or organizations like International Electrotechnical Commission (IEC), Det Norske Veritas (DNV) or Germanischer Lloyd (GL). Among these countries and organizations, IEC has issued a series of international standard for wind turbine design, which are widely used in academic research and industrial application. [Bai, 2021] has summarized most recent

IEC standard codes as shown in Table.1.2. It is worth mentioning that most of the IEC standards are still in process of updating and revision.

Except the IEC standards, there are also many other standards or norms for the wind turbine design. For instance, China have issued its own standard GB/T 13981-92 for the general design requirement of wind turbine. DNV [Standard, 2007] and GL [Lloyd and Hamburg, 2010] also issued guidelines for the wind turbines.

Design wind conditions

According the IEC 61400-1 standard [Commission et al., 2019], the wind turbine can be classified different types depending on the referenced wind speed V_{ref} and wind turbulence intensity I_{ref}. The V_{ref} is a 10-min measured mean wind speed at turbine hub height. The I_{ref} is the expected ratio of wind speed standard deviation at the hub height to the 10-min mean wind speed of 15 m/s. The wind turbine classes are shown in Table.1.3. The referenced wind speed V_{ref} categorizes the wind turbine into 3 classes, namely I, II, and III. The reference wind turbulence intensity I_{ref} categorizes also the wind turbine into 3 classes, namely A, B, and C. The special class named S, is reserved for on-site conditions where the specific values are defined by the designer.

Table 1.3 – IEC 61400-1 Wind turbine classes [Commission et al., 2019]

Wind turbine class		I	II	III	S
V_{ref} (m/s)		50	42.5	37.5	Values Specified by the designer
A	I_{ref} (-)	0.16			
B	I_{ref} (-)	0.14			
C	I_{ref} (-)	0.12			

In addition, for the design of different wind turbine classes, the wind turbine system should resist different wind conditions. The wind conditions are classified into normal wind conditions and extreme wind conditions based on the annual mean wind speed at hub heights. For the normal wind conditions, they includes normal wind profile model (NWP) and normal turbulence model (NTM). For the wind profile, it is used to describe the mean wind speed as a function of height z above the ground. The NWP with Hellmann power law can be express as follows:

$$V(z) = V_{hub}\left(\frac{z}{z_{hub}}\right)^{\alpha} \tag{1.13}$$

where z is the height above ground level, z_{hub} is the height of wind turbine hub, α is an exponent with value equal to 0.2 for Hellmann power model. The wind turbulence can represent the intensity of the changes in wind speed, shear and directions. According the IEC 61400-1, the standard deviation of tur-

Table 1.2 – IEC standards for wind energy generation systems [Bai, 2021]

Number and edition	Normative title
IEC 61400-1:2019	Part 1: Design requirements
IEC 61400-2:2019	Part 2: Small wind turbines
IEC 61400-3:2009	Part 3: Design requirements for offshore wind turbines
IEC 61400-3-1:2019	Part 3-1: Design requirements for fixed offshore wind turbines
IEC TS 61400-3-2:2019	Part 3-2: Design requirements for floating offshore wind turbines
IEC 61400-4:2012	Part 4: Design requirements wind turbine gearboxes
IEC 61400-5:2020	Part 5: Wind turbine blades
IEC 61400-6:2020	Part 6: Tower and foundation design requirements
IEC 61400-11:2019	Part 11: Acoustic noise measurement techniques
IEC 61400-12-1:2020	Part 12-1: Power performance measurements of electricity producing wind turbines
IEC 61400-12-2:2020	Part 12-2: Power performance of electricity producing wind turbines based on nacelle anemometry
IEC 61400-13:2015	Part 13: Measurement of mechanical loads
IEC 61400-14:2005	Part 14: Declaration of apparent sound power level and tonality values
IEC 61400-21-1:2019	Part 21-1: Measurement and assessment of electrical characteristics-Wind turbines
IEC 61400-21-3:2019	Part 21-3: Measurement and assessment of electrical characteristics-Wind turbine harmonic model and its application
IEC 61400-22:2010	Part 22: Conformity testing and certification
IEC 61400-23:2014	Part 23: Full-scale structural testing of rotor blades
IEC 61400-24:2019	Part 24: Lightning protection
IEC 61400-25-1:2017	Part 25-1: Communications for monitoring and control of wind power plants-Overall description of principles and models
IEC 61400-25-2:2015	Part 25-2: Communications for monitoring and control of wind power plants-Information models
IEC 61400-25-3:2015	Part 25-3: Communications for monitoring and control of wind power plants-Information exchange models
IEC 61400-25-4:2016	Part 25-4: Communications for monitoring and control of wind power plants-Mapping to communication profile
IEC 61400-25-5:2017	Part 25-5: Communications for monitoring and control of wind power plants-Compliance testing
IEC 61400-25-6:2016	Part 25-6: Communications for monitoring and control of wind power plants-Logical node classes and data classes for condition monitoring
IEC 61400-25-71:2019	Part 25-71: Communications for monitoring and control of wind power plants-Configuration description language
IEC 61400-26-1:2019	Part 26-1: Availability for wind energy generation systems
IEC 61400-27-1:2015	Part 27-1: Electrical simulation models-Wind turbines

bulence of NTM in longitudinal direction σ_1 is defined as:

$$\sigma_1 = \mathrm{I}_{ref}\,(0.75\mathrm{V}_{hub} + 5.6) \tag{1.14}$$

For the extreme wind conditions, IEC 61400-1 have defined six scenarios: (1). Extreme wind speed model (EWM). (2). Extreme operating gust (EOG) (3). Extreme turbulence model (ETM). (4). Extreme direction change (EDC) (5). Extreme coherent gust with direction change (ECD) (6). Extreme wind shear (EWS). The EOG, EDC, ECD and EWS conditions are out of the scope of this thesis and their detailed definitions can be the standard code [IEC, 2009] or other works [Bai, 2021]. For the extreme wind speed model (EWM), it is classifies into steady model and turbulent model. For the steady model, the extreme wind speed V_{e50} with a recurrence period of 50 years is expressed as follows:

$$\mathrm{V}_{e50}(z) = 1.4\mathrm{V}_{ref}\left(\frac{z}{z_{hub}}\right)^{0.11} \tag{1.15}$$

where V_{ref} is the reference wind speed listed in Table 1.3. For the turbulent extreme model, the 10-min mean speed with a recurrence period of 50 years V_{e50} is defined as:

$$\mathrm{V}_{e50}(z) = \mathrm{V}_{ref}\left(\frac{z}{z_{hub}}\right)^{0.11} \tag{1.16}$$

The standard deviation of wind speed longitudinal component if fixed as $\sigma_1 = 0.11\mathrm{V}_{hub}$.

For extreme turbulence model (ETM), the wind profile is the same as NWP. However, the standard deviation of turbulence in the longitudinal component σ_1 is given by:

$$\sigma_1 = 2\mathrm{I}_{ref}\left(0.072\left(\frac{\mathrm{V}_{avg}}{2}+3\right)\left(\frac{\mathrm{V}_{hub}}{2}-4\right)+10\right) \tag{1.17}$$

where V_{avg} equals to $0.2\mathrm{V}_{ref}$.

Design load cases

Design load cases (DLCs) are defined to take account all the operating conditions and other critical states of wind turbines. They cover various operational modes of the turbine such as start-up, normal operation, shut down and 50-year extreme condition. In total, there are 32 DLCs in the standard IEC 61400-3 [IEC, 2009]. These DLCs can be roughly categorized into two major groups namely ultimate and fatigue DLCs. Some typical DLCs are summarized in Table.1.4 [Bai, 2021]. Each DLC is assigned to an analysis of fatigue load and ultimate load. Fatigue load analysis is to assess the wind turbine fatigue strength and Ultimate load analysis is to evaluate the wind turbine under ultimate load considering blade tip deflection, material strength and structural stability.

Table 1.4 – Typical design load cases [Bai, 2021]

		Wind conditions	
		Normal	Extreme
Wind turbine states	Normal operation	DLC1.1[1],DLC1.2[2]	DLC1.3[1],DLC1.4[1],DLC1.5[1]
		DLC3.1[2]	DLC3.2[1],DLC3.3[1]
		DLC4.1[2]	DLC4.1[1]
		DLC6.4[2]	DLC6.1[1]
		DLC8.1[1]	DLC8.2[1]
	Faults and defects	DLC2.1[1],DLC2.2[1],DLC2.4[2]	DLC2.3[1]
		DLC5.1[1]	DLC6.2[1],DLC6.3[1]
			DLC7.1[1]

[1] Ultimate load analysis

[2] Fatigue load analysis

Partial safety factor based design

In the design of offshore wind turbine structures, a verified design should at least be satisfied:

$$S_d < R_d \tag{1.18}$$

where S_d and R_d are respectively the design loading and resistance. However, the structural responses from the simulation are supposed to suffer from uncertainties. Several sources of uncertainties have to be considered in the simulations, such as environmental loads or material properties. These uncertainties can be considered in a deterministic way by using partial safety factor (γ_f) [Standard, 2007, IEC, 2009], which aims at integrating all the uncertainties in the design scheme. The partial safety factors can be considered in the loads or the resistance parts. To consider the security factor in the loading part, there are two approaches as presented in Fig. 1.12. The F_k and S_k are respectively the characteristic load and load effect. Let M_a be the numerical analysis. In the first approach, the design load effect can be expressed as:

$$S_d = \gamma_f S_k = \gamma_f M_a (F_k) \tag{1.19}$$

The second approach aiming at integrating the partial safety factor before mechanical analysis, which is given by:

$$S_d = M_a \left(\gamma_f F_k\right) \tag{1.20}$$

The standards indicate that the first approach is more suitable for the analysis where the dynamic reactions need to be precisely estimated such as the design of the tower and the second approach is suitable for considering the non-linearity of model responses, for example, the design of foundation. More detailed introduction can be the related references [Standard, 2007, IEC, 2009]. The partial safety

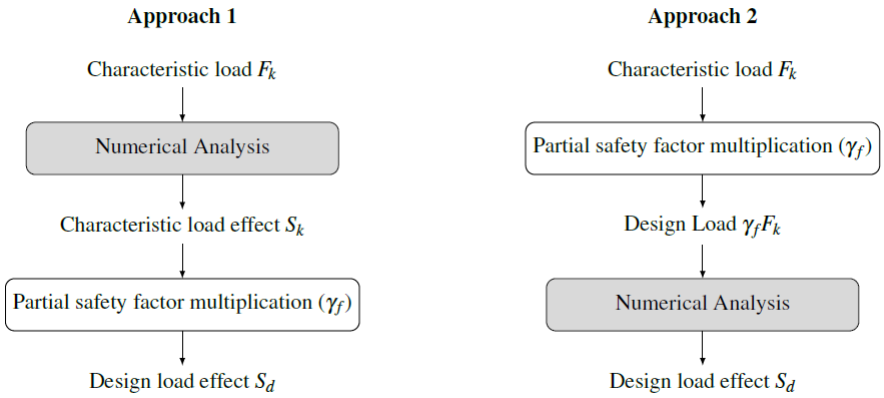

Figure 1.12 – Two approaches considering the partial safety factor in the loading [IEC, 2009]

factors being considered in resistance part can also the related references [Standard, 2007, IEC, 2009].

Reliability-based design

However, to consider the uncertainties, using partial safety factors may be too conservative or not precise. The partial safety factors are only used to ensure a minimal structural safety [Huchet, 2018]. As a alternative, the reliability based design method is more reliable and robust to take the uncertainties into account. The structural reliability or safety is that the probability of failure (Pf) will not occur or be inferior to target failure probability (Pf_t). In the other words, the reliability index (β) should be superior to the target reliability index (β_t). A reliability-based design structure should be satisfied:

$$\beta \geq \beta_t \tag{1.21}$$

where $\beta = \Phi(-Pf)$ and Φ is the cumulative density function (CDF) of the standard normal distribution. In addition, for different parts of offshore wind turbines such as blades, towers, and foundations, the target design reliability indexes may be different [Veritas, 2004, Standard, 2007]. The key point of the reliability based design is to evaluate the reliability of the structure under the uncertainties. The reliability assessment is normally time-consuming or imprecise based on the traditional approaches such as Monte Carlo simulation or first order reliability method. A detailed introduction of the reliability assessment can be found in the following section.

1.4.5 Wind turbine simulation tools

For structures as complex as wind turbines, multi-physics are involved in the modeling and simulation process. Three methods are commonly used for the wind turbine modeling process and simulations (1). Finite element method (2). Multibody simulation (3). Modal analysis. The finite element method

is general numerical method for solving differential equations arising in engineering and mathematical modeling, which are commonly used for structural analysis. Multibody simulation (MBS) is to study the dynamic behavior of interconnected structures. Each body is linked together under some constraint so that individual movement can be performed by a single body with respect to each other. The modal analysis is often used to determine the dynamic properties of the structure namely the natural frequencies and corresponding mode shapes. As for the simulation tools, until now, there is is not a single tool or method can deal with all of these aspects. However, certain subsystems of the wind turbines can be simulated by other tools. In this subsection, some popular wind turbine simulation tools are introduced.

Fatigue, Aerodynamics, Structures, and Turbulence (FAST)

FAST also named OpenFAST, is a modular computer-aided engineering (CAE) open-source software to simulate wind turbines under a given operating condition, which is design by the National Renewable Energy Lab (NREL) [Jonkman et al., 2005]. FAST employs a Multi-body/modal system (MBS) including aerodynamic, hydrodynamic and etc. The workflow of FAST is shown in Table.1.13. The aerodynamic module uses the blade element momentum (BEM) theory with empirical corrections. The hydrodynamic modules offer modeling based on Potential flow and Morison's equation. In FAST, the structural responses and control system to the wind inflow conditions are simulated in time domain. The outputs of the simulations are time series data which include the loads, power and deflections of the structural components.

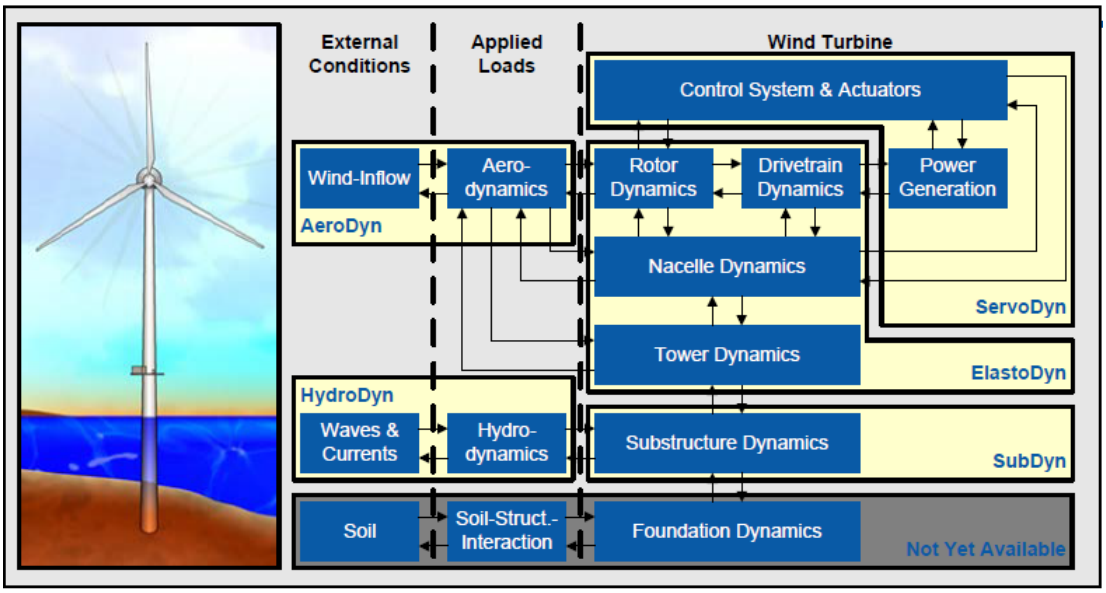

Figure 1.13 – FAST modules [Jonkman, 2014]

Horizontal Axis Wind Turbine Code-Second generation (HAWC2)

HAWC2 is a commercial package for calculating wind turbine responses in time domain that is mainly used to study the dynamics of fixed bottom OWTs operating under external loads [Larsen and Hansen, 2007]. HAWC2 also includes different models describing the the external effect, applied loads, structural dynamics and connection to the control system. The external effects models is used to model how the wind, waves and soil behave. The applied loads models is to model how the external effects interact with the structure through aerodynamic, hydrodynamic and soil models. The aerodynamic loads are based on BEM theory. The structural formulation of HAWC2 is also based on a multi-body system. The wind turbine control is performed through the external dynamic link library.

Bladed

Bladed is also a commercial software for the design and certification of onshore and offshore wind turbines.[turbine design software Bladed, 2011]. Bladed code also considers incident wave and wind loads, structural dynamics, aerodynamics, and suitable controller response. Like FAST and HAWC2, the structural dynamics of the Bladed code are based on the multibody modal system representation. The aerodynamic module uses both the momentum and blade element model. The hydrodynamic module utilizes the penal method and Morison equation. Bladed is widely used by wind turbine manufacturers and engineers to calculate loads and wind wind turbine performances. Now, Bladed has been the industry standard aero-elastic wind turbine design software.

1.5 Reliability analysis

In reality, a structure or a system is often under uncertainties. The analysis of the responses under uncertainties is important for risk assessment and decision-making. The objective of the reliability assessment is to assess the safety of a structure or a system under uncertainties. For a complex system like the wind turbine, there are many uncertainties involved in the design, such as the environmental loads and the material strength and stiffness. Therefore, for designing a wind turbine for a service life of at least 20 years, the reliability-based design of the wind turbine must be carefully considered. In this subsection, a brief introduction of the reliability analysis and applications in the wind turbines are given. The reliability-related problems can be normally classified into the three parts as shown in Fig. 1.14.

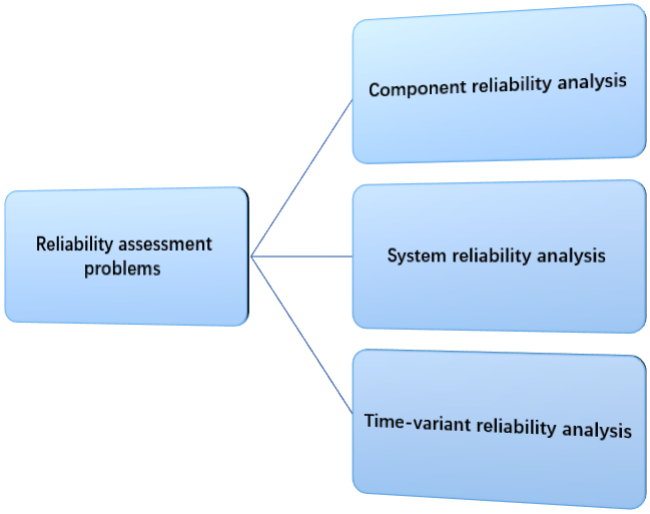

Figure 1.14 – Reliability assessment problem classification

1.5.1 Component reliability analysis

The component reliability is to compute the probability of failure P_f of a structural component with one limit state. For the response function $g(\mathbf{x})$ relating with the n-dimensional random input vector, the probability of failure of a component can be formulated as:

$$P_f = \int I_{g(\mathbf{x})\leqslant 0}(\mathbf{x}) f_{\mathbf{x}}(\mathbf{x}) dx \tag{1.22}$$

where $f_{\mathbf{x}}(\mathbf{x})$ is the joint probability density function (PDF) of the random variable vector $\mathbf{x}$. $I_{g(\mathbf{x})}$ is the failure indicator, it equals to one if $g(\mathbf{x}) \leqslant 0$ and zero otherwise. The reliability assessment approaches of the component reliability analysis can mainly classified into the following groups:(1) Approximation approaches (2) Simulation approaches (3) Surrogate models based approaches as shown in Fig.1.15.

Approximation approaches

The approximation methods are widely used for the reliability analysis, for example, first order reliability method (FORM) and second order reliability method (SORM). Before applying FORM or SORM, the input variables $\mathbf{x}$ should be transformed from physical space to standard normal space with isoprobabilistic-transformation $\mathbf{T}$.

$$\mathbf{u} = \mathbf{T}(\mathbf{x}) \tag{1.23}$$

In standard normal space, the reliability problem is simplified to find the minimum distance to the limit

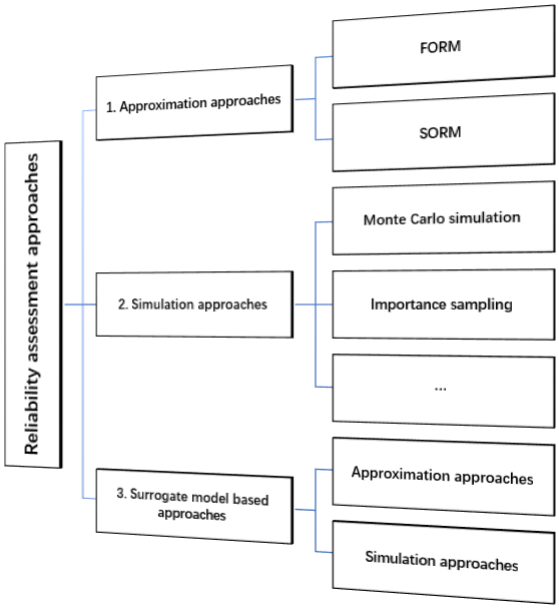

Figure 1.15 – Reliability assessment approaches classification

state:

$$\begin{aligned} \min \beta &= \left\| \mathbf{u}^{\mathrm{T}} \mathbf{u} \right\| \\ s.t. \mathrm{g}(\mathbf{u}) &= 0 \end{aligned} \tag{1.24}$$

The shortest Euclidean distance in the standard norm space is also called Hasofer-Lind reliability index β_{HL}. As shown in Fig.1.16, the probability of failure p_f can be calculated from $p_f \approx \Phi(-\beta_{\mathrm{HL}})$, where Φ is the cumulative density function (CDF) of the standard normal distribution; u^* is the corresponding most probable failure point (MPFP) in the standard space.

First Order Reliability Method (FORM) The FORM method approximates the limit state surface in the vicinity of the most probable failure point with a linear function. To solve the optimization problem in Eq.(1.24), an iterative method called HLRF is proposed by [Rackwitz and Flessler, 1978] is widely used. In HLRF method, the limit state function $\tilde{\mathrm{G}}$ at each iteration k is approximated by its tangent hyper-plane at the current MPFP u^k:

$$\tilde{\mathrm{G}}^{\mathrm{FORM}} = \mathrm{G}\left(\mathbf{u}^k\right) + \nabla \mathrm{G}\left(\mathbf{u}^k\right)^{\mathrm{T}} \left(\mathbf{u} - \mathbf{u}^k\right) \tag{1.25}$$

By iteration, the most probable failure point can be easily found. The approximate value of the failure

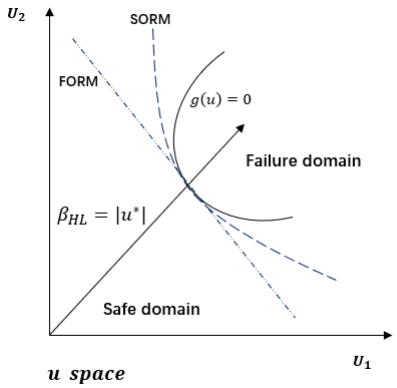

Figure 1.16 – FORM and SORM method for reliability analysis

probability is as follows:

$$\mathrm{P}_f \approx \Phi\left(-\beta_{\mathrm{HL}}\right) \tag{1.26}$$

Second Order Reliability Method (SORM) The SORM method [Low, 2014] is a second-order refinement of FORM as shown in Fig.1.16. It is thus considered as improvement of the FORM method in terms of accuracy. The tangent hyper-plane in Eq.(1.25) at each iteration k is replaced with the second order Taylor expansion at the MPFP:

$$\tilde{\mathrm{G}}^{\mathrm{SORM}} = \mathrm{G}\left(\mathbf{u}^k\right) + \nabla \mathrm{G}\left(\mathbf{u}^k\right)^{\mathrm{T}}\left(\mathbf{u}-\mathbf{u}^k\right) + \frac{1}{2}\left(\mathbf{u}-\mathbf{u}^k\right)^{\mathrm{T}} \nabla^2 \mathrm{G}\left(\mathbf{u}^k\right)\left(\mathbf{u}-\mathbf{u}^k\right) \tag{1.27}$$

where ∇^2 denotes the Hessian operator.

Simulation approaches

To get the reliability index, the approximation approaches may get inaccurate results when facing highly non-linear problems. Compared to the approximation approaches, the simulation approaches are more robust. The subsection will give a introduction typical straightforward simulation methods.

Monte Carlo Simulation Using Monte Carlo simulation for the reliability assessment is the most straightforward simulation method, which simply draws large samples. P_f in Eq.(1.22) can be estimated by MCS techniques given by:

$$\mathrm{P}_f \approx \frac{1}{\mathrm{N}_{\mathrm{MCS}}} \sum_{i=1}^{\mathrm{N}_{\mathrm{MCS}}} \mathrm{I}_{g(\mathbf{x})\leqslant 0}\left(\mathbf{x_i}\right) \tag{1.28}$$

where $\mathbf{x_i}$ is the random samples generated from the marginal density function of $f_{\mathbf{x}}(\mathbf{x})$. MCS is very robust and accurate approach if the sample size is large enough, according to the *law of large numbers*

[Loève, 1955, Robert et al., 2004]. Although it may need much computation cost, it still serves as the fundamental tool or the comparison reference for various problems [Binder et al., 1993].

Importance sampling Importance Sampling (IS)[Glynn and Iglehart, 1989, Neal, 2001] is proposed to reduce the number samples needed for MCS, or when sampling from the distribution $f_{\mathbf{x}}(\mathbf{x})$ is difficult. It focuses on input parameters that have larger importance. Eq.(1.22) can be transferred to :

$$\mathrm{P}_f = \int \mathrm{I}_{g(\mathbf{x})\leqslant 0}(\mathbf{x})\, h_{\mathbf{x}}(\mathbf{x})\, q_{\mathbf{x}}(\mathbf{x})\, dx = \mathrm{E}_q[\mathrm{I}(\mathrm{g}(\mathbf{x})\leqslant 0)\, h_{\mathbf{x}}(\mathbf{x})] \tag{1.29}$$

where $h_{\mathbf{x}}(\mathbf{x}) = \frac{f_{\mathbf{x}}(\mathbf{x})}{q_{\mathbf{x}}(\mathbf{x})}$ is the so-called importance weight function. An estimate of P_f can be obtained by generating samples from $q_{\mathbf{x}}(\mathbf{x})$ and taking the mean of $\mathrm{I}(\mathrm{g}(\mathbf{x})\leqslant 0)\, h_{\mathbf{x}}(\mathbf{x})$, i.e.

$$\hat{\mathrm{P}}_f = \mathrm{E}_q[\mathrm{I}(\mathrm{g}(\mathbf{x})\leqslant 0)\, h_{\mathbf{x}}(\mathbf{x})] = \frac{1}{n_{is}} \sum_{k=1}^{n_{is}} \mathrm{I}\left(g\left(\mathbf{x}_k\right)\leqslant 0\right) h_{\mathbf{x}}\left(\mathbf{x}_k\right) \tag{1.30}$$

In Eq.(1.29), the samples can be generated from $q_{\mathbf{x}}(\mathbf{x})$ which is a well defined distribution.

Subset simulation Subset simulation [Au and Beck, 2001, Li and Au, 2010] is an adaptive Markov Chain Monte Carlo (MCMC)[Hastings, 1970] procedure for efficiently computing the small failure probability as shown in Fig.1.17. Let F denote the final failure event and F_1,F_2...F_m be a sequence of intermediate failure events with $\mathrm{F}_1 \supset \mathrm{F}_2 \supset \cdots \supset \mathrm{F}_m = \mathrm{F}$. According to the definition of failure events in reliability analysis, each F_i is defined as $\mathrm{F}_i = \{g(\mathbf{x}) \leqslant g_i\}$, with g_i being the corresponding failure threshold ($g_1 > g_2 > \cdots > g_m = 0$). Therefore, the failure probability can be expressed as the product of $\mathrm{P}(\mathrm{F}_m)$ and a number of conditional probabilities:

$$\mathrm{P}_{\mathrm{F}} = \mathrm{P}\left(\mathrm{F}_m\right) = \mathrm{P}\left(\mathrm{F}_m \mid \mathrm{F}_{m-1}\right) \mathrm{P}\left(\mathrm{F}_{m-1}\right) = \cdots = \mathrm{P}\left(\mathrm{F}_1\right) \prod_{i=1}^{m-1} \mathrm{P}\left(\mathrm{F}_{i+1} \mid \mathrm{F}_i\right) \tag{1.31}$$

The modified Metropolis-Hastings algorithm [Au and Beck, 2001] is adopted for MCMC simulation in generating the conditional samples.

Other sampling approaches In recent decades, other sampling approaches like weighted sampling [Efraimidis and Spirakis, 2006, Braverman et al., 2015], line sampling [de Angelis et al., 2015, Depina et al., 2016], directional sampling [Bjerager, 1988, Ditlevsen et al., 1990] are also developed and used for the reliability assessment. Even though the developed sampling approaches can improve the efficiency of simulation approaches, for the real engineering problems, the simulation approaches are still computationally demanding, especially the finite element analysis based problems.

Surrogate model based approaches

To reduce computational cost of the simulation approaches for reliability analysis, the surrogate models are widely used to replace the original model with a simpler surrogate model that can be evaluated cheaply. The general concept is: given a finite set of input realizations and their corresponding

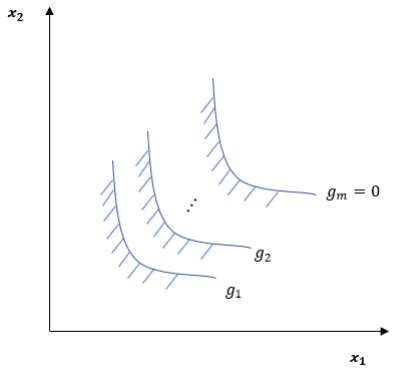

Figure 1.17 – Subset simulation

model output, known as the experimental design, a suitable parametric function is calibrated such that it accurately approximates the underlying input-output map. This process may be referred to surrogate modeling, supervised learning or meta-modeling. Many surrogate models can be found in the literature such as Response Surface Method (RSM) [Box et al., 1978, Bucher and Bourgund, 1990], the Polynomial Chaos Expansion (PCE) [Spanos and Ghanem, 1989, Sudret and Berveiller, 2008], the Artificial Neural Networks (ANN) [Papadrakakis and Lagaros, 2002], the Kriging method [Sacks et al., 1989, Kaymaz, 2005], the PC-Kriging method [Schobi et al., 2015],and the Support Vector Machine (SVM)[Hurtado, 2004, Steiner et al., 2019]. Each surrogate model is based on its own underlying assumptions and the approximation of the responses depends on the model and the problem.

The surrogate model can be used with the traditional approximation approach (FORM,SORM) for the reliability analysis. However, it will inherit the drawbacks of the approximation approaches to deal with highly non-linear problems. Therefore, the surrogate model is often used with simulation approaches.The surrogate model based simulation approaches can also be classified into (1) "one shot" (Non-adaptive) approaches and (2) Active learning (Adaptive) approaches as shown in Fig.1.18.

One shot approaches The "one shot“ approach needs to generate all sample points in advance and construct a surrogate model to ensure accuracy over the entire uncertainty space. The general process of the "one shot" approach is as shown in Fig.1.19. Normally, a large number of training samples are need to have a well-trained surrogate model. However, it is relatively simple compared with active learning approaches and less time consuming with MCS approach. Some related works can also be observed in the offshore jacket structure reliability assessment [Shittu et al., 2020, Ivanhoe et al., 2020, Chao et al., 2021].

Active learning approaches Active learning methods only select one or a few sample points at each iteration to construct the surrogate model more efficiently. Therefore, active learning approaches

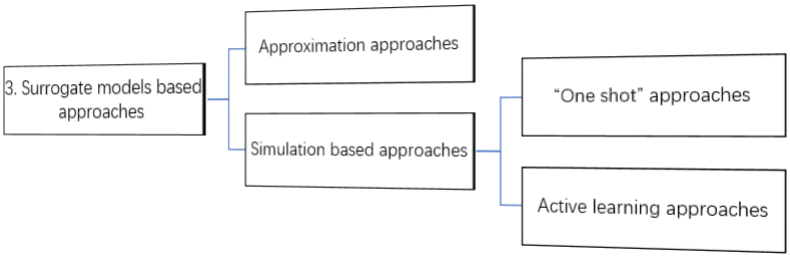

Figure 1.18 – Surrogate model based simulation approaches for reliability analysis

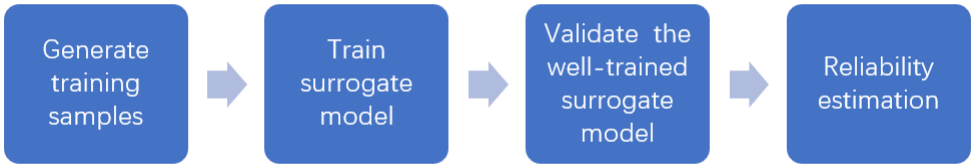

Figure 1.19 – General flowchart of "one shot" approaches with surrogate models

are generally more efficient than non-adaptive surrogate methods. The general process of the active learning approach is shown in Fig.1.20. Within the active learning approaches, a surrogate model at first is built using initial experiment design. The failure probability is then estimated by using the current surrogate and the convergence of the algorithm is assessed. If the algorithm is not converged, the enrichment of experimental design is achieved by the learning function. The main frameworks of the active learning approaches have been summarized by [Moustapha et al., 2022] in Fig.1.21, which includes four parts: surrogate model, reliability estimation, learning function, stopping criterion.

In the last decade, many active learning approaches with surrogate models have been developed for the reliability assessment. Different active learning approaches have been developed with different surrogate models, such as Kriging method [Xiao et al., 2018a, Bichon et al., 2008, Echard et al., 2011, Zhang et al., 2019], PCE [Marelli and Sudret, 2018, Zhou et al., 2020], ANN [Xiao et al., 2018b, Xiang et al., 2020], relevant vector machine [Li et al., 2021]... Other active learning approaches with different surrogate models can also be found in the review paper [Teixeira et al., 2021]. Among these approaches, Kriging is the most popular surrogate model. Many active learning approaches have been developed with Kriging method named active learning Kriging (ALK) approaches. A number of learning functions have been proposed based on Kriging model, for example, EFF learning function [Bichon et al., 2008], U learning function [Echard et al., 2011], H learning functions [Lv et al., 2015], LIF learning function[Sun et al., 2017], FNIEIF learning function [Shi et al., 2020]... Other active learning

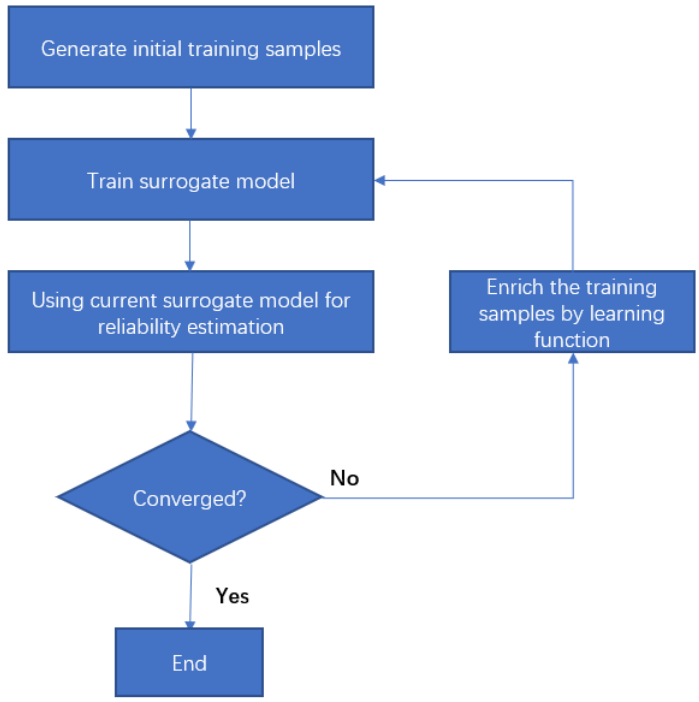

Figure 1.20 – General flowchart of active learning approaches

Kriging approaches can be found in the review paper [Fuhg et al., 2020]. The above active learning Kriging approaches are all based MCS reliability estimation. The active learning Kriging with other reliability estimation approaches are also developed in recent decades such as the Kriging with subset simulation [Huang et al., 2016, Chen et al., 2021], importance sampling [Zhang et al., 2020, Lei et al., 2021],direction sampling [Zhang et al., 2021b]... Additionally, the stopping criterion for the above active learning Kriging approaches are mostly based on the learning functions. Other stopping criterion can be found in the references [Hu and Mahadevan, 2016, Wang and Shafieezadeh, 2019a, Wang and Shafieezadeh, 2019b, Zhang et al., 2021a].

More recently, other machine learning techniques are also used for the active learning approaches such as the clustering approaches [Lelièvre et al., 2018, Xiong and Sampath, 2021], the dimensionality reduction methods[Zuhal et al., 2021], the density scanned methods[Teixeira et al., 2020]... More discussion of machine learning approaches for the reliability assessment can be found in the review papers [Xu and Saleh, 2021, Afshari et al., 2022]. Additionally, ensemble surrogate models are also proposed to deal with the reliability analysis, which aims to take advantage of the best properties of each surrogate model. Some related works can be found in the papers. [Cheng and Lu, 2020, Teixeira et al., 2020].

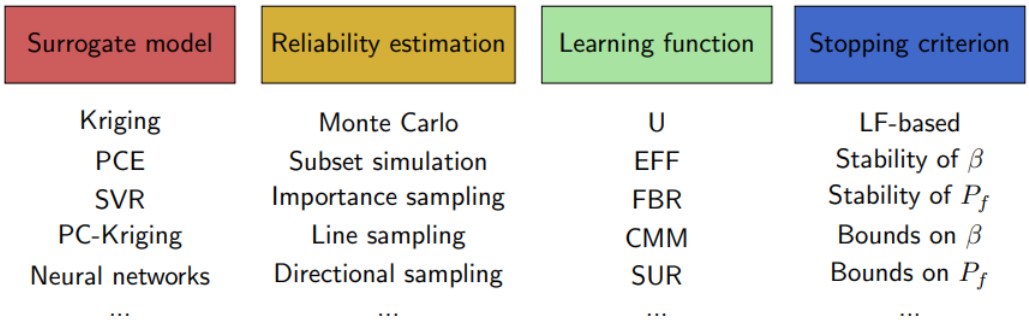

Figure 1.21 – Active learning reliability framework with example of methods [Moustapha et al., 2022]

1.5.2 System reliability analysis

A structure system commonly has multiple failure modes or components. The system reliability assessment can be formulated as :

$$\mathrm{P}_f^{sys} = \int \mathrm{I}_{g(\mathbf{x})\leqslant 0}^{sys}(\mathbf{x}) f_{\mathbf{x}}(\mathbf{x}) dx \tag{1.32}$$

where $\mathrm{I}_{g(\mathbf{x})\leqslant 0}^{sys}()$ is the failure indicator function of the system. $\mathrm{I}_{g(\mathbf{x})\leqslant 0}^{sys}$ relies on the signs of the $g_i(\mathbf{x})$ $(i = 1,...p)$. p is the number of failure modes or structural components. For a series system, $\mathrm{I}_{g(\mathbf{x})\leqslant 0}^{sys}(\mathbf{x})$ is given by:

$$\mathrm{I}_{g\leq 0}^{sys}(\mathbf{x}) = \begin{cases} 1 & \text{If} \quad \min\{g_i(\mathbf{x}) i = 1,\ldots,p\} \leq 0 \\ 0 & \text{otherwise} \end{cases} \tag{1.33}$$

For a parallel system, $\mathrm{I}_{g(\mathbf{x})\leqslant 0}^{sys}(\mathbf{x})$ is given by:

$$\mathrm{I}_{g\leq 0}^{sys}(\mathbf{x}) = \begin{cases} 1 & \text{If} \quad \max\{g_i(\mathbf{x}) i = 1,\ldots,p\} \leq 0 \\ 0 & \text{otherwise} \end{cases} \tag{1.34}$$

If there is only one component ($p = 1$), Eq.1.32 can degrade into the component reliability as expressed in Eq.1.22. To solve the system reliability problems, the approaches can also be divided into the three groups as shown in Fig.1.15.

Approximation approaches

To solve the system reliability using the approximation methods, it is normally complicated. Generally, these approaches are broken into two steps [Bichon et al., 2011]: First, the most probable failure point (MPFP) for each component is located and the reliability index β is defined for each component. Second, it is to combine the component reliability information to approximate the system reliability analysis. If only two failure modes or components are considered, the system probability can be expressed as

[Dunnett and Sobel, 1954]:

$$\begin{aligned}\Phi\left(\beta_1,\beta_2,\rho_{1,2}\right) =& \Phi\left(\beta_1\right)\Phi\left(\beta_2\right) + \int_0^{\rho_{1,2}} \frac{1}{2\pi\sqrt{1-\rho^2}} \\ & \times \exp\left[-\frac{\beta_1^2+\beta_2^2-2\rho\beta_1\beta_2}{2\left(1-\rho^2\right)}\right] d\rho\end{aligned} \tag{1.35}$$

If more than two failure modes are considered, other methods [Ditlevsen, 1979, Pandey, 1998, Dey and Mahadevan, 1998, Hohenbichler and Rackwitz, 1982] may be considered. A good summary of these approaches can be found in [McDonald and Mahadevan, 2008, Bichon et al., 2011]. However, these approaches may lead to inaccurate reliability estimation, because the MPFP may not be successfully located and the system approximation are not accurately quantified.

Simulation approaches

Using the simulation approaches for the system reliability, the concept is quite simple. The system reliability can be approximated with MCS:

$$\mathrm{P}_f^{sys} \approx \frac{1}{\mathrm{N_{MCS}}} \sum_{i=1}^{\mathrm{N_{MCS}}} \mathrm{I}_{g(\mathbf{x})\leqslant 0}^{sys}\left(\mathbf{x_i}\right) \tag{1.36}$$

For each random realization $\mathbf{x_i}$, all the component responses functions should be evaluated. The system probability of failure is just the ratio of the number of system failures between the total number of samples. Similarly, the simulation approaches require an important computational effort, which makes these approaches unrealistic for the real engineering problems.

Surrogate models based approaches

Therefore, the surrogate-based approaches for system reliability assessment get more and more popular. Like the component reliability, the surrogate-based approaches for the system reliability can be classified into: (1) Approximation approaches and (2). Simulation based approaches. Among simulation based approaches, the active learning approaches with surrogate models for system reliability are generally more efficient and accurate. Many approaches have been developed in the last decades, which can be found in the references [Bichon et al., 2011, Fauriat and Gayton, 2014, Yang et al., 2018, Yun et al., 2019, Jiang et al., 2020, Wang et al., 2021]. More details of these approaches can be found in the following section.

1.5.3 Time-variant reliability analysis

Although, the time-variant (also called time-dependent) reliability analysis is out of consideration of this thesis, a brief introduction of this type problem is given here. The time-variant failure probability is to estimate the failure probability that the time-dependent performance function $g(\boldsymbol{x},t)$ exceeds its

threshold at any instant, which is commonly formulated as:

$$P_f(t_l, t_u) = P\left\{g(\boldsymbol{x}, t) \leq 0, \exists t \in [t_l, t_u]\right\} \tag{1.37}$$

where t_l and t_u are respectively the lower-bound and upper-bound of the time interval $[t_l, t_u]$. If there exists a moment $t \in [t_l, t_u]$ satisfying $g(x,t) \leq 0$, the structure will fail. There are many approaches that have been developed in recent decades for time-variant reliability reliability. They can be roughly classified into two categories; (1). the out-crossing rate based approaches.(2) the extreme value methods.

The out-crossing rate based approaches

The out-crossing rate based approach is originally proposed [Rice, 1944]. The out-crossing rate is defined as the mean number of crossings from a safe state to an unsafe state per unit of time and the out crossing rate at time instant t can be expressed as:

$$\lambda(t) \approx \lim_{\Delta t \to 0} \frac{P\{g(\mathbf{x}, t) < 0 \cap g(\mathbf{x}, t + \Delta t) \geq 0\}}{\Delta t} \tag{1.38}$$

Extensive studies [Coleman, 1959, Rackwitz, 1998, Andrieu-Renaud et al., 2004, Der Kiureghian, 2000, Beck and Melchers, 2004, Hu and Du, 2013] on out-crossing rate approach are then followed. Coleman [Coleman, 1959] and Rackwitz [Rackwitz, 1998] have improved the methods for the computing the out crossing rate. Andrieu-Renuad et al. [Andrieu-Renaud et al., 2004] has proposed the PHI2 method which calculate the out crossing rate based on parallel static reliability method. However, the results of out crossing rate based approaches may be not accurate for highly nonlinear problems, because these approaches rely on the assumptions of independence and Poisson distribution [Du et al., 2019, Qian et al., 2021].

The extreme value based methods

To overcome the drawbacks of the out crossing rate based approaches, the extreme value based approaches are developed. The classical extreme value based approaches [Wang and Wang, 2012, Wang and Wang, 2013, Li et al., 2019] have two loops. The inner loop is to obtain extreme values using efficient global optimization and the outer loop is reliability analysis based on the extreme values. To improve efficiency, the single loop strategy[Wang and Chen, 2017, Wang and Chen, 2016, Qian et al., 2019] is also developed based on the extreme value.

The above approaches, they mainly focus on the the single time-variant limit state. More recently, the time-variant system reliability analysis can also be found in some studies [Yu et al., 2018, Xiao et al., 2020, Qian et al., 2021].

1.6 Conclusions

In this chapter, a brief introduction is given for the renewable energy development and wind energy development. The levelized cost of electricity have drop sharply in the last decade. The installed capacity of the wind energy have increased significantly in the last decade. Compared with onshore wind energy, the LCOE and installed capacity of offshore wind energy are still far behind. However, the forecast figures show that the offshore wind energy is growing very rapidly. As offshore wind technology breaks through, there will be a bigger market and a brighter future for offshore wind.

In addition, a basic introduction of wind turbine components is given. Some typical offshore wind turbine foundations are also introduced. The classical offshore wind turbine foundation design is briefly discussed. The major loads on the offshore wind turbine are summarized, which are the main part uncertainties for the reliability assessment. The modern wind turbine design standard and norms are also given and will be considered in the reliability assessment approaches. Additionally, some popular wind turbine simulation tools like FAST are introduced, which will be used for the following study.

Finally, the classical reliability analysis which including are briefly discussed. The discussions are based on the reliability problems:(1) component reliability (2) system reliability analysis (3) time-variant reliability analysis. The focus is on surrogate models assisted reliability approaches. In particular, the active learning approaches with surrogate models are of our interest, which are much efficient for the reliability assessment problems. Among these approaches, the active learning Kriging approaches have gained much attention for the reliability analysis in recent decade. Also, some popular machine learning techniques have been applied for the reliability with Kriging methods. Moreover, to take advantage of each surrogate model, the ensemble surrogate model approaches are developed for the reliability assessment, which addresses the need for using or selecting different surrogate models. However, only limited works have been done for the application of ensemble surrogate models in the reliability field.

Part II

Contributions

Chapter 2

Offshore wind turbine modeling techniques and offshore dynamic load simulation approaches

Contents

2.1 Motivation

Over the last decade, the offshore wind energy capacity has increased exponentially and more offshore wind farms are currently under construction or planned. These offshore wind farms are being installed with ever-larger turbines on sites with deeper waters. Steel jackets become the main support structures, due to the higher stiffness at the footprint and the smaller surface facing the ocean loads compared to the traditional monopiles. Many studies have been conducted with steel jacket structures. For instance, Dong et al. [Dong et al., 2011] analyses the fatigue of offshore wind turbine (OWT) jackets under different load cases in the time domain. The studies of offshore jacket structures under extreme loading can be noticed in the works of Wei et al.[Wei et al., 2014, Wei et al., 2016]. Additionally, the effects of corrosion on OWT jackets are investigated in the papers [Dong et al., 2012, Yang et al., 2019]. Other researches of OWT jacket-type structures can also be found in [Yeter et al., 2019, Chen et al., 2019].

Furthermore, for the design of OWT jackets, fatigue damage is always of interest. To evaluate the fatigue damage, the dynamic load simulation is the key point. In the OWT load simulation, the two commonly used methods are the sequentially coupled approach and the fully integrated approach. The sequential approach is widely used in industry, due to the intellectual properties and confidential issues between the foundation designer and the turbine manufacturer. The overview of this approach can be found in [Voormeeren et al., 2014, van der Valk et al., 2015]. The fully integrated method can be also found in some wind turbine simulation tools like OpenFAST [Walatka et al., 1994] and HAWC2 [Larsen and Hansen, 2007]. In addition, the comparison between these two approaches of the simulation accuracy can be found in papers [Zwick et al., 2014, Glisic et al., 2018]. However, only a few wind and wave conditions are compared in the mentioned references. As for the uncoupled simulation method, it is not commonly used, which can also have different cases. Multiphysics coupling is usually neglected in this approach, which will make the load simulations inaccurate. But the uncoupled approaches are easily carried out, which makes them popular [Ren et al., 2020, Ivanhoe et al., 2020]. Comparisons between the uncoupled and the fully coupled approaches can be found in some works [Haselbach et al., 2013, Chen Ong et al., 2017], while comparisons between the three approaches cannot be found, to the best of our knowledge.

Besides, the jacket support structures are generally modeled with beam elements to accelerate the load simulation [Dong et al., 2011, Wei et al., 2016, Dong et al., 2012]. Such a simplification may lead to inaccuracies in the results generated, due to the loss of local joint flexibility. However, a few works have focused on that. In some works, the joints of the jacket have been represented by super-elements [Tu et al., 2014, Popko et al., 2015]. It is noticed that the loads and fatigue damage of the jacket will be over/ underestimated compared to the jacket model with beam elements. However, both the references [Tu et al., 2014, Popko et al., 2015] use the sub-structuring method of Guyan reduction [Guyan, 1965], which introduces some limitations in the simulations. For instance, the inertia forces are neglected in Guyan reduction and if it is applied to dynamic problems, only an approximate solution can be found. Likewise, the damping matrices of the super-element parts of the jacket are not considered in their

studies. All the above limits will make the simulations inaccurate.

This chapter provides a summary of the modeling techniques of the offshore wind turbine jacket and different load simulation approaches. The influences of different load simulation approaches on the dynamic loading is studied. The effect of different modeling techniques on the structural response is also investigated. Section 2.2 presents the basic information for the offshore wind turbine and jacket foundation. Section 2.3 presents the basic theory of the super-element methods. The different load simulation approaches and the influences of different loads simulations are given in section 2.4. Section 2.5 shows the different modeling techniques of the offshore wind turbine jacket foundation. The last section gives some useful suggestions and recommendation for the offshore load simulations. The results obtained in this chapter are prerequisites for the following study.

2.2 A 5MW offshore wind turbine model

In this section, a brief introduction of the offshore wind turbine model and the related jacket foundation used in this work is given. The studied jacket foundation is one typical jacket model obtained from Code Comparison Collaboration Continuation (OC4) project [Vorpahl et al., 2011]. The wind turbine model is referenced from the national renewable energy laboratory (NREL) 5MW offshore Baseline Turbine [Jonkman et al., 2009]. The details information are in the followings.

2.2.1 The NREL 5MW wind turbine model

The NREL 5MW wind turbine model is widely used in the scientific studies and research. This wind turbine is a conventional 3-blade upwind variable-speed and variable blade-pitch-to-feather-controlled turbine, which is also a typical horizontal-axis wind turbine (HAWT). The main components include rotor, nacelle, tower and etc. The major properties are listed in Table.2.1.

Rotor

The rotor consists of the blades of the wind turbine and the supporting hub. It is often considered the most important components from both the performance and the cost point of view. The rotor diameter of NREL 5MW wind turbine is 126m. This value ignores the effect of blade precone which reduces the actual diameter and swept area. The exact rotor diameter is actually 125.88 and the actual swept area is 12445.3 m^2.

Table 2.1 – Gross properties of NREL 5MW reference wind turbine

Rating	5MW
Rotor Orientation, Configuration	Upwind, 3 Blades
Control	Variable Speed, Collective Pitch
Drive train	High Speed, Multiple-Stage Gearbox
Rotor, Hub Diameter	126 m, 3 m
Hub Height	90 m
Cut-In, Rated, Cut-Out Wind Speed	3 m/s, 11.4 m/s, 25 m/s
Cut-In, Rated Rotor Speed	6.9rpm, 12.1rpm
Rated Tip Speed	80 m/s
Overhang, Shaft Tilt, Precone	5 m, 5°, 2.5°
Rotor Mass	110,000 kg
Nacelle Mass	240,000 kg
Tower Mass	347,460 kg
Coordinate Location of Overall CM	(−0.2 m, 0.0 m, 64.0 m)

Blade

The NREL 5MW baseline has three 61.5m-long blades. The structural properties of each blade are based on 62.6m-long LM Glasfiber blade used in DOWEC project. So the LM Glasfiber blade is truncated at 61.5m span to obtain the structural properties. The structural property of blade tip is obtained by interpolating between the 61.2m and 61.7m stations. Additionally, NREL have specified a structural damping ratio of 0.477465% critical in all modes of the isolated blade. And they also have increased the blade section mass per unit length by 4.536% in order to scale the overall (integrated) blade mass to 17.7t. The blade structural properties are shown in Table.2.2.

Table 2.2 – Blade structural properties of 5MW wind turbine model

Length (w.r.t. Root Along Preconed Axis)	61.5 m
Mass Scaling Factor	4.536%
Overall (Integrated) Mass	17,740 kg
Second Mass Moment of Inertia (w.r.t. Root)	11,776,047 kg·m^2
First Mass Moment of Inertia (w.r.t. Root)	363,231 kg·m
CM Location (w.r.t. Root along Preconed Axis)	20.475 m
Structural-Damping Ratio (All Modes)	0.477465%

Hub and nacelle

Nacelle is the main structure of the turbine where locates the principal turbine components like generator, drive-train and brake. The hub is in the end of the slow axis and wind turbine blades are attached to the hub via the blade roots. The hub and nacelle properties of NREL 5MW wind turbines are given in Table.2.3.

Table 2.3 – Nacelle and Hub Properties

Elevation of Yaw Bearing above Ground	87.6 m
Vertical Distance along Yaw Axis from Yaw Bearing to Shaft	1.96256 m
Distance along Shaft from Hub Center to Yaw Axis	5.01910 m
Distance along Shaft from Hub Center to Main Bearing	1.912 m
Hub Mass	56,780 kg
Hub Inertia about Low-Speed Shaft	115,926 kg·m^2
Nacelle Mass	240,000 kg
Nacelle Inertia about Yaw Axis	2,607,890 kg·m^2
Nacelle CM Location Downwind of Yaw Axis	1.9 m
Nacelle CM Location above Yaw Bearing	1.75 m
Equivalent Nacelle-Yaw-Actuator Linear-Spring Constant	9,028,320,000 N·m/rad
Equivalent Nacelle-Yaw-Actuator Linear-Damping Constant	19,160,000 N·m/(rad/s)
Nominal Nacelle-Yaw Rate	0.3°/ s

Tower

The tower properties of NREL 5MW baseline wind turbine are based on the Dutch Offshore Wind Energy Converter (DOWEC) project. The outer diameter is linearly interpolated between 6.00m at the height of 0.00m (tower base) and 3.87m at the height of 87.60m (tower top). The thickness is similarly linearly interpolated from 0.0351 m to 0.0247m. The distributed tower properties are shown in Table.2.4.

Table 2.4 – Distributed tower properties

Elevation (m)	Outer diameter (m)	Thickness (m)
0.00	6.000	0.0351
8.76	5.787	0.0341
17.52	5.574	0.0330
26.28	5.361	0.0320
35.04	5.148	0.0309
43.80	4.935	0.0299
52.56	4.722	0.0289
61.32	4.509	0.0278
70.08	4.296	0.0268
78.84	4.083	0.0257
87.60	3.870	0.0247

Some key properties of the tower material are listed in Table.2.5. Beware that the effective density of tower steel is a little different from typical value (7850 kg/m^3), because this value takes into consideration the mass from the paint, bolts, welds, and flanges that are not accounted in the tower thickness data.

In this thesis, the NREL 5MW model is used for the load simulations. Other details information about the generator-torque control, drive-train, blade pitch control can be found in technical report [Jonkman et al., 2009]

Table 2.5 – Key properties of the tower material

Key Properties	Values
Young's modulus	210 (GPa)
Shear modulus	80.8 (GPa)
Poisson's radio	0.3
Density	8500 (kg/m^3)

2.2.2 The OC4 jacket model

The jacket was originally designed for the UpWind project [Vemula et al., 2010]. Then it is used with the NREL 5MW baseline turbine in the phase 1 of the OC4 project [Jonkman et al., 2012]. For the turbine model, there is one difference compared to the description in Jonkman et al. [Jonkman et al., 2009]: the hub height of the turbine is shifted from 90m to 90.55m with the jacket due to a shifted top elevation. Fig.2.1 shows the complete support structure. The jacket is designed for the 5-MW baseline turbine at the UpWind deep water reference site [Fischer et al., 2010] in 50m of water.

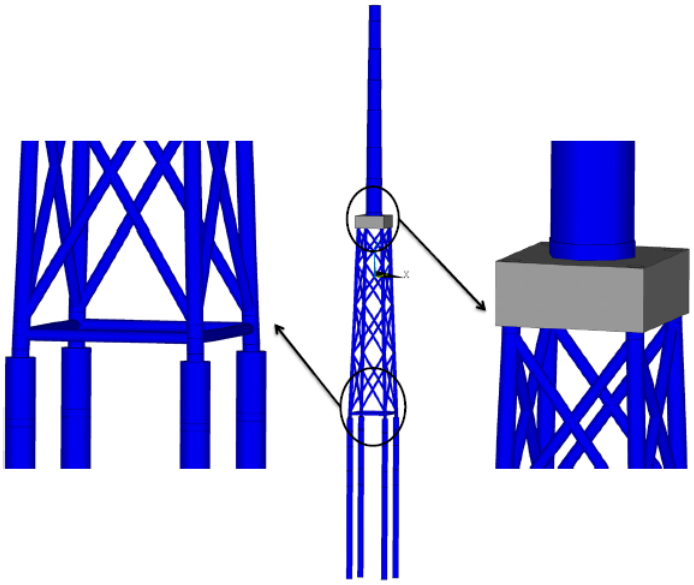

Figure 2.1 – Jacket with tower and piles (middle), concrete TP (right) and pile heads in detail (left) [Vorpahl et al., 2011]

The single jacket structure and the related positions are shown in Fig.2.2. The properties of the tubular members in the jacket are shown as described in Table.2.6, which includes the outer diameter and wall thickness of the members. The assumed steel properties of the jacket is listed in Table.2.7. The density,

Young's modulus and Poisson's ratio correspond to the values by [Kooijman et al., 2003] that were used in 5MW steel tower [Jonkman et al., 2009]. More detailed information of the jacket model can be found in the Ref.[Vorpahl et al., 2011].

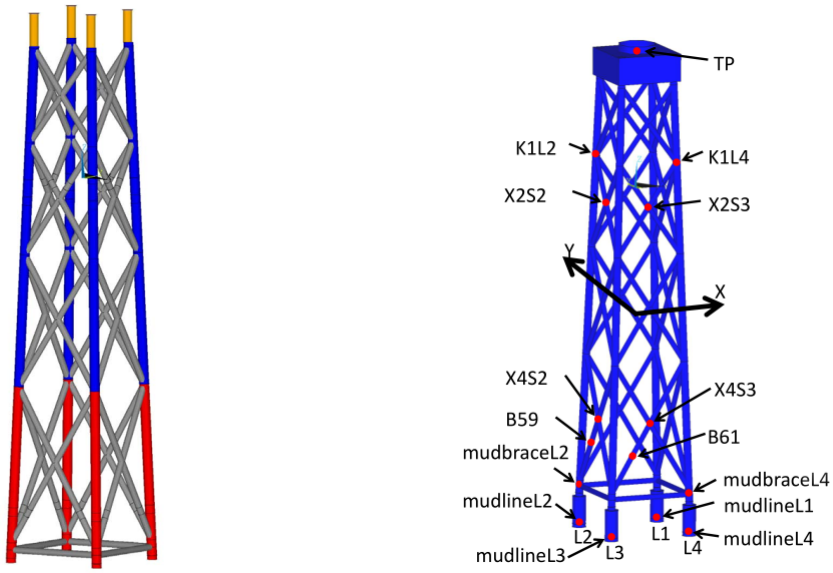

(a) OC4 jacket model [Vorpahl et al., 2011]

(b) Jacket coordinates [Popko et al., 2012]

Figure 2.2 – OC4 jacket model and related coordinates

Table 2.6 – Basic parameters of OC4 jacket

Color in Fig.2.2(a).	Outer diameter (m)	Thickness (mm)
Grey	0.8	20
Red	1.2	50
Blue	1.2	35
Orange	1.2	40

Table 2.7 – Steel properties of jacket material

Key Properties	Values
Young's modulus	210 (GPa)
Poisson's radio	0.3
Density	7850 (kg/m^3)

2.3 The theory of the super-element methods

In this section, two typical sub-structuring approaches are introduced. They are commonly used for the super-element generation, which can be noticed in the offshore wind turbine load simulation [Song et al., 2013]. The first is the Guyan reduction and the second is the Craig-Bampton reduction.

2.3.1 Guyan reduction

The Guyan reduction [Guyan, 1965] is widely used for the super-element generation. A summary of the Guyan reduction is presented below. The static equilibrium of the system is described as:

$$\mathbf{K}\boldsymbol{u} = \mathbf{F} \tag{2.1}$$

$\mathbf{K}$ is the stiffness matrix. Vector $\boldsymbol{u}$ denotes the degrees of freedom (DoF) and $\mathbf{F}$ is the external force vector.

The equation (2.1) can be written in a form that distinguishes the internal (slave) and interfaces (master) degrees of the freedom (DOFs) of a model. The subscripts m and s refer to the equation components, which are associated with the master and slave DOFs of the model, respectively.

$$\begin{bmatrix} \mathbf{K}_{mm} & \mathbf{K}_{ms} \\ \mathbf{K}_{sm} & \mathbf{K}_{ss} \end{bmatrix} \begin{bmatrix} \boldsymbol{u}_m \\ \boldsymbol{u}_s \end{bmatrix} = \begin{bmatrix} \mathbf{F}_m \\ \mathbf{F}_s \end{bmatrix} \tag{2.2}$$

The slave DOFs from Eq.(2.2) can be defined as:

$$\mathbf{u}_s = \mathbf{K}_{ss}^{-1}\left(\mathbf{F}_s - \mathbf{K}_{sm}\mathbf{u}_m\right) \tag{2.3}$$

The right side of Eq.(2.3) is used for the elimination of $\mathbf{u}_s$ from Eq.(2.2). The elimination leads to the following:

$$\left(\mathbf{K}_{mm} - \mathbf{K}_{ms}\mathbf{K}_{ss}^{-1}\mathbf{K}_{sm}\right)\mathbf{u}_m = \mathbf{F}_m - \mathbf{K}_{ms}\mathbf{K}_{ss}^{-1}\mathbf{F}_s \tag{2.4}$$

On the left side of Eq.(2.4), the condensed stiffness matrix $\tilde{\mathbf{K}}$ of the super-element can be defined as:

$$\tilde{\mathbf{K}} = \mathbf{K}_{mm} - \mathbf{K}_{ms}\mathbf{K}_{ss}^{-1}\mathbf{K}_{sm} \tag{2.5}$$

On the right side of Eq.(2.4), the generalized load vector $\tilde{\mathbf{F}}$ can be defined as:

$$\tilde{\mathbf{F}} = \mathbf{F}_m - \mathbf{K}_{ms}\mathbf{K}_{ss}^{-1}\mathbf{F}_s \tag{2.6}$$

Now Eq.(2.4) can written in a form that looks like Eq.2.1:

$$\tilde{\mathbf{K}}\mathbf{u}_m = \tilde{\mathbf{F}} \tag{2.7}$$

$\tilde{\mathbf{K}}$ and $\tilde{\mathbf{F}}$ can be formulated in a more generalized form as:

$$\tilde{\mathbf{K}} = \mathbf{R}_{\mathrm{G}}^{\mathrm{T}} \mathbf{K} \mathbf{R}_{\mathrm{G}} \tag{2.8}$$

$$\tilde{\mathbf{F}} = \mathbf{R}_{\mathrm{G}}^{\mathrm{T}} \mathbf{F} \tag{2.9}$$

where the transformation matrix $\mathbf{R}_{\mathrm{G}}$ is defined as:

$$\mathbf{R}_{\mathrm{G}} = \begin{bmatrix} \mathbf{I} \\ -\mathbf{K}_{ss}^{-1} \mathbf{K}_{sm} \end{bmatrix} \tag{2.10}$$

where $\mathbf{I}$ is the identity matrix of a size that corresponds to a number of the interface DOFs $\mathbf{u}_m$. The transformation $\mathbf{R}_{\mathrm{G}}$ is also used for the reduction of the mass matrix $\mathbf{M}$ of the super-element.

$$\tilde{\mathbf{M}} = \mathbf{R}_{\mathrm{G}}^{\mathrm{T}} \mathbf{M} \mathbf{R}_{\mathrm{G}} \tag{2.11}$$

2.3.2 Craig-Bampton reduction

Craig-Bampton (CB) reduction [Craig Jr and Bampton, 1968] is also widely used for the generation of the super-element. A short summary of CB reduction is presented in the following. As a starting point, we consider the linear equation of motion:

$$\mathbf{M}\ddot{\boldsymbol{u}} + \mathbf{C}\dot{\boldsymbol{u}} + \mathbf{K}\boldsymbol{u} = \mathbf{F} \tag{2.12}$$

Here, $\mathbf{M}$, $\mathbf{C}$ and $\mathbf{K}$ are the mass, damping and stiffness matrix, respectively. Vector $\boldsymbol{u}$ denotes the degrees of freedom (DoF). $\dot{\boldsymbol{u}}$ and $\ddot{\boldsymbol{u}}$ are its respective time derivatives and $\mathbf{F}$ is the external force vector. For simplicity, the damping component is omitted here. The DoF vector $\boldsymbol{u}$ is again partitioned into the interfaces (master) DoFs $\boldsymbol{u_m}$ and internal (slave) DoFs $\boldsymbol{u_s}$. This gives the partitioned equations of motion:

$$\begin{bmatrix} \mathbf{M}_{mm} & \mathbf{M}_{ms} \\ \mathbf{M}_{sm} & \mathbf{M}_{ss} \end{bmatrix} \begin{bmatrix} \ddot{\boldsymbol{u}}_m \\ \ddot{\boldsymbol{u}}_s \end{bmatrix} + \begin{bmatrix} \mathbf{K}_{mm} & \mathbf{K}_{ms} \\ \mathbf{K}_{sm} & \mathbf{K}_{ss} \end{bmatrix} \begin{bmatrix} \boldsymbol{u}_m \\ \boldsymbol{u}_s \end{bmatrix} = \begin{bmatrix} \mathbf{F}_m \\ \mathbf{F}_s \end{bmatrix} \tag{2.13}$$

The internal DoFs can be approximated by splitting into a 'static' and 'dynamic' part as showed below. The static response $\boldsymbol{u}_{s,\,\mathrm{stat}}$ can be obtained from second line of the partitioned equation with neglecting the inertia forces:

$$\boldsymbol{u}_s = \boldsymbol{u}_{s,\,\mathrm{stat}} + \boldsymbol{u}_{s,\,\mathrm{dyn}} \tag{2.14}$$

$$\boldsymbol{u}_{s,\,\mathrm{stat}} = \mathbf{K}_{ss}^{-1} \left(\mathbf{F}_s - \mathbf{K}_{sm} \boldsymbol{u}_m \right) \tag{2.15}$$

Furthermore, the internal force $\mathbf{F}_s$ acting on the internal DoFs is always unknown for us. Moreover, the Craig-Bampton was initially derived mainly for the purpose of vibration analysis. The force on the

internal DoFs was therefore assumed to be 0, which gives us:

$$\boldsymbol{u}_{s,\,\mathrm{stat}} = -\mathbf{K}_{ss}^{-1}\mathbf{K}_{sm}\boldsymbol{u}_m = \boldsymbol{\Psi}_s\boldsymbol{u}_m \tag{2.16}$$

Here, $\boldsymbol{\Psi}_s$ is so-called static constraint modes. The dynamic response $\boldsymbol{u}_{s,\,\mathrm{dyn}}$ is also obtained from the second line of the partitioned equations again with the internal force $\mathbf{F}_s$ equals to 0. The internal dynamic can be represented using superposition of a truncated number of vibration modes.

$$\boldsymbol{u}_{s,\mathrm{dyn}} \approx \sum_{k=1}^{n} \boldsymbol{\phi}_{s,k}\eta_{s,k} = \boldsymbol{\Phi}_s\boldsymbol{\eta}_s \tag{2.17}$$

Here, the vector $\boldsymbol{\Phi}_s$ contain n truncated fixed-interface vibration modes. In order to obtain a compact reduced model, one should choose $n << m$, where m is the original number of internal DoFs. Note that adding fixed interface vibration modes to the reduction basis, the inertia related to the internal DoFs is taken into account. Hence, the approximation found for dynamic problems can be significantly improved with respect to Guyan reduction. The vector $\boldsymbol{\eta}_s$ contains modal amplitudes and the vibration modes can be gotten by solving:

$$\left(\mathbf{K}_{ss} - \omega_{s,k}^2\mathbf{M}_{ss}\right)\boldsymbol{\phi}_{s,k} = \mathbf{0} \tag{2.18}$$

Here, $\boldsymbol{\phi}_{s,k}$ represents a single fixed-interface vibration mode with unit modal mass and $\omega_{s,k}$ its corresponding eigenfrequency. Hence, the approximation of the internal DoF is obtained and the Craig-Bampton reduction basis can be put into matrix form:

$$\boldsymbol{u}_s \approx \boldsymbol{\Psi}_s\boldsymbol{u}_m + \boldsymbol{\Phi}_s\boldsymbol{\eta}_s \tag{2.19}$$

$$\begin{bmatrix} \boldsymbol{u}_m \\ \boldsymbol{u}_s \end{bmatrix} \approx \begin{bmatrix} \mathbf{I} & \mathbf{0} \\ \boldsymbol{\Psi}_s & \boldsymbol{\Phi}_s \end{bmatrix} \begin{bmatrix} \boldsymbol{u}_m \\ \boldsymbol{\eta}_s \end{bmatrix} = \mathbf{R}_{\mathrm{CB}}\boldsymbol{q} \tag{2.20}$$

Finally, the reduction matrix $\mathbf{R}_{\mathrm{CB}}$ can be substituted in the partitioned equations to obtain:

$$\tilde{\mathbf{M}}\ddot{\boldsymbol{q}} + \tilde{\mathbf{K}}\boldsymbol{q} = \tilde{\mathbf{F}} \tag{2.21}$$

where $\tilde{\mathbf{M}}$, $\tilde{\mathbf{K}}$ and $\tilde{\mathbf{F}}$ are the reduced mass and stiffness matrix and force vector, respectively, and have the following form:

$$\begin{cases} \tilde{\mathbf{M}} = \mathbf{R}_{\mathrm{CB}}^{\mathrm{T}}\mathbf{M}\mathbf{R}_{\mathrm{CB}} \\ \tilde{\mathbf{K}} = \mathbf{R}_{\mathrm{CB}}^{\mathrm{T}}\mathbf{K}\mathbf{R}_{\mathrm{CB}} \\ \tilde{\mathbf{F}} = \mathbf{R}_{\mathrm{CB}}^{\mathrm{T}}\mathbf{F} \end{cases} \tag{2.22}$$

2.3.3 Other super-element methods

The Guyan and Craig-Bampton reductions are the two typical super-element methods. Compared to the Guyan reduction, the Craig-Bampton reduction added the fixed interface modes to the original Guyan

reduction basis in order to include the dynamic responses of the internal degree of freedom. In addition, there are other super-element methods such as the dynamic condensation [Paz, 1984], the impulse based substructuring method [Rixen and van der Valk, 2013]. A comprehensive review of these techniques can be found in [de Klerk et al., 2008, Van der Valk and Voormeeren, 2012].

2.4 Offshore wind turbine load simulation approaches

2.4.1 Offshore load simulation approaches

For the offshore load simulation, there are mainly three approaches. As shown in Fig.2.3(a), the sequentially coupled approach implies three steps: firstly, the jacket model developed in finite element analysis tool with wave loading is converted to a super-element by the sub-structuring techniques. The super-element including the mass, stiffness, damping matrices, and load vectors of the jacket with wave loading will be imported into the wind turbine analysis tools. The sub-structuring method of Craig-Bampton (CB) reduction [Craig Jr and Bampton, 1968] is applied in the sequentially coupled approach, which has been proved that it can give better results than Guyan reduction in dynamic analysis [van der Valk et al., 2015]. Then, the wind loading simulation is carried out by wind turbine analysis tools with the reduced model. The forces or displacements time series at the interface are the outputs for the last step. Finally, these time series are applied to the detailed support structure model with the same wave loading.

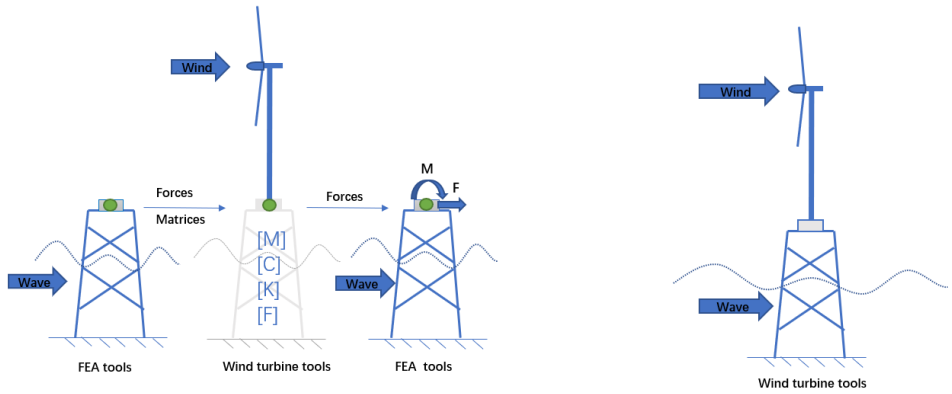

(a) Sequentially coupled

(b) Fully integrated

Figure 2.3 – The sequentially and fully coupled approaches

In contrast to the sequentially coupled method, the fully integrated approach as shown in Fig 2.3(b) will simulate the wind turbine combined with the support structure in a wind turbine tool with both wind and wave loading. In this paper, the wind turbine tool used is OpenFAST and the finite element analysis tool is ANSYS [ANSYS, 2017]. OpenFAST allows to carry out the sequentially coupled and fully integrated simulations [Branlard et al., 2020] by CB reduction. However, for the sequentially coupled approach in OpenFAST, the super-element properties (e.g. mass, stiffness, damping, and time series of excitation

forces) of the jacket must be provided by users. Hence, ANSYS software is used here to generate the super-element properties of the jacket and the wave loading for the sequentially coupled approach. Additionally, it should be mentioned that aerodynamic loads in OpenFAST are based on beam element momentum theory. The temporal wind loading at the rotor (hub) is simulated with aerodynamic loads and OpenFAST control systems. For the temporal wave loading in OpenFAST and ANSYS, the hydrodynamic loads are based on Morison equations with defined inertia and drag coefficients.

The uncoupled approach, as illustrated in Fig.2.4, may be conducted in different ways. The common situation corresponds to Fig.2.4(a), where the aerodynamic loads are determined by wind turbine tools. These loads are transferred to nodal forces and moments acting at the tower top. Hydrodynamic loads can be generated by other tools. Aero-elastic load is ignored in this case. In this paper, we focus mainly on the behaviors of the jacket under the considered loads. Hence, the case as shown in Fig.2.4(b) is investigated for the uncoupled situation. The wind turbine with the jacket support is simulated under single wind loading in OpenFAST. The forces and moments in the top of the jacket are imported to the jacket model developed in ANSYS. The wave loads are also defined in ANSYS.

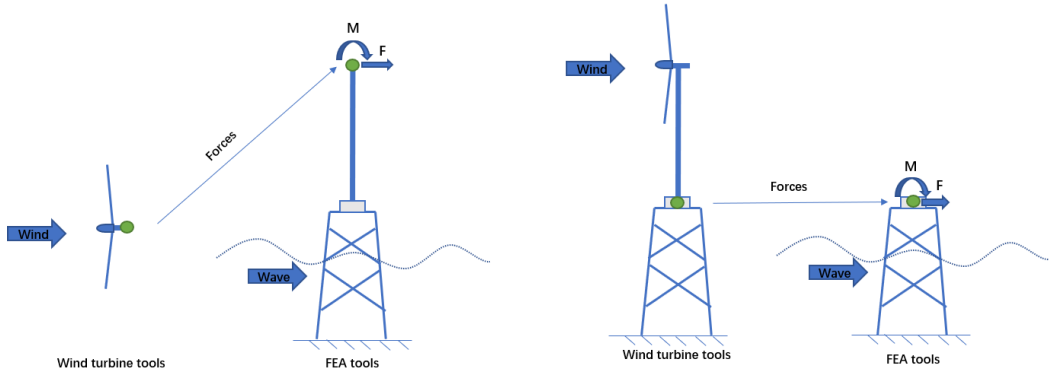

(a) Uncoupled case 1

(b) Uncoupled case 2

Figure 2.4 – The uncoupled approach in different cases

2.4.2 Comparison results of different load simulation approaches

For the study of the influences of the different load simulations on the loading, the responses on the top of the jacket (TP position) in the fully coupled and uncoupled approaches can be directly simulated with the beam jacket model in OpenFAST. While, for the sequentially coupled approach, at first, the jacket model with wave loading should be reduced into a super-element with time series of loads or displacement, which cannot be conducted in OpenFAST software. Hence, a jacket model with Timoshenko beam is developed in ANSYS, which has the same dimensions and element type as that in the OpenFAST jacket model. Table 2.8 presents the mass and modal analysis results of the jacket models furnished by OpenFAST and ANSYS. Additionally, the developed beam jacket model combined with NREL 5-MW

wind turbine is validated by the results of modal and static analysis, compared with the reference values [Song et al., 2013], which can be found in the next section.

Table 2.8 – Results obtained for the jacket models in ANSYS and OpenFAST

Jacket model	ANSYS	OpenFAST
Mass(Kg)	673881	673883
1st (x) global bending (Hz)	2.7559	2.7555
1st (y) global bending (Hz)	2.7559	2.7555
1st torsion (Hz)	5.4110	5.4133
2nd (x) global bending (Hz)	7.6240	7.6343
2nd (y) global bending (Hz)	7.6240	7.6343

Furthermore, the selected modes in the CB reduction for the sequential coupled and the fully integrated approaches are the 25 lowest ones, according to [Branlard et al., 2020]. A 10-minute loads simulation is conducted, which does not include the additional pre-simulation time. The time step is set to 0.005s. The load time series of jacket super-element for the sequential coupled method are provided with time steps equal to 0.05s. Moreover, the damping is defined with a Rayleigh damping assumption. A damping ratio of 1% is selected for the critical damping for the first two modes. More details about the above settings can be also found in [Branlard et al., 2020].

The load case set is the design load case (DLC) 1.2 of the IEC standard [IEC, 2009]. The site condition is based on the K13 Deep Water Site of the UpWind project [Fischer et al., 2010]. The wind speed is divided into 11 wind bins as done in [Tu et al., 2014], between the cut-in and cut-out wind speed, with each size 2 m/s. As depicted in Table 2.9, V, I_i, H_s, and T_p are, respectively, wind velocity, turbulence intensity, significant wave height and the peak period of the Pierson-Moskowitz (PM) spectrum.

Table 2.9 – Basic parameters of the load cases [Fischer et al., 2010]

V (m/s)	I_i (%)	H_s (m)	T_p (s)
4	20.42	1.10	5.88
6	17.50	1.18	5.76
8	16.04	1.31	5.67
10	15.17	1.48	5.74
12	14.58	1.70	5.88
14	14.17	1.91	6.07
16	13.85	2.19	6.37
18	13.61	2.47	6.71
20	13.42	2.76	6.99
22	13.26	3.09	7.40
24	13.13	3.42	7.80

In addition, the wave direction is assumed to be aligned with the wind direction. Moreover, the wind and wave simulations involve stochastic processes. The generation of wind and wave processes uses

respectively Kaimal and PM spectrum. To generate the random time series of wind and wave loading, the generation algorithm requests a "seed number" [Jonkman and Buhl Jr, 2006]. To avoid generating the same wind and wave loading, it is recommended to use at least 3 seed numbers to obtain different time histories [Tu et al., 2014]. Three seeds for wave and wind are used here to get stochastic outputs. These assumptions lead to three different settings for each wind bin during the simulation. With 11 wind bins and 3 different seeds, a total of 33 subcases are investigated, which can be seen as a representation of the required OWT simulation load cases.

Based on the load cases in Table 2.9, the loads and displacement of the TP position are compared. Here, the comparison results of the fore-aft force (Fx) and moment (My) which are the main causes of the fatigue damage, are depicted in Fig.2.5 and Fig.2.6. The platform surge (Ux) on the TP position is exhibited in Fig.2.7. In these figures, the simulation results with mean wind velocity 12m/s are shown. As we can see, the results of the sequentially coupled and the fully integrated methods are mostly in good agreement. The results of the uncoupled simulation are significantly different from those obtained by the sequentially and fully coupled approaches, particularly in Fx as shown in Fig.2.5.

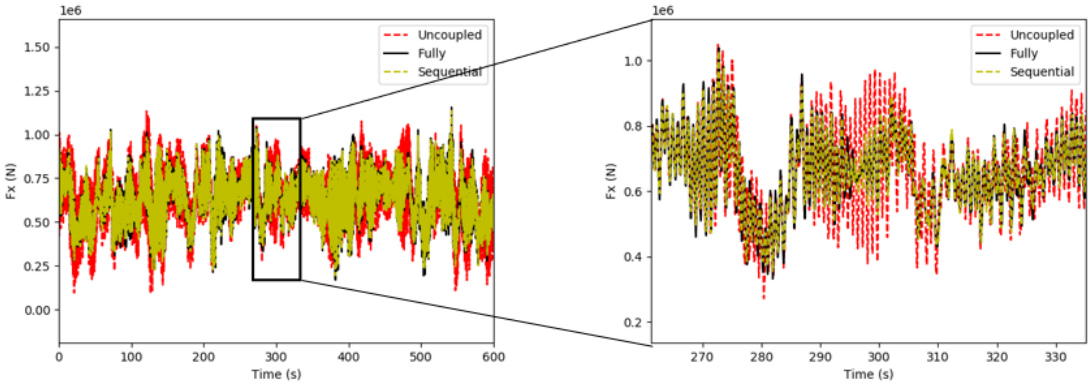

Figure 2.5 – Fx with mean wind velocity 12m/s

Moreover, the mean, absolute maximum, and standard deviation values of Fx, My, and Ux in each load case are calculated. The mean value, absolute maximum, and standard deviation values of Fx are defined as follows:

$$\overline{\mathrm{F}^{vi}} = \frac{\sum_{i=1}^{i=\mathrm{N}} \mathrm{F}_i^{vi}}{\mathrm{N}}$$

$$\mathrm{F}_{\max}^{vi} = \max\left(\left|\mathrm{F}_i^{vi}\right|\right), i = 1 \sim \mathrm{N} \tag{2.23}$$

$$\mathrm{F}_{std}^{vi} = \sqrt{\frac{\sum_{i=1}^{i=\mathrm{N}} \left(\mathrm{F}_i^{vi} - \overline{\mathrm{F}^{vi}}\right)^2}{\mathrm{N}}}$$

Here, vi, i, and N represent, respectively, the load cases with different wind velocities, time step number, and total time step number in the 10-minute simulation. Additionally, the results of the fully coupled

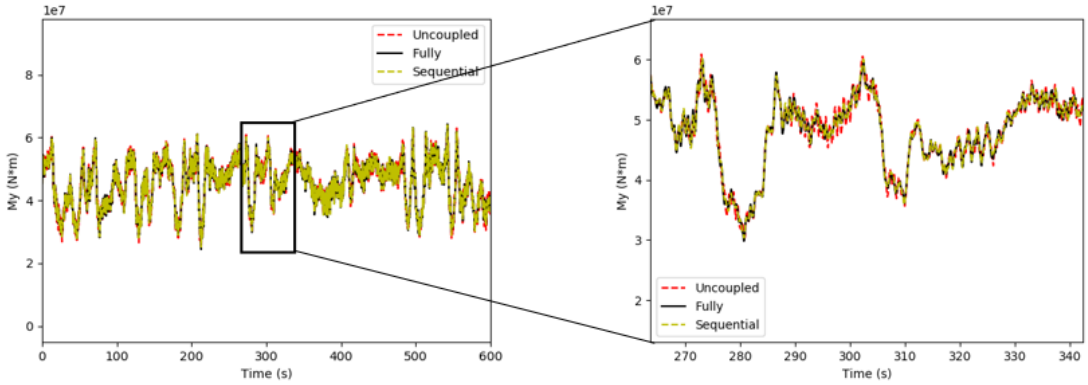

Figure 2.6 – My with mean wind velocity 12m/s

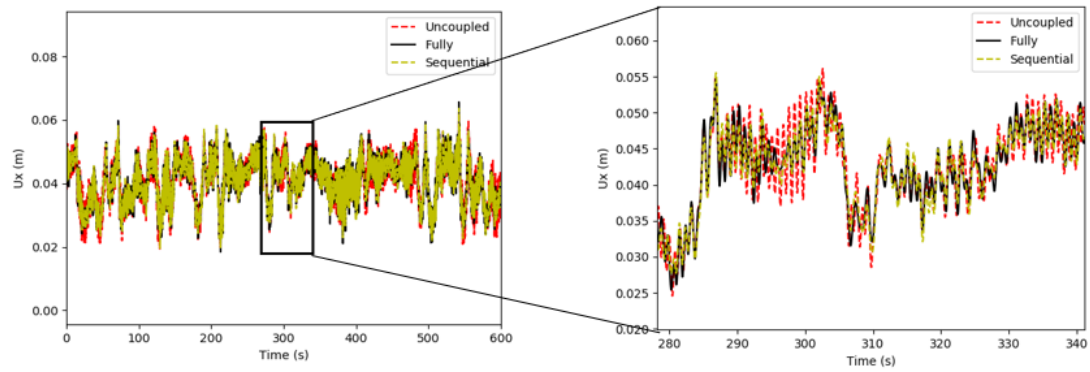

Figure 2.7 – Ux with mean wind velocity 12m/s

method are taken as references for the comparisons. The relative differences between the maximum, mean, and standard deviation values of each load case are shown in Fig.2.8, Fig.2.9, and Fig.2.10. The relative differences, for instance, in the mean values of Fx, are calculated as follows:

$$\mathrm{F}mean_{\mathrm{X}}^{vi} = \frac{\overline{\mathrm{F}_{\mathrm{X}}^{vi}} - \overline{\mathrm{F}_{Full}^{vi}}}{\overline{\mathrm{F}_{Full}^{vi}}} \times 100\% \tag{2.24}$$

Here, X represents the results of SE (the sequentially coupled approach) or Un (the uncoupled approach); Full represents the results of the fully coupled approach. In Fig.2.8, Fig.2.9, and Fig.2.10, "Max_SE_F$ully$" means the relative differences of maximum values between sequentially coupled and fully integrated approaches. As shown in the three figures, the relative differences of mean value in each load case of the three approaches are negligible. However, the differences of extreme and standard deviation values in some load cases are significant, especially in the force Fx. As depicted in Fig.2.8, in most cases, the uncoupled simulation seems to overestimate the extreme and standard deviation of the

responses in the top of the jacket. The corresponding differences can be up to 20% and 35%, respectively. In the majority of the cases, the sequentially coupled approach seems to underestimate the extreme and standard deviation of the response within -5% errors. As for My, the differences of these three simulation approaches are not obvious and the relative errors are within ± 4% as shown in Fig.2.9, which confirms the simulation results of Fig.2.6. Moreover, the extreme values and standard deviation of the displacement Ux can be over/underestimate both in the sequentially coupled and the uncoupled methods. The relative differences are within ± 6% for the sequential approach and ± 11% for the uncoupled approach.

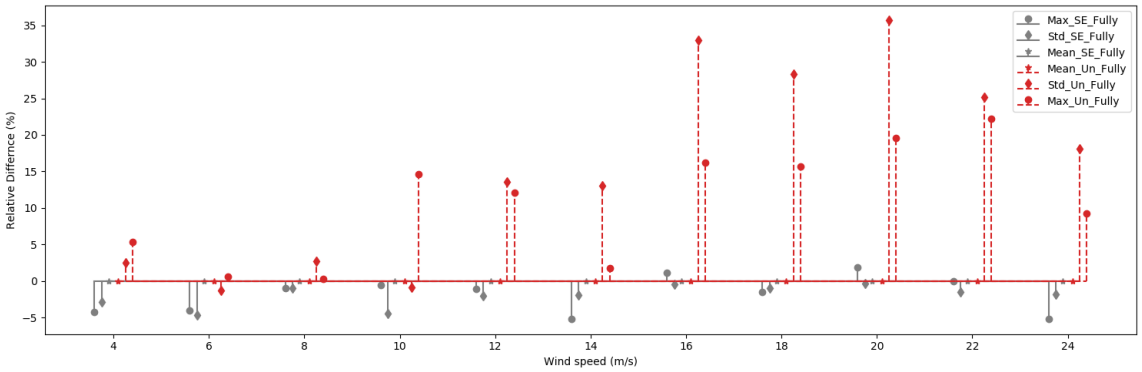

Figure 2.8 – Relative differences of Fx

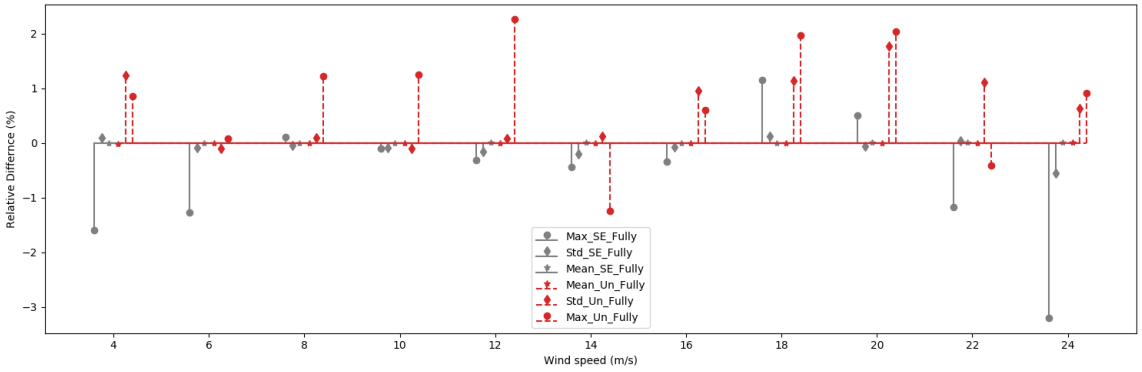

Figure 2.9 – Relative differences of My

To better compare the results, the overall mean values of absolute relative differences in the mean, extreme, and standard deviation for Fx, My, and Ux are displayed in Table 2.10 and Table 2.11. Here, "overall" means the 33 subcases, and the overall mean values of the absolute relative difference in the mean values of the force Fx are defined as follows:

$$\mathrm{O}mean_{\mathrm{X}} = \frac{\sum_{vi=1}^{vi=33} \left|\mathrm{F}mean_{\mathrm{X}}^{vi}\right|}{33} \tag{2.25}$$

As shown in the two tables, the sequentially coupled method (SE) has better overall performance than

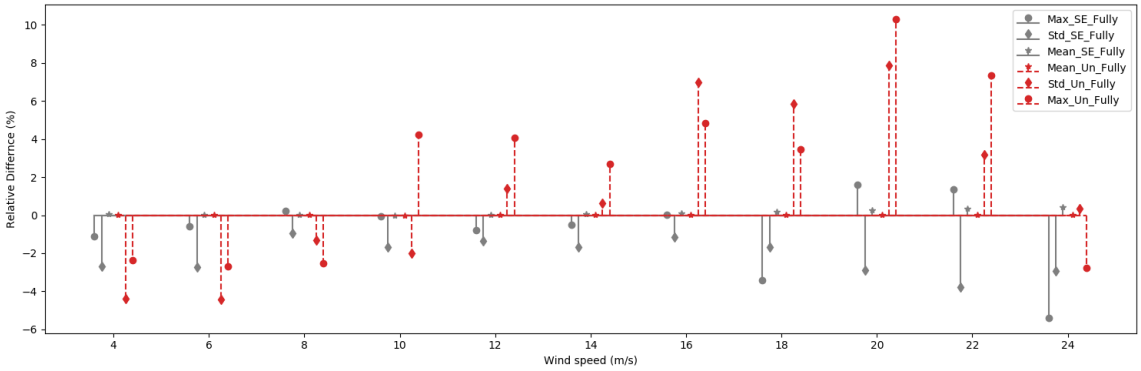

Figure 2.10 – Relative differences of Ux

the uncoupled approach (Un). It is supposed here that the overall mean values of relative differences of 5% can be acceptable. As shown in Table 2.10, the overall mean values of differences between the sequentially and fully coupled approaches in Fx, My, and Ux are inferior to 3%. These small differences between the sequentially and fully coupled methods can be generated by the CB reduction method. Indeed, the CB reduction is a linear approach and nonlinear effects like external loads generated by fluid-structure interactions are sources of error that cannot be alleviated in the sequentially coupled approach. Additionally, as mentioned in [Bredmose et al., 2013], the deflection induced by gravity and buoyancy is not considered in the CB reduction since the interface nodes are fixed during the determination of the modes, which may lead to decreased performance. Moreover, it should be mentioned that the overall mean values of differences in the mean values of the three approaches are less than 0.15%. Major differences can only be noticed in the extreme and standard deviation values, especially in the comparison of the uncoupled and the fully coupled methods. As shown in Table 2.11, the overall mean values of Fx for extreme and standard deviation are both greater than 8%. A possible source for these deviations can be the lack of hydro damping and hydroelastic coupling in the uncoupled load simulation. In the uncoupled case studied in Fig.2.4(b), the ocean environment is not considered during the wind loading simulation. Hence, the damping generated by the ocean and the interaction between the jacket and the ocean are not considered. For Ux, the sequential and uncoupled methods have close results. The overall mean values of the relative differences in Ux are less than 4%. It is also noticed that there are no obvious differences in My of the three approaches. The overall mean values of differences in My are less than 1.5% as depicted in the two tables.

Table 2.10 – Overall mean values between sequential and fully coupled approaches

Overall mean value (%)	Fx	My	Ux
Diff.Max	2.29	0.78	2.02
Diff.Mean	4.00e-3	1.90e-3	0.14
Diff.Std	2.80	0.24	2.52

From the comparative study of the three load simulation approaches, we can conclude that they have

Table 2.11 – Overall mean values between uncoupled and fully coupled approaches

Overall mean value (%)	Fx	My	Ux
Diff.Max	8.72	1.34	3.76
Diff.Mean	7.90e-3	4.00e-3	0.01
Diff.Std	12.20	0.46	2.73

little effect on the mean values of the loading and the displacement. Significant differences can be observed only in the extreme and standard deviation values. Additionally, the simulated loads and the displacement in the sequentially coupled approach are generally consistent with results obtained by the fully coupled approach. However, the calculated loads in the uncoupled approach have significant differences compared with those furnished by the fully coupled approach, particularly in Fx. Finally, the advantages and drawbacks of the three approaches are listed in Table.2.12

Table 2.12 – Summary of the different load simulation approaches

Methods	Fully coupled approach	Sequentially coupled	Uncoupled (case 2)
Main steps	1. Modeling the jacket structure by using beam model in OpenFAST 2. Simulate the wave and the wind loading and perform structural analysis by using the beam jacket model in OpenFAST	1. Modeling the jacket model and wave loadling by finite element tool,e.g. ANSYS 2. Generate the super-element of the jacket and wave loading by using CB reduction method 3. Import the super-element time series matrices and vectors to OpenFAST and simulate time series wind load 4. Extract time series loads and apply them on the top of the jacket with the same wave loading 5. Perform the structural analysis of the jacket using finite element software	1. Modeling the jacket model by finite element tool 2. Simulate wind loading by wind turbine simulation tool 3. Extract the time series wind loading from wind turbine tools and apply them to the finite element model with wave loading
Advantages	1. Strong coupling between multiphysics 2. Reference results for comparisons	1. Can be used for the advanced finite element model 2. Acceptable accuracy 3. Commonly used in industry	1. Easy implementation 2. Can also be used for the advanced jacket model
Drawbacks	1. Cannot be used for advanced finite element model	1. Difficult implementation due to different interactions between different software	1. Lack of the accuracy

2.5 Offshore wind turbine jacket modeling techniques

2.5.1 Traditional modeling techniques and super-element techniques

Offshore wind turbine jackets have been widely used in the offshore wind turbine jacket. The jacket models are always modeling beam model, which can be found in the studies [Dong et al., 2011, Dong et al., 2012, Wei et al., 2016]. Such a simplification may lead to inaccuracies. However, the simulation of the jacket models with pure shell or solid elements is often much time-consuming. To keep joint flexibility and also reduce simulation time, Tu [Tu et al., 2014], Popko [Popko et al., 2015] and Vorpahl [Vorpahl, 2015] proposed to use super-element modeling techniques for a more accurate representation of joints in the jacket model as shown in Fig.2.11.

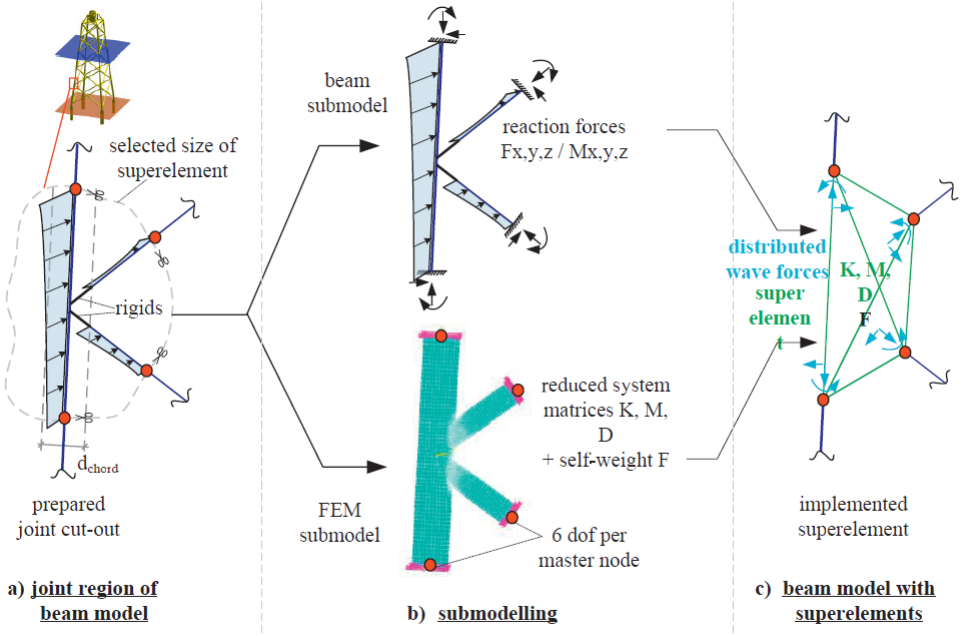

Figure 2.11 – Steps of the super-element implementation [DUB, 2013]

In this section, the influence of different jacket models on the structural responses is investigated. Two numerical jacket models are compared. One (Beam model) is set up with Timoshenko beam elements as presented in Fig.2.12(a) with 3D visualization. All joints are modeled by beam elements that are rigidly connected at the intersection points of their central axes. The second model (Super-element model as shown in Fig.2.12(b)) uses super-elements for the joints' representation and Timoshenko beam elements for the rest parts. All the joints are originally modeled with shell elements and all dimensions of the joints follow the recommendations in [DUB, 2013].The joints modeled by shell elements will be reduced to super-elements by the CB reduction method. As for the CB reduction modes of the joints, a common method of mode selection consists of using the modes with the lowest frequencies. As mentioned pre-

viously, the 25 lowest frequency modes are also selected here. The sequentially coupled load simulation approach is applied for both the two jacket models, which has more accurate load simulation ability than the uncoupled approach as demonstrated in the previous section. For the beam jacket model, the loading in the top of the jacket can be simulated as shown in Fig.2.3(a). For the loading of the super-element model, we perform two steps: at first, the joints are reduced to super-elements and imported to main jacket structures as depicted in Fig.2.12(b). After that, the super-element jacket model with wave loading will be reduced to a new super-element with time series of loads for sequentially coupled load simulation. Furthermore, to validate the developed numerical models, modal and static analysis are performed and the results are compared with the reference values as listed in Table 2.13 and Table 2.14. Here, the NREL 5-MW wind tower and rotor nacelle assembly (RNA) [Jonkman et al., 2009] are adopted for the modal and static analysis with developed jacket models. As shown in Table 2.13 and Table 2.14, the developed beam model exhibits close results in the modal and static analyses compared with the reference values, which are also based on beam elements. For the super-element model, the natural frequencies decrease a little. Due to the precise representation of the joints of the jacket, the mass and stiffness of the super-element jacket model also decrease, which can also be noticed in [Tu et al., 2014]. That's why the displacement at RNA of the super-element model with the same thrust load will be bigger than the beam model.

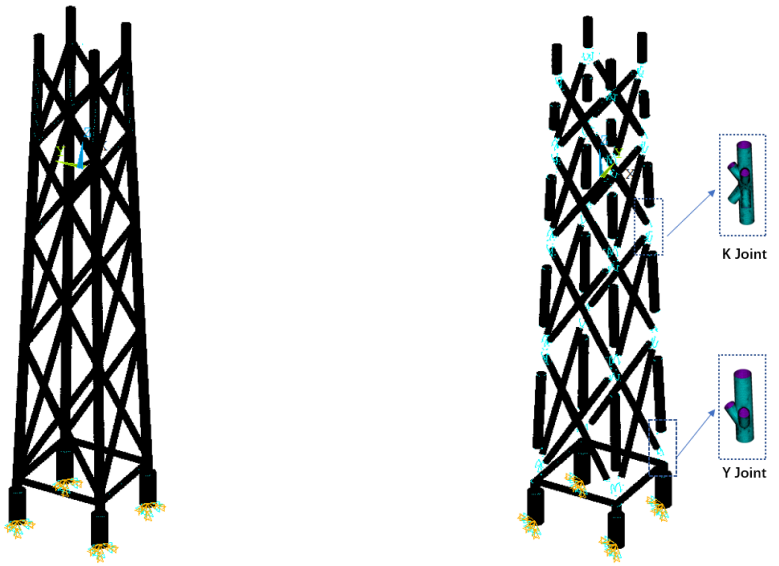

(a) Beam model (b) Model with super-elements

Figure 2.12 – Jacket models

Table 2.13 – Comparison of modal analysis of complete wind turbine

Modal analysis	Ref.[Song et al., 2013]	Beam (Diff.)	Super-element (Diff.)
1st Fore-aft	0.3190	0.3196 (0.19%)	0.3108 (-2.57%)
2nd Fore-aft	1.1936	1.1789 (-1.23%)	1.1388 (-4.59%)

Table 2.14 – Comparison of static analysis of complete wind turbine

Thrust load at RNA (kN)	Displacement(m) at RNA		
	Ref.[Song et al., 2013]	Beam (Diff.)	Super-element (Diff.)
2000	1.2089	1.1975 (-0.94%)	1.2736 (5.35%)
4000	2.4178	2.3950 (-0.94%)	2.5472 (5.35%)

2.5.2 Comparison results of different jacket models

To investigate the influence of different jacket models, at first, the mass and modal analysis results of two jacket models (Beam and Super-element models) are compared in Table 2.15. The mass of the super-element jacket model is inferior to that of the beam jacket model, since the overlapping parts of joints in the beam model are excluded in the super-element model. In addition, the first 5 eigenfrequencies of the super-element jacket model are smaller than those of the beam model, which means that the stiffness of the super-element model also decreases. Additionally, the load cases considered in the comparison are the same as shown in Table 2.9. The settings of the OpenFAST tool are the same as those in section 3.2.

Jacket model in ANSYS	Beam	Super-element	Difference (%)
Mass(Kg)	673881	636920	-5.8031
1st (x) global bending (Hz)	2.7559	2.7156	-1.4840
1st (y) global bending (Hz)	2.7559	2.7157	-1.4803
1st torsion (Hz)	5.4110	5.3385	-1.3581
2nd (x) global bending (Hz)	7.6240	7.2741	-4.8102
2nd (y) global bending (Hz)	7.6240	7.2745	-4.8045

Table 2.15 – Mass and modal comparison of jacket models in ANSYS

Also, the fore-aft force (Fx), moment (My), and displacement (Ux) of TP are compared. The results of load cases with mean wind velocity 12m/s are plotted in Fig.2.13, Fig.2.14, and Fig.2.15. The differences between the two models in My are little but the differences in Fx are easier to observe. As for Ux, the beam and the super-element models have the same trend in the time series. But the displacement (Ux) furnished by the super-element model is always superior to the same quantity evaluated by the beam model.

Here, the mean, absolute maximum, and standard deviation are also calculated from simulation results in each load case. The results of super-element models are taken as the reference. The relative differences between the beam and super-element models are plotted in Fig.2.16 and Fig.2.17. Here, only the relative differences of Fx and Ux are given, since the differences between the values of My are small as shown

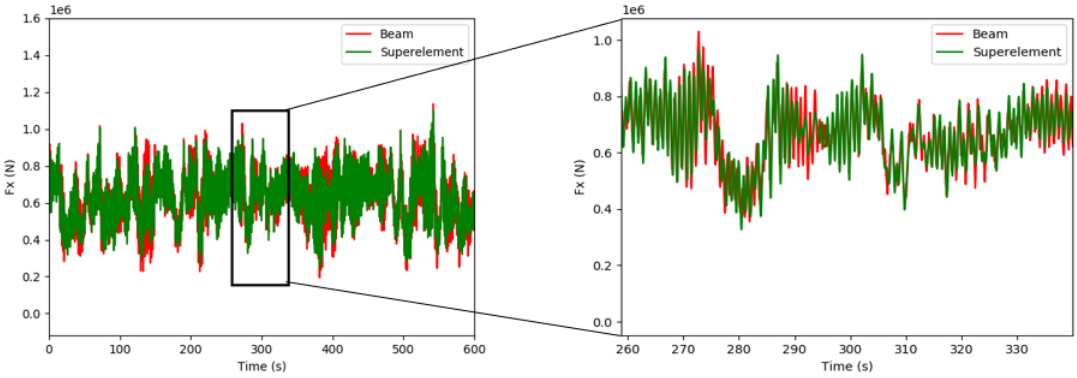

Figure 2.13 – Fx with mean wind velocity 12m/s

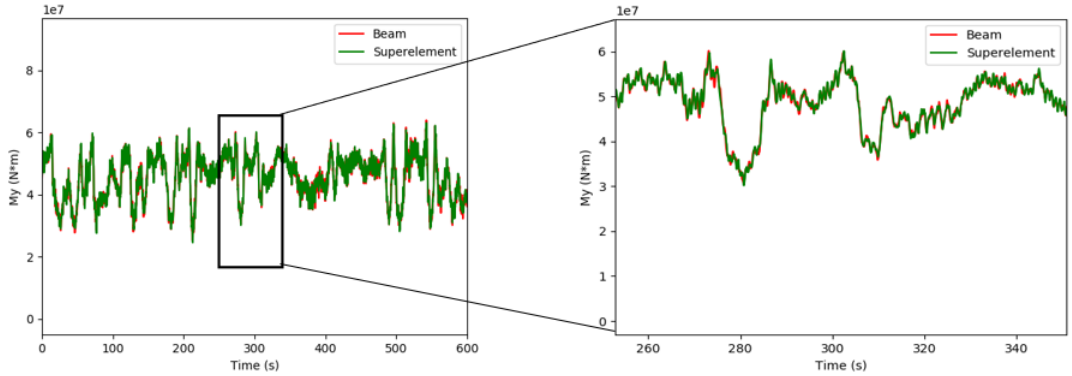

Figure 2.14 – My with mean wind velocity 12m/s

in Fig.2.14. The overall mean values of absolute relative differences of the three parameters (Fx, My, Ux) are given in Table 2.16. As shown in Fig.2.16, the differences in Fx mainly occur in the extreme and standard deviation values. The differences in extreme and standard deviation values can be up to 10% and 15% respectively. The overall mean values of differences are also greater than 5%. As for My, the overall mean values of relative differences are small (within 3%). More importantly, it should be noticed that great differences can be observed in Ux as shown in Fig.2.17. It seems that the use of beam elements at the joints of the jacket tends to underestimate the displacement Ux of the jacket. The mean values of Ux in each load case are underestimated by nearly 12%. Also, the extreme and standard deviation will be underestimated. The overall mean values of Ux in extreme and standard deviation values are also superior to 5%. These differences can be explained by the fact that the use of super-elements not only reduces the mass of joint parts of the jacket but also reduces the stiffness of the whole jacket structure.

The results of the two jacket models show that the use of a more detailed representation of the joints leads to significant differences in the jacket displacement, which can be observed in the overall mean values of the relative difference in Ux. Moreover, some differences can be also observed in extreme and standard

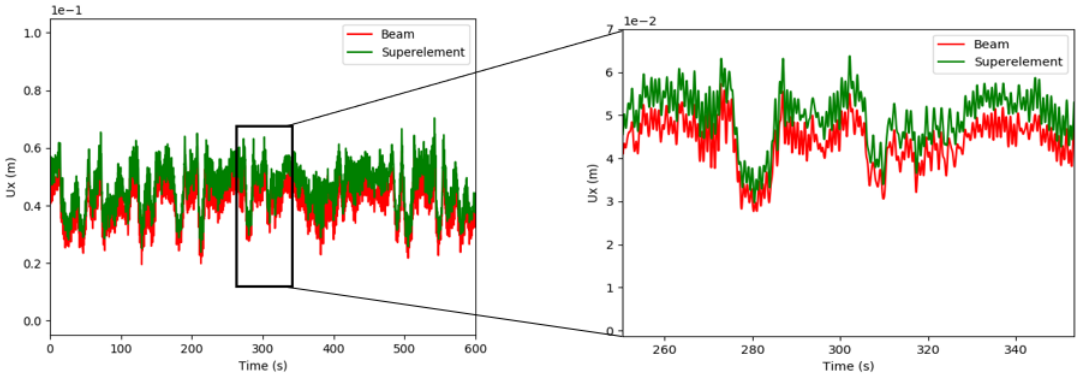

Figure 2.15 – Ux with mean wind velocity 12m/s

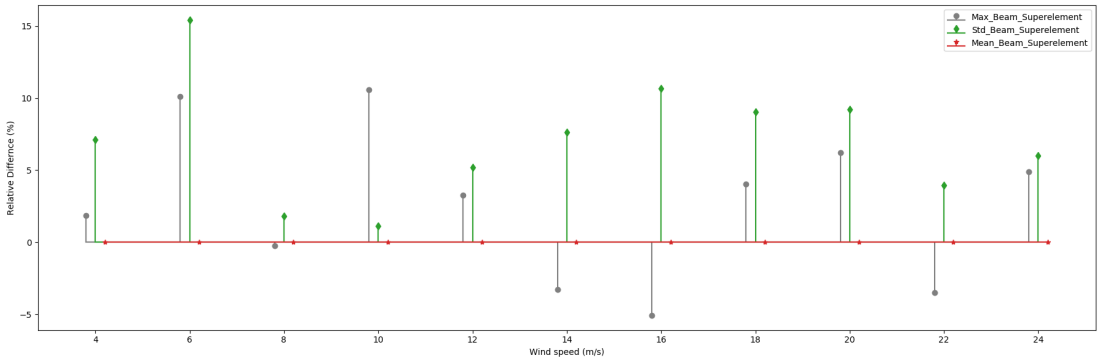

Figure 2.16 – Relative differences of Fx

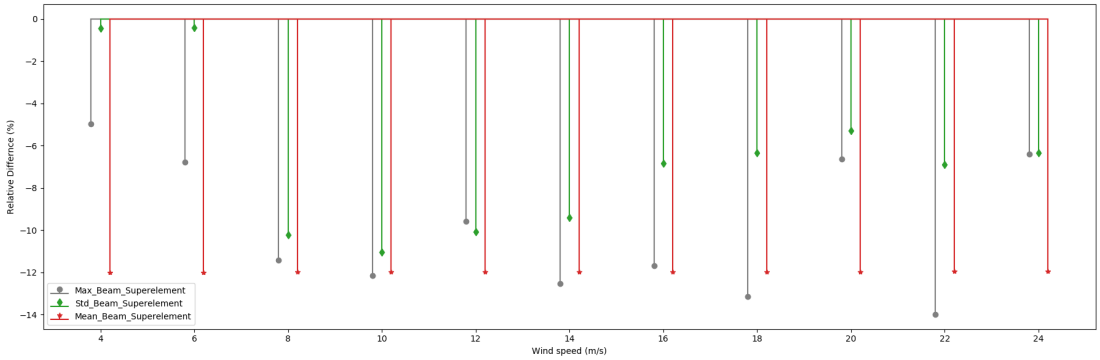

Figure 2.17 – Relative differences of Ux

values of the force (Fx). Concerning the load (My), the differences between the two jacket models are negligible.

Table 2.16 – Overall mean values between beam and super-element model

Overall mean value (%)	Fx	My	Ux
Diff.Max	5.14	1.68	9.45
Diff.Mean	0.01	0.14	11.98
Diff.Std	7.03	2.50	7.20

2.6 Conclusions

In this chapter, at first, the basic information of the 5MW offshore wind turbine and OC4 jacket model used in this study is introduced. The related design load cases are also briefly discussed. Then, the basic theory of the substructuring (super-element) methods are given in this chapter. Then, the influence of different load simulation approaches and jacket models on the structural responses are studied. Firstly, three load simulation methods used for OWT structures are compared. In this comparison, the beam jacket model is applied in all three approaches. One uncoupled case which focuses on the behavior of the jacket is compared with the fully and sequentially coupled approaches. Secondly, the effect of two different numerical jacket models on the loading is also investigated. The sequentially coupled load simulation is used for both the two jacket models. One jacket model uses only Timoshenko beam and the other model uses super-elements for representation of the junctions in the jacket model. The comparison work mainly focuses on the behaviors of the top of the jacket. The analysis of the results leads to the following conclusions:

Using different load simulation approaches does not make many differences in the mean values of the simulation results. Major differences can only be observed in the extreme and standard deviation values. Moreover, the sequential method has better performance than the uncoupled approach. The overall mean values of the absolute relative differences are less than 3%. The small differences between the sequentially and fully coupled method may come from the inherent problem of the CB method applied in the sequential approaches. When comparing the uncoupled and the fully coupled methods, the overall mean values of relative differences in My and Ux are small. However, the overall mean values of maximum and standard deviation values in Fx are greater than 5%. Such a difference may lead to under/overestimation namely when evaluating the extreme responses and fatigue damage of the jacket. The differences between the uncoupled and the fully coupled approaches are mainly because hydro-damping and hydro-elastic coupling are not included in the uncoupled simulation.

For the comparison of the two jacket models, firstly, a small difference is observed in the eigenfrequencies. The total mass of the jacket in the beam model is higher due to overlapping parts of the joints. These overlaps are excluded from the super-element model, which makes the total mass of the super-element model decrease. The first 5 natural frequencies of the super-element model are also lower than those of the beam model, which means that the stiffness of the jacket in the super-element model also decreases. In addition, at the top of the jacket, the simulation results of the super-element model are different from those of the beam model in the displacement (Ux). The mean values of displacement Ux in the

super-element model are superior to those furnished by the beam model. The overall mean value of relative differences in the mean values of Ux is about 11.98%. For the loads (Fx, My), some differences appear in the extreme and standard deviation of Fx. These differences may generate some errors in the evaluation of the extreme responses of the jacket. The differences observed can be explained by the reduction of stiffness in the super-element jacket model, which makes the jacket model more realistic.

In conclusion, from the comparison of the load simulation methods, it is found that the results of the uncoupled case as shown in Fig.2.4(b) can present significant differences when compared to the results of the fully coupled method. The load calculations of the sequential approach are mostly in good agreement with those furnished by the fully coupled method. Thus, the sequential approach and the fully integrated method are recommended for OWT load calculations. Furthermore, for the comparison of different models of the jacket, the responses of the super-element model exhibit significant differences compared to the beam model. To better model the jacket behaviors, the jacket model with super-elements appears as the best solution among those studied. In the future, the jacket model with super-elements and the sequentially coupled approach will be used in reliability analysis of the jacket system, because they can better simulate the loading and jacket behaviors.

Chapter 3

Reliability assessment with ensemble surrogate models

Contents

3.1 Motivation

Uncertainties in material properties, loads, and geometrical parameters widely exist in real-world engineering problems and will affect structural safety in practical engineering. Therefore, in order to enable reliable designs, the different sources of uncertainty must be analyzed during the life cycle assessment. In this context, reliability analysis is an approach that aims to assess the probability of failure of systems with uncertainties. Since the introduction of reliability assessment, many reliability methods have been developed [Ang and Cornell, 1974, Tamimi et al., 1989, Tvedt, 1990, Ang et al., 1992, Au and Beck, 2001, Nie and Ellingwood, 2000, Blatman and Sudret, 2010, Bichon et al., 2008, Echard et al., 2011, Alban et al., 2017]. Among these approaches, the first-order reliability method (FORM)[Ang and Cornell, 1974] and second-order reliability method (SORM)[Tvedt, 1990] are two representative approximation methods [Zhao and Ono, 1999]. They focus on finding a single most probable point and provide a good balance between accuracy and computational efficiency. However, the accuracy of these methods cannot meet the requirements in the case of highly nonlinear problems or multiple most probable points. Compared to these approximation approaches, Monte Carlo simulation (MCS) [Kalos and Whitlock, 2009, Alban et al., 2017] is a very robust reliability method that is generally used as a reference and its results are compared to those furnished by other reliability assessment methods. The main shortcoming of MCS is that it requires a large number of samples and is time-consuming for many real engineering problems. Even though some variance reduction techniques were developed such as Importance Sampling (IS) [Ang et al., 1992], Subset Simulation (SS) [Au and Beck, 2001] and Directional Simulation (DS) [Nie and Ellingwood, 2000], the computational cost remain high and impractical for rare event problems.

In order to obtain accurate and efficient reliability analysis results, surrogate-assisted reliability analysis became increasingly important in the last decade. The basic idea is to replace the performance function by constructing a surrogate model (also known as metamodel), such as Response Surface (RS) [Roussouly et al., 2013, Dong et al., 2018], Artificial Neural Network (ANN)[Hurtado and Alvarez, 2001, Schueremans and Van Gemert, 2005, Li et al., 2018a], Support Vector Machine (SVM) [Basudhar and Missoum, 2008, Bourinet et al., 2011], Polynomial Chaos Expansion (PCE)[Blatman and Sudret, 2010, Marelli and Sudret, 2018], and Gaussian process also called Kriging model [Kaymaz, 2005, Echard et al., 2011]. Furthermore, the strategy for constructing a surrogate model can generally be classified into two types (1) "one shot" (non-adaptive) and (2) active learning approaches (adaptive). The "one shot" method requires generating all sample points in advance and performing the reliability analysis by using the validated surrogate model. However, active learning methods select one or several sample points at each iteration to construct the surrogate model, which is updated at each iteration efficiently until the convergence. Hence, active learning approaches based on metamodeling techniques [Echard et al., 2011, Blatman and Sudret, 2010, Bourinet, 2016, Li et al., 2018b, Marelli and Sudret, 2018] have gained considerable interest. Among all the active learning approaches, the Kriging model is widely used. Bichon et al. [Bichon et al., 2008] proposed an active learning approach based on the expected fea-

sibility learning function with Kriging. Echard et al.[Echard et al., 2011] proposed a U-function with Kriging named AK-MCS. Based on AK-MCS, some studies [Hu and Mahadevan, 2016, Peijuan et al., 2017] are also conducted to enhance the computational efficiency. Additionally, other learning functions [Lv et al., 2015, Sun et al., 2017, Zhang et al., 2019, Shi et al., 2020] based on Kriging model have also been developed in recent years. Moreover, the cross-validation techniques are then used to develop active learning approaches with Kriging model [Zhang et al., 2015, Xiao et al., 2018a]. However, active learning approaches based on Kriging model may become less efficient when facing high-dimensional and nonlinear problems. Therefore, some attention [Hurtado and Alvarez, 2001, Chojaczyk et al., 2015] has been turned to artificial neural networks for reliability assessment due to their powerful ability to deal with high-dimensional and highly nonlinear problems. Eason and Cremaschi [Eason and Cremaschi, 2014] applied the active learning method in ANN with two adaptive sampling algorithms. Then, Xiao et al.[Xiao et al., 2018b] proposed three universal learning functions which can be applied in ANN. More recently, Xiang et al.[Xiang et al., 2020] proposed an active learning approach in ANN with weighted sampling. As we can see, many works have been conducted based on one of these two metamodels (Kriging and ANN). However, it is still hard to know which surrogate model is more suitable for an unknown problem. To solve this difficulty, the ensemble of surrogate models seems to be a better approach.

Ensemble of surrogates was firstly introduced by the work [Zerpa et al., 2005, Goel et al., 2007] which considers different metamodels, which aims to take advantage of the best properties of each metamodel. The strategy of the ensemble of surrogates can be mainly classified in two approaches: on the one hand, the weighted average surrogate (WAS) and, on the other hand, the best surrogate (BS) approaches. A surrogate model with higher accuracy should be assigned a large weight or selected as the best surrogate in the ensemble of surrogates. Moreover, the goodness (accuracy) of each surrogate model can be measured globally and locally. Goel et al [Goel et al., 2007] propose a global weight selection scheme based on global data-driven measures of goodness, which can be used in all the surrogate models. Zerpa et al.[Zerpa et al., 2005] construct a local weighted average model based on the variance predicted by three surrogate models. The method proposed by Zerpa et al.[Zerpa et al., 2005] cannot be extended to other surrogate models that do not provide sample's variances. Furthermore, all the above-mentioned methods mainly focus on constructing the ensemble of surrogate models to ensure accuracy over the entire uncertainty space. However, the construction of an ensemble of surrogates in reliability analysis is different, since we only care about the contour line of the performance function corresponding to the zero value. More recently, Cheng et Lu [Cheng and Lu, 2020] proposed an active learning approach using PCE, Kriging, and Support Vector Regression (SVR) based on WAS for reliability assessment. The goodness of the metamodels is measured globally and the weights are determined by leave-one-out (LOO) errors of the metamodels and change at each iteration. Teixeira et al.[Teixeira et al., 2020] proposed an active learning method based on BS approach named multi-metamodel complement-basis with linear regression, PCE, and Kriging. The goodness of each surrogate model is also measured globally, and the active (best) metamodel is determined by the absolute LOO errors of the metamodels at each iteration. However, in [Cheng and Lu, 2020] and [Teixeira et al., 2020], the weight or the best surrogate model

is fixed for all the candidate samples at each iteration. As mentioned in [Goel et al., 2007], when the weights are selected based on the global measures of goodness of the surrogate models, they are fixed in design space and may not be able to capture local behaviors. In this case, the ensemble of surrogate models with active learning approaches may be less efficient in selecting the updating points for the construction of an ensemble of surrogates. In this chapter, we propose a data-driven approach to locally measure the goodness of the surrogate models and directly relate the weights or the best surrogate to candidate samples. The weights or the best surrogate in the ensemble of surrogates will vary with the candidate samples. In the proposed approaches, cross-validation and Jackknife techniques are firstly used to estimate prediction errors of the surrogate models. Additionally, two methods are developed to locally measure the goodness of the surrogate models and calculate the prediction errors of the ensemble of surrogates. The ensemble of surrogates is updated by selecting new sample points that have large prediction errors as well as near the limit state.

In this chapter, some typical surrogate models are presented in section 3.2. The previous methods for constructing ensemble surrogate models are given in section 3.3. The proposed methods with ensemble surrogate models for reliability analysis are given in section 3.4. The application examples are studied in section 3.5. Conclusions are given in section 3.6.

3.2 Surrogate models

A variety of surrogate modeling techniques is available in the literature. They can be mainly classified into two groups: localised surrogates and global surrogates as shown in Table 3.1. The localised surrogates rely on the availability of local information, where the predictions in proximity to the points in the training set are accurate. The global surrogates achieve good accuracy in terms of global error measures, thus offering some degree of extrapolation capabilities, but potentially worse local accuracy than their localised counterparts. Note that the choice for these surrogates are normally problem oriented. It is hard to figure out which surrogate model is the best for the given problems. In this section, several popular surrogate models used in reliability analysis are presented.

Table 3.1 – Surrogate models classification

Localised surrogates	Global surrogates
Kriging [Krige, 1951]	Linear regression [Nelder and Wedderburn, 1972]
Spline [Reinsch, 1967]	Polynomial chaos expansions [Askey and Wilson, 1985]
Sparse grids [Bungartz and Griebel, 2004]	Poincare expansions [Roustant et al., 2017]
Support vector machine [Smola and Schölkopf, 2004]	Artificial neural networks [Cheng and Titterington, 1994]
...	...

3.2.1 Kriging model

The Kriging model, also known as Gaussian process, was first introduced by [Krige, 1951] in the field of geostatistics. It is based on the assumption that the response function consists of a regression model and a stochastic process, given by:

$$g(\mathbf{x}) = \mathbf{f}(\mathbf{x})^{\mathrm{T}}\boldsymbol{\beta} + z(\mathbf{x}) \tag{3.1}$$

where $\mathbf{f}(\mathbf{x})$ is the basic function vector, $\boldsymbol{\beta}$ is the corresponding regression coefficient vector, and $z(\mathbf{x})$ represents a stationary Gaussian process with zero mean and the covariance between two points,$\mathbf{x_i}$ and $\mathbf{x_k}$:

$$\mathrm{cov}(z(\mathbf{x_i})z(\mathbf{x_k})) = \sigma^2 \mathrm{R}_\theta(\mathbf{x_i}, \mathbf{x_k}) \tag{3.2}$$

where σ^2 and $\mathrm{R}_\theta(\mathbf{x_i}, \mathbf{x_k})$ are respectively the process variance and a Gaussian correlation function defined by a vector of parameters θ. Several correlation functions are available for the Kriging model. In this paper, the Gaussian correlation function used is the squared exponential kernel, which reads as: :

$$\mathrm{R}_\theta(\mathbf{x}_i, \mathbf{x}_k) = \prod_{j=1}^{n} \exp\left[-\theta_j \left(\mathrm{x}_\mathrm{i}^{(\mathrm{j})} - \mathrm{x}_\mathrm{k}^{(\mathrm{j})}\right)^2\right] \tag{3.3}$$

where $\mathrm{x}_\mathrm{i}^{(\mathrm{j})}$ and $\mathrm{x}_\mathrm{k}^{(\mathrm{j})}$ are the j-th values of the vectors $\mathbf{x_i}$ and $\mathbf{x_k}$. θ_j is a scalar which gives the multiplicative inverse of the correlation length in the j-th direction. The unknown parameters ($\boldsymbol{\beta}$, σ^2,θ) of the Kriging model can be optimized by maximum likelihood estimation. Once the optimal values of the three parameters are obtained, the expected value $\mu_{\hat{g}}$ and the variance $\sigma^2_{\hat{g}}$ at a point $\mathbf{x}$ can be determined by the equations:

$$\mu_{\hat{g}}(\mathbf{x}) = \beta + \mathbf{r}(\mathbf{x})\mathbf{R}_\theta^{-1}(\mathbf{Y} - \mathbf{1}\beta) \tag{3.4}$$

$$\sigma^2_{\hat{g}}(\mathbf{x}) = \sigma^2\left(1 + u(\mathbf{x})^{\mathrm{T}}\left(\mathbf{1}^{\mathrm{T}}\mathbf{R}_\theta^{-1}\mathbf{1}\right)^{-1} u(\mathbf{x}) - \mathbf{r}(\mathbf{x})^{\mathrm{T}}\mathbf{R}_\theta^{-1}\mathbf{r}(\mathbf{x})\right) \tag{3.5}$$

where $\mathbf{r}(\mathbf{x}) = \{\mathrm{R}(\mathbf{x}, \mathbf{x}_1), \mathrm{R}(\mathbf{x}, \mathbf{x}_2), \ldots, \mathrm{R}(\mathbf{x}, \mathbf{x}_n)\}$ represents the correlation vector between the unknown point $\mathbf{x}$ and n all known experimental points and $u(\mathbf{x})$ can be expressed as $u(\mathbf{x}) = \mathbf{1}^{\mathrm{T}}\mathbf{R}_\theta^{-1}\mathbf{r}(\mathbf{x}) - 1$. The expected value $\mu_{\hat{g}}$ is always considered as the prediction of the Kriging model.

3.2.2 Polynomial Chaos Expansion

Polynomial Chaos Expansion (PCE) was first proposed by Wiener [Wiener, 1938]. The random response Y(X) is represented in a suitable functional space, like Hilbert space L^2. Assume a physical model with a finite second order measure, such as $\mathbb{E}\left(\|\mathrm{Y}(\mathrm{X})\|^2\right) < +\infty$, then PCE approximation of this model can expressed as:

$$\hat{\mathrm{Y}}^{\mathrm{PCE}}(\mathrm{X}) \approx \sum_{\alpha \in \mathrm{A}} y_\alpha \Psi_\alpha(\mathrm{X}) \tag{3.6}$$

$\Psi_\alpha(X)$ is the given basis; y_α is the finite subsets of coefficients from a truncated basis $A \subset \mathbb{N}^M$. Different truncation plan, with parameters p and q can be used:

$$A^{n,p,q} = \{\alpha \in A^{n,p} : \|\alpha\|_q \leq p\} \tag{3.7}$$

here n is the number of inputs and p is the maximum degree. For $q = 1$, this corresponds a standard truncation, and for $q < 1$, this corresponds a hyperbolic truncation which includes high-degree terms in each single variable, while avoiding high order interaction terms. The basis can adopt different types and their supported distributions are summarized as Askey-Scheme [Xiu and Karniadakis, 2002] listed in Table 3.2.

Due to the orthonormality of the polynomial basis as respect to their joint probability density (PDF), the inner product of the basis satisfy:

$$\langle \Psi_\alpha(x), \Psi_\beta(x) \rangle = \mathbb{E}\left(\Psi_\alpha(x), \Psi_\beta(x)\right) = \delta_{\alpha\beta} \tag{3.8}$$

where $\delta_{\alpha\beta} = 1$, only if $\alpha = \beta$; otherwise, $\delta_{\alpha\beta} = 0$. For the calculation of coefficients (y_α), two types of methods are available,referred as intrusive stochastic collocation method and non-intrusive Galerkin projection. The performances of the two approaches are similar and non-intrusive method is widely used for its easier implementation [Eldred and Burkardt, 2009].

Table 3.2 – Variable distribution and associated orthonormal families

Random variable distribution	Wiener-Askey chaos	Support
Gaussian	Hermite	(-∞,∞)
Gamma	Laguerre	[0,∞)
Beta	Jacobi	[a,b]
Uniform	Legendre	[a.b]
Poisson	Charlier	{0,1,2,...}
Binomial	Krawtchouk	{0,1,...N}
Negative Binomial	Meixner	{0,1,2,...}
Hypergeometric	Hahn	{0,1,„,N}

3.2.3 Artificial neural networks

Artificial neural networks (ANN) are widely used in many fields. The basic structure of an Artificial neural networks is composed of three or more layers of neurons as shown in Fig.3.1. The neurons of the neighboring layers are connected by weights, and the output of each neuron can be expressed as:

$$H_i^{(l)} = f\left(\sum_{j=1}^{n} w_{ij}^{(l)} H_j^{(l-1)} + b_i^{(l)}\right) \tag{3.9}$$

where $H_i^{(l)}$ is the output of the ith neuron of the lth layer, $w_{ij}^{(l)}$ are the weights of the jth input, $b_i^{(l)}$ is the bias, n is the number of the neurons of the $(l-1)$th layer, and $f()$ is the activation function. The multi-

layer perceptron (MLP) with backpropagation algorithm is widely used in the literature. Concerning the activation function, the rectified linear unit (RELU) function is commonly used in the literature, since it can efficiently prevent vanishing and exploding gradient problems. The RELU activation function can be expressed as:

$$f(x) = \begin{cases} x, x > 0 \\ 0, x \leqslant 0 \end{cases} \tag{3.10}$$

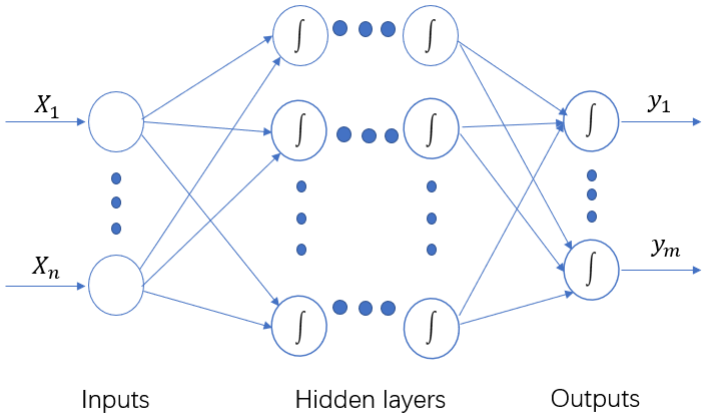

Figure 3.1 – Structures of Artificial neural networks

Furthermore, as shown in the study [Xiao et al., 2018b], a backpropagation (BP) neural network with three layers (input layer, hidden layer, and output layer) can approximate any continuous functions. Therefore, a BP neural network with three layers is applied in the present work.

3.3 Ensemble surrogate models

Ensemble of surrogates was firstly introduced by the work [Zerpa et al., 2005, Goel et al., 2007] which considers different metamodels, which aims to take advantage of the best properties of each metamodel. The strategy of the ensemble of surrogates can be mainly classified in two approaches: on the one hand, the weighted average surrogate (WAS) and, on the other hand, the best surrogate (BS) approaches. A surrogate model with higher accuracy should be assigned a large weight or selected as the best surrogate in the ensemble of surrogates. Moreover, the goodness (accuracy) of each surrogate model can be measured globally and locally.

3.3.1 Global goodness measurement of ensemble surrogate models

Goel et al [Goel et al., 2007] proposed a global weight selection scheme based on global data-driven measures of goodness, which can be used in all the surrogate models. The weighted average model can be

expressed as:

$$\hat{y}_{was} = \sum_{i}^{\mathrm{N_M}} w_i \hat{y}_i \tag{3.11}$$

where w_i is the weight associated with ith surrogate model and $\mathrm{N_M}$ is the total number of surrogate models. Furthermore, the sum of weights equals to one $\left(\sum_{i=1}^{\mathrm{N_M}} w_i = 1\right)$. w_i can be calculated by the proposed approaches in [Goel et al., 2007]. A surrogate model that is deemed more accurate should be assigned a large weight, and the less accurate model should have less influence on the predictions. Three approaches have been proposed for the weight calculation by [Goel et al., 2007]. They are summarized as follows:

(1). Weight calculation equation one

The weight associated with ith surrogate model is given as:

$$w_i = \frac{\sum_{j=1, j\neq i}^{\mathrm{N_M}} \mathrm{E}_j}{(\mathrm{N_M}-1)\sum_{j=1}^{\mathrm{N_M}} \mathrm{E}_j} \tag{3.12}$$

where E_j is the global data-based error measure for the jth surrogate model.

(2). Weight calculation equation two

The second weighted calculation function is expressed as:

$$\begin{aligned} w_i^* &= \left(\mathrm{E}_i + \alpha \mathrm{E}_{avg}\right)^{\beta}, \quad w_i = w_i^* / \sum_i w_i^* \\ \mathrm{E}_{avg} &= \sum_{i=1}^{\mathrm{N_M}} \mathrm{E}_i / \mathrm{N_{SM}}; \quad \beta < 0, \alpha < 1 \end{aligned} \tag{3.13}$$

This weighting scheme requires the user to specify two parameters α and β, which control the importance of averaging and importance of individual surrogate, respectively. Small values of α and large negative values of β impart high weights to the best surrogate model. Large values α and small negative β values represent high confidence in the averaging scheme.

(3). Best surrogate selection

The best surrogate selection can be seen as the special case of weighted average surrogate model, which aims to select the best model among all considered surrogate models.The best surrogate model is revisited for each new design of experiment. The weighting scheme can be consider where the model with least global data-based error is assigned a weight of one and all other models are assigned zero weight. The data-based error (E) mentioned in above is used with generalized mean square cross-validation error.

3.3.2 Local goodness measurement of ensemble surrogate models

Zerpa et al.[Zerpa et al., 2005] presented a local weighed average surrogate approach, which can be expressed as:

$$\hat{y}_{lwas}(\mathrm{x}) = \sum_{i}^{\mathrm{N_M}} w_i(\mathrm{x})\,\hat{y}_i(\mathrm{x}) \tag{3.14}$$

where $\hat{y}_i(\mathbf{x})$ is the predicted response by ith surrogate model at the point $\mathbf{x}$. $w_i(\mathbf{x})$ is the weight associated with ith surrogate model at the point $\mathbf{x}$. $w_i(\mathbf{x})$ can be calculated by:

$$w_i(\mathbf{x}) = \frac{\frac{1}{\mathrm{V}_i(\mathbf{x})}}{\sum_{j=i}^{k} \frac{1}{\mathrm{V}_j(\mathbf{x})}} \tag{3.15}$$

where $\mathrm{V}_i(\mathbf{x})$ is the prediction variance of the i surrogate model at the point $\mathbf{x}$. Zerpa et al. [Zerpa et al., 2005] used Polynomial regression model, Kriging model and Radial basis function model for ensemble surrogate models. The proposed approach can be only used to the surrogate model which can provide the variance of samples. Need to be mentioned, the variances calculated in the surrogate models are not uniform.

All the above-mentioned methods mainly focus on constructing the ensemble of surrogate models to ensure accuracy over the entire uncertainty space. However, the construction of an ensemble of surrogates in reliability analysis is different, since we only care about the contour line of the performance function corresponding to the zero value. More recently, Cheng et Lu [Cheng and Lu, 2020] and Teixeira et al.[Teixeira et al., 2020] have proposed two approaches for reliability analysis with ensemble surrogate models. However, in [Cheng and Lu, 2020] and [Teixeira et al., 2020], the weight or the best surrogate model is fixed for all the candidate samples at each iteration. As mentioned in [Goel et al., 2007], when the weights are selected based on the global measures of goodness of the surrogate models, they are fixed in design space and may not be able to capture local behaviors. In this case, the ensemble of surrogate models with active learning approaches may be less efficient in selecting the updating points for the construction of an ensemble of surrogates. In following section, we propose a data-driven approach to locally measure the goodness of the surrogate models and directly relate the weights or the best surrogate to candidate samples. The weights or the best surrogate in the ensemble of surrogates will vary with the candidate samples.

3.4 Ensemble surrogate models with local goodness measurement for reliability analysis

3.4.1 Prediction errors of candidate samples

In the proposed approaches, a key point is the evaluation of the prediction errors at the candidate samples of each surrogate model. Jin et al. [Jin et al., 2002] proposed a cross-validation approach to estimate

the prediction error at a given point **x**. By K-fold cross-validation approach, the predicted errors that are not provided by the original metamodel techniques such as PCE, SVR can be easily estimated. In addition, Kleijen et al.[Kleijnen and Van Beers, 2004] and Xiao et al. [Xiao et al., 2018b] implement cross-validation with jackknife technique respectively in Kriging and ANN metamodels to estimate the errors. Jackknife method is a classical resampling technique especially useful for error (variance) estimation and is also applied in this paper. According to [Kleijnen and Van Beers, 2004], the jackknife's pseudo-value at the candidate sample **x** is given by:

$$\hat{y}^i(\mathbf{x}) = \mathrm{K} \times \hat{y}(\mathbf{x}) - (\mathrm{K}-1) \times \hat{y}^{(-i)}(\mathbf{x}) \tag{3.16}$$

where $\hat{y}(\mathbf{x})$ denotes the prediction values on **x** based on the metamodel trained by all K fold samples; $\hat{y}^{(-i)}(\mathbf{x})$ denotes the predicted values on **x** using metamodel created based on K − 1 fold samples with ith fold moved out ($i = 1, 2...\mathrm{K}$). From the pseudo-values in Eq.(3.16), the jackknife's error at candidate point **x** is defined as follows:

$$e^2(\mathbf{x}) = \frac{1}{\mathrm{K}(\mathrm{K}-1)} \sum_{i=1}^{\mathrm{K}} \left(\hat{y}^i(\mathbf{x}) - \overline{\hat{y}}(\mathbf{x}) \right)^2 \quad \text{with} \quad \overline{\hat{y}} = \frac{1}{\mathrm{K}} \sum_{i=1}^{\mathrm{K}} \hat{y}^i(\mathbf{x}) \tag{3.17}$$

In the cross-validation approach, 5 and 10 folds cross-validation are commonly used. Hence, the 5-fold cross validation is used in the present work with K equals to 5.

3.4.2 Proposed local goodness measurement approaches

For the local goodness assessment, Zerpa et al. [Zerpa et al., 2005] proposed a local measure approach based on the variance of the estimator provided by surrogate models. However, this approach cannot be extended for other surrogate models, such as ANN, PCE, and SVM. Because these surrogate models cannot provide the variance of the estimator. In this section, the local goodness measure is based on the errors calculated by cross-validation with Jackknife techniques, which is a data-based approach and can be used for any surrogate model. The basic principle is that the metamodel that has a smaller predicted error will be assigned a greater weight or selected as the best surrogate. The details of the proposed local measure approaches are listed in the following subsections.

Proposed local weighted average surrogate approach

In the proposed local weighted average surrogate (LWAS) approach, the predictor of LWAS at point **x** is defined as y_{lwas}, which can be expressed as [Goel et al., 2007]:

$$\hat{y}_{lwas}(\mathbf{x}) = \sum_i^{\mathrm{N_M}} w_i(\mathbf{x})\, \hat{y}_i(\mathbf{x}) \tag{3.18}$$

For the prediction error (e_{lwas}) in LWAS approach at the point **x** is not given in previous works. Here, the

prediction error (e_{lwas}) is defined as follows:

$$e_{lwas}(\mathbf{x}) = \sum_{i}^{\mathrm{N_M}} w_i(\mathbf{x}) e_i(\mathbf{x}) \tag{3.19}$$

where $\hat{y}_i(\mathbf{x})$ and $e_i(\mathbf{x})$ respectively are the predicted response and error by ith surrogate model at the point $\mathbf{x}$. Here, it should be mentioned that all the prediction errors in each surrogate model are calculated by using the cross-validation and Jackknife techniques. $w_i(\mathbf{x})$ is the weight associated with ith surrogate model at the point $\mathbf{x}$ and $\mathrm{N_M}$ is the total number of surrogate models. Furthermore, the sum of weights equals to one $\left(\sum_{i=1}^{\mathrm{N_M}} w_i(\mathbf{x}) = 1\right)$. $w_i(\mathbf{x})$ can be calculated by the adapted functions WAT1 and WAT3 in [Goel et al., 2007], where the original functions are developed to measure the global goodness of the surrogate models. Here, the adapted function WAT1 is applied as follows:

$$w_i(\mathbf{x}) = \frac{\sum_{j=1, j\neq i}^{\mathrm{N_M}} e_j(\mathbf{x})}{(\mathrm{N_M}-1)\sum_{j=1}^{\mathrm{N_M}} e_j(\mathbf{x})} \tag{3.20}$$

It should be noticed that $e_j(\mathbf{x})$ is the predicted error of jth metamodel at the point $\mathbf{x}$.

Proposed local best surrogate approach

In the proposed local best surrogate (LBS) approach, the idea is that if the ith surrogate model in the $\mathrm{N_M}$ surrogate models gives the minimum predicted error e_i at the point $\mathbf{x}$,the predictor and prediction error of the ith surrogate model at the point $\mathbf{x}$ will be considered as the predicted response ($\hat{y}_{lbs}$) and the error (e_{lbs}) of LBS approach at the point $\mathbf{x}$. They can be defined as follows:

$$\begin{aligned} &[e_i(\mathbf{x}), i] = \min\left(e_j(\mathbf{x})\right), j = 1..\mathrm{N_M} \\ &\hat{y}_{lbs}(\mathbf{x}) = \hat{y}_i(\mathbf{x}) \\ &\mathrm{e}_{lbs}(\mathbf{x}) = e_i(\mathbf{x}) \end{aligned} \tag{3.21}$$

3.4.3 Active learning approaches for reliability analysis with ensemble surrogate models

In the proposed active learning approach, Kriging and ANN model are used to construct the ensemble surrogate models. Kriging is one of the most popular surrogate models used in the active learning approach. Recently, artificial neural networks (ANN) have also attracted a lot of interest for structural reliability assessment due to their powerful capability. Many active learning approaches have been developed based on Kriging models and ANN. But selecting an appropriate model or technique for a reliability assessment problem with limited knowledge of the limit state function remains a challenging task. Ensemble of surrogates seems to be a good approach to tackle this challenge. Additionally, the values predicted by ANN and Kriging at the point $\mathbf{x}$ are noted respectively as $\hat{y}_{nn}(\mathbf{x})$ and $\hat{y}_k(\mathbf{x})$. The corresponding errors calculated by 5-fold cross-validation and Jackknife techniques are noted as $e_{nn}(\mathbf{x})$ and

$e_k(\mathbf{x})$.

Learning function

The learning function is the key for active learning methods because it is the guideline for the selection of new training sample points to construct an efficient surrogate model. There are three basic ideas to construct the learning function (a) select the points near the limit state function ; (b) select the points with large predicted errors or variances ; (c) select the points far away from existing training points. Generally speaking, any combination of two or three above ideas can be used to construct the learning function. The most commonly used function is U function which is combined with (a) and (b) expressed as:

$$\mathrm{U}(\mathbf{x}) = \frac{\left|\hat{y}(\mathbf{x})\right|}{e(\mathbf{x})} \tag{3.22}$$

where $\hat{y}(\mathbf{x})$ and $e(\mathbf{x})$ are respectively the predicted response and error at point $\mathbf{x}$ by the surrogate model. Here, the U function is also applied in our proposed approaches, which reads:

$$\mathrm{U}_m(\mathbf{x}) = \frac{\left|\hat{y}_m(\mathbf{x})\right|}{e_m(\mathbf{x})} \tag{3.23}$$

Here, m represents $lwas$ (the proposed LWAS approach) or lbs (the proposed LBS approach).

Convergence criterion

Two stopping criterions for the proposed active learning approaches are considered:
(1). For many practical structural reliability problems, the computational resources are limited due to time-consuming FEA simulation[Aute et al., 2013]. Therefore, the proposed method will be stopped when a maximum number of evaluations are reached.
(2). The second stop criterion is to estimate the maximum relative difference ($e_{\mathrm{P}f}$) between the probability of failure ($\mathrm{P}f$) predicted by the ensemble of surrogate models and the probability of failure predicted by the single surrogate model, which reads:

$$\frac{e_{\mathrm{P}f}}{\mathrm{P}f} \leq \xi \tag{3.24}$$

Here, $e_{\mathrm{P}f} = \max\left\{\left|\mathrm{P}f - \mathrm{P}f_k\right|, \left|\mathrm{P}f - \mathrm{P}f_{nn}\right|\right\}$. $\mathrm{P}f_k$ and $\mathrm{P}f_{nn}$ are respectively the probability of failure estimated by Kriging and ANN surrogate models. The value ξ can be selected as a very small value (e.g. 0.01 in this thesis) to obtain an acceptable level of accuracy by considering computational efficiency.

Main steps of the proposed active learning approach

The main steps of the proposed methods as shown in Fig.3.2 and Algorithm 3.1 are summarized as follows:
(1). Generate a small number of initial points ($\mathbf{X_{DoE}}$) by Latin Hypercube Sampling (LHS) technique and

compute the corresponding model response $\mathbf{Y_{DoE}}$. Also, generate a large number population $\mathbf{S}$ of N_{mcs} samples with MCS.

(2). Train the surrogate models (Kriging and ANN) with $\mathbf{X_{DoE}}$ and $\mathbf{Y_{DoE}}$. Then estimate the predictor at each point $\mathbf{x}$ of the whole population $\mathbf{S}$ by Kriging and ANN. Calculate related prediction errors with Jackknife techniques. Also, estimate the probability of failure by Kriging ($P f_k$) and ANN ($P f_{nn}$).

(3). Calculate the weights for LWAS approach or select the best surrogate model for LBS approach at each sample $\mathbf{x}$ in $\mathbf{S}$.

(4). Calculate predicted responses and errors of each sample $\mathbf{x}$ in the ensemble of surrogate models (LWAS or LBS). Then, estimate the probability of failure ($P f$) of the ensemble of surrogates of the population $\mathbf{S}$.

(5). Search a new point $\mathbf{x_u}$ from $\mathbf{S}$ by minimizing $U_m(\mathbf{x})$, and compute the true model response $\mathbf{y_u}$. Then, update $\mathbf{X_{DoE}}$ and $\mathbf{Y_{DoE}}$ by adding $\mathbf{x_u}$ and $\mathbf{y_u}$ respectively.

(6). Repeat steps (2)-(5) until the stopping criterion is satisfied.

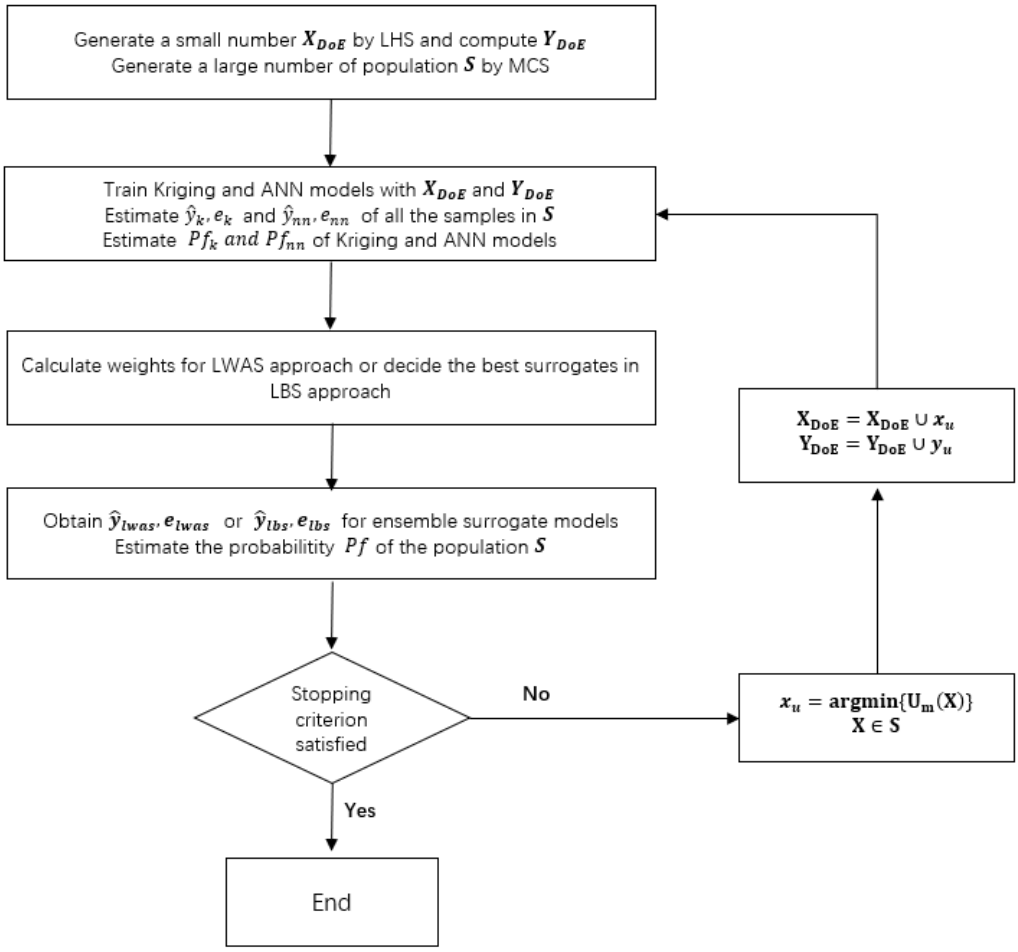

Figure 3.2 – Flowchart of the active learning algorithm.

Algorithm 3.1 Ensemble surrogate model combined with Kriging and ANN based on local goodness assessment

Input: Generate a small number (N_{call}) of initial samples X_{DoE} by LHS and compute the related Y_{DoE};
Generate a large number of population **S** by MCS for the failure probability estimation.

while $\xi \leqslant e_{pf}$ **do**:
  (Train Kriging and ANN)
  Train Kriging models and ANN models with X_{DoE} and Y_{DoE};
  (Get the predicted values and probabilities of falure in each surrogate model)
  Predict the values of all the samples **S** with the current Kriging ($\hat{y}_k$) and ANN ($\hat{y}_{nn}$) ;
  Calculate the probability of failure in Kriging (Pf_k) and ANN (Pf_{nn});
  (Get the cross-validation errors for all the samples in Kriging and ANN)
  Estimate the sample errors with cross-validation approaches in Kriging (e_k) and ANN (e_{nn});
  (Get the predicted values and errors in ensemble surrogate models)
  Calculate the weights (w_i) for all the samples in LWAS approach;
  (Or select the best for all the samples in LBS approach;)
  Calculate $\hat{y}_{lwas}$ and e_{lwas} for all the samples **S** in LWAS approach;
  (Or calculate $\hat{y}_{lbs}$ and e_{lbs} for all the samples **S** in LBS approach;)
  (Get the probability of failure in the ensemble surrogate model)
  Calculate the probability of failure (Pf) in ensemble surrogate model $\hat{y}_{lwas}$ (or $\hat{y}_{lbs}$);
  (Calculate the value to decide the stopping criterion)
  Recalculate the value of e_{pf};
  (Select the new added sample)
  Select the new sample (x_u) for minimizing U_{lwas} (or U_{lbs}) and get the true response y_u;
  Enrich respectively X_{DoE} and Y_{DoE} with x_u and y_u
  N_{call}=N_{call}+1
end while

Output: Get the probability value of ensemble surrogate model Pf
Get the total number of calls to the performance functions (N_{call})

3.5 Examples and applications

In this section, 4 representative examples and one finite element example are investigated to demonstrate the accuracy and efficiency of the proposed methods. The first example is a series system with four performance functions; the second example is a highly nonlinear oscillator; the third example is a cantilever tube with a medium number of variables and a highly nonlinear function; the fourth is a high dimension analytical problem with 40 and 100 variables; the last example is an engineering problem with an offshore wind turbine jacket foundation with 15 variables. Furthermore, the accuracy and efficiency comparisons between the proposed approaches and AK-MCS are discussed in these 5 examples. The results of crude MCS approach is also given in the examples. Additionally, the total number of original function evaluations ($Ncall$), the percentage error (ε) compared to MCS, and the coefficient of variation of the estimated probability of failure (CoV) are also reported in these examples. The percentage error

and the coefficient of variation are defined as:

$$\begin{aligned} \varepsilon &= \frac{\left|\hat{\mathrm{P}f} - \mathrm{P}f_{\mathrm{mcs}}\right|}{\mathrm{P}f_{\mathrm{mcs}}} \times 100\% \\ CoV &= \sqrt{\frac{1-\mathrm{P}f}{\mathrm{N}_{\mathrm{mcs}}\,\mathrm{P}f}} \end{aligned} \tag{3.25}$$

where $\mathrm{P}f$ is the probability of failure, $\mathrm{P}f_{mcs}$ is the probability of failure estimated by crude MCS with a large population N_{mcs} and $\hat{\mathrm{P}f}$ is the probability of failure estimated by the proposed methods and AK-MCS. In addition, the contribution weights of ANN and Kriging models in the proposed approaches of each iteration are also given in these 5 examples. They are defined as follows:

$$\begin{aligned} \mathrm{W}_i^{\mathrm{lwas}} &= \frac{\sum_{k=1}^{\mathrm{N}_{mcs}} w_i^k}{\mathrm{N}_{mcs}} \\ \mathrm{W}_i^{lbs} &= \frac{\sum_{k=1}^{\mathrm{N}_{mcs}} 1_{lbs=i}^k}{\mathrm{N}_{mcs}} \end{aligned} \tag{3.26}$$

where W_i^{lwas} is the contribution weight of the ith surrogate model in LWAS approach and w_i^k is the weight of ith surrogate model in the kth point of the whole population (N_{mcs}); W_i^{lbs} is the contribution weight of the ith metamodel in LBS approach and $1_{lbs=i}^k$ means that the predicted value in kth point of LBS approach comes from ith surrogate model. Moreover, to reduce the uncertainty of different initial points of LHS technique, the average results of 10 repeated runs are compared. Also, it should be mentioned that the proposed approaches and AK-MCS are implemented by using Python scikit-learn toolbox [Pedregosa et al., 2011].

3.5.1 Example 1: A series system with four branches

The series system is one of the most widely studied examples in reliability analysis, which has already been investigated in [Echard et al., 2011, Xiao et al., 2018b, Cheng and Lu, 2020, Teixeira et al., 2020]. The performance function is given by:

$$g(\boldsymbol{x}) = \min \left\{ \begin{array}{c} 3 + 0.1\,(x_1 - x_2)^2 - (x_1 + x_2)/\sqrt{2} \\ 3 + 0.1\,(x_1 - x_2)^2 + (x_1 + x_2)/\sqrt{2} \\ (x_1 - x_2) + 6/\sqrt{2} \\ (x_2 - x_1) + 6/\sqrt{2} \end{array} \right\} \tag{3.27}$$

where x_1 and x_2 are independent standard normal distributed random variables. In this example, 12 initial points are generated for the proposed methods and AK-MCS by LHS. Only 10 neurons are used in the hidden layer of ANN model. Generally, it is a tricky thing to select the number of neurons in the hidden layer, which is always tuned by optimization tools. The number of neurons in the hidden layer will depend on the random dimension and complexity of the problem. However, only a small set of training data are available in active learning approaches. Hence, a small number (less than 100 in this paper) of neurons in the hidden layer are sufficient. Additionally, 10^6 samples are generated by MCS to

estimate the probability of failure. The average results of 10 repeated runs are compared in Table 3.3. The proposed two approaches provide comparative results with much fewer model evaluations compared to AK-MCS method. Moreover, the proposed two approaches have better performances in efficiency and accuracy than WAS-Ensemble approach developed by Cheng and Lu [Cheng and Lu, 2020]. The proposed two approaches have nearly the same performance as Complement-basis approach developed by Teixeira et al. [Teixeira et al., 2020] in this example. The convergence of the proposed approaches is achieved after 45 iterations.

Table 3.3 – Average results for the proposed methods, AK-MCS and MCS in 10 repeated runs and relative comparison with other two ensemble of metamodeling methods. * denoted the results reported in references

Method	Pf(10^{-3})	CoV(%)	ε (%)	Ncall
MCS	4.471	1.49	-	1×10^6
AK-MCS+U	4.471	1.49	0.00	123
WAS-Ensemble *[Cheng and Lu, 2020]	4.37	1.51	1.13	73.0
Complement-basis approach *[Teixeira et al., 2020]	4.437	1.50	0.44	55.2
Proposed LWAS approach	4.435	1.50	0.80	57.8
Proposed LBS approach	4.453	1.50	0.41	54.2

Fig.3.3 shows the final limit state of the two proposed models and the corresponding design of experiments (DoEs). The enriched points (EPs) are selected by U learning function and most of the selected sample points are around the true limit-state functions. Furthermore, the iteration processes of the proposed methods including ANN and Kriging models given in Fig.3.4 and Fig.3.5. It should be mentioned that the ANN and Kriging models are both enriched by the samples which are selected by the proposed LWAS or LBS approaches. For the proposed approaches, in the beginning, the Kriging model contributes more to estimate the probability of failure of the ensemble surrogate models. In the proposed LWAS approach, with the enrichment of DoEs, the ANN model has nearly the same contribution as the Kriging model. In the proposed LBS approaches, Kriging will take a dominant place after about 30 calls.

Moreover, to better understand the proposed approaches, the proposed LWAS approach is compared with the independent Kriging, ANN models, and AK-MCS approach. Here, the independent Kriging and ANN models mean that the enriched points are selected based on U function but with their own prediction values and cross-validation errors ($\frac{|\hat{y}_k|}{e_k}$, $\frac{|\hat{y}_{nn}|}{e_{nn}}$), which is different from the Kriging and ANN models in the proposed LWAS approach ($\frac{|\hat{y}_{lwas}|}{e_{lwas}}$). The convergence plots of these approaches are shown in Fig.3.6(a). The number of iterations in the independent Kriging and ANN models is taken as the same as the proposed LWAS approach. It is clear, in this example, that the independent ANN (IANN) can reach the true probability of failure (Pf_{mcs}) more efficiently compared to the independent Kriging (IK) and AK-MCS. Also, the independent Kriging model cannot reach the true probability of failure as efficiently as the Kriging model in the proposed LWAS approach in Fig.3.4. It means that, without the use of ANN model, the Kriging model cannot achieve such good performance as shown in Fig.3.4. However, the Kriging model in the proposed LWAS approach seems closer to the LWAS ensemble surrogate in Fig.3.4.

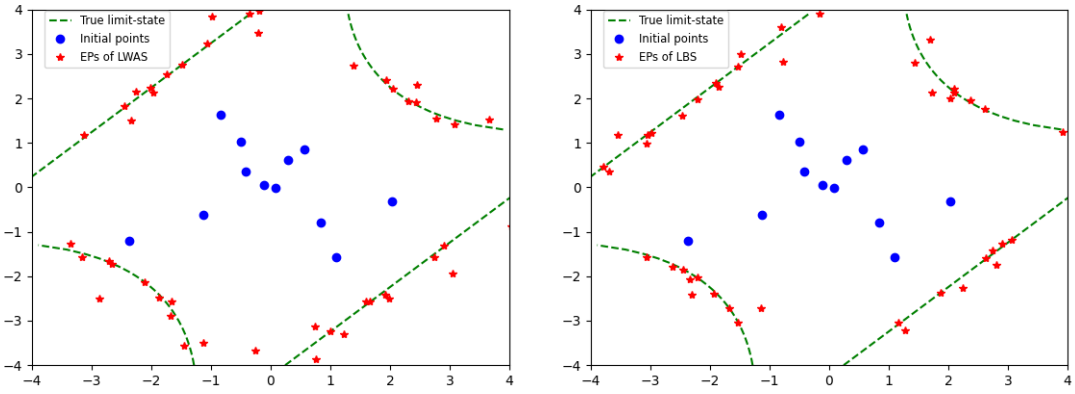

(a) LWAS approach (b) LBS approach

Figure 3.3 – Enrich points of the proposed two approaches in example 1.

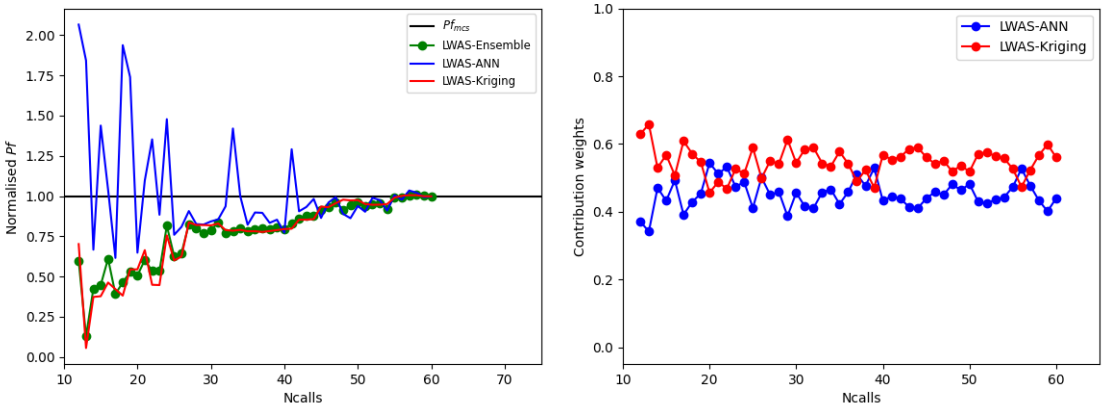

(a) Evolution of P$\hat{f}$ normalized by Pf_{mcs} (b) Contribution weights of Kriging and ANN

Figure 3.4 – Convergence curve of the proposed LWAS approach in example 1.

We can explain this by the fact that the Kriging model is an exact interpolator, where the predicted values at the observed input values are exactly equal to the observed output values. Hence, compared to the ANN model, the Kriging model may have closer performance to the proposed ensemble surrogate with the same enriched points. Compared with AK-MCS approach, the proposed LWAS approach is also more efficient to approximate the true probability of failure. Additionally, the convergence criterion of the proposed approach is related directly to the probability of failure, which can make the convergence faster.

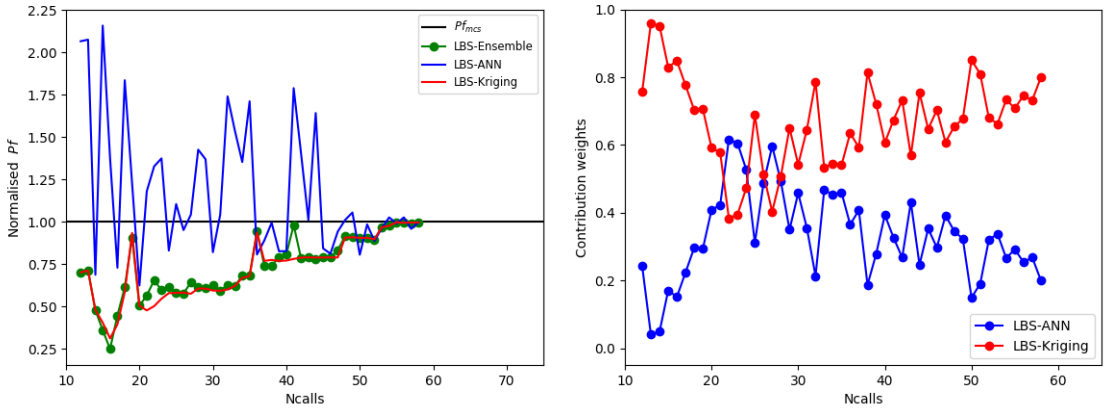

(a) Evolution of P$\hat{f}$ normalized by Pf_{mcs} (b) Contribution weights of Kriging and ANN

Figure 3.5 – Convergence curve of the proposed LBS approach in example 1.

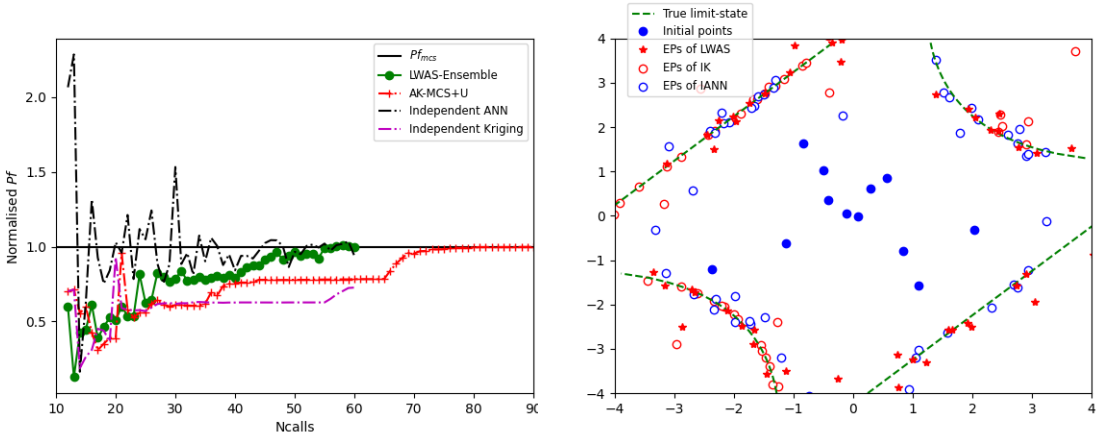

(a) Evolution of P$\hat{f}$ normalized by Pf_{mcs} (b) Comparison of the enriched points

Figure 3.6 – Comparison results of the proposed LWAS approach in example 1.

To better demonstrate the differences between the proposed LWAS approach, independent Kriging, and independent ANN model, the enriched points of these three models are depicted in Fig.3.6(b). The results show that the enriched points in the proposed LWAS are not only different from the independent Kriging model but also different from the independent ANN model. The enriched points in the independent ANN model can take into account all the limit states, but some points are far away from the true limit states. The independent Kriging model can only take into account some limit states in this example. That's why it cannot reach efficiently the true probability of failure in this example. However, the proposed LWAS approach can consider all the limit states and the enriched points are closer to the true

limit states.

3.5.2 Example 2: A highly nonlinear oscillator

A nonlinear oscillator as showed in Fig.3.7, consists of a non-linear undamped single degree of freedom system. The performance function is defined as [Echard et al., 2011, Schueremans and Van Gemert, 2005, Rajashekhar and Ellingwood, 1993, Xiao et al., 2018b]:

$$g\left(c_1, c_2, m, r, t_1, \mathrm{F}_1\right) = 3r - \left| \frac{2\mathrm{F}_1}{m\omega_0^2} \sin\left(\frac{\omega_0 t_1}{2}\right) \right| \tag{3.28}$$

with $\omega_0 = \sqrt{\frac{c_1+c_2}{m}}$. The six random variables are listed in Table 3.4. 12 initial points are generated for the proposed methods and AK-MCS using LHS. 10 neurons are used in the hidden layer of ANN model. 7×10^4 samples are generated by MCS to estimate the probability of failure. The average results of 10 repeated runs are compared in Table 3.5. Compared to AK-MCS approach, the proposed methods almost have the same accuracy but less than half the number of calls to the performance functions. Compared with complement-basis approach, the proposed two methods also outperform. It should be mentioned here, in the reference [Teixeira et al., 2020], complement-basis approach estimates the probability of failure with a smaller population size of 5×10^4. Usually, when the population size increases, the number of calls of the performance function will also increase. Fig.3.8 and Fig.3.9 show the iteration processes of the proposed approaches. In the proposed LWAS approach as illustrated in Fig.3.8, at the start, the ANN model seems to have more effect on the probability of failure. But after 16 function evaluations, the Kriging model has a greater contribution weight. In the proposed LBS approach. Similarly, the Kriging model will play a more important role after 16 function evaluations.

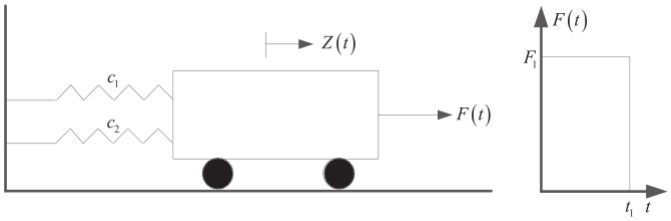

Figure 3.7 – A nonlinear oscillator.

Table 3.4 – Random variables in Example 2

Variable	Distribution	Mean	Standard deviation
m	Normal	1	0.05
c_1	Normal	1	0.1
c_2	Normal	0.1	0.01
r	Normal	0.5	0.05
F_1	Normal	1	0.2
t_1	Normal	1	0.2

Table 3.5 – Average results for the proposed methods, AK-MCS and MCS in 10 repeated runs and relative comparison with Complement-basis approach . * denoted the results reported in reference

Method	Pf(10^{-2})	CoV(%)	ε (%)	Ncall
MCS	2.888	2.19	-	7×10^4
AK-MCS+U	2.888	2.19	0.00	76.7
Complement-basis approach *[Teixeira et al., 2020]	2.846	2.61	0.20	43.1
Proposed LWAS approach	2.892	2.19	0.14	29.5
Proposed LBS approach	2.871	2.20	0.61	32.9

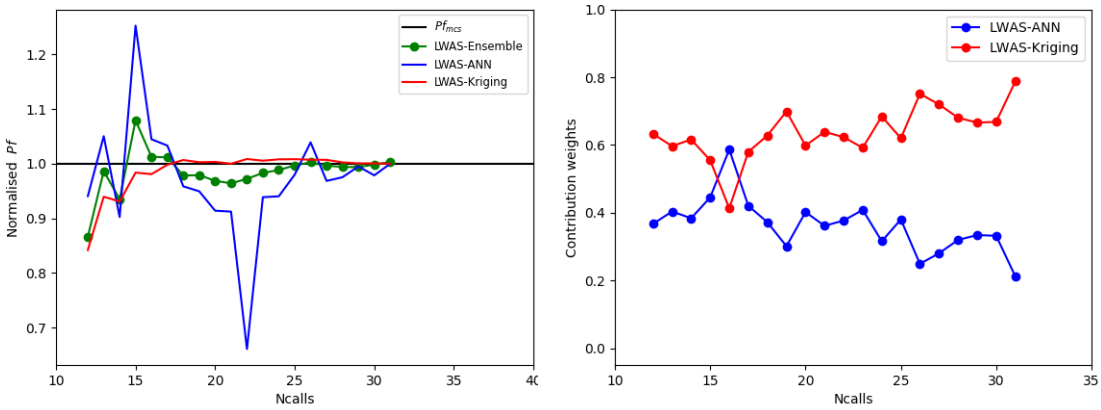

(a) Evolution of P$\hat{f}$ normalized by Pf_{mcs} (b) Contribution weights of Kriging and ANN

Figure 3.8 – Convergence curve of the proposed LWAS approach in example 2.

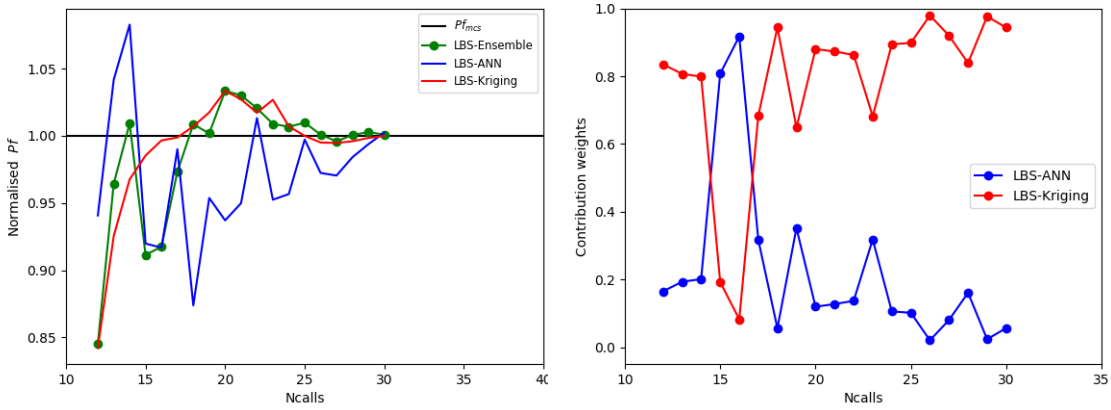

(a) Evolution of P$\hat{f}$ normalized by Pf_{mcs} (b) Contribution weights of Kriging and ANN

Figure 3.9 – Convergence curve of the proposed LBS approach in example 2.

3.5.3 Example 3: A cantilever tube

A cantilever tube as showed in Fig.3.10 is also a widely studied example in [Xiao et al., 2018b, Teixeira et al., 2020]. It is subjected to external forces F_1, F_2 P and torsion T. The performance function is given by:

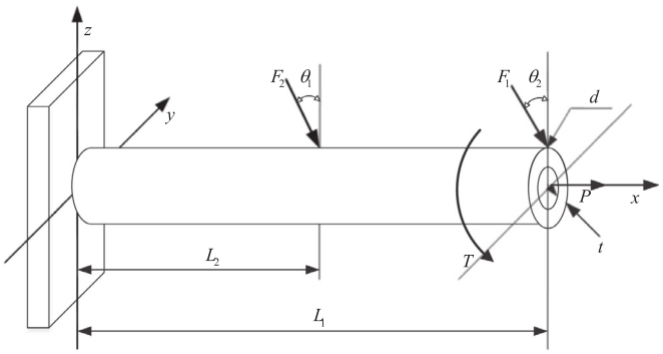

Figure 3.10 – A cantilever tube.

$$g = \mathrm{S}_y - \sqrt{\sigma_x^2 + 3\tau_{zx}^2}, \quad \text{with} \tag{3.29}$$

$$\sigma_x = \frac{\mathrm{P} + \mathrm{F}_1 \sin\theta_1 + \mathrm{F}_2 \sin\theta_2}{\mathrm{A}} + \frac{\mathrm{M}r}{\mathrm{I}} \tag{3.30}$$

$$\tau_{xz} = \frac{\mathrm{TD}}{2\mathrm{J}} \tag{3.31}$$

$$\mathrm{M} = \mathrm{F}_1 \mathrm{L}_1 \cos\theta_1 + \mathrm{F}_2 \mathrm{L}_2 \cos\theta_2 \tag{3.32}$$

$$\mathrm{A} = \frac{\pi}{4}\left[\mathrm{D}^2 - (\mathrm{D} - 2t)^2\right], \quad \mathrm{I} = \frac{\pi}{64}\left[\mathrm{D}^4 - (\mathrm{D} - 2t)^4\right], \quad r = \frac{\mathrm{D}}{2}, \quad \mathrm{J} = 2\mathrm{I} \tag{3.33}$$

11 random variables are involved in this example. Here, the distribution type of these 11 parameters are referenced in [Teixeira et al., 2020] are listed in Table 3.6. In this example, 12 initial points are generated for the proposed methods and AK-MCS using LHS. 20 neurons are considered in the hidden layers for the ANN model. 10^6 samples are generated by MCS to estimate the probability of failure. The average results of 10 repeated runs are compared in Table 3.7. The proposed methods are also more efficient than Complement-basis and AK-MCS approaches. Nearly half number calls to performance functions are required, compared with AK-MCS approach. The iteration processes of the proposed approaches are depicted in Fig.3.11 and Fig.3.12. The Kriging model appears to have a great contribution in this example. The ANN model, only at the start point, shows an important influence on the evaluation of the probability of failure. However, with enrichment of DoEs, the Kriging model starts to take the dominant places, which is more obvious in the proposed LBS approaches.

Table 3.6 – Random variables in example 3

Variable	Mean (Lower bound)	Standard deviation (Upper bound)	Distribution
t (mm)	5	0.1	Normal
D (mm)	42	0.5	Normal
L_1 (mm)	119.75	120.25	Uniform
L_2 (mm)	59.75	60.25	Uniform
F_1 (kN)	3	0.3	Normal
F_2 (kN)	3	0.3	Normal
P (kN)	12	1.2	Normal
T (N·m)	90	9	Gumbel
S_y (MPa)	210	21	Normal
θ_1 (°)	5	0.5	Normal
θ_2 (°)	10	1	Normal

Table 3.7 – Average results for the proposed methods, AK-MCS and MCS in 10 repeated runs and relative comparison with Complement-basis approach . * denoted the results reported in reference

Method	Pf(10^{-4})	CoV(%)	ε (%)	Ncall
MCS	4.767	4.58	-	1×10^6
AK-MCS+U	4.767	4.58	0.00	100.9
Complement-basis approach *[Teixeira et al., 2020]	4.304	4.82	0.88	83.6
Proposed LWAS approach	4.779	4.57	0.25	59.5
Proposed LBS approach	4.761	4.58	0.13	57

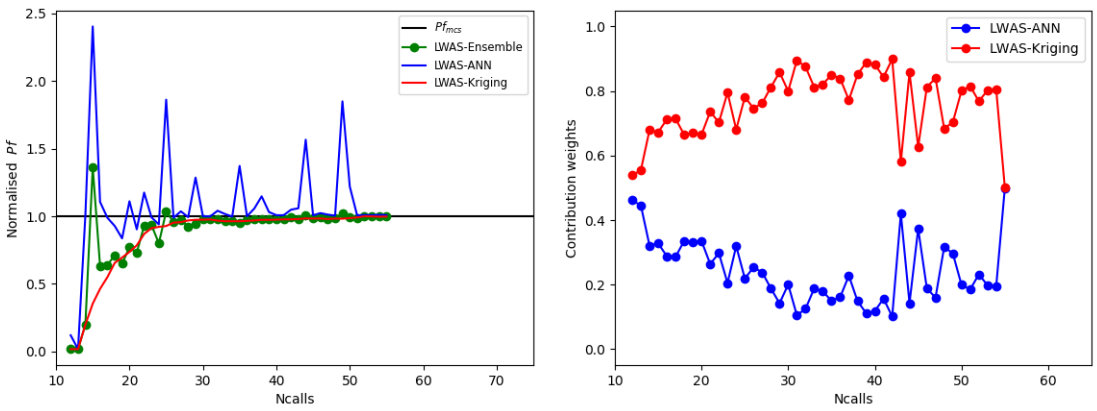

(a) Evolution of P$\hat{f}$ normalized by Pf_{mcs}

(b) Contribution weights of Kriging and ANN

Figure 3.11 – Convergence curve of the proposed LWAS approach in example 3.

Furthermore, to consider a rare event problem ($P_f \leqslant 10^{-5}$), the second case of this example is considered by taking a smaller standard deviation of the yield strength S_y. In the second case, only the standard deviation of the parameter (S_y) in Table 3.6 is changed to 16.8 and the other random variables rest the

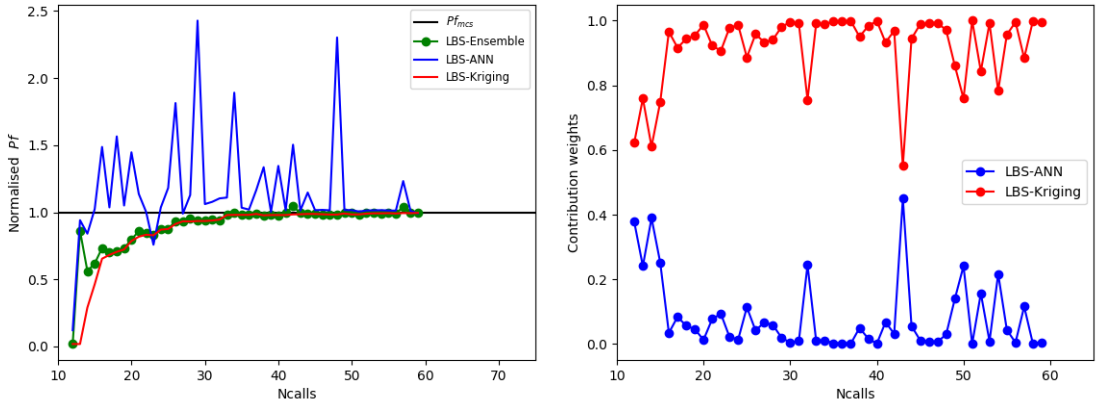

(a) Evolution of P$\hat{f}$ normalized by Pf_{mcs}

(b) Contribution weights of Kriging and ANN

Figure 3.12 – Convergence curve of the proposed LBS approach in example 3.

same as the original. The numbers of initial points and neurons in the hidden layers are the same as the first case. 10^7 samples are generated by MCS to estimate the probability of failure. The average results of 10 repeated runs are compared in Table 3.8. It is clear that the proposed approaches are also more efficient than AK-MCS method to estimate such a small probability of failure.

Table 3.8 – Average results for proposed methods, AK-MCS and MCS in 10 repeated runs.

Method	Pf(10^{-5})	CoV(%)	ε (%)	Ncall
MCS	4.429	4.75	-	1×10^7
AK-MCS+U	4.429	4.75	0.00	95.4
Proposed LWAS approach	4.417	4.76	0.27	58.2
Proposed LBS approach	4.436	4.75	0.16	55.8

3.5.4 Example 4: A high dimensional example

The fourth example with high dimension consists of an analytical performance function, where the number of variables can be changed without altering the level of failure probability. The performance function is defined as [Echard et al., 2011, Huang et al., 2016, Xiang et al., 2020]:

$$g(x_1,\ldots,x_n) = (n+3\sigma\sqrt{n}) - \sum_{i=1}^{n} x_i \tag{3.34}$$

where x_i are considered as lognormal random variables with unit mean and standard deviation of $\sigma = 0.2$; and n is the number of random variables. Two studies are performed on this example: 40 and 100 random variables. 12 initial points are generated for the proposed methods and AK-MCS by LHS in both two cases. The numbers of neurons in the hidden layer are respectively 20 and 50 for the first and

second case. 3×10^5 samples are generated by MCS to estimate the probability of failure.

The results are summarized in the Table 3.9. In the case with 40 random variables, only about 65 calls of the performance functions are required in the proposed methods to obtain the same probability of failure of MCS method. The AK-MCS approach needs about 120 calls to achieve the same accuracy. In the case with 100 random variables, the superiority of the proposed methods is also demonstrated, where about 150 calls are needed to achieve the same accuracy as crude MCS method compared to 170 calls in AK-MCS approach. But it seems that with the increase of dimension, the efficiency superiority of the proposed methods compared to AK-MCS will decrease a little. Additionally, the iteration processes of the proposed methods with 40 random variables are given in Fig.3.13 and Fig.3.14. The ANN models contribute more at the beginning of the iteration processes and have more contribution on the probability of failure on the proposed methods. With the enrichment of DoEs, the Kriging model starts to have a greater contribution weight in both two proposed approaches.

Table 3.9 – Average results for the proposed methods, AK-MCS and MCS in 10 repeated runs

Method	n	Pf(10^{-3})	CoV(%)	ε (%)	Ncall
MCS	40	1.829	4.26	-	3×10^5
	100	1.648	4.49	-	3×10^5
AK-MCS+U	40	1.829	4.26	0.00	121
	100	1.648	4.49	0.00	170.4
Proposed LWAS approach	40	1.826	4.27	0.19	65.7
	100	1.647	4.49	0.04	150.8
Proposed LBS approach	40	1.821	4.27	0.41	66.3
	100	1.647	4.50	0.06	148

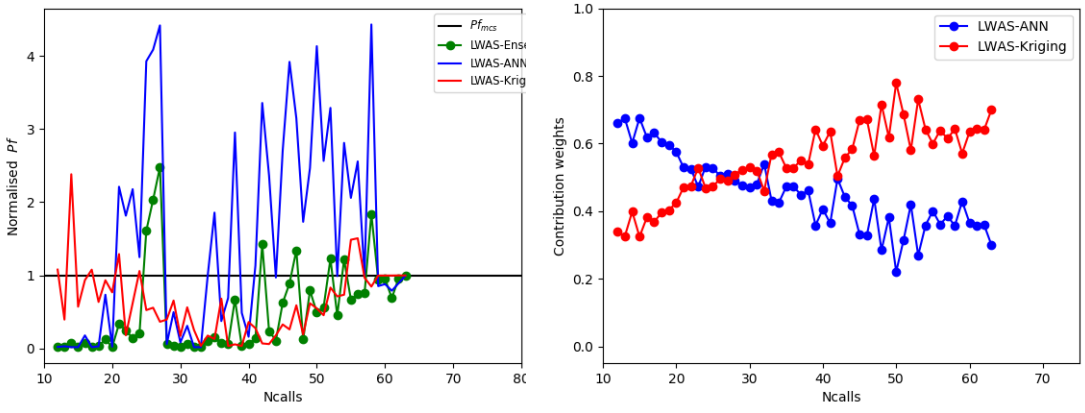

(a) Evolution of P$\hat{f}$ normalized by Pf_{mcs}

(b) Contribution weights of Kriging and ANN

Figure 3.13 – Convergence curve of the proposed LWAS approach in example 4 with 40 variables.

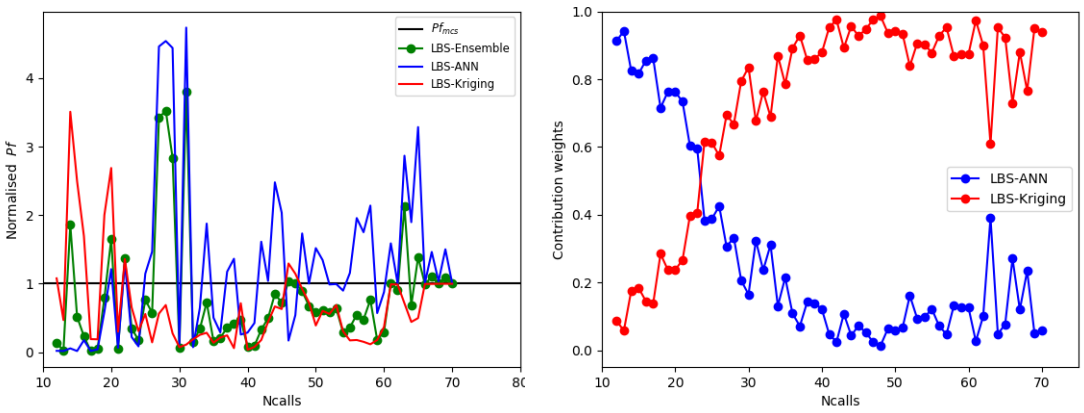

(a) Evolution of P$\hat{f}$ normalized by Pf_{mcs}

(b) Contribution weights of Kriging and ANN

Figure 3.14 – Convergence curve of the proposed LBS approach in example 4 with 40 variables.

Moreover, the influence of MCS population sizes on the convergence speed of the proposed methods in the case with 40 random variables is also investigated. With the increase of the population size from 3×10^5 to 1.5×10^6 samples, the average results in 10 repeated runs are plotted in Fig.3.15. It is clear that AK-MCS method is sensitive to the population size, whose convergence criterion depends directly on total sampling points. The total number of calls of the performance function will increase from about 120 to 160. However, the proposed approaches appear not sensitive to the population size. Only about 65 calls of the performance function are needed to reach a similar probability of failure as MCS method, even though with the increase of population sizes.

3.5.5 Example 5: An offshore wind turbine jacket

The fifth example is an engineering problem concerning an offshore wind turbine jacket referenced in OC4 project [Vorpahl et al., 2011]. The reliability of the jacket under one extreme load case (DLC 6.1b in the standard IEC-2009 [IEC, 2009]) is investigated. The jacket model is subjected to the loads from the wind turbine and the ocean (wave and current) loads. The loads from wind turbine are simulated by wind turbine tools (i.e. OpenFAST) and the wave and current loading are calculated in the finite element software (i.e. ANSYS). A reliability analysis is conducted considering the uncertainties of geometry, material, and load parameters based on the jacket model. There are 15 random variables as listed in Table 3.10. The limit state function is given by:

$$g(\mathrm{X}) = \sigma_m - \sigma_{max}(\mathrm{X}) \tag{3.35}$$

X denotes the random variables, where σ_m is the yield strength and σ_{max} is the maximum Von-Mises stress which depends on the first 14 variables in Table 3.10. The Von-Mises stress is simulated by finite element software ANSYS [ANSYS, 2017] as shown in Fig.3.16. The developed jacket model is modeled

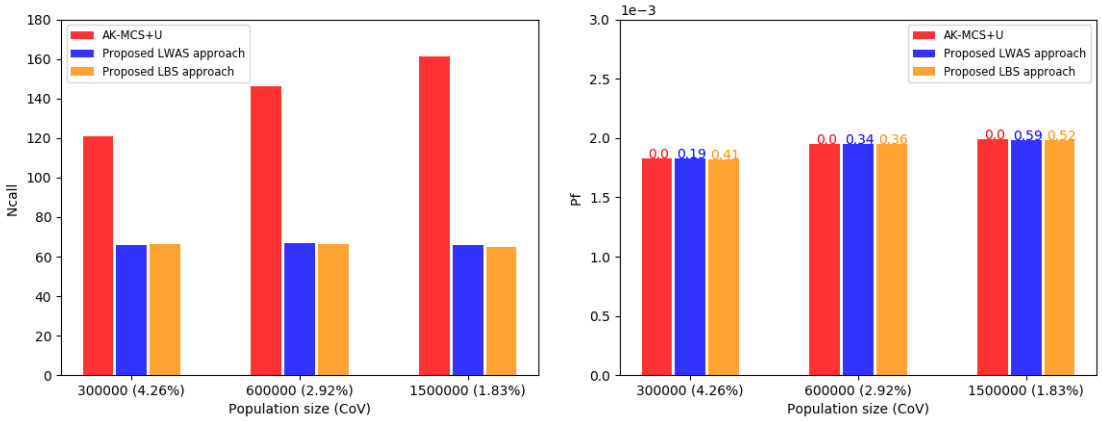

(a) Number of calls to functions

(b) Probability of failure

Figure 3.15 – Influences of different population sizes on the proposed approaches and AK-MCS. ε (%) is presented above the bars of P_f in (b).

by beam element and the mesh convergence results of the developed model is checked as shown in Table.3.11. In Table 3.10, the mean value of the loads (Fx, Fy, Fz, Mx, My, Mz) are calculated in wind turbine tool OpenFAST [Walatka et al., 1994]; the mean value of wave height (Hs), wave period (Tp) and current speed (Vc) are referenced in [Fischer et al., 2010]; the mean values of thicknesses ($T1, T2, T3, T4$) are the original ones of the jacket referenced in [Vorpahl et al., 2011] ; E is the Young modulus with the mean value equal to 210 GPa and σ_m is the yield strength of steel material with a mean value of 323 MPa. Here, all the parameters are assumed to follow the normal distribution with coefficients of variation (C_i).

Table 3.10 – Random variables with normal distribution in example 5

Variable	mean	Standard deviation
Fx (kN)	660	C_1*660
Fy (kN)	9	C_1*9
Fz (kN)	11851	C_1*11851
Mx (kN·m)	4479	C_1*4479
My (kN·m)	29368	C_1*29368
Mz (kN·m)	371	C_1*371
Hs (m)	10.34	C_2*10.34
Tp (s)	10.87	C_2*10.87
Vc (m/s)	1.2	C_2*1.2
T1 (mm)	50	C_3*50
T2 (mm)	20	C_3*20
T3 (mm)	35	C_3*35
T4 (mm)	40	C_3*40
E (GPa)	210	C_4*210
σ_m (MPa)	323	C_5*323

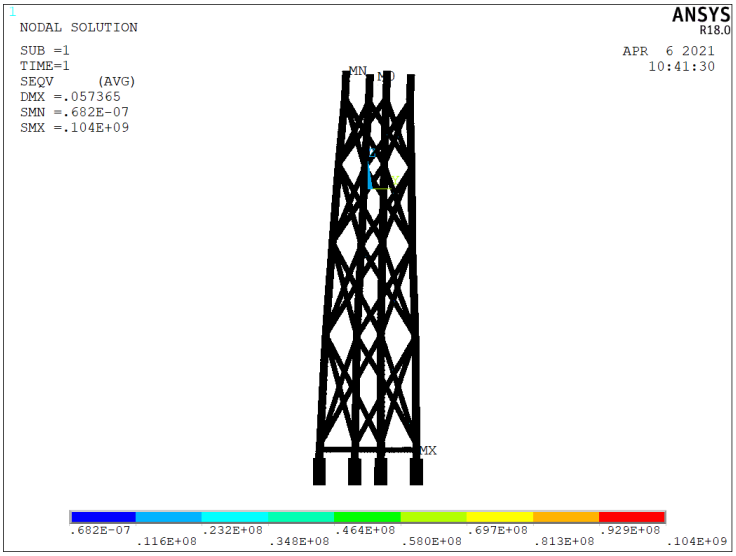

Figure 3.16 – Finite element analysis of the jacket model.

Table 3.11 – Mesh convergence results of the developed jacket model

Mesh size	Maximum stress(MPa)	Diff.(%)
1	103.54	-
refinement 1	105.73	2.12
refinement 2	106.30	0.54
refinement 3	106.49	0.18
refinement 4	106.52	0.03

According to standard codes [Veritas, 2004], the target reliability index of offshore wind turbine structure is typically 3.71, corresponding to a probability of failure 10^{-4}. To evaluate such a probability of failure, crude MCS approach will have a great computational burden. Hence, in this example, two cases are investigated with different values of C_i. In the first case, the thickness parameter (T_i) and material properties (E,σ_m) are given a bigger coefficient (C_i) to increase the probability of failure, in order to compare the proposed approaches with crude MCS approach. In the second case, the typical coefficients (C_i) are given for each variable. Only the results of the AK-MCS and the proposed approaches are compared. For the two cases, 30 initial samples are generated for the proposed methods and AK-MCS using LHS. The number of neurons in the hidden layer is set to 30 for both two cases. 5×10^4 samples generated by MCS are used to evaluate the probability of failure for the first case. Here, only one run is conducted due to the expensive computation of crude MCS with finite element analysis. In the second case, 3×10^6 samples are generated for the estimation of the probability of failure. The total computational time of the proposed approaches, AK-MCS, and MCS are also given in this example. The time calculation is based on an Intel(R) Core(TM) i7-8750H CPU @ 2.20GHz with a total memory of 32GB. The results are summarized in Table 3.12.

Table 3.12 – Results of the proposed approaches, AK-MCS and MCS

Method	Case 1: C_1=C_2=C_3=C_4=0.14, C_5=0.28				
	Pf(10^{-3})	CoV(%)	ε(%)	Ncall	CPU time(s)
MCS	8.72	4.77	-	5×10^4	864379
AK-MCS+U	8.70	4.77	0.23	301	2432
Proposed LWAS approach	8.64	4.79	0.92	165	1886
Proposed LBS approach	8.80	4.75	0.92	135	1351
Method	Case 2: C_1=0.25, C_2=0.1, C_3=0.03, C_4=0.08, C_5=0.2				
	Pf(10^{-4})	CoV(%)	ε(%)	Ncall	CPU time(s)
AK-MCS+U	3.00	3.33	-	532	33769
Proposed LWAS approach	2.98	3.34	-	241	20604
Proposed LBS approach	3.00	3.33	-	236	20209

It is clear that the proposed approaches are more efficient than AK-MCS method in both two cases. To achieve the same accuracy as MCS method in the first case, only about 165 and 135 calls of the performance functions are needed, which are nearly the half number calls of AK-MCS. The iteration process of the proposed methods are given in Fig.3.17 and Fig.3.18. It indicates that at the beginning Kriging model contributes more in both two proposed approaches. With the enrichment of DoEs, the contribution weights of ANN model gradually increase. At last, ANN model shows more influence on the predicted probability of failure, especially in the proposed LWAS approach. In the second case, the efficiency superiority of the proposed approaches is also observed. AK-MCS approach needs about 532 calls to finite element simulations. The proposed approaches need only about 236 (LBS approach) and 241 (LWAS approach) calls to finite element simulations. As mentioned in the previous examples, this is because the convergence criterion of AK-MCS method depends on each sample point. With a large population size, the calls of performance function will also increase in AK-MCS approach. As for the computational time, the proposed approaches need less CPU time to estimate the probability of failure and outperform in the both two cases, compared with crude MCS and AK-MCS approaches.

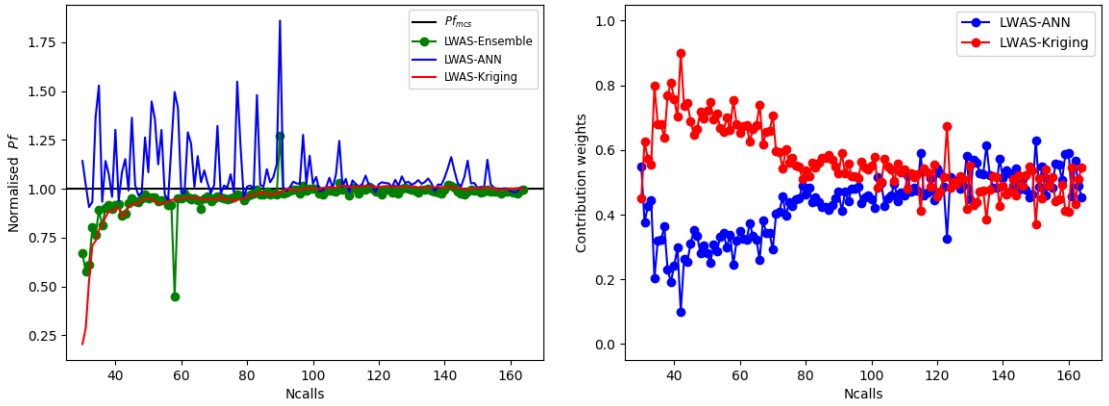

(a) Evolution of P$\hat{f}$ normalized by Pf_{mcs} (b) Contribution weights of Kriging and ANN

Figure 3.17 – Convergence curve of the proposed LWAS approach in the first case of example 5.

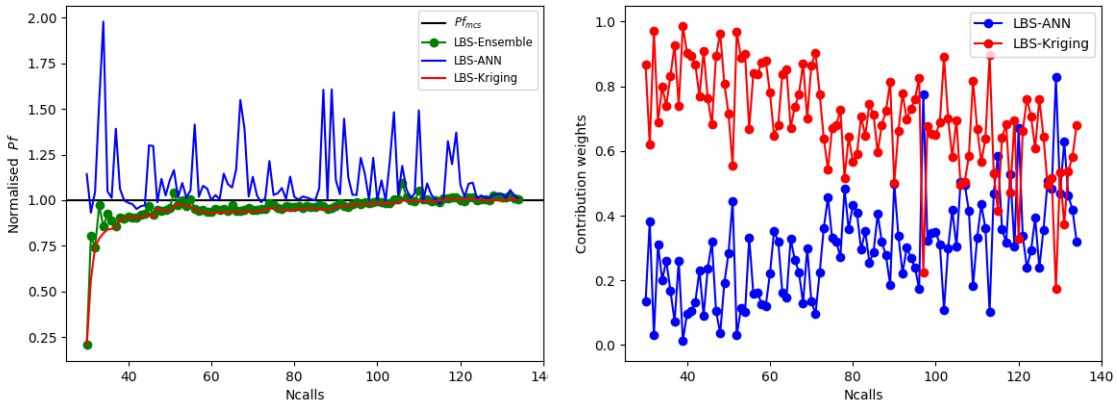

(a) Evolution of P$\hat{f}$ normalized by Pf_{mcs} (b) Contribution weights of Kriging and ANN

Figure 3.18 – Convergence curve of the proposed LBS approach in the first case of example 5.

3.6 Conclusions

In this chapter,the basic structures and principle of some classic surrogate models (Kriging, PCE and ANN) are also introduced. Furthermore, the basic principle of the ensemble surrogates are briefly discussed. More importantly, two approaches are proposed to assess the probability of failure with ensemble surrogate models based on the local goodness assessment. In the proposed approaches, classic cross-validation and Jackknife techniques are used to predict the errors of the surrogate models. Additionally, two methods are proposed to measure the local goodness of the surrogate models and estimate the prediction errors of the ensemble of surrogates. Moreover, two active learning approaches

are proposed based on the ensemble of surrogates with ANN and Kriging. Compared to other active learning approaches with ensemble of surrogate models [Cheng and Lu, 2020, Teixeira et al., 2020], the weights of the proposed LWAS approaches and the best surrogates of the proposed LBS approaches are directly associated with candidate samples and vary with each sample point. The efficiency and accuracy of the proposed approaches are validated by 4 benchmark examples and one finite element problems.

In the five examples, the proposed two approaches that combine kriging and artificial neural networks with local goodness measurement are efficient. In most cases, compared with AK-MCS, nearly half the number of calls of the performance function are required to reach a similar probability of failure as the crude MCS. There are two reasons for such a behavior, as mentioned above. First, the proposed approaches seems to be more efficient in approximating the true probability of failure than AK-MCS. Secondly, the stopping criterion of the proposed methods is directly related to the probability of failure. In addition, it should be noted that another advantage of the proposed methods is that they are not sensitive to the population sizes, when compared to AK-MCS approach. Moreover, compared with the ensemble of surrogates based on global goodness assessment, the proposed approaches also outperform in the most cases. The reason may be that the weight [Cheng and Lu, 2020] or the best (active) surrogate [Teixeira et al., 2020] fixed for all the candidate samples cannot select the updated points as efficiently as the proposed approaches.However, through the five numerical applications, the proposed ensemble surrogate approaches seem to have different numerical behaviors. In fact, this numerical behaviors of the proposed approaches depend on the number of initial sampling points, the position of these sampling points, the enriched points and the number of neurons in the hidden layer of the ANN model. For this reason, the contribution of the ANN and the Kriging models in the ensemble of surrogates can be different from one example to another, even in the same example when the initial sampling points are different.

Finally, it should be mentioned that the proposed approaches are not only suitable for combining Kriging and ANN but can also be extended to other surrogate models including PCE, SVR, etc. Future researches may focus on using the proposed active learning approaches in the ensemble of surrogates for time-dependent reliability problems.

Chapter 4

System reliability assessment with active learning Kriging approaches

Contents

4.1 Motivation

Wind energy has been considered as one of the most promising among renewable energies. In recent decades, wind energy has been experiencing rapid worldwide development [Manwell et al., 2010]. Europe and Asia already have installed a significant capacity of wind energy [Henderson et al., 2003, Sun et al., 2012]. Compared to land-based wind energy, there is more space and more stable and high wind speed for offshore wind energy. More and more offshore wind turbines are currently under construction or planned. These offshore wind farms are being installed with ever-larger turbines in deeper waters. The support structure has been identified as a vital contribution to cost-effective installations in deep water. Traditional monopile and tripod foundations are mainly used for shallow water of 20-30m. Jacket support structures have become the main support structures in deep water (50-100m), due to higher stiffness at the footprint and the smaller surface-facing ocean loads compared to the monopile structures.

Many research works have been done based on steel jacket structures. Dong et al.[Dong et al., 2011] at first did the long-term fatigue and fatigue reliability analysis of offshore wind turbine (OWT) jacket under different load cases in the time domain. And after, the effect of corrosion and inspection is also considered their works [Dong et al., 2012]. Wei et al [Wei et al., 2014, Wei et al., 2016, Wei et al., 2017] conducted a few studies about the jacket responses under extreme wind and wave loading. While, to accelerate the simulation, the jacket models are often modeling with beam elements in the above researches, which will over/underestimate the responses of the jackets especially in the joints of the jacket structures. For instance, the stress concentration exists in the joint parts of the offshore jackets, which can be found in many related works [Ahmadi and Lotfollahi-Yaghin, 2012, Ahmadi, 2016, Cheng et al., 2018]. However, the simulation of the jacket models with pure shell or solid elements is often much time-consuming. To keep joint flexibility and also reduce simulation time, Tu et al. [Tu et al., 2014], Vorpahl [Vorpahl, 2015] and Ren et al. [Ren et al., 2021] proposed to use super-element modeling techniques for a more accurate representation of joints in the jacket model. Thus, in this thesis, a jacket model (Super-element model) with the super-element modeling technique is developed. In addition, another jacket model (beam model) with beam elements is also developed. The stress concentration phenomenon of the joints in the jacket model is investigated, compared with the beam and the super-element models.

Furthermore, for the reliability analysis, the system might consist of only a single component that is subject to multiple different failure mechanisms (e.g. stress and buckling in a mechanical component), or it might be made up of multiple components. The analysis of such systems is called system reliability analysis (SRA) where multiple failure modes are considered, as opposed to component reliability analysis (CRA) where only a single failure mode is considered. Generally, there are three common approaches used for the reliability assessment. The sampling-based approaches (e.g.MCS) are easy to use. but it requires too many evaluations of the performance functions. To improve the efficiency of MCS, various variance reduction techniques such as IS [Glynn and Iglehart, 1989], LS [de Angelis et al., 2015], SS [Au and Beck, 2001] were developed. However, these methods inherit the disadvantages of MCS,

they still need thousands of function evaluations. For the analytical approach, the first/second-order methods (FORM/SORM) were proposed to solve the CRA or SRA problems. Although the number of the limit state functions evaluations decreased a lot, the inaccuracy of FORM and SORM methods cannot be guaranteed when facing highly nonlinear problems.

In recent decades, surrogate models-based approaches for reliability assessment have gained much attention. The basic idea is to replace the computationally expensive simulation by constructing a surrogate model (also known as metamodel), such as response surface (RS) [Roussouly et al., 2013], artificial neural network (ANN)[Hurtado and Alvarez, 2001] and Kriging model [Kaymaz, 2005]. Additionally, the strategy of constructing a surrogate model can generally be classified into (1) non-adaptive and (2) adaptive (active learning) approaches. The non-adaptive methods need to generate all sample points in advance and construct a surrogate model to ensure accuracy over the entire uncertainty space, which can be found in some works of offshore jacket structure reliability assessment [Shittu et al., 2020, Ivanhoe et al., 2020, Chao et al., 2021]. Ivanhoe et al. [Ivanhoe et al., 2020] used least-squared regression for reliability assessment of an offshore wind turbine jacket. REN et al.[Chao et al., 2021] conducted the reliability assessment of the offshore wind turbine jacket with ANN considering corrosion effect. While the reliability analysis with active learning approaches in the offshore wind turbine structures cannot be found in the literature. Active learning methods [Bichon et al., 2008, Echard et al., 2011, Bourinet, 2016, Zhang et al., 2019] only select one or a few sample points at each iteration to construct the surrogate model more efficiently. Therefore, active learning approaches are generally more efficient than non-adaptive surrogate methods. Moreover, many active learning approaches [Bichon et al., 2011, Fauriat and Gayton, 2014, Zhou et al., 2020, Jiang et al., 2020] have been developed for system reliability assessment. In these approaches, the active learning approaches with Kriging model are much popular. Hence, in this work, Kriging-based active learning approaches are used to solve SRA problems.

However, for the most active learning approaches, they are always facing the high dimension problem also known as the "curse of dimension". With the increase of the dimension of the random parameters, the efficiency of active learning approaches will decrease a lot. To tackle this challenge, sensitivity analysis can be used to reduce stochastic dimensions. The sensitivity analysis (SA) is widely used to quantify the effects of random parameters on the model responses and reduce the stochastic dimensions of the reliability analysis. Over the few decades, many global sensitivity analysis (GSA) techniques [Morris, 1991, Sobol, 2001, Campolongo et al., 2007, Kucherenko and Song, 2016, Papaioannou and Straub, 2021] have been developed. Additionally, the global sensitivity analysis of offshore wind turbines can also be noticed in many related works[Hübler et al., 2017b, Velarde et al., 2019a, Ren et al., 2020]. Hulbler et al.[Hübler et al., 2017b] proposed a hierarchical four-step global sensitivity analysis of offshore turbines. It is found that, for different offshore support structures, only a small parameter subset is influential. Velarde et al.[Velarde et al., 2019a] also conducted a global sensitivity of offshore wind turbine foundation under fatigue loads using linear regression of Monte Carlo simulation and Morris screening method.

It concluded that the parameter significance may vary with different design load cases. More recently, Ren et al. [Ren et al., 2020] did the global sensitivity analysis of an offshore wind turbine jacket structure with Morris screening and Fourier amplitude sensitivity test methods. The results showed that ultimate stresses in different parts of jacket structures were affected by different parameters. In this work, Morris screening method [Morris, 1991, Campolongo et al., 2007] is used here for global sensitivity analysis to reduce random parameter dimensions considering ultimate load cases. The non-influential parameters will be considered deterministic variables for reliability assessment.

In this chapter, at first, the reliability analysis with active learning Kriging model is presented in section 4.2. Section 4.3 presents the system reliability analysis approaches with active learning Kriging approaches. Section 4.4 presents problem of AK-SYS and AK-SYSi and proposes a new composite learning function for the system reliability analysis. The adaption H learning function for the system reliability analysis are in section 4.5. The examples and applications of are given section 4,6. The application on offshore wind turbine jacket is given in 4.7. The conclusions are given section 4.8.

4.2 Active learning Kriging approaches for component reliability analysis

The application of the Kriging model is also classified into two approaches (1).Non-adaptive approaches (2).Adaptive Kriging approaches. The non-adaptive methods need to generate all sample points in advance and construct a surrogate model to ensure accuracy over the entire uncertainty space, which can be found in some works of offshore jacket structure reliability assessment [Shittu et al., 2020, Ivanhoe et al., 2020, Chao et al., 2021]. Active learning methods [Bichon et al., 2008, Echard et al., 2011, Bourinet, 2016, Zhang et al., 2019] only select one or a few sample points at each iteration to construct the surrogate model more efficiently. Therefore, active learning approaches are generally more efficient than non-adaptive surrogate methods. Among these approaches, the active learning approaches with Kriging model are very popular. The general process of the active learning approach with Kriging model is as shown in Fig.4.1. The key point of the active learning Kriging is to define the learning function and the stopping condition. In this section, some popular learning functions are summarized.

4.2.1 Learning function EFF

The learning function EFF is proposed by [Bichon et al., 2008] and measures how well the true value of the performance function at a point is expected to satisfy the limit state equation over a given region,

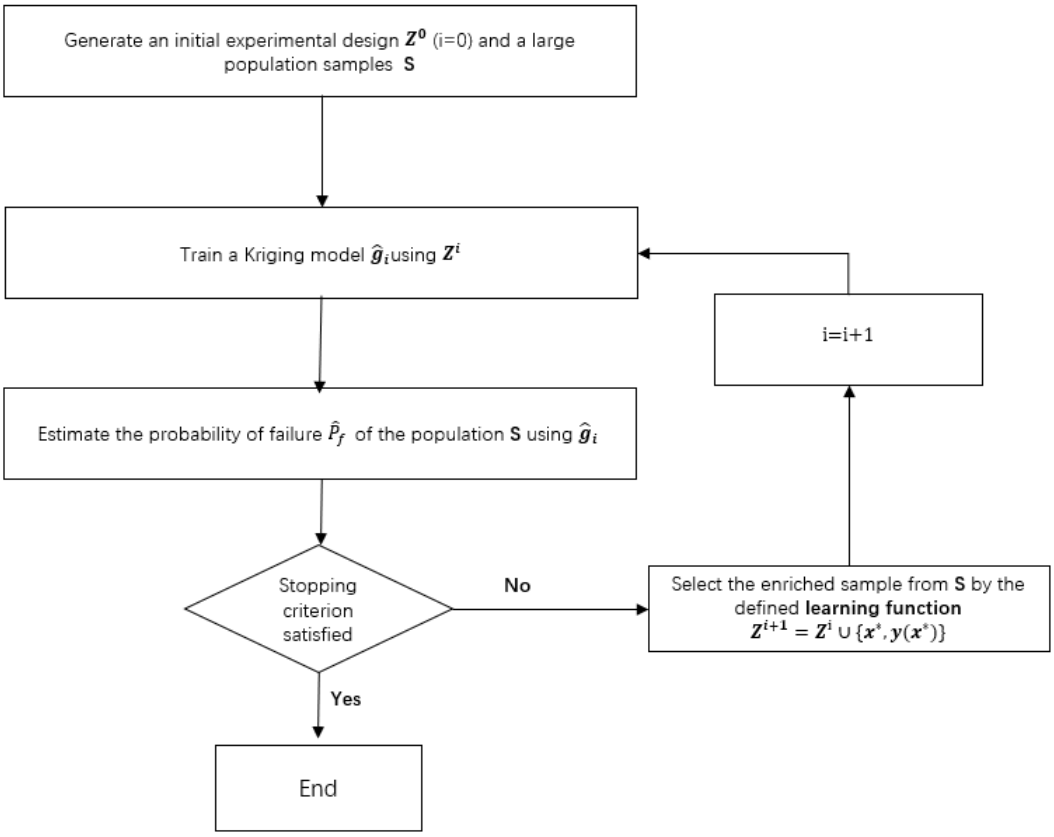

Figure 4.1 – Active learning approaches with Kriging model

which has the following expression.

$$\begin{aligned}\mathrm{EFF}(x) = \mu_{\hat{g}}(x)\left[2\Phi\left(\frac{-\mu_{\hat{g}}(x)}{\sigma_{\hat{g}}(x)}\right) - \Phi\left(\frac{-\varepsilon\mathrm{EFF}(x) - \mu_{\hat{g}}(x)}{\sigma_{\hat{g}}(x)}\right) - \Phi\left(\frac{\varepsilon\mathrm{EFF}(x) - \mu_{\hat{g}}(x)}{\sigma_{\hat{g}}(x)}\right)\right] \\ -\sigma_{\hat{g}}(x)\left[2\phi\left(\frac{-\mu_{\hat{g}}(x)}{\sigma_{\hat{g}}(x)}\right) - \phi\left(\frac{-\varepsilon\mathrm{EFF}(x) - \mu_{\hat{g}}(x)}{\sigma_{\hat{g}}(x)}\right) - \phi\left(\frac{\varepsilon\mathrm{EFF}(x) - \mu_{\hat{g}}(x)}{\sigma_{\hat{g}}(x)}\right)\right] \\ +\varepsilon_{\mathrm{EFF}}(x)\left[\Phi\left(\frac{\varepsilon\mathrm{EFF}(x) - \mu_{\hat{g}}(x)}{\sigma_{\hat{g}}(x)}\right) - \Phi\left(\frac{-\varepsilon_{\mathrm{EFF}}(x) - \mu_{\hat{g}}(x)}{\sigma_{\hat{g}}(x)}\right)\right]\end{aligned} \tag{4.1}$$

where $\mu_{\hat{g}}(x)$ and $\sigma^2_{\hat{g}}(x)$ are respectively the prediction mean value and variance of the Kriging model. $\phi(\cdot)$ is the PDF of standard normal variable, $\varepsilon_{\mathrm{EFF}}(x) = 2\sigma_{\hat{g}}(x)$ is the threshold function. $\mathrm{EFF}(x)$ gets to be large when the point is close to the limit state equation or the predicted variance is large. Therefore, the point that can maximize the response of $\mathrm{EFF}(x)$ is always selected to be the best new training sampling. The stopping condition of learning function $\mathrm{EFF}(x)$ is often set to be $\max\{\mathrm{EFF}(x)\} \leq 0.001$.

4.2.2 Learning function U

The learning function U is proposed by [Echard et al., 2011] and quantifies the misclassification probability of the sign of the prediction. The probability of making a wrong sign estimation is given by:

$$\mathrm{P}_{\text{sign}}(\boldsymbol{x}) = \Phi\left(-\frac{\left|\mu_{\hat{g}}(\boldsymbol{x})\right|}{\sigma_{\hat{g}}(\boldsymbol{x})}\right) \tag{4.2}$$

where $\Phi(\cdot)$ represents the Cumulative Distribution Function (CDF) of a standard normal variable. Normally, the following U function is used to substitute the misclassification probability.

$$\mathrm{U}(x) = \frac{\left|\mu_{\hat{g}}(x)\right|}{\sigma_{\hat{g}}(x)} \tag{4.3}$$

The point that minimizes $\mathrm{U}(x)$ has the most probability to make a wrong sign estimation and thus it is the best point to refine the surrogate model. The stopping criterion of the learning function $\mathrm{U}(x)$ is often set to be $\min\{\mathrm{U}(x)\} \geq 2$, which represents that the probability of making wrong sign estimation is less than $\Phi(-2) \approx 0.023$. The active learning Kriging approach with U function is also named AK-MCS, which is commonly used for research and study. An overall process of AK-MCS approach with U function is detailed in Algorithm 4.1.

Algorithm 4.1 AK-MCS: Active learning Kriging approaches with Monte Carlo simulation

Input: Generate a small number (N_{call}) of initial samples $\mathrm{X}_{\mathrm{DoE}}$ by LHS and compute the related $\mathrm{Y}_{\mathrm{DoE}}$;
Generate a large number of population **S** by MCS for the failure probability estimation.

while $\mathrm{U}_{min} \leqslant 2$ **do**:
  (Train Kriging model and get the prediction values)
  Train Kriging model with $\mathrm{X}_{\mathrm{DoE}}$ and $\mathrm{Y}_{\mathrm{DoE}}$;
  Predict the values ($\mu_{\hat{g}}$ and $\sigma_{\hat{g}}$) of all the samples **S** with the current Kriging;
  (Get the probability of failure in current Kriging model)
  Estimate the probability of failure ($\mathrm{P}f$) based on the Kriging prediction $\mu_{\hat{g}}$;
  (Select the new added point and the minimum value of U function)
  Calculate the U values for all the samples;
  Select the new sample x_u that has the minimum U value (U_{min}) and get the true response y_u;
  Enrich respectively $\mathrm{X}_{\mathrm{DoE}}$ and $\mathrm{Y}_{\mathrm{DoE}}$ with x_u and y_u
  N_{call}=N_{call}+1
end while

Output: Get the probability value of ensemble surrogate model $\mathrm{P}f$
Get the total number of calls to the performance functions (N_{call})

4.2.3 Learning function H

The learning function H is proposed by [Lv et al., 2015], which is based on the information entropy theory and is used to measure the uncertainty of the prediction. The prediction is more certain when the

information entropy is lower, The learning function H is expressed by .

$$H(x) = \left| \begin{array}{l} \ln\left(\sqrt{2\pi}\sigma_{\hat{g}}(x) + \frac{1}{2}\right)\left[\Phi\left(\frac{\varepsilon_H(x)-\mu_{\hat{g}}(x)}{\sigma_{\hat{g}}(x)}\right) - \Phi\left(\frac{-\varepsilon_H(x)-\mu_{\hat{g}}(x)}{\sigma_{\hat{g}}(x)}\right)\right] \\ -\left[\frac{\varepsilon_H(x)-\mu_{\hat{g}}(x)}{2}\phi\left(\frac{\varepsilon_H(x)-\mu_{\hat{g}}(x)}{\sigma_{\hat{g}}(x)}\right) + \frac{\varepsilon_H(x)+\mu_{\hat{g}}(x)}{2}\phi\left(\frac{-\varepsilon_H(x)-\mu_{\hat{g}}(x)}{\sigma_{\hat{g}}(x)}\right)\right] \end{array} \right| \tag{4.4}$$

where $\varepsilon_H(\boldsymbol{x}) = 2\sigma_{\hat{g}}(\boldsymbol{x})$ is the threshold function. The point that maximizes the response of $H(x)$ is chosen to be the new training sample to refine the surrogate model in each iteration. Lv et al.[Lv et al., 2015] concluded that it is reasonable to define the stopping criterion as $\max\{H(x)\} \leq 1$ or a smaller one for higher precision and $\max\{H(x)\} \leq 0.5$ is used.

4.2.4 Other learning functions

More recently, some other learning function based Kriging model are also developed [Sun et al., 2017, Zhang et al., 2019, Shi et al., 2020]. The learning function LIF [Sun et al., 2017] measures how much the estimation accuracy of the failure probability will be improved if a new training point is added to update the surrogate model, which takes the joint PDF of the random input vector into account. The learning functions REIF and REIF2 [Zhang et al., 2019] are proposed to construct folded normal distribution of prediction, which is based on the theory that the point satisfying the equation $|\hat{g}(x)| = 0$ can be used to update the surrogate model. The learning function FNEIF [Shi et al., 2020] measures the contribution degree of a point to the approximate limit state equation improvement of surrogate model in view of folded normal distribution. The details of these learning functions and the related stopping criterion can be found in [Shi et al., 2020]. However, for a given problem, it is also hard to figure out which learning function is more suitable. It is up to the users to try it out and no learning function can be guaranteed to work for all problems.

4.3 Active learning Kriging approaches for system reliability analysis

The above learning functions are typically used for the component reliability analysis. However, for the system reliability analysis, the active learning Kriging approaches can be different. Three common approaches [Bichon et al., 2011, Fauriat and Gayton, 2014] for adaptation component reliability analysis to system reliability analysis are summarized in the following subsection. Also, the classical active learning Kriging approaches for system reliability analysis are briefly introduced.

4.3.1 Adaptation component reliability analysis to system reliability analysis with active learning Kriging approaches

Component solutions

The first and easiest strategy is estimate system probability of failure to carry out the classification of the population using a surrogate model of each failure mode. This probability is then estimated through the number of failed configurations of the system with respect to the total number of simulations. First,

a Kriging model is trained on the initial design of experiments for each performance function. Then the active learning on each model is performed with the learning function, for example with U learning function:

$$\mathrm{U}_j(\mathbf{x}) = \frac{\left|\hat{g}_j(\mathbf{x})\right|}{\sigma_{\hat{g}_j(\mathbf{x})}} \tag{4.5}$$

This technique may be extended to system that are not simple series or parallel arrangements. However, consider the case where one (or more) component limit state does not contribute to the system probability of failure because the system probability of failure violating this limit state is much smaller than that of other components. In such a case, the effort spent constructing the Kriging model for this performance function is essentially wasted. Hence, the efficiency of this approach can be further improved.

Composite limit state

In the second approach, rather than construct an independent Kriging model for each of the components, now we try to train a single Kriging model to capture the so-called "composite" limit state. The system problem is converted into a single component reliability problem. g_{com} being the composite performance function is defined as follows:

$$\begin{aligned} g_{com}(\mathbf{X}) &= \max_{j=1,\ldots,p} g_j(\mathbf{X}) \quad \text{for parallel systems} \\ g_{com}(\mathbf{X}) &= \min_{j=1,\ldots,p} g_j(\mathbf{X}) \quad \text{for series systems} \end{aligned} \tag{4.6}$$

where p is the total number of limit state functions. The problem with this approach is that it is necessary to fit a Kriging model to a performance that may be highly irregular, especially around the intersection of different limit states. The stopping condition being very hard to reach, it can generate intensive calculation.

$$\min_{i=1,\ldots,\mathrm{N_{MC}}} \mathrm{U}_{com}\left(\mathbf{x}^{(i)}\right) = \min_{i=1,\ldots,\mathrm{N_{MC}}} \frac{\left|\hat{g}_{comp}\left(\mathbf{x}^{(i)}\right)\right|}{\sigma_{\hat{g}_{comp}(\mathbf{x}^{(i)})}} \geq 2 \tag{4.7}$$

Composite learning function

The third approach is so-called "composite learning function". The first step is to compute the Kriging model on the initial DoE. Then, the active learning is only performed on the performance functions that influence the system failure domain. The composite learning function with AK-SYS [Fauriat and Gayton, 2014] is defined as:

$$\mathrm{U}_s\left(\mathbf{x}^{(i)}\right) = \frac{\left|\hat{g}_{\mathrm{S}}\left(\mathbf{x}^{(i)}\right)\right|}{\sigma_{\hat{g}_s(\mathbf{x}^{(i)})}} \tag{4.8}$$

where s is the index of the performance function that minimizes $\hat{g}_j(\mathbf{x}^{(i)})$, for $j = 1,\ldots,p$, at a given point $\mathbf{x}^{(i)}$, for a series system of p failure modes (or maximizes it for a parallel systems). At this point $\mathbf{x}^{(i)}$, only

the true performance function g_s is evaluated and added for the calculation of the Kriging model $\hat{g}_s$. The advantage given by this approach is that no calls (or at most a small number) will be made to true performance functions that have little on the system failure domain.

4.3.2 Classical active learning Kriging approaches for the system reliability analysis

From the study of [Bichon et al., 2011, Fauriat and Gayton, 2014], the composite learning function can be seen as a better approach for system reliability analysis with active learning approaches. In this subsection, some typical active learning Kriging approaches used for system reliability analysis are summarized:

EGRA-SYS

Efficient global reliability analysis for system reliability analysis was introduced in Ref. [Bichon et al., 2011], which is based on the expected feasible function (EFF). The composite EFF is now written as:

$$\begin{aligned}\mathrm{EFF}(\mathbf{x}) = &\left(\mu_{\mathbf{g}}^{*} - \bar{z}\right)\left[2\Phi\left(\frac{\bar{z}-\mu_{\mathrm{g}}^{*}}{\sigma_{\mathrm{g}}^{*}}\right) - \Phi\left(\frac{z^{-}-\mu_{\mathrm{g}}^{*}}{\sigma_{\mathrm{g}}^{*}}\right) - \Phi\left(\frac{z^{+}-\mu_{\mathrm{g}}^{*}}{\sigma_{\mathrm{g}}^{*}}\right)\right] \\ &- \sigma_{\mathrm{g}}^{*}\left[2\phi\left(\frac{\bar{z}-\mu_{\mathrm{g}}^{*}}{\sigma_{\mathrm{g}}^{*}}\right) - \phi\left(\frac{z^{-}-\mu_{\mathrm{g}}^{*}}{\sigma_{\mathrm{g}}^{*}}\right) - \phi\left(\frac{z^{+}-\mu_{\mathrm{g}}^{*}}{\sigma_{\mathrm{g}}^{*}}\right)\right] \\ &+ \varepsilon\left[\Phi\left(\frac{z^{+}-\mu_{\mathrm{g}}^{*}}{\sigma_{\mathrm{g}}^{*}}\right) - \Phi\left(\frac{z^{-}-\mu_{\mathrm{g}}^{*}}{\sigma_{\mathrm{g}}^{*}}\right)\right]\end{aligned} \tag{4.9}$$

where $\bar{z}$ is a constant and ε is proportional to the standard deviation of the Kriging model. z^{-} and z^{+} are respectively denoted $\bar{z}\pm\varepsilon$. The selection of the mean value used in the composite EFF μ_{g}^{*} depends on the type of system and the definition of failure for the components as shown in Table. 4.1. The value used for the composite standard deviation, σ_{g}^{*}, is then the standard deviation from the corresponding model i that maximized/minimized the function in Table.4.1.

Table 4.1 – Selection of the composite mean value among the component Kriging models

System type	$g_i \leq 0$	$g_i \geq 0$
Parallel	$\mu_{\mathrm{g}}^{*} = \max\left[\mu_{\mathrm{g}}^{i}\right]$	$\mu_{\mathrm{g}}^{*} = \min\left[\mu_{\mathrm{g}}^{i}\right]$
Series	$\mu_{\mathrm{g}}^{*} = \min\left[\mu_{\mathrm{g}}^{i}\right]$	$\mu_{\mathrm{g}}^{*} = \max\left[\mu_{\mathrm{g}}^{i}\right]$

Once the point $\mathbf{x}$ which maximizes the function EFF($\mathbf{x}$) is found, the EFF value for each of the components is calculated at this point. Only the component with a non-converged EFF value are evaluated and added to that component's Kriging training data. The stopping condition is that the maximum composite expected feasibility is less than a specified tolerance (i.e. max(EFF) < 0.0001)

AK-SYS

The AK-SYS method [Fauriat and Gayton, 2014] is an adaptation of the AK-MCS method for system reliability, which is based on U learning function. The composite U function is expressed as:

$$\mathrm{U}(\mathbf{x}) = \frac{|\mu_{\mathrm{g}}^*|}{\sigma_{\mathrm{g}}^*} \tag{4.10}$$

The selection of the mean value of Kriging prediction is defined as the following. The value used for the composite standard deviation, σ_{g}^*, is then the standard deviation from the corresponding model i. The stopping criterion of learning function $\mathrm{U}(\mathbf{x})$ is often set to be $\min\{\mathrm{U}(\mathbf{x})\} \geq 2$. An overall process of AK-SYS approach for series system is detailed in Algorithm 4.2.

$$\begin{aligned} \mu_{\mathrm{g}}^* &= \max(\mu_g^i) \quad i = 1 \ldots p \quad \text{for parallel system} \\ \mu_{\mathrm{g}}^* &= \min(\mu_g^i) \quad i = 1 \ldots p \quad \text{for series system} \end{aligned} \tag{4.11}$$

Algorithm 4.2 AK-SYS: an adaption of AK-MCS for system reliability analysis

Input: Generate a small number (N_{call}) of initial samples $\mathrm{X}_{\mathrm{DoE}}$ by LHS and compute the related values for each failure mode (i) $\mathrm{Y}^i_{\mathrm{DoE}}$ and note that N^i_{call}=N_{call} and $\mathrm{X}^i_{\mathrm{DoE}}$=$\mathrm{X}_{\mathrm{DoE}}$;
Generate a large number of population **S** by MCS for the failure probability estimation.

1: **while** $\mathrm{U}_{min} \leqslant 2$ **do**:
2: **(Train Kriging model and get the prediction values in each failure mode)**
3: Train Kriging models ($\hat{g}^i$) with $\mathrm{X}^i_{\mathrm{DoE}}$ and $\mathrm{Y}^i_{\mathrm{DoE}}$;
4: Predict the values ($\mu^i_{\hat{g}}$ and $\sigma^i_{\hat{g}}$) of all the samples **S** with $\hat{g}^i$;
5: **(Get the system probability of failure)**
6: For the series system, search minimum value $\mu^j_{\hat{g}}(x) = min(\mu^i_{\hat{g}}(x))$ with x in the samples S,
7: where j is the failure mode number that has the minimum prediction value at the sample x;
8: The related standard deviation of $\mu^j_{\hat{g}}$ is denoted $\sigma^j_{\hat{g}}$;
9: Get the system probability of failure $\mathrm{P}f_{sys}$ based on $\mu^j_{\hat{g}}$;
10: **(Select the new added point, the minimum value of U function and the related failure mode)**
11: Calculate the U values for all the samples with $\mu^j_{\hat{g}}$ and $\sigma^j_{\hat{g}}$;
12: Select the new sample x^j_u that has the minimum U value (U_{min}) and get the true response y^j_u;
13: Enrich respectively $\mathrm{X}^j_{\mathrm{DoE}}$ and $\mathrm{Y}^j_{\mathrm{DoE}}$ with x^j_u and y^j_u
14: N^j_{call}=N^j_{call}+1
15: **end while**

Output: Get the probability value of ensemble surrogate model $\mathrm{P}f_{sys}$
Get the total number of calls to the performance functions (sum(N^i_{call}))

AK-SYSi

The AK-SYSi method [Yun et al., 2019] proposed an improved AK-SYS by using a refined U learning function. The AK-SYSi method updates the Kriging meta-model from the most easily identifiable failure mode among the multiple failure modes and this strategy can avoid identifying the minimum mode or

the maximum mode by the initial and the in-process Kriging model. For a series system, only if one mode among all the failure modes is failed, the system is failed. All the modes are safe, so the system is safe. Therefore, for system safe state,the states of all modes are accurately identified. For system failed state, just one mode in the failure state is accurately identified (if more than one mode are in failed states.) Thus, the refined composite U function for series system is defined as:

$$\begin{aligned} \mathrm{U}(\mathbf{x}) &= \min \frac{\left|\mu_g^i\right|}{\sigma_g^i} \text{ If } \mu_g^i > 0 \ \forall i = 1, \dots p \\ \mathrm{U}(\mathbf{x}) &= \max \frac{\left|\mu_g^i\right|}{\sigma_g^i} \text{ If } \mu_g^i \leq 0 \ \exists i = 1, \dots p \end{aligned} \tag{4.12}$$

For the parallel system, only if one mode is safe state, the system is safe. All the modes are failed, the system is failed. Therefore, for safe system state, only one safe mode is accurately identified. For system failed state, the states of all the modes are accurately identified. Thus,the refined composite U function for series system is defined as:

$$\begin{aligned} \mathrm{U}(\mathbf{x}) &= \min \frac{\left|\mu_g^i\right|}{\sigma_g^i} \text{ If } \mu_g^i < 0 \ \forall i = 1, \dots p \\ \mathrm{U}(\mathbf{x}) &= \max \frac{\left|\mu_g^i\right|}{\sigma_g^i} \text{ If } \mu_g^i > 0 \ \exists i = 1, \dots p \end{aligned} \tag{4.13}$$

The stopping criterion of composite learning function $\mathrm{U}(\mathbf{x})$ is often set to be $\min\{\mathrm{U}(\mathbf{x})\} \geq 2$ for both series and parallel system.

4.3.3 Other active leaning Kriging approaches for system reliability analysis

More recently, many active learning Kriging approaches are developed for system reliability analysis. Hu et al [Hu et al., 2017] proposed an active learning Kriging approach based on singular value decomposition. Yang et al.[Yang et al., 2018] proposed active learning Kriging with truncated candidate region named ALK-TCR, which is capable to recognize and avoid approximating the unimportant component(s). Then active learning Kriging model with importance sampling for system reliability analysis are also developed in [Guo et al., 2021, Wang et al., 2021]. Yuan et al.[Yuan et al., 2020] have combined structure function with active learning for system reliability analysis, which is easily implemented for complex systems,such as bridge network systems. Jiang et al.[Jiang et al., 2020] have proposed an active learning Kriging with error-guided estimation. Jia et al.[Jiang et al., 2021] proposed to combine hierarchical fuzzy simulation with active learning Kriging for system reliability analysis. Although, many active learning approach methods have been developed for system reliability, we do not know which one is more applicable for a particular problem. However, compared with other approaches, the system reliability analysis with U learning functions

4.4 A new composite U learning function for system reliability analysis

Among all these active learning Kriging for system reliability, the Kriging model with U learning function is widely used for the comparison and application. However, the existing approaches based on U learning function (AK-SYS-U and AK-SYSi-U) have some inherent problems. In this subsection, a new composite U learning function is proposed for the system reliability analysis.

4.4.1 The problem of composite learning function of AK-SYS

As mentioned in [Yun et al., 2019], the composite learning function in AK-SYS will face the limitation that the false identification of minimum mode or maximum mode may occur by using the last calibrated Kriging and may further mislead the next refinement of Kriging. Use a simple three-failure-mode series system to illustrate. If the true values of these three limit state function are:

$$\begin{cases} g_1(\boldsymbol{x}^*) = 1 \\ g_2(\boldsymbol{x}^*) = 2 \\ g_3(\boldsymbol{x}^*) = -1 \end{cases} \tag{4.14}$$

at a given point $\boldsymbol{x}^*$. The prediction of the limit state values by the last calibrated Kriging are:

$$\begin{cases} \hat{g}_1(\boldsymbol{x}^*) = 1 \\ \hat{g}_2(\boldsymbol{x}^*) = 0.5 \\ \hat{g}_3(\boldsymbol{x}^*) = 2 \end{cases} \tag{4.15}$$

Eq.(4.15) shows that the first mode is accurately estimated; the second and the third mode are inaccurately estimated. By Eq.(4.11), the next process will update the second mode because it is considered as the minimum failure mode by mistake. By updating, the predictions are updated as:

$$\begin{cases} \hat{g}_1(\boldsymbol{x}^*) = 1 \\ \hat{g}_2(\boldsymbol{x}^*) = 2 \\ \hat{g}_3(\boldsymbol{x}^*) = 2 \end{cases} \tag{4.16}$$

Then, the minimum failure mode identified by the current Kriging is the first mode. Due to the first mode's accurate estimation, the updating of the point $\boldsymbol{x}^*$ is stopped. The false identification of maximum mode in the parallel system can also illustrated by the three-failure-mode system. If the true values of these three limit state function are:

$$\begin{cases} g_1(\boldsymbol{x}^*) = -1 \\ g_2(\boldsymbol{x}^*) = -0.5 \\ g_3(\boldsymbol{x}^*) = 0.5 \end{cases} \tag{4.17}$$

at a given point $\boldsymbol{x}^*$. The prediction of the limit state values by the last calibrated Kriging are:

$$\begin{cases} \hat{g}_1(\boldsymbol{x}^*) = -1 \\ \hat{g}_2(\boldsymbol{x}^*) = 0.5 \\ \hat{g}_3(\boldsymbol{x}^*) = -1.5 \end{cases} \tag{4.18}$$

Eq.(4.17) shows that the first mode is accurately estimated; the second and the third mode is inaccurately estimated. By Eq.(4.17), the next process will update the second mode because it is considered as the maximum failure mode by mistake. By updating, the predictions are updated as:

$$\begin{cases} \hat{g}_1(\boldsymbol{x}^*) = -1 \\ \hat{g}_2(\boldsymbol{x}^*) = -0.5 \\ \hat{g}_3(\boldsymbol{x}^*) = -1.5 \end{cases} \tag{4.19}$$

Then, the maximum failure mode identified by the current Kriging is the second mode. Due to the second mode's accurate estimation, the updating of the point $\boldsymbol{x}^*$ is stopped. From the above description, it can be seen that the final Kriging may give a false prediction of the state of the realization $\boldsymbol{x}^*$, due to the false identification of minimum mode or maximum mode.

4.4.2 The problem of composite learning function of AK-SYSi

To avoid identifying the minimum mode or the maximum mode by the initial and the in-process Kriging, an improved AK-SYS by using a refined U learning function is proposed [Yun et al., 2019], which updates the Kriging from easily identifiable failure mode among the multiple failure modes. However, as observed in [Jiang et al., 2020], the AK-SYSi method may tend to terminate prematurely or too late, Also, use the three-failure-mode series system to illustrate. If the true values of these limit state function are:

$$\begin{cases} g_1(\boldsymbol{x}^*) = 1 \\ g_2(\boldsymbol{x}^*) = 2 \\ g_3(\boldsymbol{x}^*) = 1 \end{cases} \tag{4.20}$$

at a given point $\boldsymbol{x}^*$. The prediction of the limit state values by the last calibrated Kriging and the related U values are:

$$\begin{cases} \hat{g}_1(\mathbf{x}^*) = -1, \quad \mathrm{U}_1(\mathbf{x}^*) = 0.1 \\ \hat{g}_2(\mathbf{x}^*) = 1, \quad \mathrm{U}_2(\mathbf{x}^*) = 0.2 \\ \hat{g}_3(\mathbf{x}^*) = 1.5, \quad \mathrm{U}_3(\mathbf{x}^*) = 0.15 \end{cases} \tag{4.21}$$

Eq.(4.21) shows all the modes are inaccurately estimated. By Eq.(4.12), the next process will update the second mode because it is considered as the most easily identifiable mode by mistake. By updating, the

predictions are updated as:

$$\begin{cases} \hat{g}_1(\mathbf{x}^*) = -1, \quad \mathrm{U}_1(\mathbf{x}^*) = 0.1 \\ \hat{g}_2(\mathbf{x}^*) = 2, \quad \mathrm{U}_2(\mathbf{x}^*) = +\infty \\ \hat{g}_3(\mathbf{x}^*) = 1.5, \quad \mathrm{U}_3(\mathbf{x}^*) = 0.15 \end{cases} \tag{4.22}$$

Then, the most easily identifiable failure mode in the series system is the second mode. Due to the second mode's accurate estimation, the updating of the point $\boldsymbol{x}^*$ is stopped. Similarly, the false identification of mode in the parallel system can also be illustrated by the three-failure mode system. If the true values of these limit states are:

$$\begin{cases} g_1(\boldsymbol{x}^*) = -1 \\ g_2(\boldsymbol{x}^*) = -0.5 \\ g_3(\boldsymbol{x}^*) = -0.3 \end{cases} \tag{4.23}$$

at a given point $\boldsymbol{x}^*$. The prediction of the limit state values by the last calibrated Kriging and the related U values are:

$$\begin{cases} \hat{g}_1(\mathbf{x}^*) = 1, \quad \mathrm{U}_1(\mathbf{x}^*) = 0.1 \\ \hat{g}_2(\mathbf{x}^*) = 1.5, \quad \mathrm{U}_2(\mathbf{x}^*) = 0.2 \\ \hat{g}_3(\mathbf{x}^*) = -0.5, \quad \mathrm{U}_3(\mathbf{x}^*) = 0.15 \end{cases} \tag{4.24}$$

Eq.(4.24) shows all the modes are inaccurately estimated. By Eq.(4.13), the next process will update the second mode because it is considered as the most easily identifiable mode by mistake. By updating, the predictions are updated as:

$$\begin{cases} \hat{g}_1(\mathbf{x}^*) = 1, \quad \mathrm{U}_1(\mathbf{x}^*) = 0.1 \\ \hat{g}_2(\mathbf{x}^*) = -0.5, \quad \mathrm{U}_2(\mathbf{x}^*) = +\infty \\ \hat{g}_3(\mathbf{x}^*) = -0.5, \quad \mathrm{U}_3(\mathbf{x}^*) = 0.15 \end{cases} \tag{4.25}$$

Then, the most easily identified mode by the current Kriging is the second mode. Due to the second mode's accurate estimation, the updating of the point $\boldsymbol{x}^*$ is stopped. From the above description, it can be seen that the final Kriging may also give a false prediction of the state of the realization $\boldsymbol{x}^*$ in the AK-SYSi method.

4.4.3 The proposed composite U learning function for system reliability analysis

As demonstrated in the previous study, the AK-SYS and AK-SYSi will face the same limitation about the false identification failure mode. AK-SYSi seems to solve the false identification of minimum or maximum mode problem, but the false identification of the failure mode still exist. Therefore, a refined composite learning function is proposed in this section, which can take advantage of both AK-SYS and AK-SYSi composite learning function. In this thesis, the new composite learning function with Kriging is

named AK-SYSm. The new composite function for the series system is defined as:

$$\begin{aligned} \mathrm{U(x)} &= \min \frac{\left|\mu_g^i\right|}{\sigma_g^i},\ \text{If } \mu_g^i > 0\ \forall i = 1,\dots p \\ \mathrm{U}(\mathbf{x}) &= \max \frac{\left|\mu_g^i\right|}{\sigma_g^i},\ \text{If } \mu_g^i < 0\ \forall i = 1,\dots p \\ \mathrm{U}(\mathbf{x}) &= \frac{\left|\mu_{\mathrm{g}}^*\right|}{\sigma_{\mathrm{g}}^*}, \mu_{\mathrm{g}}^* = \min\left(\mu_{\mathrm{g}}^i\right), \text{Otherwise} \end{aligned} \tag{4.26}$$

The new composite function for the parallel system is defined as:

$$\begin{aligned} \mathrm{U(x)} &= \max \frac{\left|\mu_g^i\right|}{\sigma_g^i},\ \text{If } \mu_g^i > 0\ \forall i = 1,\dots p \\ \mathrm{U}(\mathbf{x}) &= \min \frac{\left|\mu_g^i\right|}{\sigma_g^i},\ \text{If } \mu_g^i < 0\ \forall i = 1,\dots p \\ \mathrm{U}(\mathbf{x}) &= \frac{\left|\mu_{\mathrm{g}}^*\right|}{\sigma_{\mathrm{g}}^*}, \mu_{\mathrm{g}}^* = \max\left(\mu_{\mathrm{g}}^i\right), \text{Otherwise} \end{aligned} \tag{4.27}$$

The proposed new composite learning function can deal with the above-mentioned problems of AK-SYS and AK-SYSi.

4.5 Adaptation H learning function for the system reliability analysis

For the reliability analysis with active learning Kriging model, different learning functions may have different performances. However, for a given problem, no one knows which learning function is better. In addition, the active learning Kriging for component reliability analysis can always be adapted to the system reliability analysis. In this chapter, active learning Kriging with H function is adapted for the system reliability analysis.

4.5.1 Composite H learning function: AK-SYS-H

The first composite function is based on the idea of AK-SYS method. Actually, the composite learning function method of AK-SYS can be extended to all active learning Kriging problems. The composite H learning function is defined as:

$$\mathrm{H}^*(x) = \left| \begin{array}{l} \ln\left(\sqrt{2\pi}\sigma_{\hat{g}}^* + \frac{1}{2}\right)\left[\Phi\left(\frac{\varepsilon_{\mathrm{H}}^* - \mu_{\hat{g}}^*}{\sigma_{\hat{g}}^*}\right) - \Phi\left(\frac{-\varepsilon_{\mathrm{H}}^* - \mu_{\hat{g}}^*}{\sigma_{\hat{g}}^*}\right)\right] \\ -\left[\frac{\varepsilon_{\mathrm{H}}^* - \mu_{\hat{g}}^*}{2}\phi\left(\frac{\varepsilon_{\mathrm{H}}^* - \mu_{\hat{g}}^*}{\sigma_{\hat{g}}^*}\right) + \frac{\varepsilon_{\mathrm{H}}^* + \mu_{\hat{g}}^*}{2}\phi\left(\frac{-\varepsilon_{\mathrm{H}}^* - \mu_{\hat{g}}^*}{\sigma_{\hat{g}}^*}\right)\right] \end{array} \right| \tag{4.28}$$

where $\varepsilon_{\mathrm{H}}^* = 2\sigma_{\hat{\mathrm{g}}}^*$ is the threshold function. The selection of the mean value of Kriging prediction is defined

in the following equation (4.29). The value used for the composite standard deviation, σ_g^*, is then the standard deviation from the corresponding model i.

$$\begin{aligned} \mu_g^* &= \max(\mu_g^i) \quad i = 1 \dots p \quad \text{for parallel system} \\ \mu_g^* &= \min(\mu_g^i) \quad i = 1 \dots p \quad \text{for series system} \end{aligned} \tag{4.29}$$

4.5.2 Composite H learning function: AK-SYSi-H

The second composite learning function is based on the idea of AK-SYSi. The composite H learning function for the series system is defined as:

$$\begin{aligned} \mathrm{H(x)} &= \min\left(\mathrm{H}^i(x)\right), \text{ If } \mu_g^i > 0, \forall\, i = 1, \dots p \\ \mathrm{H(x)} &= \max\left(\mathrm{H}^i(x)\right), \text{ If } \mu_g^i \leq 0, \exists i = 1, \dots p \end{aligned} \tag{4.30}$$

For the parallel system, the composite H learning function is defined as:

$$\begin{aligned} \mathrm{H(x)} &= \min\left(\mathrm{H}^i(x)\right), \text{ If } \mu_g^i < 0, \forall\, i = 1, \dots p \\ \mathrm{H(x)} &= \max\left(\mathrm{H}^i(x)\right), \text{ If } \mu_g^i > 0, \exists i = 1, \dots p \end{aligned} \tag{4.31}$$

where the $\mathrm{H}^i(x)$ is expressed as the following:

$$\mathrm{H}^i(x) = \left| \begin{array}{l} \ln\left(\sqrt{2\pi}\sigma_{\hat{g}}^i + \frac{1}{2}\right)\left[\Phi\left(\frac{\varepsilon_{\mathrm{H}}^i - \mu_{\hat{g}}^i}{\sigma_{\hat{g}}^i}\right) - \Phi\left(\frac{-\varepsilon_{\mathrm{H}}^i - \mu_{\hat{g}}^i}{\sigma_{\hat{g}}^i}\right)\right] \\ -\left[\frac{\varepsilon_{\mathrm{H}}^i - \mu_{\hat{g}}^i}{2}\phi\left(\frac{\varepsilon_{\mathrm{H}}^i - \mu_{\hat{g}}^i}{\sigma_{\hat{g}}^i}\right) + \frac{\varepsilon_{\mathrm{H}}^i + \mu_{\hat{g}}^i}{2}\phi\left(\frac{-\varepsilon_{\mathrm{H}}^i - \mu_{\hat{g}}^i}{\sigma_{\hat{g}}^i}\right)\right] \end{array} \right| \tag{4.32}$$

where $\varepsilon_{\mathrm{H}}^i = 2\sigma_{\hat{g}}^i$ is the threshold function.

4.5.3 Composite H learning function: AK-SYSm-H

The final composite learning function is based on the proposed AK-SYSm method. The composite H learning function for the series problem is defined as:

$$\begin{aligned} \mathrm{H(x)} &= \max\left(\mathrm{H}^i(x)\right), \text{ If } \mu_g^i > 0, \forall \mathrm{i} = 1, \dots p \\ \mathrm{H(x)} &= \min\left(\mathrm{H}^i(x)\right), \text{ If } \mu_g^i < 0, \forall \mathrm{i} = 1, \dots p \\ \mathrm{H}(x) &= \mathrm{H}^*(x), \mu_g^* = \min\left(\mu_g^i\right), \text{ Otherwise} \end{aligned} \tag{4.33}$$

For the parallel system, the composite learning function is defined as:

$$\begin{aligned} \mathrm{H(x)} &= \min\left(\mathrm{H}^i(x)\right), \text{ If } \mu_g^i > 0, \forall \mathrm{i} = 1, \dots p \\ \mathrm{H(x)} &= \max\left(\mathrm{H}^i(x)\right), \text{ If } \mu_g^i < 0, \forall \mathrm{i} = 1, \dots p \\ \mathrm{H}(x) &= \mathrm{H}^*(x), \mu_g^* = \max\left(\mu_g^i\right), \text{ Otherwise} \end{aligned} \tag{4.34}$$

As for the stopping condition for the system reliability analysis, $\max\{\mathrm{H}(x)\} \leq 0.5$ is considered in this work. However, it should be mentioned that the composite learning function AK-SYS-H and AK-SYSi-H will inherit the problems of AK-SYS and AK-SYSi.

4.6 Examples and applications

In this section, two examples are studied to demonstrate the performance of the proposed composite learning function and the adaption of H learning function for system reliability analysis. The first example is a numerical example of the parallel system with three limit states. The second example is a series system of roof truss structure with three performance functions. To ensure the stability of the results, all the methods are repeated 50 times for each example. The average results are listed in the following tables, where N_{call} represents the mean value of the number of limit state function calls. Moreover, in order to demonstrate the performance of AK-SYS-H,AK-SYSi-H and AK-SYSm-H, different thresholds in the example 1 are tested. As for the threshold for the AK-SYS-U,AK-SYSi-U,AK-SYSm-U, the stopping criterion of $\mathrm{U}(\mathbf{x})$ is set to be $\min\{\mathrm{U}(\mathbf{x})\} \geq 2$. Additionally, the relative error of each method in 50 runs are plotted by boxplot. The relative error is calculated by:

$$\varepsilon = \frac{\left| p_f^{mcs} - \hat{p}_f \right|}{p_f^{mcs}} \times 100\% \tag{4.35}$$

where p_f^{mcs} is the failure probability estimated by MCS, and p_f is the failure probability estimated by active learning Kriging methods. Furthermore, the coefficient of variation (C.O.V) of the system failure probability is given by:

$$\mathrm{C.O.V}\left(\hat{\mathrm{P}}_f\right) = \sqrt{\frac{1-\hat{p}_f}{\mathrm{N}_{mcs}\hat{p}_f}} \tag{4.36}$$

where N_{mcs} is the population samples generated by Monte Carlo simulation.

4.6.1 Example 1: A numerical example of parallel system

The first numerical example is a non-linear parallel system [Bichon et al., 2011, Fauriat and Gayton, 2014, Zhou et al., 2020], which has two random input variables X_1 and X_2, with three performance functions.

$$\begin{aligned} g_1(\mathbf{X}) &= 8\mathrm{X}_1^2 - 8\mathrm{X}_2^2 - \left(\mathrm{X}_1^2 + \mathrm{X}_2^2\right)^2 \\ g_2(\mathbf{X}) &= 2\mathrm{X}_2^2 - 2\mathrm{X}_1^2 - \left(\mathrm{X}_1^2 + \mathrm{X}_2^2\right)^2 \\ g_3(\mathbf{X}) &= 8\mathrm{X}_1^2 - 8\mathrm{X}_2^2 + \left(\mathrm{X}_1^2 + \mathrm{X}_2^2\right)^2 \end{aligned} \tag{4.37}$$

where two Gaussian input variables $X_1 \sim N(0,1)$ and $X_2 \sim N(0,1)$ are independent. The parallel system problem can be formulated as:

$$P_f = \text{Prob}\left(g_1(\mathbf{X}) < 0 \cap g_2(\mathbf{X}) < 0 \cap g_3(\mathbf{X}) < 0\right) \tag{4.38}$$

For this example, 1×10^5 random points are generated by MCS. Concerning the active learning Kriging approaches, a dozen of initial sample points are generated by LHS. Table. 4.2 presents the average results of active learning approaches with composite U function. As shown in Table.4.2, the proposed composite learning function in AK-SYSm-U can achieve to evaluate the system reliability as efficiently and accurately as the AK-SYS-U and AK-SYSi-U. To demonstrate the robustness of the proposed composite learning function, the relative error (ε) of 50 repeated runs in each method is shown in Fig.4.2(a). The proposed composite U learning function is robust compared with AK-SYS and AK-SYSi approach. Furthermore, Table. 4.3 presents the average results of active learning Kriging model with composite H function. Also, three different stopping conditions (0.5,0.1,0.01) in composite H function are considered in Table. 4.3. First, the adaptation of active learning Kriging with three composite H learning function can be used for the system reliability analysis. Secondly, with more strict threshold, the mean value of relative error will decrease. Hence, for the reader or users, they can select the threshold value according to their requirement about accuracy and efficiency. In the following examples, the stopping condition of H learning function is set to max(H) ≤ 0.5. In addition, the relative errors in the 50 repeated runs with three composite H functions with threshold equals to 0.01 is plotted in Fig.4.2(b). Similarly, as shown in Fig.4.2(b), the active learning Kriging with the proposed idea of composite H learning function (AK-SYSm-H) is more robust.

Table 4.2 – Average results of active learning Kriging with U function in 50 repeated runs of example 1

Methods	g_1	g_2	g_3	Total	Pf	C.O.V(%)	ε(%)
MCS	1×10^5	1×10^5	1×10^5	3×10^5	0.1926	0.65	-
AK-SYS-U	37.94	34.16	17.92	90.02	0.1926	0.65	0.14
AK-SYSi-U	39.08	32.26	23.64	94.98	0.1926	0.65	0.13
AK-SYSm-U	37.78	34.88	23.80	96.46	0.1926	0.65	0.12

4.6.2 Example 2: A series system of roof truss structure

The second example is a series system of roof truss structure [Yun et al., 2019, Jiang et al., 2020]. As shown in Fig. 4.3, the top chords and compression bars of the roof truss are made of the steel reinforced concrete, while the bottom chords and tension bars are made of steel. Assume the uniformly distributed load q that can be transformed into the nodal load $P = ql/4$ is applied on the roof truss structure, where l is the length of the truss. This roof truss structure takes into account three failure modes. The first failure mode considers the perpendicular defection of the truss peak node C, which is derived as $\Delta_C = \frac{ql^2}{2}\left(\frac{3.81}{A_C E_C} + \frac{1.13}{A_S E_S}\right)$, where A_C, A_S are the cross-sectional areas of the steel reinforced concrete and the steel bars respectively, and E_C, E_S are the corresponding elastic modulus. For this mode, the fail-

Table 4.3 – Average results of active learning Kriging with H function in 50 repeated runs of example 1

Methods	g_1	g_2	g_3	Total	Pf	C.O.V(%)	ε(%)
MCS	1×10^5	1×10^5	1×10^5	3×10^5	0.1926	0.65	-
AK-SYS-H (0.5)	41	39.6	17.10	97.7	0.1923	0.65	0.31
AK-SYS-H (0.1)	42.28	40.66	18.10	101.04	0.1926	0.65	0.1
AK-SYS-H (0.01)	42.9	41.18	18.16	102.24	0.1926	0.65	0.09
AK-SYSi-H (0.5)	40.64	36.36	33.44	110.44	0.1926	0.65	0.2
AK-SYSi-H (0.1)	41.26	36.96	33.78	112	0.1926	0.65	0.14
AK-SYSi-H (0.01)	41.52	37.28	33.90	112.7	0.1926	0.65	0.13
AK-SYSm-H (0.5)	41.18	41.5	25.86	108.54	0.1925	0.65	0.2
AK-SYSm-H (0.1)	42.4	42.3	26.58	111.28	0.1927	0.65	0.1
AK-SYSm-H (0.01)	43	42.8	26.96	112.76	0.1926	0.65	0.07

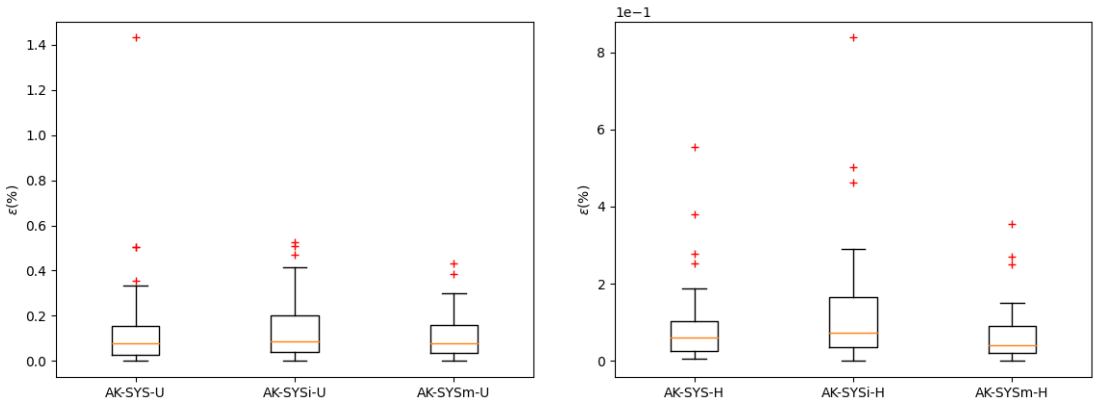

(a) Composite U learning functions

(b) Composite H learning functions

Figure 4.2 – Boxplots of the relative error (ε) in example 1.

ure event occurs when Δ_C exceeds 0.03m. The second failure mode is that the internal force of AD bar ($1.185ql$) exceeds the ultimate stress $f_C A_C$, where f_C is the compressive strength of AD bar. For the third mode, the failure occurs when the internal force of EC bar ($0.75ql$) exceeds the ultimate stress $f_S A_S$, where f_S is the tensile strength of EC bar. Therefore, the LSFs of the three failure modes are given by

$$\begin{aligned} g_1 &= 0.03 - \frac{ql^2}{2}\left(\frac{3.81}{A_C E_C} + \frac{1.13}{A_{SES}}\right) \\ g_2 &= f_C A_C - 1.185ql \\ g_3 &= f_S A_S - 0.75ql \end{aligned} \tag{4.39}$$

As the roof truss structure is a series system, the failure probability is defined as:

$$P_f = \text{Prob}\left(g_1 < 0 \cup g_2 < 0 \cup g_3 < 0\right) \tag{4.40}$$

There are eight random variables in this case and they are all assumed to follow the lognormal distribution. Additionally, all the random variables are mutually independent and the statistical information is listed in Table.4.4

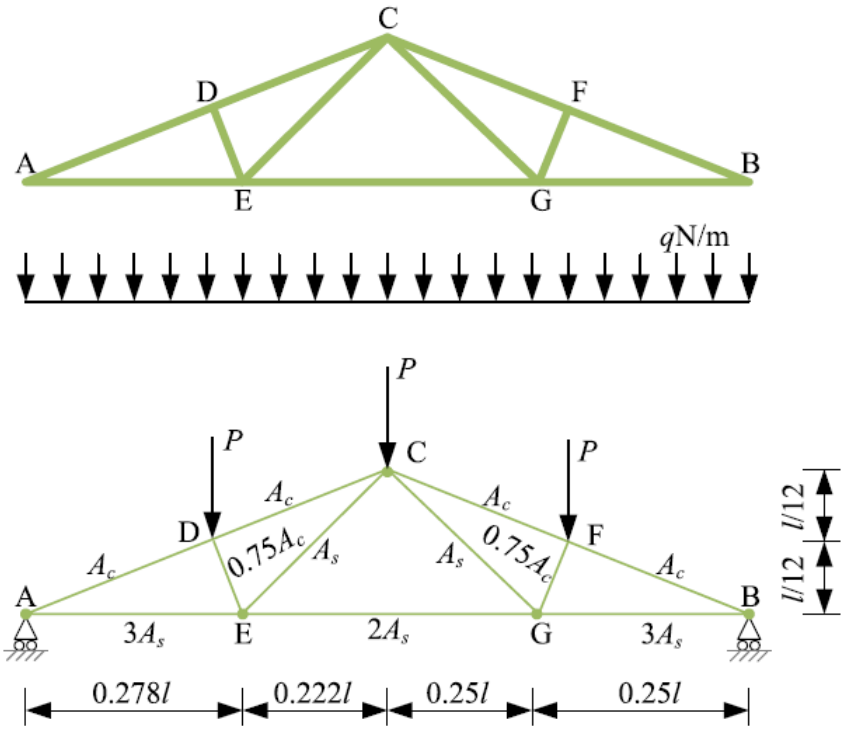

Figure 4.3 – The roof truss structure [Jiang et al., 2020]

Table 4.4 – Distribution parameters of roof truss structures

Variable	Description	Mean	Coefficient of variation
q(N/m)	Uniform load	20000	0.07
l(m)	Length	12	0.01
A_S (m^2)	Cross-sectional area	9.82×10^{-4}	0.06
A_C (m^2)	Cross-sectional area	0.04	0.12
E_S (N/m^2)	Elastic modulus	2×10^{11}	0.06
E_C (N/m^2)	Elastic modulus	3×10^{10}	0.06
f_S (N/m^2)	Tensile strength	3.35×10^{8}	0.12
f_C (N/m^2)	Compressive strength	1.34×10^{7}	0.18

In this example, 2×10^5 random points are generated by MCS. A dozen of initial sample points are generated by LHS for the active learning Kriging approaches. The results of the composite U and H function are listed in Table.4.5. All the active learning Kriging approaches have obtained the relatively accurate results compared to MCS. As shown in Table.4.5, all the methods pay no attention to the first limit state and little attention to the third limit state. More training samples are expected to be generated for the second limit state, which is the most significant one of the system failure domain. The proposed AK-SYS-H method seem more efficient in this example and the efficiency of AK-SYSi and AK-SYSm approaches has little differences. Furthermore, the proposed composite idea (AK-SYSm-U and AK-SYSm-H) are more robust compared to other composite ideas with the same learning function. The relative error (ε) of 50 repeated runs in each method are also shown in Fig.4.4. It is clear that the proposed composite idea of learning function is more robust.

Table 4.5 – Average results of active learning Kriging methods in 50 repeated runs of example 2

Methods	g_1	g_2	g_3	Total	Pf	C.O.V(%)	ε(%)
MCS	2×10^5	2×10^5	2×10^5	6×10^5	0.003410	3.82	-
AK-SYS-U	12	43.32	20.92	76.24	0.003408	3.82	0.27
AK-SYSi-U	12	50.14	24.20	86.34	0.003415	3.82	0.15
AK-SYSm-U	12	52.9	24.94	89.84	0.003410	3.82	0.09
AK-SYS-H	12.02	41.04	20.84	73.9	0.003415	3.82	0.19
AK-SYSi-H	12	45.22	28.20	85.42	0.003434	3.81	0.24
AK-SYSm-H	12	48.8	29.92	90.72	0.003410	3.82	0.1

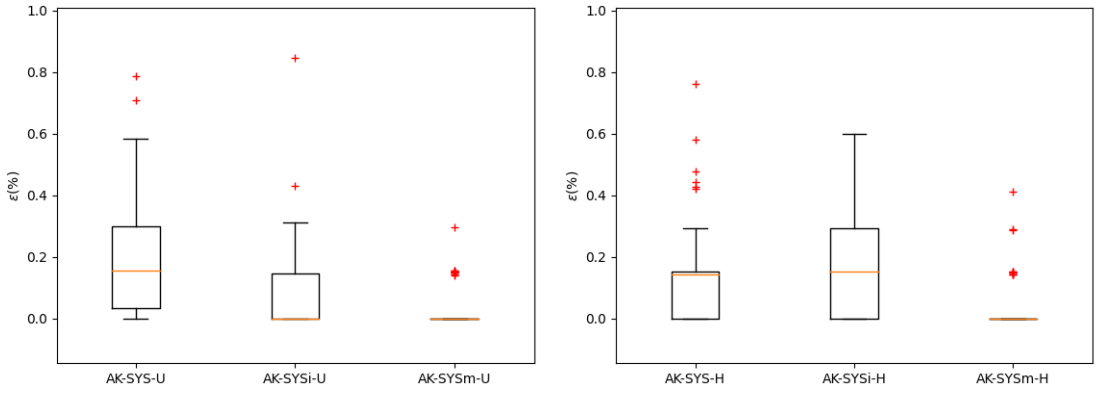

(a) Composite U learning functions

(b) Composite H learning functions

Figure 4.4 – Boxplots of the relative error (ε) in example 2.

4.7 Application on the offshore wind turbine jacket model

In the section, we have applied the developed approaches for the offshore wind turbine jacket models. The overview of this section is as shown Fig.**??**. At first, the finite element models of the jacket are developed and validated with the reference values in the green part. Next, in the blue part, one ultimate limit state is defined and the sensitivity analysis is conducted based on the beam jacket model to select the influential parameters for the reliability assessment. Finally, active learning approaches are used to assess the probability of failure in the orange part. The layout of this section is as follows. The design load case, and limit state are given in section 2. Section 3 shows that parameter selection and sensitivity analysis results. The jacket model validation and stress concentration study are discussed in section 4. Section 5 gives the results of the reliability analysis results with active learning approaches.

4.7.1 Design load case, Loads, and Limit state function

Design load case

In the standard codes IEC 61400-3 [IEC, 2009], 32 DLCs (design load cases) are defined covering various operational modes of the turbine such as normal operation, shut down, and 50-years extreme conditions. They can be mainly categorized into two major groups, namely ultimate and fatigue DLCs. The typical load cases applied in the structural design of OWT are the fatigue load under normal sea conditions and the ultimate load under 50-year extreme condition [Gentils et al., 2017]. All the DLCs should be carefully considered in the design of the jacket. While, in this paper, our focus is mainly on the ultimate DLCs. The 50-year return period is generally considered as a critical ultimate load case as shown in Table 4.6, which is mostly considered to correspond to the parked turbine, under the 50-year EWM (extreme wind model) with a 50-years RWH (reduced wave height) and ECM (extreme current model) as described in DLC.6.1b IEC 61400-3 [IEC, 2009].

Table 4.6 – Design load case

Load cases	Wind condition	Wave conditions
Ultimate load case DLC.6.1b	EWM:V_{e50}	RWH: H_{red50}

Loads from wind turbine

The loads from wind turbines mainly consist of aerodynamic and inertia loads. Aerodynamic loads are transferred from the rotor. Inertial load is mainly due to the mass of the RNA (rotor-nacelle assembly). The above loads are among the most important load sources to be considered in the reliability assessment of the support structure. They can be simulated from the wind turbine tools like OpenFAST [Walatka et al., 1994] and HAWC2 [Larsen and Hansen, 2007]. In this work, the loads from wind turbines are simulated with OpenFAST using sequentially coupled approaches. The mean values of the loads for DLC.6.1b are listed in Table 4.7.

Table 4.7 – Mean values of loads from wind turbine

Load case	Fx (kN)	Fy (kN)	Fz (kN)	Mx (kN*m)	My (kN*m)	Mz (kN*m)
DLC 6.1b	660	9	-11851	-4479	29368	371

Hydrodynamic loads

Hydrodynamic loads mainly consist of wave and current loads. It is critical to properly estimate the wave load because waves will cause a significant force on the jacket. The choice of wave theory to apply to the model depends on the site characteristics. The decision of wave theory is also dependent on the ratio of the height to diameter of the structural member. When the diameter of the structure is less than one-fifth of the wave length, Morrison's equation can be applied for the wave force estimation [Veritas, 2004]:

$$\mathrm{F_{wave}}\,(z) = \frac{1}{4}\rho_w \pi \mathrm{D}^2 \mathrm{C_M}\,\dot{u}(z,t) + \frac{1}{2}\rho_w \mathrm{D}\mathrm{C_D}\,u(z,t)|u(z,t)| \tag{4.41}$$

where D and ρ_w are the diameter of jacket members and the density of the water with a typical value of 1025 kg/m^3, $\mathrm{C_M}$ and $\mathrm{C_D}$ are the coefficient of inertia and drag of the jacket members respectively, and their corresponding values are 1.6 and 1.0 respectively, according to [DNV, 2016]. $\dot{u}(z,t)$ and $u(z,t)$ are respectively horizontal acceleration and velocity of water particles, which can be obtained from linear/Airy wave theory. z and t are respectively the reference depth and time.

Current can induce a drag load acting on the jacket structure. The current velocity can be estimated using an exponential profile as follows [IEC, 2009]:

$$u_c(z) = u_{\mathrm{MSL}}\left(\frac{d+z}{d}\right)^{\frac{1}{7}} \tag{4.42}$$

where u_{MSL} is the current velocity at mean sea level (MSL), d is the depth of water and z is the reference depth. In this paper, both wave and current loads are defined in ANSYS ocean loading module [ANSYS, 2017] by giving the related wave and current parameters such as wave height, wave period, and current velocity at MSL. The effect of direction in wave and current is also taken into account.

Limit state function

For an OWT jacket support structure, the performance function of the ultimate limit state based on the Von-Mises criterion is given by:

$$g_u = \sigma_m - \sigma_{\max} \tag{4.43}$$

where σ_m is the allowable stress with a mean value of 355 Mpa for steel S355 and $\sigma_{\max}$ is the maximum Von-Mises stress calculated by the finite element analysis tools.

4.7.2 Parameter selection and Sensitivity analysis

Parameter selection

For the selection of the random parameters, the uncertainties of environmental parameters, operational loads, and material property are taken into account. All the random parameters and related distribution are listed in Table 4.8. The mean values of the loads (Fx,Fy,Fz,Mx,My,Mz) are from the wind turbines simulated by OpenFAST tool. In addition, Hs, Tp, and Cmsl are respectively the significant wave height, wave peak period, and the current speed at mean sea level (MSL). E is Young's modulus of the jacket material. Here, the mean values of wave and current parameters in 50-year return period are referenced in [Fischer et al., 2010]. Furthermore, according to the references [Lee et al., 2014, Velarde et al., 2019b], the loads on the top of the jacket can be assumed to follow the Gumbel distribution for the extreme load cases and the coefficients of variation equal to 0.1 [Lee et al., 2014]. Hs, Tp and Cmsl can be assumed to follow respectively Weibull, Lognormal and Weibull as suggested in the references [Taflanidis et al., 2013, Wang and Kolios, 2017, Hübler et al., 2017a] and the coefficients of variation also equal to 0.1 [Wang and Kolios, 2017, Ivanhoe et al., 2020]. As for the direction of the wave (Dw) and current (Dc), normally they are different from each other. However, during the sequentially coupled approach, it is assumed that wave and current are aligned with the wind loading. Hence, to consider the influence of the wave and current direction, a small angle of ±30° in wave and current direction is investigated in this work. The directions of the wave and current are assumed here to follow uniform distributions. The material properties (E, σ_m) can be seen to follow the Lognormal distribution [Velarde et al., 2019b, Stieng and Muskulus, 2020] with the coefficients of variation respectively equal to 0.03 [Velarde et al., 2019b] and 0.1 [Stieng and Muskulus, 2020]. Also, it should be mentioned that all the parameters as shown in Table 4.8 are assumed to be independent in this study.

Sensitivity analysis

Sensitivity analysis (SA) aims to quantify the influence of all uncertain input parameters on considered model outputs. It is widely used to identify the parameters that are influential or non-influential. Those non-influential parameters can be considered as deterministic variables. In this work, one global sensitivity analysis (GSA) method named Morris screening method [Morris, 1991, Campolongo et al., 2007] is used to classify the parameters. In Morris screening method, two sensitivity indexes are calculated: μ^*, which estimates the overall influence of the factor on the output, and σ, which assesses the totality of the factor's higher order effects, i.e. non-linear and interaction effects. A high value of μ_j^* indicates that the j-th parameter gives an important overall influence on the output. Similarly, a high value σ_j means that the j-th parameter is involved in interaction with other parameters.

The parameters (except σ_m) in Table 4.8 are considered as random parameters and the sensitivity of the maximum stress in the beam jacket model is analyzed. The developed beam jacket model is validated by modal and static analysis, which can be found in section 4. The maximum Von-mises stress is simulated with ANSYS in linear static analysis. Morris screening method is performed based on Python SALib

Table 4.8 – Random parameters before sensitivity analysis

Parameters	Mean (Lower bound)	Standard deviation (Upper bound)	Distribution
Operational loading from wind turbines			
Fx (kN)	660	0.1*660	Gumbel [Lee et al., 2014, Velarde et al., 2019b]
Fy (kN)	9	0.1*9	Gumbel [Lee et al., 2014, Velarde et al., 2019b]
Fz (kN)	11851	0.1*11851	Gumbel [Lee et al., 2014, Velarde et al., 2019b]
Mx (kN*m)	4479	0.1*4479	Gumbel [Lee et al., 2014, Velarde et al., 2019b]
My (kN*m)	29368	0.1*29368	Gumbel [Lee et al., 2014, Velarde et al., 2019b]
Mz (kN*m)	371	0.1*371	Gumbel [Lee et al., 2014, Velarde et al., 2019b]
Environmental parameters			
Hs (m)	10.34[Fischer et al., 2010]	0.1*10.34	Weibull [Taflanidis et al., 2013, Wang and Kolios, 2017, Hübler et al., 2017a]
Tp (s)	10.87 [Fischer et al., 2010]	0.1*10.87	Lognormal [Taflanidis et al., 2013, Wang and Kolios, 2017]
Dw (°)	-30	30	Uniform
Cmsl (m/s)	1.2 [Fischer et al., 2010]	0.1*1.2	Weibull [Wang and Kolios, 2017, Hübler et al., 2017a]
Dc (°)	-30	30	Uniform
Material properties			
E (Gpa)	210	0.03*210	Lognormal [Velarde et al., 2019b]
σ_m (Mpa)	355	0.1*355	Lognormal [Velarde et al., 2019b, Stieng and Muskulus, 2020]

toolbox [Herman and Usher, 2017]. For the sensitivity analysis, all the parameters are assumed to be uniformly distributed and 4-σ_{std} intervals are taken for the non-uniform parameter distributions as done in Ref.[Hübler et al., 2017b]. The total number of simulation evaluations (n) for the sensitivity analysis is given by $n = r(k+1)$, where r is the number of trajectories and $k = 12$ is the number of parameters. In this work, different values of r are investigated to observe the convergence of the sensitivity analysis results. In addition, the Morris indexes μ^* and σ, are normalized using the following equations:

$$\begin{aligned} \mu^*_{n_j} &= \frac{\mu^*_j}{\max(\mu^*, \sigma)} \\ \sigma_{n_j} &= \frac{\sigma_j}{\max(\mu^*, \sigma)} \end{aligned} \tag{4.44}$$

The sensitivity analysis results are depicted in Fig.4.5. With the increase in the number of evaluations, the sensitivity analysis results converged. As shown in Fig.4.5.(d), the wave and current parameters have the most important influences on the maximum stress of the jacket model. The wave height (H_s) and current velocity (C_{msl}) have important overall influence on the maximum stress. The wave direction (D_c) and current direction D_w have great interactions with other parameters. Also, the wave peak period (T_p) has certain influence on the stress. In addition, compared with wave and current parameters, the loads parameters (Fx,Fz,My) have limited overall effect on the maximum stress. However, the loads (Fy,Mx.Mz) and the material property (E) seem non-influential to the maximum stress. Hence, in the reliability assessment, they will be considered as deterministic variables with their mean values, and the final random parameters considered for reliability analysis are given in Table 4.9.

4.7.3 Jacket model validation and Stress concentration study

Jacket model validation

Two numerical jacket models are developed in this paper. One (Beam model) is set up with Timoshenko beam element as presented in Fig.4.6(a) with 3D visualization. All joints are modeled by beams that are rigidly connected at the intersection points of their central axes. The other model (Super-element model as shown in Fig.4.6(b)) uses the super-elements for the joints' representation and Timoshenko beam element for the rest parts. All the joints are originally modeled with shell elements and all the dimensions of the joint follow the recommendations in [DUB, 2013]. In addition, because in this paper only linear static analysis is considered in finite element analysis, the Guyan [Guyan, 1965] reduction method can be applied to reduce the joints with shell elements to super-elements. Furthermore, to validate the developed numerical models, the modal and static analysis results are compared with the reference values as listed in Table 4.10 and Table 4.11. Here, the NREL 5-MW wind tower and rotor nacelle assembly (RNA) [Jonkman et al., 2009] are adopted for the modal and static analysis with developed jacket models. As shown in Table 4.10 and Table 4.11, the developed beam model has little differences in the modal and static analysis compared with the reference values, which are also based on beam elements. For the super-element model, the natural frequencies decrease a bit. Due to the precise representation of the joints in the jacket, the mass and stiffness of the super-element jacket model also decrease, which can

Table 4.9 – Random parameters after sensitivity analysis

Parameters	Mean (Lower bound)	Standard deviation (Upper bound)	Distribution
Operational loading from wind turbines			
Fx (kN)	660	0.1*660	Gumbel [Lee et al., 2014, Velarde et al., 2019b]
Fz (kN)	11851	0.1*11851	Gumbel [Lee et al., 2014, Velarde et al., 2019b]
My (kN*m)	29368	0.1*29368	Gumbel [Lee et al., 2014, Velarde et al., 2019b]
Environmental parameters			
Hs (m)	10.34 [Fischer et al., 2010]	0.1*10.34	Weibull [Taflanidis et al., 2013, Wang and Kolios, 2017, Hübler et al., 2017a]
Tp (s)	10.87 [Fischer et al., 2010]	0.1*10.87	Lognormal [Taflanidis et al., 2013, Wang and Kolios, 2017]
Dw (°)	-30	30	Uniform
Cmsl (m/s)	1.2 [Fischer et al., 2010]	0.1*1.2	Weibull [Wang and Kolios, 2017, Hübler et al., 2017a]
Dc (°)	-30	30	Uniform
Material property			
σ_m (Mpa)	355	0.1*355	Lognormal [Velarde et al., 2019b, Stieng and Muskulus, 2020]

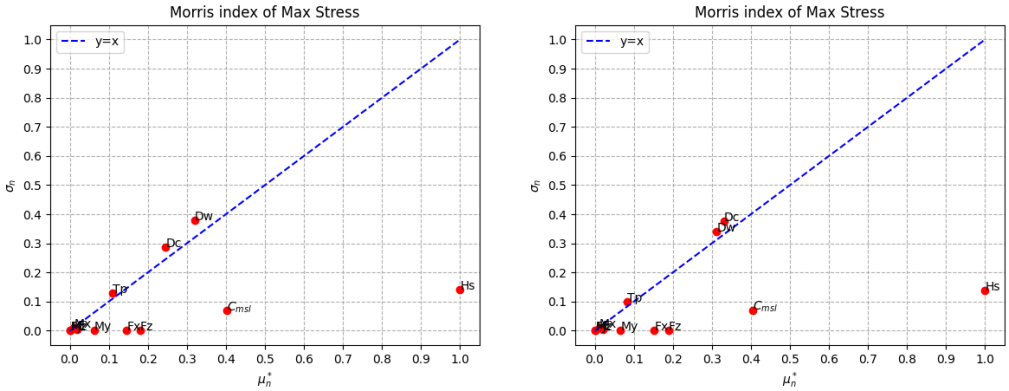

(a) r=50 and n=520

(b) r=60 and n=650

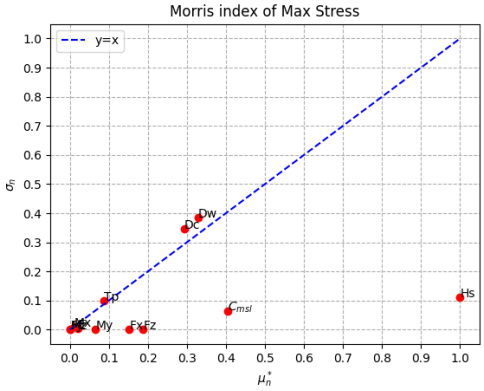

(c) r=70 and n=780

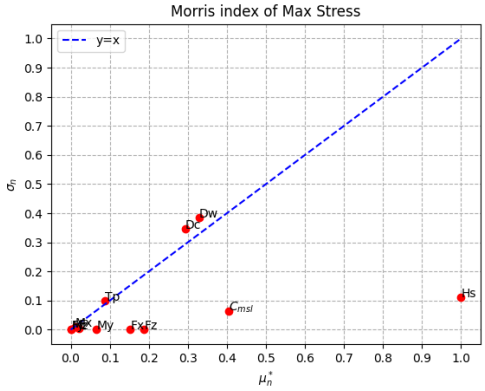

(d) r=80 and n=910

Figure 4.5 – Convergence of the sensitivity analysis results

also be noticed in the study [Tu et al., 2014]. That's why the displacement at RNA of super-element model with the same thrust load will be bigger than the beam model.

Table 4.10 – Modal analysis results

Modal analysis	Ref.[Song et al., 2013]	Beam (Diff.)	Super-element (Diff.)
1st Fore-aft	0.3190	0.3196 (0.19%)	0.3065 (-3.92%)
2nd Fore-aft	1.1936	1.1789 (-1.23%)	1.1052 (-7.41%)

Table 4.11 – Static analysis results

Thrust load at RNA (kN)	Displacement(m) at RNA		
	Ref.[Song et al., 2013]	Beam (Diff.)	Super-element (Diff.)
2000	1.2089	1.1975 (-0.94%)	1.2842 (6.23%)
4000	2.4178	2.3950 (-0.94%)	2.5684 (6.23%)

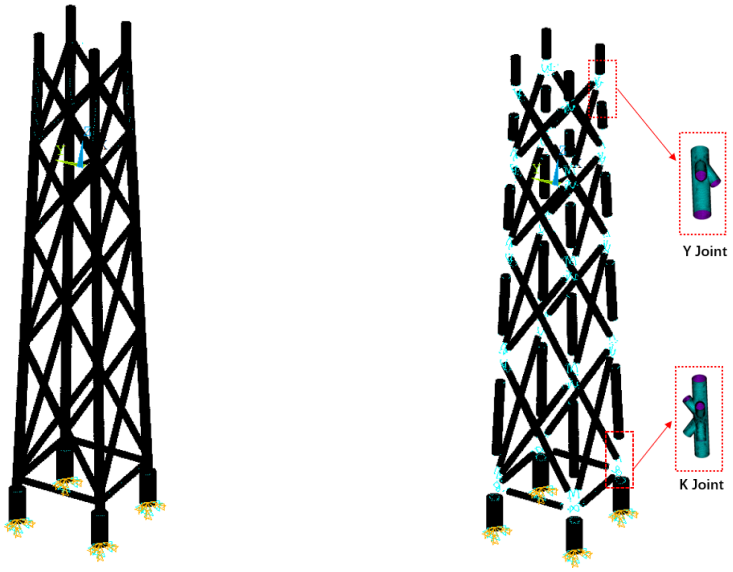

(a) Beam model (b) super-element model

Figure 4.6 – Jacket model

Stress concentration study

One simple stress concentration study is demonstrated by using the two jacket models. To study the stress concentration in the jacket joints, the joints of the jacket are classified into 5 zones (Yup, K1, K2, K3, Mud) as shown in Fig.4.7 . The Von-Mises stress in the 5 zones of the beam and the super-element models are compared. The maximum Von-Mises stress calculated in the joints of the super-element model is depicted in Fig.4.8. At first, the joints are modeled with shell elements and then converted to super-elements with Guyan reduction. The linear static analysis is conducted based on the jacket model with super-elements. At last, the maximum stresses in the joints of shell elements can be obtained after post-process.

Table 4.12 – Stress concentration factor (SCF) results

Max.Von-Mises Stress (Mpa)	Beam model	Super-element model	SCFs
Yup zone	59.98	118.33	1.97
K1 zone	52.02	178.57	3.43
K2 zone	67.45	180.75	2.68
K3 zone	68.25	225,43	3.30
Mud zone	89.90	267.39	2.97

The mean values of the loads, wave, current, and material parameters as shown in Table 4.9 are taken for this stress concentration factor study. The maximum stress of different zones in the beam and the

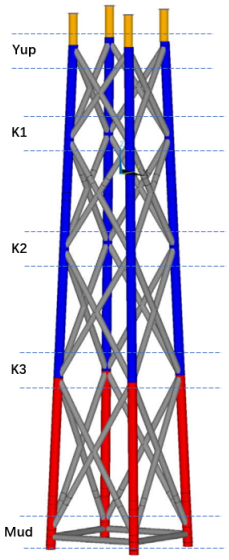

Figure 4.7 – Joint zone classification

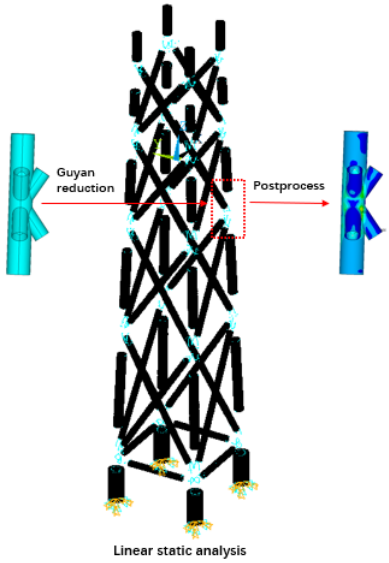

Figure 4.8 – Von-Mises stress of K2 joint in super-element model

super-element model are listed in Table 4.12. The super-element model has higher stress than the beam model in different zones of the jacket model due to the stress concentration. Moreover, the stress concentration factors (SCFs) in different zones are also different, due to different load-bearing behaviors in the different joints. It is clear that the stress concentration in the joints of the jacket model cannot be neglected when conducing reliability assessment of the jacket model.

Additionally, to observe the changes of the stress concentration factor, another 100 simulations results of the super-element and beam jacket models are compared. The 100 simulation samples are generated with the parameters in Table 4.9 (except σ_m) using Latin Hypercube sampling (LHS). The maximum stress of the whole jacket and the maximum stress in the different zones of the jacket models are depicted in Fig.4.9 and the related stress concentration factors of the maximum Von-Mises stress are shown in Fig.4.10. As shown in Fig.4.10, the stress concentration factors in the same zones will vary with the change of the random parameters. Furthermore, as shown in Fig.4.9, it is found that the maximum stress is always at the bottom of the jacket (Mud zone). Hence, for the reliability analysis of the jacket model considering ultimate stress, our focus will be on the bottom of the jacket.

4.7.4 Reliability analysis of the super-element jacket model

System reliability problem formulation

As discussed in the last section, the maximum stress of the super-element model is always at the bottom of the jacket (Mud zone). There are four joints in the mud zone as shown in Fig.4.11. Due to the uncertainty of the direction of the wave and current, the ultimate stress can be located in any joint of the mud

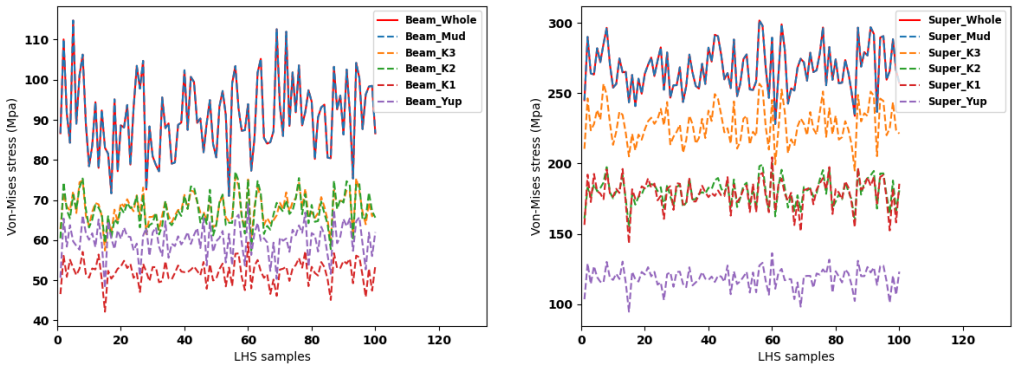

(a) Beam model (b) Super-element model

Figure 4.9 – Ultimate stresses in different zones of the jacket models

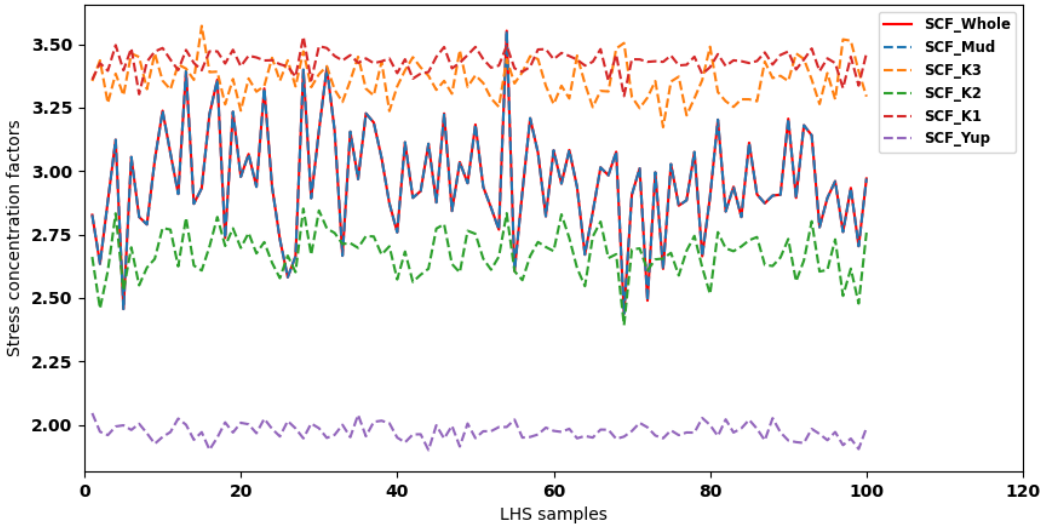

Figure 4.10 – Stress concentration factors in different zones

zone. Hence, the ultimate limit states of the super-element jacket model can be formulated as follows:

$$\begin{aligned} g_{us1} &= \sigma_m - \sigma_{s1} \\ g_{us2} &= \sigma_m - \sigma_{s2} \\ g_{us3} &= \sigma_m - \sigma_{s3} \\ g_{us4} &= \sigma_m - \sigma_{s4} \end{aligned} \tag{4.45}$$

where σ_{si} represents the maximum Von-Mises stress of ith joint in the mud zone, which is also simulated

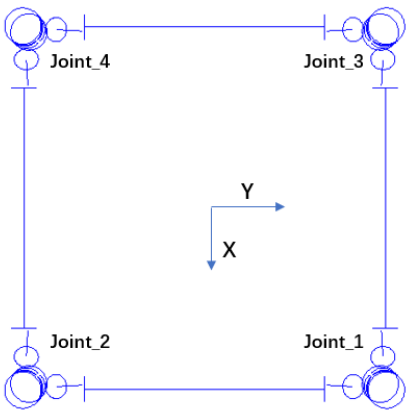

Figure 4.11 – Joints in the mud zone of the super-element model

in ANSYS software. The probability of failure of the jacket is considered as a series system, which can be expressed as:

$$\mathrm{P}f_{sys} = \mathrm{Prob}\left\{g_{us1} < 0 \cup g_{us2} < 0 \cup g_{us3} < 0 \cup g_{us4} < 0\right\} \tag{4.46}$$

For the system reliability analysis, the AK-SYS and the proposed approaches are used to for the reliability assessment. Similarly, to reduce the influence of the uncertainty of initial points, 20 repeated runs are conducted for the reliability assessment of each active learning approach. The initial sample size is set to 30 and all the initial samples are generated by using Latin Hypercube sampling (LHS). Monte Carlo simulation (MCS) is used to generate the total population of 1×10^5 for reliability assessment. The average results of the 20 runs are listed in Table.4.13. The system probabilities of failure and the coefficient of variation in 20 runs are also plotted as shown in Fig.4.12

Table 4.13 – Average reliability analysis results of the super-element model in 20 runs

Methods	g_{u1}	g_{u2}	g_{u3}	g_{u4}	Total calls	$\mathrm{P}f_{sys}$	C.O.V (%)
AK-SYS-U	234.40	30.00	111.15	30.00	405.55	7.27×10^{-3}	3.70
AK-SYSm-U	240.05	32.00	115.40	31.75	419.2	7.27×10^{-3}	3.70
AK-SYS-H	198.25	30.00	127.7	31.00	385.95	7.32×10^{-3}	3.68
AK-SYSm-H	204.55	58.85	186.05	46.7	496.15	7.31×10^{-3}	3.69

At first, it should be mentioned that for the system reliability approaches based on the improved composite learning function (AK-SYSi), they cannot convergence (after 1000 iterations) in this example. Therefore, only the results of the approaches based on the original (AK-SYS) and proposed (AK-SYSm) composite learning function are given in Table.4.13. All the active learning Kriging approaches can nearly get the same results of the probability of failure. The relative errors of the average probability of failure

between different approaches are less than 1%, which can confirm the results of the reliability assessment. The AK-SYS-H seems more efficient among these approaches. Moreover, the results show that two joints (joint 1 and joint 3) in the bottom of the jacket have dominated the failure domain of the ultimate limit states. Particularly, the joint 1 plays the most important role in the series systems of ultimate stress. More importantly, the probabilities of failure in two approaches are both bigger than the design probability of failure when considering stress concentration of the jacket joints under ultimate load case. The reliability-based design optimization should be considered in the future.

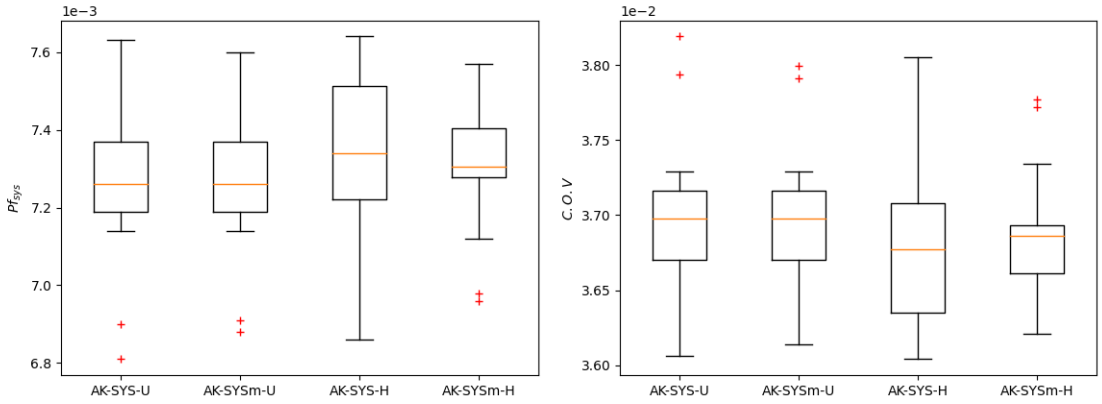

(a) Probability of failure (Pf_{sys})

(b) Coefficient of variations (C.O.V)

Figure 4.12 – Boxplots of the probability of failure and coefficient of variation.

4.8 Conclusions

In this chapter, the active learning Kriging approaches used for the system reliability analysis have been summarized. The Kriging model is a very popular surrogate model and is commonly used in the reliability analysis of the structure. In recent decade, the active learning Kriging approaches have gained much attention. In this chapter, at first, the typical learning functions used for component reliability are briefly introduced. Also, the typical active learning Kriging approaches of system reliability analysis are also discussed. Among these approaches, the composite learning functions can be seen as both efficient and accurate for the system reliability analysis. Some typical active learning approaches for system reliability analysis based on the composite learning function are introduced including AK-SYS and AK-SYSi.

Furthermore, the problems of the composite learning function approaches in the AK-SYS and AK-SYSi are discussed. Then, a new composite learning function based on U function for system reliability analysis is proposed, which enable the algorithm more robust for reliability assessment. In addition, the H learning function of the active learning Kriging is also adapted to the system reliability analysis,

this is because, for a given problem, we do not know which active learning function is better. Two numerical examples are used to demonstrate the robustness and efficiency of the proposed approaches. The results show that the adapted H learning function can assess the probability of failure of the system efficiently and accurately.

Finally, the proposed composite learning function and the developed approaches are also applied to the super-element model of the offshore wind turbine. A general framework is proposed to conduct the reliability assessment with active learning approaches. At first, the numerical modeling of physic model should be validated. Secondly, the sensitivity analysis should be conducted to select the influential parameters for the reliability assessment. The reliability analysis with active learning approaches is conducted in the end. From the sensitivity analysis study, it is found that wave and current parameters have important influences on the ultimate stress. In particular, the wave and current directions have nonlinear interactions with other parameters, which are usually assumed to be aligned in most researches. The loads ($\mathrm{F}x, \mathrm{F}z, \mathrm{M}y$) from wind turbines also have an effect on the ultimate stress. Concerning the stress concentration study, it is clear that the stress concentration phenomenon cannot be ignored in the joints part of the jacket. Additionally, the stress concentration factors are variant with the different parts of the jacket, due to the different load-bearing behaviors. Also, the stress concentration factors in the same zones will vary with the change of the random parameters.

For the reliability analysis with active learning approaches, the probabilities of failure in the four approaches are nearly the same, which confirms the reliability assessment results. Moreover, the results show that two joints (joint 1 and joint 3) in the bottom of the jacket have dominated the failure domain of the ultimate limit states. Particularly, the joint 1 plays the most important role in the series systems of ultimate stress. More importantly, the probabilities of failure in two approaches are both bigger than the design probability of failure when considering stress concentration of the jacket joints under the ultimate load case. The reliability-based design optimization should be considered in the future. Last but not least, it is noticed that the surrogate-based active learning approaches are much efficient for the reliability assessment. Only A few hundred simulations are needed to achieve the reliability analysis, which is much more efficient compared to the traditional reliability assessment approaches (e.g. MCS). In recent decades, many active learning methods have been developed, which can be benefited for the real engineering application and simulation.

Chapter 5

Conclusions and Perspectives

Contents

5.1 Conclusions

In this thesis, the reliability analysis of an offshore wind turbine jacket with active learning approaches is conducted. In the chapter one, the overview of the wind energy and the development of the offshore wind turbine is reviewed. Also, different offshore wind turbine foundations are briefly introduced. Additionally, the typical reliability analysis approaches and the application on the wind turbine are also discussed.

In the chapter two, the influences of different load simulations approaches and modeling of the jacket on the loading are considered. Three typical load simulation approaches (the fully coupled, sequentially coupled and uncoupled) are compared and the load differences between these approaches are also analyzed. The results show that the load simulation results in the sequentially coupled approach are mostly in good agreement with those of the fully coupled approaches. Moreover, two finite element models of the jacket model are developed. One is with purely beam element. The other is with the super-element for detailed representation of the joints in the jacket model, where the rest parts of the jacket are with beam elements. The results show that with different jacket models, the extreme values of the loading may have significant differences, but the mean values of the loading do not have many differences. Moreover, the values of the displacement in the different jacket structure can be much different, due to the change of the stiffness of the jacket structure. From this study, the more accurate load simulation approaches and the jacket model is chosen for the reliability analysis.

In the chapter three, some typical surrogate models are also summarized and the idea of ensemble surrogate models is introduced. Two approaches are proposed to combine the ensemble surrogate for reliability analysis with active learning based on local goodness assessment. One is the local weighted average surrogate (LWAS) approach and the other is the local best surrogate (LBS) approach. The Kriging and ANN models are used to construct the ensemble surrogate model. The results show that the proposed approaches are efficient for reliability assessment. Four examples and the beam jacket model under one ultimate limit state are used to demonstrate the efficiency and accuracy of the proposed approaches. Compared with the traditional AK-MCS approach, in most cases, the proposed approaches only require half the number of calls of the performance functions to reach the reference probability of failure obtained by crude MCS. In addition, it should be mentioned that the proposed approaches are not only suitable for combining Kriging and ANN, but also can be extended to other surrogate models. Additionally, more restrictive convergence condition could be considered for more accurate prediction of the failure probability.

In the chapter four, the active learning Kriging approaches for system reliability analysis are introduced. At first, the active learning functions of the Kriging model used for component reliability are summarized. Then, the typical approaches based on the active learning Kriging for system reliability analysis are discussed. Our focus is on the composite learning function approach, which is more efficient and accurate. The problems of the existing composite U learning functions are also discussed and a new

composite U learning function is proposed, which is more robust and solve the inherited problems of other composite U functions. Furthermore, for a given problem, we have no idea which learning function is better. Therefore, active learning Kriging approaches with H learning function are also adapted for the system reliability analysis. Two numerical examples and the super-element jacket model under several ultimate limit state are used to demonstrate the efficiency and robustness of the proposed approaches. The results show that the proposed composite learning function is more accurate for the system reliability analysis both in U and H functions. Moreover, the adapted H learning function can efficiently and accurately assess the probability of failure of the system. Hence, for the real engineering application, we can choose the suitable approaches for their problems.

Finally, from this thesis, readers may notice that the active learning approaches used for the reliability analysis are efficient, which can save a lot of model evaluations. For an advanced engineering problem, especially based on finite element analysis, the active learning approaches can save computational cost. In recent decades, many surrogate-assisted reliability approaches have been developed for the component, system, time-variant reliability analysis.

5.2 Perspectives

No work is perfect. In this thesis, for the offshore wind turbine jacket, in view of the increase of the extreme weather conditions, the author have considered the reliability analysis of the jacket model under one ultimate limit state. However, for the buckling, fatigue limit states of offshore wind turbines, there are still a lot of work need to do. Furthermore, for the ensemble surrogate models, they are only used for the component reliability analysis. As for the system reliability analysis and time-variant reliability analysis, the related approaches of the ensemble surrogate models should also be considered. In the following, several perspectives can be considered for future works.

For the reliability assessment approaches:
(1).Adapt the ensemble surrogate model for the system reliability analysis with active learning approaches.
(2).Develop the time-variant reliability analysis with ensemble surrogate models.
(3).Combine the ensemble surrogate models with other sampling approaches (Importance sampling, Subset Simulations, etc.) for reliability analysis.
(4).Develop reliability-based design optimization by using ensemble of surrogates.
For the application on the offshore wind turbine jacket:
(1).System reliability assessment of the offshore wind turbine jacket considering other limit state (Modal, Buckling, Fatigue...).
(2).Time-variant reliability analysis of the offshore wind turbine jacket.
(3).Reliability-based design optimization of the offshore wind turbine jacket.

Part III

French Abstract

Annexe A

Résumé en français

Contents

A.1 Résumé

Cette thèse vise à développer une approche pour une évaluation efficace et précise de la fiabilité du jacket des éoliennes offshore. Le jacket d'une éolienne offshore est soumise à diverses incertitudes. L'analyse de la fiabilité de la fondation du jacket est généralement effectuée en utilisant des approches d'approximation traditionnelles (par exemple FORM/SORM) ou la méthode des simulations de Monte Carlo. La modélisation mécanique du jacket d'une éolienne offshore nécessite généralement des modèles de simulations complexes et une analyse dynamique très couteuse en temps de calcul. L'utilisation des méthodes traditionnelles (FORM/SORM, simulations de Monte Carlo, etc.) pour l'analyse de fiabilité de ces structures peut-être inadaptée. En effet, les méthodes d'approximation souffrent souvent de problèmes de convergence numérique surtout lorsque l'analyse dynamique des structures est impliquée, voire de précision lorsque le problème contient plusieurs point de défaillance. Les méthodes de simulations de Monte Carlo sont robustes, toutefois elles sont très coûteuses en temps de calcul et elles sont impraticables pour calculer des faibles probabilités de défaillance.

La première partie de cette thèse vise la comparaison de trois approches de simulation des charges utilisées pour l'analyse dynamique des structures d'éoliennes offshore. Les approches étudiées sont respectivement la méthode non couplée, l'approche séquentielle et l'approche entièrement couplée. Ensuite, deux modèles numériques du jacket sont développés afin d'étudier l'influence des techniques de modélisation du jacket. le premier modèle utilise des éléments de poutre de Timoshenko pour l'ensemble des éléments du jacket. Le deuxième modèle utilise une modélisation avancée à l'aide de la technique des super-éléments. Les éléments du jacket sont modélisés par des éléments de poutre et les assemblages entre ces éléments sont modélisés à l'aide des éléments de coque. Des comparaisons entre ces deux modèles sont également effectuées. La comparaison des approches de simulation des charges a montré que les résultats de l'approche séquentielle sont pour la plupart en bon accord avec ceux de l'approche entièrement couplée. L'approche non couplée peut conduire à des erreurs importantes dans les réponses extrêmes de l'analyse dynamique. En outre, pour la comparaison entre les deux modèles du jacket, nous constatons que les réponses du modèle du jacket à super-éléments sont différentes de celles du modèle de poutre, en particulier pour les déplacements du jacket.

La deuxième partie de ce travail de thèse propose deux approches d'apprentissage actif pour l'évaluation de la fiabilité basée sur des modèles de substitution d'ensemble. Les modèles de krigeage (kriging) et les réseaux de neurones artificiels (ANN : *Artificiel Neural Network*) sont combinés pour constituer le modèle de substitution d'ensemble. L'efficacité et la précision des approches proposées sont démontrées par 4 exemples académiques et le modèle de poutre du jacket. Les résultats de l'analyse de fiabilité des exemples traités en utilisant les modèles de substitution d'ensemble avec les approches proposées d'apprentissage actif montrent l'efficacité et la robustesse de ces méthodes. D'ailleurs, même pour des problèmes de grande dimension et d'événement rare (probabilité de défaillance trés très faible), ces approches montrent des performances numériques remarquables par rapport au modèle de substitution unique avec des approches d'apprentissage actif (par exemple AK-MCS). La dernière

partie de cette thèse est dédiée à l'analyse de fiabilité système défini par plusieurs fonctions de performances. Une nouvelle fonction d'apprentissage composite est proposée pour le krigeage basé sur l'apprentissage actif avec la fonction U. Le modèle de krigeage à apprentissage actif avec la fonction d'apprentissage dite H est également adapté à l'analyse de fiabilité système. L'efficacité et la précision des approches proposées pour l'évaluation de la fiabilité système sont également montrées à travers deux exemples numériques et le modèle de super-éléments du jacket. Les résultats montrent que la fonction d'apprentissage composite proposée rend l'analyse de la fiabilité système plus robuste. Par ailleurs, la méthode d'apprentissage actif développée avec la fonction d'apprentissage H peut estimer efficacement et précisément la probabilité de défaillance système.

Mots-clés : Jacket d'éolienne offshore, Simulation des charges offshore, Super-élément, analyse par éléments finis, évaluation de la fiabilité, apprentissage actif, fiabilité système, probabilité de défaillance.

A.2 Introduction générale

Il ne fait aucun doute que les énergies renouvelables sont actuellement la forme d'énergie la plus prometteuse pour le respect de l'environnement. L'énergie éolienne en général et récemment l'énergie éolienne offshore, en particulier, ont pris de plus en plus d'importance sur le marché des énergies renouvelables. Pour les éoliennes offshores, les sous-structures et les fondations représentent une part importante des coûts de construction des éoliennes. Les fondations conventionnelles de type monopieu et tripode sont principalement utilisées pour les eaux peu profondes de 20 à 40 mètres. Les structures de support de type jacket sont devenues les principales structures de support dans les eaux profondes (50-100 m). Comme la plupart des structures offshores, les structures de support en jacket doivent résister aux charges complexes, à des conditions environnementales extrêmes, qui peuvent entraîner une défaillance structurelle et parfois même à des accidents graves. En particulier, l'augmentation des conditions météorologiques extrêmes (typhon, tsunami, etc.) au cours des dernières décennies nécessite des structures de support de jacket avec une fiabilité très élevée. Par conséquent, l'évaluation de la fiabilité et l'optimisation de la conception basée sur la fiabilité des structures de jacket sont devenues des domaines de recherche majeurs. Cependant, il existe de nombreuses incertitudes dans la conception d'une structure de jacket : (1) le caractère aléatoire naturel des facteurs environnementaux tels que le vent, les vagues et les courants, (2) les incertitudes dues aux modèles physiques des structures flexibles, et les modèles de simulation aéro-hydro-servo-mécanique (3) fluctuations des résistances des matériaux et les dimensions géométriques. Toutes ces incertitudes rendent l'évaluation de la fiabilité des structures jacket indispensable.

En ce qui concerne le chargement agissant sur la fondation de l'éolienne offshore, il est généralement simulé à l'aide des outils aéro-hydro-servo-dynamique tels que FAST et HAWC2, qui sont souvent basés sur trois approches. La première est la simulation découplée, la deuxième est l'approche séquentielle couplée et la troisième est l'approche entièrement couplée. L'approche séquentielle est largement utilisée dans l'industrie, en raison des propriétés intellectuelles et des questions de confidentialité entre le concepteur de la fondation et le fabricant de l'éolienne. Les approches entièrement couplées et les approches non couplées sont couramment utilisées dans la recherche fondamentale et les études universitaires. Cependant, à notre connaissance, la précision et l'efficacité de ces trois approches ne sont pas comparées et étudiées. De plus, les structures de support du jacket sont généralement modélisées avec des éléments de poutre afin d'accélérer la simulation des charges. Une telle simplification peut conduire à des inexactitudes dans les résultats générés, car la flexibilité locale des joints du jacket n'est pas prise en compte. L'influence des techniques de modélisation du jacket sur le chargement n'a pas encore été étudiée.

En ce qui concerne les approches d'évaluation de la fiabilité, les méthodes de fiabilité basées sur les approches d'approximation telles que FORM/SORM sont souvent utilisées pour l'évaluation de la probabilité de défaillance des structures. Ces méthodes offrent un bon équilibre entre la précision et le coût de calcul. Toutefois, ces méthodes sont basées sur la recherche du point de défaillance le

plus probable d'une part, d'autre part elles souffrent des problèmes de convergence numérique lorsque les fonctions d'état limites sont fortement non-linéaires, particulièrement de dynamiques des structures.

Les simulations de Monte Carlo (MCS : *Monte Carlo Simulations*) est une méthode très robuste pour l'évaluation de la fiabilité et la probabilité de défaillance. Cette méthode repose sur la génération d'un grand nombre de tirages aléatoires et l'estimation de la fonction d'état limite pour chaque tirage. Le principal inconvénient de la MCS est qu'elle nécessite un temps de calcul important. D'ailleurs, la méthode MCS s'avère impraticable pour des problèmes d'ingénierie avancée nécessitant des couplages multiphysiques. Bien que certaines techniques de réduction de la variance ont été développées, comme la simulation par importance (IS : *Importance Sampling*), les simulations stratifiées (*SS : Subsest Simulations*) et les simulations directionnelles (DS : *Directional Simulations*). Cependant, le coût de calcul reste toujours élevé et peu pratique pour les problèmes d'événements rares. Au cours des deux dernières décennies, l'analyse de fiabilité assistée par des modèles de substitution est devenue de plus en plus importante. L'idée de base est de remplacer la fonction de performance en construisant un modèle de substitution, également appelé méta-modèle. En outre, la stratégie de construction d'un modèle de substitution peut généralement être classée en deux types : (1) la méthode "one shot" (méthodes non adaptatives) et (2) les approches d'apprentissage actif (méthodes adaptatives). La méthode "one shot" nécessite de générer tous les points d'échantillonnage à l'avance et d'effectuer l'analyse de fiabilité en utilisant le modèle de substitution validé. D'autre part, les méthodes d'apprentissage actif sélectionnent un ou plusieurs points d'échantillonnage à chaque itération pour construire le modèle de substitution, qui est mis à jour à chaque itération de manière efficace jusqu'à la convergence. Par conséquent, les approches d'apprentissage actif sont normalement plus efficaces que les approches "one shot". Dans ce travail de thèse, différentes approches sont proposées pour l'évaluation de la fiabilité des structures à l'aide des méthodes d'apprentissage actif.

Dans cette thèse, nous avons mis l'accent également sur les approches de simulation des charges et les techniques de modélisation du jacket. Nous avons étudié l'influence des différentes approches de simulation des charges et de la modélisation du jacket sur les charges elle-mêmes. D'autre part, les approches d'apprentissage actif sont proposées pour l'évaluation de la fiabilité du jacket. Deux approches d'apprentissage actif basées sur un modèle de substitution d'ensemble avec mesure de la qualité locale sont développées pour l'analyse de la fiabilité d'une seule fonction d'état limite. Cependant, lorsque plusieurs fonctions d'état limites sont définies, l'analyse de fiabilité du système est préconisée. Pour cela, une nouvelle fonction d'apprentissage composite est proposée pour l'analyse de la fiabilité du système avec la méthode de Krigeage et la fonction d'apprentissage de type U. L'apprentissage actif des approches de Krigeage avec la fonction d'apprentissage H est également adapté à l'analyse de la fiabilité des systèmes.

Le plan de cette thèse est le suivant :
Le premier chapitre présente les récents développements de l'énergie éolienne et vue d'ensemble

sur les approches de conception des structures éoliennes, particulièrement les structures Jacket. Le développement des énergies renouvelables et de l'énergie éolienne est présenté dans la section 1.2. Les composants modernes des éoliennes offshores et les fondations des éoliennes offshores sont présentés dans la section 1.3. La section 1.4 présente les principales charges, les normes de conception et certains outils de simulation d'éoliennes typiques. Les approches d'évaluation de la fiabilité sont résumées dans la section 1.5. Les conclusions sont présentées dans la section 1.6.

Le chapitre 2 étudie l'influence des différentes approches de simulation de charge et des modèles du jacket sur les réponses. La section 2.2 présente les paramètres de base du modèle d'éolienne 5MW du NREL et de la fondation du jacket de l'éolienne offshore, qui sont utilisés pour l'étude suivante. Les théories de base de l'approche de simulation des charges et des techniques de modélisation sont données dans la section 2.3. Les résultats de comparaison des approches de simulation des charges sont présentés dans la section 2.4. La section 2.5 présente l'influence des différentes modélisations du jacket sur les charges. La section 2.6 présente les conclusions de l'étude et quelques recommandations.

Le chapitre 3 présente la proposition de l'utilisation des modèles de substitution d'ensemble avec des approches d'apprentissage actif pour évaluation de la probabilité de défaillance. L'approche proposée combine les réseaux de neurones artificiels et la méthode de Krigeage. La section 3.2 énumère quelques modèles de substitution typiques et les hypothèses de base des modèles de substitution. La section 3.3 résume les méthodes précédentes de modèles de substitution d'ensemble et leurs limites. Les détails du modèle de substitution d'ensemble proposé avec des mesures locales sont donnés dans la section 3.4. Des exemples et des applications des approches proposées sont présentés dans la section 3.5. Les conclusions et les discussions sont présentées dans la section 3.6.

Le chapitre 4 présente la seconde proposition pour l'analyse de fiabilité des systèmes. Les fonctions d'apprentissages de type H et composite sont proposées pour l'apprentissage actif du modèle de substitution de Krigeage utilisé dans l'analyse de fiabilité des systèmes. Certaines fonctions d'apprentissage typiques pour les modèles de substitution de Krigeage sont résumées dans la section 4.2. La section 4.3 présente quelques approches typiques de Krigeage par apprentissage actif pour l'analyse de la fiabilité des systèmes. La section 4.4 présente le problème de AK-SYS et AK-SYSi et la nouvelle fonction d'apprentissage composite. En outre, nous proposons dans la section 4.5 l'adaptation de la fonction d'apprentissage H pour l'apprentissage actif du modèle de substitution de Krigeage utilisé également pour l'analyse de la fiabilité des systèmes. Quelques exemples et applications numériques sont présentés dans la section 4.6. L'utilisation des approches proposées pour l'évaluation de la fiabilité système du jacket d'une éolienne offshore est présentée dans la section 4.7.

Le chapitre 5 présente la conclusion générale de cette thèse et quelques perspectives pour le futur.

A.3 Chapitre 1 : Objectifs

Les Énergies renouvelables sont considérées comme la source d'énergie durable et respectueuse de l'environnement. L'énergie éolienne est l'une des plus prometteuses des énergies renouvelables pour atteindre la neutralité carbone. Au cours de la dernière décennie, la capacité en énergie éolienne a augmenté rapidement. Le coût nivelé de l'énergie éolienne terrestre a atteint un niveau compétitif par rapport aux énergies conventionnelles. Cependant, le coût de l'énergie éolienne offshore reste élevé, en raison des coûts associés au transport, à l'installation et à la maintenance. Par rapport à l'énergie éolienne terrestre, les éoliennes en mer sont soumises à des vitesses de vent plus élevées et plus stables, ce qui permet de rendre l'énergie moins intermittente. De plus, les éoliennes en mer permettent également de réduire leur impact sur les activités humaines. Afin de promouvoir l'utilisation de l'énergie éolienne en mer, de nombreuses politiques nationales et régionales ont été élaborées. De plus en plus de parcs éoliens offshores sont construits et planifiés.

Dans l'énergie éolienne offshore, les fondations des éoliennes offshores représentent une part importante des coûts. Les fondations offshores sont utilisées pour soutenir l'éolienne et assurer son bon fonctionnement. Les fondations d'éoliennes offshores peuvent être classées en deux catégories : les éoliennes offshores fixées au fond marin et les éoliennes offshores flottantes. Le choix de la fondation dépend des conditions du fond marin et de la profondeur de l'eau. Toutefois, la technologie et la chaîne industrielle des éoliennes flottantes ne sont pas encore matures, par rapport aux éoliennes offshores fixées au fond marin. Pour les éoliennes offshores fixées au fond marin, il existe plusieurs types de fondations, comme le monopieu et le jacket. Le monopieu représente actuellement 90 % des fondations d'éoliennes offshores et sont principalement installés en eaux peu profondes. Comme la profondeur d'eau des installations d'éoliennes offshores augmente, les fondations de type jacket sont devenues le principal support des éoliennes offshores. Comme la plupart des structures offshores, les fondations en jacket sont soumises à des charges extrêmes et stochastiques. De plus, Pour assurer le fonctionnement de l'éolienne offshore, une plus grande fiabilité est requise pour les fondations offshores, en particulier avec l'augmentation des conditions météorologiques extrêmes (typhons, tsunamis, etc.). Par conséquent, l'analyse de la fiabilité des fondations des éoliennes offshores est devenue un outil majeur.

Pour évaluer la fiabilité du jacket d'une éolienne offshore, la quantification des incertitudes et les approches d'analyse de la fiabilité sont cruciales. La simulation de la charge de l'éolienne offshore est souvent basée sur des outils numériques tels que FAST et ANSYS. Dans cette thèse, nous nous concentrons sur les approches de simulation numérique des charges appliquées sur une éolienne offshore. L'évaluation de la fiabilité du jacket de l'éolienne offshore est généralement basée sur les simulations de Monte Carlo, qui nécessitent beaucoup de temps de calcul. Pour cela, nous proposons une approche efficace et précise pour l'évaluation la fiabilité de la fondation de type jacket d'une éolienne offshore.

A.4 Chapitre 2 : Approches de simulation des charges utilisées pour l'analyse dynamique d'un jacket d'éolienne offshore avec différentes techniques de modélisation

Ce chapitre présente tout d'abord les informations de base sur l'éolienne offshore de 5 MW et le modèle du Jacket OC4 utilisés dans cette étude. Les cas de charge de conception correspondants sont également brièvement abordés. Ensuite, la théorie de base des méthodes de sous-structuration (super-éléments) est présentée dans ce chapitre. Ensuite, l'influence des différentes approches de simulation de charge et des modèles du Jacket sur les réponses structurelles est étudiée.

Pour les approches de simulation des charges, trois approches de simulation des charges sont comparées comme le montre Fig.A.1 et A.2. Dans cette comparaison, le modèle du jacket de poutre est utilisé pour les trois approches. Les approches non couplée, séquentielle et entièrement couplée sont respectivement étudiées et comparées. Cette étude comparative des trois approches de simulation des charges nous permet de conclure que les différentes approches ont peu d'effet sur les valeurs moyennes des charges et des déplacements. Des différences significatives ne peuvent être observées que dans les valeurs extrêmes et l'écart-type de ces quantités d'intérêt. En outre, les charges et les déplacements simulés par l'approche séquentiellement couplée est généralement conformes aux résultats obtenus par l'approche entièrement couplée. Cependant, les charges calculées par l'approche non couplée présentent des différences significatives par rapport à celles fournies par l'approche entièrement couplée.

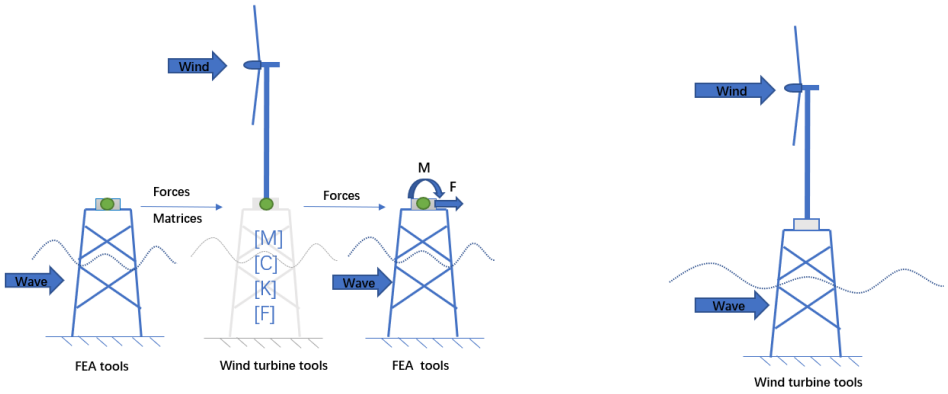

(a) Séquentiellement couplée (b) Entièrement couplée

FIGURE A.1 – Les approches séquentiellement et entièrement couplées

En ce qui concerne l'influence du type de modèlisation du jacket sur les réponses structurelles, deux modèles numériques du jacket sont developpés et étudiés comme le montre Fig.A.3. Le premier modèle (modèle de poutre) est établi avec des éléments de poutre de Timoshenko, comme présenté dans la visualisation 3D. Tous les joints sont modélisés par des éléments de poutre qui sont reliés de manière rigide aux points de jonction de leurs axes centraux. Le deuxième modèle (modèle de super-éléments)

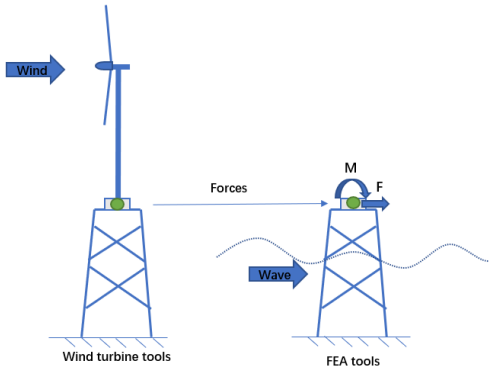

FIGURE A.2 – Cas non-couplé

utilise des super-éléments pour la représentation des joints et des éléments de poutre Timoshenko pour les autres parties. Les résultats montrent qu'une petite différence est observée dans les fréquences propres des deux modèles. La masse totale du jacket dans le modèle de poutre est plus élevée en raison du chevauchement des parties des joints. Ces chevauchements sont évités dans le modèle à super-éléments, ce qui fait que la masse totale du modèle à super-éléments diminue. Les cinq premières fréquences naturelles du modèle à super-éléments sont également inférieures à celles du modèle à poutre, ce qui signifie que la rigidité du Jacket dans le modèle à super-éléments diminue également. En outre, au sommet du jacket, les résultats de simulation du modèle à super-éléments sont différents de ceux du modèle de poutre en ce qui concerne les déplacements (Ux). Les valeurs moyennes des déplacements Ux dans le modèle à super-éléments sont supérieures à celles fournies par le modèle de poutres. Pour les charges (Fx, My), des différences apparaissent dans les valeurs extrêmes et l'écart-type de Fx. Ces différences peuvent générer des erreurs dans l'évaluation des réponses extrêmes du jacket.

En conclusion, la comparaison des méthodes de simulation des charges a montré que les résultats de l'approche non couplée, comme indiqué sur la Fig.A.2, peuvent présenter des différences significatives par rapport aux résultats de l'approche entièrement couplée. Les calculs des charges en utilisant l'approche séquentielle sont pour la plupart en bon accord avec ceux calculées par la méthode entièrement couplée. Ainsi, l'approche séquentielle et la méthode entièrement couplée sont recommandées pour le calcul des charges des éoliennes offshores. En outre, pour la comparaison des différents modèles de Jacket, les réponses du modèle à super-éléments présentent des différences significatives par rapport au modèle de poutre. Pour mieux modéliser le comportement du jacket, le modèle de super-éléments apparaît comme la meilleure solution parmi celles étudiées. D'ailleurs, le modèle du jacket avec super-éléments et l'approche séquentielle pour l'estimation des charges seront utilisés dans l'analyse de fiabilité système du jacket.

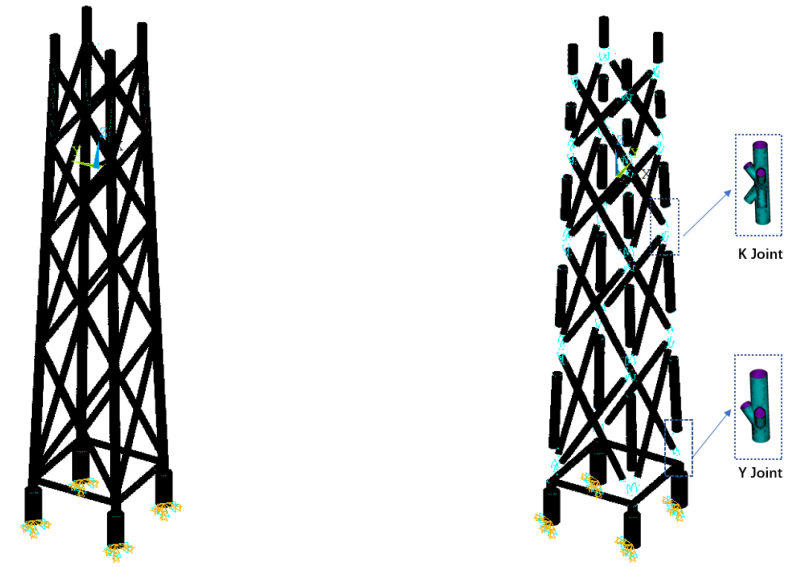

(a) Modèle de poutre (b) Modèle à super-éléments

FIGURE A.3 – Les Modèles du jacket

A.5 Chapitre 3 : Évaluation de la fiabilité à l'aide des modèles de substitution d'ensemble

Dans ce chapitre, les principes de base de certains modèles de substitution classiques (Kriging, Polynômes de chaos (PCE) et les réseaux de neurones artificiels (ANN)) sont présentés. En outre, le principe de base des modèles de substitution d'ensemble est brièvement discuté. Plus important encore, deux approches sont proposées pour évaluer la probabilité de défaillance avec des modèles de substitution d'ensemble basés sur l'évaluation de la qualité locale de prédiction. Dans les approches proposées, les techniques classiques de validation croisée et de Jackknife sont utilisées pour prédire les erreurs des modèles de substitution. De plus, deux méthodes sont proposées pour mesurer la qualité locale de prédiction des modèles de substitution et estimer l'erreur de prédiction de l'ensemble des modèles de substitution. En outre, l'évaluation de l'erreur de la prédiction est directement associée aux échantillons candidats et varient avec chaque point d'échantillon. Les modèles de substitution d'ensemble utilisées dans cette thèse sont les réseaux de neurones artificiels (ANN : *Artificial Neural Network*) et le Krigeage. L'apprentissage actif des deux modèles de substitution d'ensemble comme indiqué dans l'algorithme 1.1 s'appuie sur les deux méthodes d'évaluation de la qualité locale de prédiction, LWAS (Local Weighted Average Surrogate) et LBS (Local Best Surrogate). Ces deux méthodes sont basées respectivement sur les poids de la prédiction des modèles de substitution (pour LWAS) et la meilleure prédiction des modèles de substitution.L'efficacité et la précision des approches proposées sont validées par 4 exemples de référence et un problème d'éléments finis.

Dans les cinq exemples, la méthode proposée qui combine le krigeage (Kriging) et les réseaux neuronaux artificiels (ANN) basée sur les deux approches d'apprentissage actif montre qu'elle est efficace. Dans la plupart des exemples étudiés, la méthode proposée de deux modèles de substitution d'ensemble nécessite la moitié du nombre d'appels à la fonction de performance par rapport à la méthode dite AK-MCS, pour atteindre la probabilité de défaillance estimée par les simulations de Monte-Carlo. Il y a deux raisons à un tel comportement numérique Premièrement, l'approche proposée semble être plus efficace que l'approche AK-MCS pour l'approximation de la probabilité de défaillance. Deuxièmement, le critère d'arrêt des méthodes proposées est directement lié à la probabilité de défaillance. En outre, il convient de noter qu'un autre avantage de la méthode proposée est qu'elle n'est pas sensible à la taille de la population, par rapport à l'approche AK-MCS. De plus, les méthodes existantes des modèles de substitution d'ensemble sont basées sur l'évaluation de la qualité globale de la prédiction, les approches proposées pour l'évaluation de la qualité locale de la prédiction sont plus performantes pour la plupart des exemples étudiés. En effet, les modèles de substitution d'ensemble existants [Cheng and Lu, 2020, Teixeira et al., 2020] sont basées sur l'évaluation globale de l'erreur de la prédiction, ainsi le modèle de substitution actif (le modèle ayant le poids le plus élevé ou ayant l'erreur de prédiction la plus faible) est fixé pour tous les échantillons candidats. Par ailleurs, les deux approches proposées pour l'apprentissage actif sont basées sur une mesure locale de la prédiction. Pour cela, les points candidats pour la mise à jour des modèles de substitution sont sélectionnés à chaque itération en

fonction de l'erreur de la prédiction. Cela semble la raison pour laquelle les approches proposées sont plus efficaces. Cependant, à travers les cinq applications numériques traités, les approches de modèles de substitution d'ensemble proposées semblent avoir des comportements numériques différents. En fait, ces comportements numériques dépendent du nombre de points d'échantillonnage initiaux, de la position de ces points d'échantillonnage, des points enrichis et du nombre de neurones dans la couche cachée du modèle ANN. Pour cette raison, la contribution des modèles ANN et du Kriging dans l'ensemble des modèles de substitution peut être différente d'un exemple à l'autre, même dans le même exemple lorsque les points d'échantillonnage initiaux sont différents.

Enfin, il convient de mentionner que les approches proposées ne sont pas seulement adaptées à la combinaison du Krigeage et de l'ANN, mais qu'elles peuvent également être étendues à d'autres modèles de substitution, notamment le PCE, le SVR, etc.

Algorithm 1.1 Modèle de substitution d'ensemble combinant le krigeage (kriging) et les réseaux de neurones artificiels (ANN) basé sur l'évaluation de la qualité locale de la prédiction

Input : Générer un petit nombre (N_{call}) d'échantillons initiaux. X_{DoE} par LHS et calculer le Y_{DoE} correspondant. ;

Générer un grand nombre de populations **S** par MCS pour l'estimation de la probabilité de défaillance.

while $\xi \leqslant e_{pf}$ **do** :
(Entraîner le Krigeage et l'ANN)
Entraîner les modèles de krigeage et les modèles ANN avec X_{DoE} et Y_{DoE} ;
(Obtenir les valeurs prédites et les probabilités de défaillance dans chaque modèle de substitution)
Prédire les valeurs de tous les échantillons **S** avec le Krigeage actuel ($\hat{y}_k$) et l'ANN ($\hat{y}_{nn}$) ;
Calculer la probabilité de défaillance en utilisant les modèles de substitution de Krigeage (Pf_k) et de l'ANN (Pf_{nn}) ;
(Estimation les erreurs de validation croisée pour tous les échantillons des modèles de Krigeage et de l'ANN)
Estimation des erreurs d'échantillonnage avec les approches de validation croisée des modèles de Krigeage (e_k) et de l'ANN (e_{nn}) ;
(Calculer les valeurs prédites et les erreurs dans les modèles de substitution d'ensemble)
Calculer les poids (w_i) pour tous les échantillons dans l'approche LWAS ;
(Ou sélectionner le meilleur modèle de substitution pour tous les échantillons dans l'approche LBS)
Calculer $\hat{y}_{lwas}$ et e_{lwas} pour tous les échantillons **S** par l'approche LWAS ;
(Ou calculer $\hat{y}_{lbs}$ et e_{lbs} pour tous les échantillons **S** par l'approche LBS)
(Calculer la probabilité de défaillance par le modèle de substitution d'ensemble)
Calculer la probabilité de défaillance (Pf) par le modèle de substitution d'ensemble $\hat{y}_{lwas}$. (or $\hat{y}_{lbs}$) ;
(Calculer la valeur pour décider du critère d'arrêt)
Recalculez la valeur de e_{pf} ;
(Sélectionnez le nouvel échantillon ajouté)
Sélectionner le nouvel échantillon (x_u) pour minimiser U_{lwas} (ou U_{lbs}) et obtenir la vraie réponse y_u ;
Enrichir respectivement X_{DoE} et Y_{DoE} avec x_u et y_u ;
N_{call}=N_{call}+1
end while

Output : Calculer la valeur de la probabilité de défaillance par le modèle de substitution d'ensemble. Pf
Obtenir le nombre total d'appels aux fonctions de performance (N_{call})

A.6 Chapitre 4 : Évaluation de la fiabilité des systèmes à l'aide de l'apprentissage actif du krigeage

Dans ce chapitre, les fonctions d'apprentissage utilisées pour l'analyse de fiabilité d'une seule fonction de performance sont brièvement présentées. Les approches utilisées pour l'extension de l'analyse de la fiabilité d'une seule fonction d'état limite à l'analyse de la fiabilité d'un système composé de plusieurs fonctions de performances sont également discutées. Parmi ces approches, les fonctions d'apprentissage composites, qui peuvent être considérées comme efficaces et précises pour l'analyse de la fiabilité des systèmes. Certaines approches d'apprentissage actif pour l'analyse de la fiabilité des systèmes basées sur la fonction d'apprentissage composite sont également présentées, notamment AK-SYS et AK-SYSi.

En outre, les problèmes rencontrés par l'utilisation de la fonction d'apprentissage composite dans les méthodes AK-SYS et AK-SYSi sont discutés. Nous proposons dans ce travail de thèse une nouvelle fonction d'apprentissage composite basée sur la fonction U. Cela permet de rendre l'algorithme plus robuste pour l'évaluation de la fiabilité système. En outre, la fonction d'apprentissage H de l'apprentissage actif de Kriging est également adaptée à l'analyse de la fiabilité des systèmes. En effet, pour un problème donné, nous ne savons pas la meilleure fonction d'apprentissage actif à utiliser. Deux exemples numériques sont utilisés pour démontrer la robustesse et l'efficacité des approches proposées. Les résultats montrent que la fonction d'apprentissage adaptée dite H peut évaluer la probabilité de défaillance du système de manière efficace et précise.

Enfin, la fonction d'apprentissage proposée et les approches développées sont également appliquées au modèle de super-élément du jacket de l'éolienne offshore. Un cadre général est proposé pour mener l'évaluation de la fiabilité système avec des approches d'apprentissage actif. Dans un premier temps, la modélisation numérique du modèle physique doit être validée. Ensuite, l'analyse de sensibilité doit être menée pour sélectionner les paramètres influents pour l'évaluation de la fiabilité. Finalement, l'analyse de fiabilité système du jacket est réalisée à l'aide des approches d'apprentissage actif. L'analyse de sensibilité révèle que les paramètres de la vague et du courant ont une influence importante sur la contrainte ultime de Von-Mises. En particulier, les directions des vagues et du courant ont des interactions non linéaires avec d'autres paramètres, qui sont généralement supposés être alignés dans la plupart des recherches. Les charges ($\mathrm{F}x, \mathrm{F}z, \mathrm{M}y$) des éoliennes ont également un effet sur la contrainte ultime. De plus, cette étude montre que le phénomène de concentration des contraintes ne peut pas être ignoré dans la partie des joints de jacket. Les facteurs de concentration des contraintes varient selon les différentes parties de jacket, en raison des différents comportements de support de charge. De plus, les facteurs de concentration des contraintes dans les mêmes zones varient en fonction de la modification des paramètres aléatoires.

Les probabilités de défaillance obtenues en utilisant les approches d'apprentissage actif proposées pour

le krigeage sont presque identiques, ce qui confirme les résultats de l'évaluation de la fiabilité système du jacket. De plus, les résultats montrent que deux joints (joint 1 et joint 3) dans la partie inférieure de jacket ont dominé le domaine de défaillance des états limites ultimes. En particulier, le joint 1 joue le rôle le plus important dans les systèmes en série de la contrainte ultime. Par ailleurs, la probabilité de défaillance du jacket en tenant compte de la concentration des contraintes des joints dans le cas de l'état limite ultime, est supérieure à la probabilité de défaillance cible recommandée par les normes en vigueur [Veritas, 2002, 1990, 2003]. L'optimisation de la conception basée sur la fiabilité semble être envisagée dans les perspectives de ce travail. Finalement, nous constatons que les approches d'apprentissage actif basées sur les modèles de substitution sont très efficaces pour l'évaluation de la fiabilité. Quelques centaines de simulations seulement peuvent être suffisantes pour réaliser l'analyse de fiabilité. Cela permet d'effectuer les analyses de fiabilité des systèmes complexes à un coût de calcul abordable. En outres, ces approches sont beaucoup plus efficaces que les approches traditionnelles d'évaluation de la fiabilité (par exemple, MCS). Au cours des dernières décennies, de nombreuses méthodes d'apprentissage actif ont été développées, qui peuvent être utiles pour les applications d'ingénierie avancée basée sur des modèles de simulation très couteux en temps de calcul.

A.7 Chapitre 5 : Conclusions et perspectives

Dans le cadre de ce travail de thèse, nous avons réalisé l'analyse de fiabilité d'un jacket d'éolienne offshore à l'aide des approches d'apprentissage actif. Le premier chapitre présente une vue d'ensemble de l'énergie éolienne et les développements récents de l'éolienne offshore. Les types de fondations des éoliennes offshore sont également brièvement présentés. Enfin, les différentes approches de l'analyse de fiabilité et leur application aux éoliennes sont également brièvement abordées.

Dans le chapitre 2, les influences des différentes approches de simulation des charges et de la modélisation du jacket sur les charges sont examinées. Trois approches de simulation des charges (entièrement couplée, séquentiellement couplée et découplée) sont comparées et les différences en valeurs moyenne, écart-types et valeurs extrêmes sont également analysées. Les résultats montrent que les résultats de la simulation des charges dans l'approche séquentielle sont généralement en bon accord avec ceux de l'approche entièrement couplée. En outre, deux modèles d'éléments finis du modèle du jacket sont développés. L'un en utilisant des éléments de poutre. Le deuxième modèle en utilisant la technique de super-éléments pour la représentation détaillée des joints du jacket. Ces super-éléments sont combinés aux éléments de poutre pour les autres parties du jacket. Les résultats obtenus montre que les valeurs des déplacements du jacket calculés par les deux modélisations du jacket sont différentes, en raison du changement de la rigidité de la structure du jacket en utilisant la modélisation des joint par les super-éléments. Les valeurs extrêmes des charges présentent des différences significatives, mais les valeurs moyennes des charges présentent des différences légères. Cette étude nous a permis d'une part de sélectionner l'approche de simulation des charges la plus précise et efficace ; d'autre part de choisir la modélisation mécanique la plus appropriée du jacket pour l'analyse de fiabilité.

Dans le chapitre 3, certains modèles de substitution sont résumés et l'idée de modèles de substitution d'ensemble est introduite. Deux approches sont proposées pour combiner les modèles de substitution d'ensemble pour l'analyse de fiabilité avec l'apprentissage actif basé sur l'évaluation de la qualité locale de la prédiction. La première approche est basée sur la moyenne pondérée locale de substitution (LWAS). La deuxième approche est basée sur le meilleur modèle de substitution locale (LBS). Nous avons proposé une approche de modèles de substitution d'ensemble en combinant le Krigeage (Kriging) et les réseaux de neurones artificiels (ANN). Les résultats montrent que les approches proposées sont efficaces pour l'évaluation de la fiabilité. Quatre exemples et le modèle du jacket en considérant l'état limite ultime sont utilisés pour démontrer l'efficacité et la précision des approches proposées. Pour la plupart des exemples étudiés, les approches proposées nécessitent que la moitié du nombre d'appels des fonctions de performance par rapport à la méthode AK-MCS ; pour atteindre la probabilité de défaillance de référence obtenue par les simulations de Monte Carlo. En outre, il convient de mentionner que les approches proposées ne sont pas seulement adaptées à la combinaison du Krigeage et de l'ANN, mais peuvent également être étendues à d'autres modèles de substitution. En outre, l'obtention d'une évaluation plus précise de la probabilité de défaillance est conditionnée au critère de convergence des algorithmes proposées.

Le chapitre 4 présente l'utilisation des méthodes de Krigeage avec un apprentissage actif pour l'analyse de la fiabilité des systèmes. Dans un premier temps, les fonctions d'apprentissage actif du modèle de Krigeage utilisé pour l'analyse de fiabilité d'une seule fonction de performance sont résumées. Ensuite, les approches de krigeage avec l'apprentissage actif pour l'analyse de la fiabilité des systèmes sont discutées. Nous nous concentrons sur l'approche de la fonction d'apprentissage composite, qui est plus efficace et plus précise. Les problèmes des fonctions d'apprentissage U composites existantes sont également discutés et une nouvelle fonction d'apprentissage U composite est proposée. Cette fonction d'apprentissage est plus robuste et résout les problèmes posés par les autres fonctions U composites. En outre, pour un problème donné, nous n'avons aucune idée de la meilleure fonction d'apprentissage à utiliser. Par conséquent, nous avons également adapté la fonction d'apprentissage H pour l'analyse de la fiabilité du système avec trois fonctions d'apprentissage composites. Trois exemples numériques et le modèle de jacket sont utilisés pour montrer les bonnes performances numériques des fonctions d'apprentissage proposées. En outre, ces approches ont été utilisées pour l'évaluation de la fiabilité système du jacket modélisé par les super-éléments pour la prise en compte de la concentration des contraintes dans l'état limite ultime. Les résultats montrent que la fonction d'apprentissage composite proposée est plus robuste pour l'analyse de la fiabilité système, tant pour les fonctions U que H. De plus, la fonction d'apprentissage H adaptée peut évaluer efficacement et précisément la probabilité de défaillance du système. Par conséquent, pour les applications d'ingénierie avancée, ces approches peuvent être utilisées efficacement pour l'estimation de la fiabilité système.

Aucun travail n'est parfait. Dans cette thèse, nous avons considérer que l'état limite ultime dans l'analyse de fiabilité du jacket. Cependant, les états limites de flambement et de fatigue peuvent être considérés également dans des travaux futurs. En outre, les modèles de substitution d'ensemble ne sont utilisés que pour l'analyse de la fiabilité d'une seule fonction de performance. L'utilisation de l'approche proposée basée sur la combinaison du krigeage et des réseaux de neurones artificiels pour l'analyse de la fiabilité des systèmes semble réalisable dans les futurs travaux de recherche. Cette perspective permet même de l'utiliser pour l'analyse de fiabilité dépendant du temps. Plusieurs perspectives sont énumérées pour la suite de ces travaux de recherche.

(1).Adaptation des modèles de substitution d'ensemble avec des approches d'apprentissage actif pour l'analyse de la fiabilité système.
(2).Développement de l'analyse de fiabilité dépendant du temps en utilisant les modèles de substitution d'ensemble.
(3).Combiner les modèles de substitution d'ensemble avec d'autres approches d'échantillonnage (tirages d'importance, Subset, etc.) pour l'analyse de fiabilité.
4).Développement d'une approche d'optimisation basée sur la fiabilité en utilisant les modèles de substitution d'ensemble.

Part IV

Bibliography

Bibliography

[DUB, 2013] (2013). Advanced representation of tubular joints in jacket models for offshore wind turbine simulation. Energy Procedia, 35:234 – 243.

[1990, 2003] 1990, N. E. (2003). Eurocodes structuraux : base de calcul des structures. France.

[Afshari et al., 2022] Afshari, S. S., Enayatollahi, F., Xu, X., and Liang, X. (2022). Machine learning-based methods in structural reliability analysis: A review. Reliability Engineering & System Safety, 219:108223.

[Agency, 2021] Agency, I. R. E. (2021). Renewable electricity and generation statistics, august 2021.

[Ahmadi, 2016] Ahmadi, H. (2016). A probability distribution model for scfs in internally ring-stiffened tubular kt-joints of offshore structures subjected to out-of-plane bending loads. Ocean Engineering, 116:184–199.

[Ahmadi and Lotfollahi-Yaghin, 2012] Ahmadi, H. and Lotfollahi-Yaghin, M. A. (2012). A probability distribution model for stress concentration factors in multi-planar tubular dkt-joints of steel offshore structures. Applied Ocean Research, 34:21–32.

[Alban et al., 2017] Alban, A., Darji, H. A., Imamura, A., and Nakayama, M. K. (2017). Efficient Monte Carlo methods for estimating failure probabilities. Reliability Engineering & System Safety, 165:376–394.

[Andrieu-Renaud et al., 2004] Andrieu-Renaud, C., Sudret, B., and Lemaire, M. (2004). The phi2 method: a way to compute time-variant reliability. Reliability Engineering & System Safety, 84(1):75–86.

[Ang and Cornell, 1974] Ang, A. H. and Cornell, C. A. (1974). Reliability bases of structural safety and design. Journal of the Structural Division, 100(Proc. Paper 10777).

[Ang et al., 1992] Ang, G. L., Ang, A. H.-S., and Tang, W. H. (1992). Optimal importance-sampling density estimator. Journal of engineering mechanics, 118(6):1146–1163.

[ANSYS, 2017] ANSYS (2017). 18.0 user's guide. 2017.

[Askey and Wilson, 1985] Askey, R. and Wilson, J. A. (1985). Some basic hypergeometric orthogonal polynomials that generalize Jacobi polynomials, volume 319. American Mathematical Soc.

[Au and Beck, 2001] Au, S.-K. and Beck, J. L. (2001). Estimation of small failure probabilities in high dimensions by subset simulation. Probabilistic engineering mechanics, 16(4):263–277.

[Aute et al., 2013] Aute, V., Saleh, K., Abdelaziz, O., Azarm, S., and Radermacher, R. (2013). Cross-validation based single response adaptive design of experiments for kriging metamodeling of deterministic computer simulations. Structural and Multidisciplinary Optimization, 48(3):581–605.

[Bachynski and Moan, 2012] Bachynski, E. E. and Moan, T. (2012). Design considerations for tension leg platform wind turbines. Marine Structures, 29(1):89–114.

[Bai, 2021] Bai, H. (2021). Machine learning assisted probabilistic prediction of long-term fatigue damage and vibration reduction of wind turbine tower using active damping system. PhD thesis, Normandie.

[Basudhar and Missoum, 2008] Basudhar, A. and Missoum, S. (2008). Adaptive explicit decision functions for probabilistic design and optimization using support vector machines. Computers & Structures, 86(19-20):1904–1917.

[Beck and Melchers, 2004] Beck, A. T. and Melchers, R. E. (2004). On the ensemble crossing rate approach to time variant reliability analysis of uncertain structures. Probabilistic Engineering Mechanics, 19(1-2):9–19.

[Bichon et al., 2008] Bichon, B. J., Eldred, M. S., Swiler, L. P., Mahadevan, S., and McFarland, J. M. (2008). Efficient global reliability analysis for nonlinear implicit performance functions. AIAA journal, 46(10):2459–2468.

[Bichon et al., 2011] Bichon, B. J., McFarland, J. M., and Mahadevan, S. (2011). Efficient surrogate models for reliability analysis of systems with multiple failure modes. Reliability Engineering & System Safety, 96(10):1386–1395.

[Binder et al., 1993] Binder, K., Heermann, D., Roelofs, L., Mallinckrodt, A. J., and McKay, S. (1993). Monte Carlo simulation in statistical physics. Computers in Physics, 7(2):156–157.

[Bjerager, 1988] Bjerager, P. (1988). Probability integration by directional simulation. Journal of Engineering Mechanics, 114(8):1285–1302.

[Blatman and Sudret, 2010] Blatman, G. and Sudret, B. (2010). An adaptive algorithm to build up sparse polynomial chaos expansions for stochastic finite element analysis. Probabilistic Engineering Mechanics, 25(2):183–197.

[Bourinet, 2016] Bourinet, J.-M. (2016). Rare-event probability estimation with adaptive support vector regression surrogates. Reliability Engineering & System Safety, 150:210–221.

[Bourinet et al., 2011] Bourinet, J.-M., Deheeger, F., and Lemaire, M. (2011). Assessing small failure probabilities by combined subset simulation and support vector machines. Structural Safety, 33(6):343–353.

[Box et al., 1978] Box, G. E., Hunter, W. H., Hunter, S., et al. (1978). Statistics for experimenters, volume 664. John Wiley and sons New York.

[Branlard et al., 2020] Branlard, E., Shields, M., Anderson, B., Damiani, R., Wendt, F., Jonkman, J., Musial, W., and Foley, B. (2020). Superelement reduction of substructures for sequential load calculations in openfast. In Journal of Physics: Conference Series, volume 1452, page 012033.

[Braverman et al., 2015] Braverman, V., Ostrovsky, R., and Vorsanger, G. (2015). Weighted sampling without replacement from data streams. Information Processing Letters, 115(12):923–926.

[Bredmose et al., 2013] Bredmose, H., Mariegaard, J., Paulsen, B., Jensen, B., Schløer, S., Larsen, T., Kim, T., and Hansen, A. (2013). The Wave Loads project. Number 0045 in DTU Wind Energy E. DTU Wind Energy, Denmark.

[Bucher and Bourgund, 1990] Bucher, C. G. and Bourgund, U. (1990). A fast and efficient response surface approach for structural reliability problems. Structural safety, 7(1):57–66.

[Bungartz and Griebel, 2004] Bungartz, H.-J. and Griebel, M. (2004). Sparse grids. Acta numerica, 13:147–269.

[Burton et al., 2011] Burton, T., Jenkins, N., Sharpe, D., and Bossanyi, E. (2011). Wind energy handbook. John Wiley & Sons.

[Campolongo et al., 2007] Campolongo, F., Cariboni, J., and Saltelli, A. (2007). An effective screening design for sensitivity analysis of large models. Environmental modelling & software, 22(10):1509–1518.

[Chao et al., 2021] Chao, R., Aoues, Y., Lemosse, D., and DE CURSI, E. S. (2021). Structural reliability assessment of offshore wind turbine jacket considering corrosion degradation. In 14th WCCM-ECCOMAS Congress 2020.

[Chen et al., 2021] Chen, J., Chen, Z., Xu, Y., and Li, H. (2021). Efficient reliability analysis combining kriging and subset simulation with two-stage convergence criterion. Reliability Engineering & System Safety, 214:107737.

[Chen et al., 2019] Chen, T., Wang, X., Gu, X., Zhao, Q., Yuan, G., and Liu, J. (2019). Axial compression tests of grouted connections in jacket and monopile offshore wind turbine structures. Engineering Structures, 196:109330.

[Chen Ong et al., 2017] Chen Ong, M., Bachynski, E. E., and David Økland, O. (2017). Dynamic responses of jacket-type offshore wind turbines using decoupled and coupled models. Journal of Offshore Mechanics and Arctic Engineering, 139(4).

[Cheng et al., 2018] Cheng, B., Li, C., Lou, Y., and Zhao, X. (2018). Parametric FE modeling to predict hot spot stress concentrations of bird-beak SHS joints in offshore structures. Ocean Engineering, 160:54–67.

[Cheng and Titterington, 1994] Cheng, B. and Titterington, D. M. (1994). Neural networks: A review from a statistical perspective. Statistical science, pages 2–30.

[Cheng and Lu, 2020] Cheng, K. and Lu, Z. (2020). Structural reliability analysis based on ensemble learning of surrogate models. Structural Safety, 83:101905.

[Chojaczyk et al., 2015] Chojaczyk, A. A., Teixeira, A. P., Neves, L. C., Cardoso, J. B., and Soares, C. G. (2015). Review and application of artificial neural networks models in reliability analysis of steel structures. Structural Safety, 52:78–89.

[Coleman, 1959] Coleman, J. J. (1959). Reliability of aircraft structures in resisting chance failure. Operations Research, 7(5):639–645.

[Commission et al., 2019] Commission, I. E. et al. (2019). Iec 61400-1: 2019: Wind energy generation systems-part 1: Design requirements.

[Council, 2021] Council, G. W. E. (2021). Gwec: Global wind report 2021.

[Craig Jr and Bampton, 1968] Craig Jr, R. R. and Bampton, M. C. (1968). Coupling of substructures for dynamic analyses. AIAA journal, 6(7):1313–1319.

[de Angelis et al., 2015] de Angelis, M., Patelli, E., and Beer, M. (2015). Advanced line sampling for efficient robust reliability analysis. Structural safety, 52:170–182.

[de Klerk et al., 2008] de Klerk, D., Rixen, D. J., and Voormeeren, S. (2008). General framework for dynamic substructuring: history, review and classification of techniques. AIAA journal, 46(5):1169–1181.

[De Valk, 2013] De Valk, P. (2013). Accuracy of calculation procedures for offshore wind turbine support structures.

[Depina et al., 2016] Depina, I., Le, T. M. H., Fenton, G., and Eiksund, G. (2016). Reliability analysis with metamodel line sampling. Structural Safety, 60:1–15.

[Der Kiureghian, 2000] Der Kiureghian, A. (2000). The geometry of random vibrations and solutions by FORM and SORM. Probabilistic Engineering Mechanics, 15(1):81–90.

[Dey and Mahadevan, 1998] Dey, A. and Mahadevan, S. (1998). Ductile structural system reliability analysis using adaptive importance sampling. Structural safety, 20(2):137–154.

[Ditlevsen, 1979] Ditlevsen, O. (1979). Narrow reliability bounds for structural systems. Journal of structural mechanics, 7(4):453–472.

[Ditlevsen et al., 1990] Ditlevsen, O., Melchers, R. E., and Gluver, H. (1990). General multi-dimensional probability integration by directional simulation. Computers & Structures, 36(2):355–368.

[DNV, 2016] DNV, G. (2016). DNVGL-ST-0126: Support structures for wind turbines. Oslo, Norway: DNV GL.

[Dong et al., 2011] Dong, W., Moan, T., and Gao, Z. (2011). Long-term fatigue analysis of multi-planar tubular joints for jacket-type offshore wind turbine in time domain. Engineering Structures, 33(6):2002–2014.

[Dong et al., 2012] Dong, W., Moan, T., and Gao, Z. (2012). Fatigue reliability analysis of the jacket support structure for offshore wind turbine considering the effect of corrosion and inspection. Reliability Engineering & System Safety, 106:11–27.

[Dong et al., 2018] Dong, Y., Teixeira, A., and Soares, C. G. (2018). Time-variant fatigue reliability assessment of welded joints based on the phi2 and response surface methods. Reliability Engineering & System Safety, 177:120–130.

[Du et al., 2019] Du, W., Luo, Y., and Wang, Y. (2019). Time-variant reliability analysis using the parallel subset simulation. Reliability Engineering & System Safety, 182:250–257.

[Dunnett and Sobel, 1954] Dunnett, C. W. and Sobel, M. (1954). A bivariate generalization of student's t-distribution, with tables for certain special cases. Biometrika, 41(1-2):153–169.

[Eason and Cremaschi, 2014] Eason, J. and Cremaschi, S. (2014). Adaptive sequential sampling for surrogate model generation with artificial neural networks. Computers & Chemical Engineering, 68:220–232.

[Echard et al., 2011] Echard, B., Gayton, N., and Lemaire, M. (2011). AK-MCS: an active learning reliability method combining kriging and Monte Carlo simulation. Structural Safety, 33(2):145–154.

[Efraimidis and Spirakis, 2006] Efraimidis, P. S. and Spirakis, P. G. (2006). Weighted random sampling with a reservoir. Information Processing Letters, 97(5):181–185.

[Eldred and Burkardt, 2009] Eldred, M. and Burkardt, J. (2009). Comparison of non-intrusive polynomial chaos and stochastic collocation methods for uncertainty quantification. In 47th AIAA aerospace sciences meeting including the new horizons forum and aerospace exposition, page 976.

[Fauriat and Gayton, 2014] Fauriat, W. and Gayton, N. (2014). AK-SYS: an adaptation of the AK-MCS method for system reliability. Reliability Engineering & System Safety, 123:137–144.

[Fischer et al., 2010] Fischer, T., De Vries, W., and Schmidt, B. (2010). Upwind design basis. Upwind deliverable (WP4: Offshore foundations and support structures), Endowed Chair of Wind Energy (SWE) at the Institute of Aircraft Design Universit at Stuttgart.

[Freeman et al., 2016] Freeman, K., Hundleby, G., Nordstrom, C., Roberts, A., Valpy, B., Willow, C., Torato, P., Ayuso, M., and Boshell, F. (2016). Floating foundations: A game changer for offshore wind power.

[Fuhg et al., 2020] Fuhg, J. N., Fau, A., and Nackenhorst, U. (2020). State-of-the-art and comparative review of adaptive sampling methods for kriging. Archives of Computational Methods in Engineering, pages 1–59.

[Gentils et al., 2017] Gentils, T., Wang, L., and Kolios, A. (2017). Integrated structural optimisation of offshore wind turbine support structures based on finite element analysis and genetic algorithm. Applied energy, 199:187–204.

[Glisic et al., 2018] Glisic, A., Nguyen, N.-D., Schaumann, P., et al. (2018). Comparison of integrated and sequential design approaches for fatigue analysis of a jacket offshore wind turbine structure. In The 28th International Ocean and Polar Engineering Conference. International Society of Offshore and Polar Engineers.

[Glynn and Iglehart, 1989] Glynn, P. W. and Iglehart, D. L. (1989). Importance sampling for stochastic simulations. Management science, 35(11):1367–1392.

[Goel et al., 2007] Goel, T., Haftka, R. T., Shyy, W., and Queipo, N. V. (2007). Ensemble of surrogates. Structural and Multidisciplinary Optimization, 33(3):199–216.

[Guo et al., 2021] Guo, Q., Liu, Y., Chen, B., and Yao, Q. (2021). A variable and mode sensitivity analysis method for structural system using a novel active learning kriging model. Reliability Engineering & System Safety, 206:107285.

[Guyan, 1965] Guyan, R. J. (1965). Reduction of stiffness and mass matrices. AIAA journal, 3(2):380–380.

[Haselbach et al., 2013] Haselbach, P., Natarajan, A., Jiwinangun, R. G., and Branner, K. (2013). Comparison of coupled and uncoupled load simulations on a jacket support structure. Energy Procedia, 35:244–252.

[Hasselmann et al., 1973] Hasselmann, K. F., Barnett, T. P., Bouws, E., Carlson, H., Cartwright, D. E., Eake, K., Euring, J., Gicnapp, A., Hasselmann, D., Kruseman, P., et al. (1973). Measurements of windwave growth and swell decay during the joint north sea wave project (jonswap). Ergaenzungsheft zur Deutschen Hydrographischen Zeitschrift, Reihe A.

[Hastings, 1970] Hastings, W. K. (1970). Monte Carlo sampling methods using markov chains and their applications.

[Henderson et al., 2003] Henderson, A. R., Morgan, C., Smith, B., Sørensen, H. C., Barthelmie, R. J., and Boesmans, B. (2003). Offshore wind energy in europe—a review of the state-of-the-art. Wind Energy: An International Journal for Progress and Applications in Wind Power Conversion Technology, 6(1):35–52.

[Herman and Usher, 2017] Herman, J. D. and Usher, W. (2017). SALib: An open-source python library for sensitivity analysis. J. Open Source Software, 2(9):97.

[Hermans and Peeringa, 2016] Hermans, K. and Peeringa, J. (2016). Future XL monopile foundation design for a 10 MW wind turbine in deep water. ECN.

[Hohenbichler and Rackwitz, 1982] Hohenbichler, M. and Rackwitz, R. (1982). First-order concepts in system reliability. Structural safety, 1(3):177–188.

[Hu and Du, 2013] Hu, Z. and Du, X. (2013). Time-dependent reliability analysis with joint upcrossing rates. Structural and Multidisciplinary Optimization, 48(5):893–907.

[Hu and Mahadevan, 2016] Hu, Z. and Mahadevan, S. (2016). Global sensitivity analysis-enhanced surrogate (GSAS) modeling for reliability analysis. Structural and Multidisciplinary Optimization, 53(3):501–521.

[Hu et al., 2017] Hu, Z., Nannapaneni, S., and Mahadevan, S. (2017). Efficient kriging surrogate modeling approach for system reliability analysis. AI EDAM, 31(2):143–160.

[Huang et al., 2016] Huang, X., Chen, J., and Zhu, H. (2016). Assessing small failure probabilities by AK–SS: an active learning method combining kriging and subset simulation. Structural Safety, 59:86–95.

[Hübler et al., 2017a] Hübler, C., Gebhardt, C. G., and Rolfes, R. (2017a). Development of a comprehensive database of scattering environmental conditions and simulation constraints for offshore wind turbines. Wind Energy Science, 2(2):491–505.

[Hübler et al., 2017b] Hübler, C., Gebhardt, C. G., and Rolfes, R. (2017b). Hierarchical four-step global sensitivity analysis of offshore wind turbines based on aeroelastic time domain simulations. Renewable Energy, 111:878–891.

[Huchet, 2018] Huchet, Q. (2018). Kriging based methods for the structural damage assessment of offshore wind turbines. PhD thesis, Université Clermont Auvergne.

[Hurtado, 2004] Hurtado, J. E. (2004). An examination of methods for approximating implicit limit state functions from the viewpoint of statistical learning theory. Structural Safety, 26(3):271–293.

[Hurtado and Alvarez, 2001] Hurtado, J. E. and Alvarez, D. A. (2001). Neural-network-based reliability analysis: a comparative study. Computer methods in applied mechanics and engineering, 191(1-2):113–132.

[IEC, 2009] IEC, I. (2009). 61400-3, wind turbines-part 3: Design requirements for offshore wind turbines. International Electrotechnical Commission, Geneva.

[Ingram, 2011] Ingram, G. (2011). Wind turbine blade analysis using the blade element momentum method. version 1.1. Durham University, Durham.

[Ivanhoe et al., 2020] Ivanhoe, R., Wang, L., and Kolios, A. (2020). Generic framework for reliability assessment of offshore wind turbine jacket support structures under stochastic and time dependent variables. Ocean Engineering, 216:107691.

[Jiang et al., 2020] Jiang, C., Qiu, H., Gao, L., Wang, D., Yang, Z., and Chen, L. (2020). EEK-SYS: System reliability analysis through estimation error-guided adaptive kriging approximation of multiple limit state surfaces. Reliability Engineering & System Safety, 198:106906.

[Jiang et al., 2021] Jiang, X., Lu, Z., Wei, N., and Hu, Y. (2021). An efficient method for solving the system failure possibility of multi-mode structure by combining hierarchical fuzzy simulation with kriging model. Structural and Multidisciplinary Optimization, pages 1–20.

[Jiang, 2021] Jiang, Z. (2021). Installation of offshore wind turbines: A technical review. Renewable and Sustainable Energy Reviews, 139:110576.

[Jin et al., 2002] Jin, R., Chen, W., and Sudjianto, A. (2002). On sequential sampling for global metamodeling in engineering design. In International Design Engineering Technical Conferences and Computers and Information in Engineering Conference, volume 36223, pages 539–548.

[Jonkman and Buhl Jr, 2006] Jonkman, B. J. and Buhl Jr, M. L. (2006). Turbsim user's guide. Technical report, National Renewable Energy Lab.(NREL), Golden, CO (United States).

[Jonkman, 2014] Jonkman, J. (2014). Overview of offshore features of fast–hydrodyn, subdyn & map. In NREL Workshop, September.

[Jonkman et al., 2009] Jonkman, J., Butterfield, S., Musial, W., and Scott, G. (2009). Definition of a 5-MW reference wind turbine for offshore system development. Technical report, National Renewable Energy Lab.(NREL), Golden, CO (United States).

[Jonkman et al., 2012] Jonkman, J., Robertson, A., Popko, W., Vorpahl, F., Zuga, A., Kohlmeier, M., Larsen, T., Yde, A., and Knut M. Oksta, K. S., Nichols, J., Nygaard, T., Gao, Z., Manolas, D., Kim, K., Yu, Q., Shi, W., Park, H., Vasquez-Rojas, A., Dubois, J., Kaufer, D., Thomassen, P., de Ruiter, M., Peering, J., Zhiwen, H., and von Waade, H. (2012). Offshore code comparison collaboration continuation (OC4), Phase I – Results of coupled simulations of an offshore wind turbine with jacket support structure. Technical report, NREL.

[Jonkman et al., 2005] Jonkman, J. M., Buhl Jr, M. L., et al. (2005). FAST user's guide.

[Kalos and Whitlock, 2009] Kalos, M. H. and Whitlock, P. A. (2009). Monte carlo methods. John Wiley & Sons.

[Kausche et al., 2018] Kausche, M., Adam, F., Dahlhaus, F., and Großmann, J. (2018). Floating offshore wind-economic and ecological challenges of a TLP solution. Renewable Energy, 126:270–280.

[Kaymaz, 2005] Kaymaz, I. (2005). Application of kriging method to structural reliability problems. Structural Safety, 27(2):133–151.

[Kleijnen and Van Beers, 2004] Kleijnen, J. P. and Van Beers, W. C. (2004). Application-driven sequential designs for simulation experiments: Kriging metamodelling. Journal of the operational research society, 55(8):876–883.

[Kooijman et al., 2003] Kooijman, H., Lindenburg, C., Winkelaar, D., and Van der Hooft, E. (2003). DOWEC 6 MW pre-design: Aero-elastic modeling of the DOWEC 6 MW pre-design in PHATAS. DOWEC Dutch Offshore Wind Energy Converter 1997–2003 Public Reports.

[Krige, 1951] Krige, D. G. (1951). A statistical approach to some basic mine valuation problems on the witwatersrand. Journal of the Southern African Institute of Mining and Metallurgy, 52(6):119–139.

[Kucherenko and Song, 2016] Kucherenko, S. and Song, S. (2016). Derivative-based global sensitivity measures and their link with sobol'sensitivity indices. In Monte Carlo and Quasi-Monte Carlo Methods, pages 455–469. Springer.

[Larsen and Hansen, 2007] Larsen, T. J. and Hansen, A. M. (2007). How 2 HAWC2, the user's manual. target, 2(2).

[Lee et al., 2014] Lee, Y.-S., Choi, B.-L., Lee, J. H., Kim, S. Y., and Han, S. (2014). Reliability-based design optimization of monopile transition piece for offshore wind turbine system. Renewable Energy, 71:729–741.

[Lei et al., 2021] Lei, J., Lu, Z., and Wang, L. (2021). An efficient method by nesting adaptive kriging into importance sampling for failure-probability-based global sensitivity analysis. Engineering with Computers, pages 1–16.

[Lelièvre et al., 2018] Lelièvre, N., Beaurepaire, P., Mattrand, C., and Gayton, N. (2018). AK-MCSi: A kriging-based method to deal with small failure probabilities and time-consuming models. Structural Safety, 73:1–11.

[Li and Au, 2010] Li, H.-S. and Au, S.-K. (2010). Design optimization using subset simulation algorithm. Structural Safety, 32(6):384–392.

[Li et al., 2019] Li, H.-S., Wang, T., Yuan, J.-Y., and Zhang, H. (2019). A sampling-based method for high-dimensional time-variant reliability analysis. Mechanical Systems and Signal Processing, 126:505–520.

[Li et al., 2021] Li, T., Pan, Q., and Dias, D. (2021). Active learning relevant vector machine for reliability analysis. Applied Mathematical Modelling, 89:381–399.

[Li et al., 2018a] Li, X., Ding, Q., and Sun, J.-Q. (2018a). Remaining useful life estimation in prognostics using deep convolution neural networks. Reliability Engineering & System Safety, 172:1–11.

[Li et al., 2018b] Li, X., Gong, C., Gu, L., Gao, W., Jing, Z., and Su, H. (2018b). A sequential surrogate method for reliability analysis based on radial basis function. Structural Safety, 73:42–53.

[Liu et al., 2016] Liu, Y., Li, S., Yi, Q., and Chen, D. (2016). Developments in semi-submersible floating foundations supporting wind turbines: A comprehensive review. Renewable and Sustainable Energy Reviews, 60:433–449.

[Lloyd and Hamburg, 2010] Lloyd, G. and Hamburg, G. (2010). Guideline for the certification of wind turbines. July 1st.

[Loève, 1955] Loève, M. (1955). Probability theory (New York, 1955). and, 407:384.

[Lombardi et al., 2017] Lombardi, P., Balischewski, S., Hauer, I., Wolter, M., and Wenge, C. (2017). Battery storage services that minimize wind farm operating costs: A case study.

[Low, 2014] Low, B. (2014). FORM, SORM, and spatial modeling in geotechnical engineering. Structural Safety, 49:56–64.

[Lv et al., 2015] Lv, Z., Lu, Z., and Wang, P. (2015). A new learning function for kriging and its applications to solve reliability problems in engineering. Computers & Mathematics with Applications, 70(5):1182–1197.

[Manwell et al., 2010] Manwell, J. F., McGowan, J. G., and Rogers, A. L. (2010). Wind energy explained: theory, design and application. John Wiley & Sons.

[Marelli and Sudret, 2018] Marelli, S. and Sudret, B. (2018). An active-learning algorithm that combines sparse polynomial chaos expansions and bootstrap for structural reliability analysis. Structural Safety, 75:67–74.

[McDonald and Mahadevan, 2008] McDonald, M. and Mahadevan, S. (2008). Design optimization with system-level reliability constraints.

[Micallef and Rezaeiha, 2021] Micallef, D. and Rezaeiha, A. (2021). Floating offshore wind turbine aerodynamics: Trends and future challenges. Renewable and Sustainable Energy Reviews, 152:111696.

[Morris, 2011] Morris, L. (2011). Direct drive vs. gearbox: progress on both fronts: will the wind turbine technology showdown leave just one technology standing? Power Engineering, 115(3):38–42.

[Morris, 1991] Morris, M. D. (1991). Factorial sampling plans for preliminary computational experiments. Technometrics, 33(2):161–174.

[Moulas et al., 2017] Moulas, D., Shafiee, M., and Mehmanparast, A. (2017). Damage analysis of ship collisions with offshore wind turbine foundations. Ocean Engineering, 143:149–162.

[Moustapha et al., 2022] Moustapha, M., Marelli, S., and Sudret, B. (2022). Active learning for structural reliability: Survey, general framework and benchmark. Structural Safety, page 102174.

[Neal, 2001] Neal, R. M. (2001). Annealed importance sampling. Statistics and computing, 11(2):125–139.

[Nelder and Wedderburn, 1972] Nelder, J. A. and Wedderburn, R. W. (1972). Generalized linear models. Journal of the Royal Statistical Society: Series A (General), 135(3):370–384.

[Nie and Ellingwood, 2000] Nie, J. and Ellingwood, B. R. (2000). Directional methods for structural reliability analysis. Structural Safety, 22(3):233–249.

[Pandey, 1998] Pandey, M. (1998). An effective approximation to evaluate multinormal integrals. Structural safety, 20(1):51–67.

[Papadrakakis and Lagaros, 2002] Papadrakakis, M. and Lagaros, N. D. (2002). Reliability-based structural optimization using neural networks and Monte Carlo simulation. Computer methods in applied mechanics and engineering, 191(32):3491–3507.

[Papaioannou and Straub, 2021] Papaioannou, I. and Straub, D. (2021). Variance-based reliability sensitivity analysis and the form α-factors. Reliability Engineering & System Safety, 210:107496.

[Paz, 1984] Paz, M. (1984). Dynamic condensation. AIAA journal, 22(5):724–727.

[Pedregosa et al., 2011] Pedregosa, F., Varoquaux, G., Gramfort, A., Michel, V., Thirion, B., Grisel, O., Blondel, M., Prettenhofer, P., Weiss, R., Dubourg, V., Vanderplas, J., Passos, A., Cournapeau, D., Brucher, M., Perrot, M., and Duchesnay, E. (2011). Scikit-learn: Machine learning in Python. Journal of Machine Learning Research, 12:2825–2830.

[Peijuan et al., 2017] Peijuan, Z., Ming, W. C., Zhouhong, Z., and Liqi, W. (2017). A new active learning method based on the learning function U of the AK-MCS reliability analysis method. Engineering Structures, 148:185–194.

[Pierson Jr and Moskowitz, 1964] Pierson Jr, W. J. and Moskowitz, L. (1964). A proposed spectral form for fully developed wind seas based on the similarity theory of sa kitaigorodskii. Journal of geophysical research, 69(24):5181–5190.

[Popko et al., 2015] Popko, W., Georgiadou, S., Loukogeorgaki, E., Vorpahl, F., et al. (2015). Influence of joint flexibility on local dynamics of a jacket support structure. In The Twenty-fifth International Ocean and Polar Engineering Conference. International Society of Offshore and Polar Engineers.

[Popko et al., 2012] Popko, W., Vorpahl, F., Zuga, A., Kohlmeier, M., Jonkman, J., Robertson, A., Larsen, T. J., Yde, A., Saetertro, K., Okstad, K. M., et al. (2012). Offshore code comparison collaboration continuation (OC4), phase I-Results of coupled simulations of an offshore wind turbine with jacket support structure. Technical report, National Renewable Energy Lab.(NREL), Golden, CO (United States).

[Qian et al., 2019] Qian, H.-M., Huang, H.-Z., and Li, Y.-F. (2019). A novel single-loop procedure for time-variant reliability analysis based on kriging model. Applied Mathematical Modelling, 75:735–748.

[Qian et al., 2021] Qian, H.-M., Huang, T., and Huang, H.-Z. (2021). A single-loop strategy for time-variant system reliability analysis under multiple failure modes. Mechanical Systems and Signal Processing, 148:107159.

[Rackwitz, 1998] Rackwitz, R. (1998). Computational techniques in stationary and non-stationary load combination-a review and some extensions. Journal of Structural Engineering, 25(1)):1–20.

[Rackwitz and Flessler, 1978] Rackwitz, R. and Flessler, B. (1978). Structural reliability under combined random load sequences. Computers & Structures, 9(5):489–494.

[Rajashekhar and Ellingwood, 1993] Rajashekhar, M. R. and Ellingwood, B. R. (1993). A new look at the response surface approach for reliability analysis. Structural safety, 12(3):205–220.

[Reinsch, 1967] Reinsch, C. H. (1967). Smoothing by spline functions. Numerische mathematik, 10(3):177–183.

[Ren et al., 2020] Ren, C., Aoues, Y., Lemosse, D., and De Cursi, E. S. (2020). Global sensitivity analysis of offshore wind turbine jacket. In International Symposium on Uncertainty Quantification and Stochastic Modeling, pages 35–48. Springer.

[Ren et al., 2021] Ren, C., Aoues, Y., Lemosse, D., and De Cursi, E. S. (2021). Comparative study of load simulation approaches used for the dynamic analysis on an offshore wind turbine jacket with different modeling techniques. Engineering Structures, 249:113308.

[Rice, 1944] Rice, S. O. (1944). Mathematical analysis of random noise. The Bell System Technical Journal, 23(3):282–332.

[Rixen and van der Valk, 2013] Rixen, D. J. and van der Valk, P. L. (2013). An impulse based substructuring approach for impact analysis and load case simulations. Journal of Sound and Vibration, 332(26):7174–7190.

[Robert et al., 2004] Robert, C. P., Casella, G., and Casella, G. (2004). Monte Carlo statistical methods, volume 2. Springer.

[Roussouly et al., 2013] Roussouly, N., Petitjean, F., and Salaun, M. (2013). A new adaptive response surface method for reliability analysis. Probabilistic Engineering Mechanics, 32:103–115.

[Roustant et al., 2017] Roustant, O., Barthe, F., and Iooss, B. (2017). Poincaré inequalities on intervals–application to sensitivity analysis. Electronic journal of statistics, 11(2):3081–3119.

[Sacks et al., 1989] Sacks, J., Welch, W. J., Mitchell, T. J., and Wynn, H. P. (1989). Design and analysis of computer experiments. Statistical science, 4(4):409–423.

[Schobi et al., 2015] Schobi, R., Sudret, B., and Wiart, J. (2015). Polynomial-chaos-based kriging. International Journal for Uncertainty Quantification, 5(2).

[Schueremans and Van Gemert, 2005] Schueremans, L. and Van Gemert, D. (2005). Benefit of splines and neural networks in simulation based structural reliability analysis. Structural safety, 27(3):246–261.

[Sclavounos et al., 2010] Sclavounos, P. D., Lee, S., DiPietro, J., Potenza, G., Caramuscio, P., and De Michele, G. (2010). Floating offshore wind turbines: tension leg platform and taught leg buoy concepts supporting 3-5 mw wind turbines. In European wind energy conference EWEC, pages 20–23.

[Secretariat, 2020] Secretariat, R. (2020). Renewables 2020 global status report. Rep. Paris: REN12.

[Shi et al., 2020] Shi, Y., Lu, Z., He, R., Zhou, Y., and Chen, S. (2020). A novel learning function based on kriging for reliability analysis. Reliability Engineering & System Safety, 198:106857.

[Shittu et al., 2020] Shittu, A. A., Mehmanparast, A., Shafiee, M., Kolios, A., Hart, P., and Pilario, K. (2020). Structural reliability assessment of offshore wind turbine support structures subjected to pitting corrosion-fatigue: A damage tolerance modelling approach. Wind Energy, 23(11):2004–2026.

[Smola and Schölkopf, 2004] Smola, A. J. and Schölkopf, B. (2004). A tutorial on support vector regression. Statistics and computing, 14(3):199–222.

[Sobol, 2001] Sobol, I. M. (2001). Global sensitivity indices for nonlinear mathematical models and their Monte Carlo estimates. Mathematics and computers in simulation, 55(1-3):271–280.

[Song et al., 2013] Song, H., Damiani, R., Robertson, A., and Jonkman, J. (2013). New structural-dynamics module for offshore multimember substructures within the wind turbine computer-aided engineering tool fast. Technical report, National Renewable Energy Lab.(NREL), Golden, CO (United States).

[Spanos and Ghanem, 1989] Spanos, P. D. and Ghanem, R. (1989). Stochastic finite element expansion for random media. Journal of engineering mechanics, 115(5):1035–1053.

[Standard, 2007] Standard, O. (2007). Design of offshore wind turbine structures. DET NOR SKE VERITAS, 581.

[Steiner et al., 2019] Steiner, M., Bourinet, J.-M., and Lahmer, T. (2019). An adaptive sampling method for global sensitivity analysis based on least-squares support vector regression. Reliability Engineering & System Safety, 183:323–340.

[Stieng and Muskulus, 2020] Stieng, L. E. S. and Muskulus, M. (2020). Reliability-based design optimization of offshore wind turbine support structures using analytical sensitivities and factorized uncertainty modeling. Wind Energy Science, 5(1):171–198.

[Sudret and Berveiller, 2008] Sudret, B. and Berveiller, M. (2008). Stochastic finite element methods in geotechnical engineering. Reliability-Based design in Geotechnical Engineering: Computations and applications, Taylor & Francis (Eds.), New York, USA, pages 260–297.

[Sun et al., 2012] Sun, X., Huang, D., and Wu, G. (2012). The current state of offshore wind energy technology development. Energy, 41(1):298–312.

[Sun et al., 2017] Sun, Z., Wang, J., Li, R., and Tong, C. (2017). LIF: A new Kriging based learning function and its application to structural reliability analysis. Reliability Engineering & System Safety, 157:152–165.

[Taflanidis et al., 2013] Taflanidis, A. A., Loukogeorgaki, E., and Angelides, D. C. (2013). Offshore wind turbine risk quantification/evaluation under extreme environmental conditions. Reliability Engineering & System Safety, 115:19–32.

[Tamimi et al., 1989] Tamimi, S., Amadei, B., and Frangopol, D. M. (1989). Monte Carlo simulation of rock slope reliability. Computers & structures, 33(6):1495–1505.

[Teixeira et al., 2020] Teixeira, R., Martinez-Pastor, B., Nogal, M., and O'Connor, A. (2020). Reliability analysis using a multi-metamodel complement-basis approach. Reliability Engineering & System Safety, 205:107248.

[Teixeira et al., 2021] Teixeira, R., Nogal, M., and O'Connor, A. (2021). Adaptive approaches in metamodel-based reliability analysis: A review. Structural Safety, 89:102019.

[Thomsen, 2014] Thomsen, K. (2014). Offshore wind: a comprehensive guide to successful offshore wind farm installation. Academic Press.

[Tu et al., 2014] Tu, Y., Vorpahl, F., et al. (2014). Influence of superelement support structure modeling on the loads on an offshore wind turbine with a jacket support structure. In The Twenty-fourth International Ocean and Polar Engineering Conference. International Society of Offshore and Polar Engineers.

[turbine design software Bladed, 2011] turbine design software Bladed, W. (2011). Wind turbine design software - bladed - dnv gl.

[Tvedt, 1990] Tvedt, L. (1990). Distribution of quadratic forms in normal space—application to structural reliability. Journal of engineering mechanics, 116(6):1183–1197.

[Uzunoglu and Soares, 2020] Uzunoglu, E. and Soares, C. G. (2020). Hydrodynamic design of a free-float capable tension leg platform for a 10 mw wind turbine. Ocean Engineering, 197:106888.

[Van der Valk and Voormeeren, 2012] Van der Valk, P. and Voormeeren, S. (2012). An overview of modeling approaches for complex offshore wind turbine support structures. Proceedings of ISMA2012-USD2012, pages 17–19.

[van der Valk and Rixen, 2014] van der Valk, P. L. and Rixen, D. J. (2014). An impulse based substructuring method for coupling impulse response functions and finite element models. Computer Methods in Applied Mechanics and Engineering, 275:113–137.

[van der Valk et al., 2015] van der Valk, P. L., Voormeeren, S. N., de Valk, P. C., and Rixen, D. J. (2015). Dynamic models for load calculation procedures of offshore wind turbine support structures: Overview, assessment, and outlook. Journal of Computational and Nonlinear Dynamics, 10(4).

[Van der Valk, 2014] Van der Valk, P. L. C. (2014). Coupled simulations of wind turbines and offshore support structures: Strategies based on the dynamic substructuring paradigm.

[Velarde et al., 2019a] Velarde, J., Kramhøft, C., and Sørensen, J. D. (2019a). Global sensitivity analysis of offshore wind turbine foundation fatigue loads. Renewable Energy, 140:177–189.

[Velarde et al., 2019b] Velarde, J., Vanem, E., Kramhøft, C., and Sørensen, J. D. (2019b). Probabilistic analysis of offshore wind turbines under extreme resonant response: Application of environmental contour method. Applied Ocean Research, 93:101947.

[Vemula et al., 2010] Vemula, N. K., De Vries, W., Fischer, T., Cordle, A., and Schmidt, B. (2010). Design solution for the upwind reference offshore support structure.

[Veritas, 2002] Veritas, D. N. (2002). Guidelines for design of wind turbines. Wind Energy Departement, Riso National Laboratory.

[Veritas, 2004] Veritas, D. N. (2004). DNV-OS-J101-design of offshore wind turbine structures. Det Norske Veritas.

[Voormeeren et al., 2014] Voormeeren, S., van der Valk, P., Nortier, B., Molenaar, D.-P., and Rixen, D. (2014). Accurate and efficient modeling of complex offshore wind turbine support structures using augmented superelements. Wind Energy, 17(7):1035–1054.

[Vorpahl et al., 2011] Vorpahl, F., Popko, W., and Kaufer, D. (2011). Description of a basic model of the "upwind reference jacket" for code comparison in the oc4 project under iea wind annex xxx. Technical report.

[Vorpahl, 2015] Vorpahl, F. R. (2015). Modeling of offshore wind turbines with braced support structures. PhD thesis, Hannover: Gottfried Wilhelm Leibniz Universität Hannover.

[Walatka et al., 1994] Walatka, P. P., Clucas, J., McCabe, R. K., Plessel, T., Potter, R., and Cooper, D. (1994). Fast user guide.

[Wang et al., 2021] Wang, J., Sun, Z., and Cao, R. (2021). An efficient and robust kriging-based method for system reliability analysis. Reliability Engineering & System Safety, 216:107953.

[Wang and Kolios, 2017] Wang, L. and Kolios, A. (2017). A generic framework for reliability assessment of offshore wind turbine monopiles considering soil-solid interaction and harsh marine environments. In Proceedings of the 5th International Conference on Marine Structures, MARSTRUCT, Lisbon, Portugal, pages 8–10.

[Wang and Chen, 2016] Wang, Z. and Chen, W. (2016). Time-variant reliability assessment through equivalent stochastic process transformation. Reliability Engineering & System Safety, 152:166–175.

[Wang and Chen, 2017] Wang, Z. and Chen, W. (2017). Confidence-based adaptive extreme response surface for time-variant reliability analysis under random excitation. Structural Safety, 64:76–86.

[Wang and Shafieezadeh, 2019a] Wang, Z. and Shafieezadeh, A. (2019a). ESC: an efficient error-based stopping criterion for kriging-based reliability analysis methods. Structural and Multidisciplinary Optimization, 59(5):1621–1637.

[Wang and Shafieezadeh, 2019b] Wang, Z. and Shafieezadeh, A. (2019b). REAK: Reliability analysis through Error rate-based Adaptive Kriging. Reliability Engineering & System Safety, 182:33–45.

[Wang and Wang, 2012] Wang, Z. and Wang, P. (2012). A nested extreme response surface approach for time-dependent reliability-based design optimization. Journal of Mechanical Design, 134(12).

[Wang and Wang, 2013] Wang, Z. and Wang, P. (2013). A new approach for reliability analysis with time-variant performance characteristics. Reliability Engineering & System Safety, 115:70–81.

[Wei et al., 2014] Wei, K., Arwade, S. R., and Myers, A. T. (2014). Incremental wind-wave analysis of the structural capacity of offshore wind turbine support structures under extreme loading. Engineering Structures, 79:58–69.

[Wei et al., 2016] Wei, K., Arwade, S. R., Myers, A. T., and Valamanesh, V. (2016). Directional effects on the reliability of non-axisymmetric support structures for offshore wind turbines under extreme wind and wave loadings. Engineering Structures, 106:68–79.

[Wei et al., 2017] Wei, K., Myers, A. T., and Arwade, S. R. (2017). Dynamic effects in the response of offshore wind turbines supported by jackets under wave loading. Engineering Structures, 142:36–45.

[Wiener, 1938] Wiener, N. (1938). The homogeneous chaos. American Journal of Mathematics, 60(4):897–936.

[Wisatesajja et al., 2019] Wisatesajja, W., Roynarin, W., and Intholo, D. (2019). Comparing the effect of rotor tilt angle on performance of floating offshore and fixed tower wind turbines. Journal of Sustainable Development, 12(5).

[Wu et al., 2019] Wu, X., Hu, Y., Li, Y., Yang, J., Duan, L., Wang, T., Adcock, T., Jiang, Z., Gao, Z., Lin, Z., et al. (2019). Foundations of offshore wind turbines: A review. Renewable and Sustainable Energy Reviews, 104:379–393.

[Xiang et al., 2020] Xiang, Z., Chen, J., Bao, Y., and Li, H. (2020). An active learning method combining deep neural network and weighted sampling for structural reliability analysis. Mechanical Systems and Signal Processing, 140:106684.

[Xiao et al., 2020] Xiao, N.-C., Yuan, K., and Zhou, C. (2020). Adaptive kriging-based efficient reliability method for structural systems with multiple failure modes and mixed variables. Computer Methods in Applied Mechanics and Engineering, 359:112649.

[Xiao et al., 2018a] Xiao, N.-C., Zuo, M. J., and Guo, W. (2018a). Efficient reliability analysis based on adaptive sequential sampling design and cross-validation. Applied Mathematical Modelling, 58:404–420.

[Xiao et al., 2018b] Xiao, N.-C., Zuo, M. J., and Zhou, C. (2018b). A new adaptive sequential sampling method to construct surrogate models for efficient reliability analysis. Reliability Engineering & System Safety, 169:330–338.

[Xiong and Sampath, 2021] Xiong, Y. and Sampath, S. (2021). A fast-convergence algorithm for reliability analysis based on the AK-MCS. Reliability Engineering & System Safety, 213:107693.

[Xiu and Karniadakis, 2002] Xiu, D. and Karniadakis, G. E. (2002). The Wiener–Askey polynomial chaos for stochastic differential equations. SIAM journal on scientific computing, 24(2):619–644.

[Xu and Saleh, 2021] Xu, Z. and Saleh, J. H. (2021). Machine learning for reliability engineering and safety applications: Review of current status and future opportunities. Reliability Engineering & System Safety, page 107530.

[Yang et al., 2018] Yang, X., Liu, Y., Mi, C., and Tang, C. (2018). System reliability analysis through active learning kriging model with truncated candidate region. Reliability Engineering & System Safety, 169:235–241.

[Yang et al., 2019] Yang, Y., Wu, Q., He, Z., Jia, Z., and Zhang, X. (2019). Seismic collapse performance of jacket offshore platforms with time-variant zonal corrosion model. Applied Ocean Research, 84:268–278.

[Yeter et al., 2019] Yeter, B., Garbatov, Y., and Guedes Soares, C. (2019). Ultimate strength assessment of jacket offshore wind turbine support structures subjected to progressive bending loading. Ships and Offshore Structures, 14(2):165–175.

[Yu et al., 2018] Yu, S., Wang, Z., and Meng, D. (2018). Time-variant reliability assessment for multiple failure modes and temporal parameters. Structural and Multidisciplinary Optimization, 58(4):1705–1717.

[Yuan et al., 2020] Yuan, K., Xiao, N.-C., Wang, Z., and Shang, K. (2020). System reliability analysis by combining structure function and active learning kriging model. Reliability Engineering & System Safety, 195:106734.

[Yun et al., 2019] Yun, W., Lu, Z., Zhou, Y., and Jiang, X. (2019). AK-SYSi: an improved adaptive kriging model for system reliability analysis with multiple failure modes by a refined u learning function. Structural and Multidisciplinary Optimization, 59(1):263–278.

[Zerpa et al., 2005] Zerpa, L. E., Queipo, N. V., Pintos, S., and Salager, J.-L. (2005). An optimization methodology of alkaline–surfactant–polymer flooding processes using field scale numerical simulation and multiple surrogates. Journal of Petroleum Science and Engineering, 47(3-4):197–208.

[Zhang et al., 2021a] Zhang, C., Wang, Z., and Shafieezadeh, A. (2021a). Error quantification and control for adaptive kriging-based reliability updating with equality information. Reliability Engineering & System Safety, 207:107323.

[Zhang et al., 2015] Zhang, L., Lu, Z., and Wang, P. (2015). Efficient structural reliability analysis method based on advanced kriging model. Applied Mathematical Modelling, 39(2):781–793.

[Zhang et al., 2021b] Zhang, X., Lu, Z., and Cheng, K. (2021b). AK-DS: An adaptive Kriging-based directional sampling method for reliability analysis. Mechanical Systems and Signal Processing, 156:107610.

[Zhang et al., 2019] Zhang, X., Wang, L., and Sørensen, J. D. (2019). REIF: a novel active-learning function toward adaptive Kriging surrogate models for structural reliability analysis. Reliability Engineering & System Safety, 185:440–454.

[Zhang et al., 2020] Zhang, X., Wang, L., and Sørensen, J. D. (2020). AKOIS: an adaptive Kriging oriented importance sampling method for structural system reliability analysis. Structural Safety, 82:101876.

[Zhao and Ono, 1999] Zhao, Y.-G. and Ono, T. (1999). A general procedure for First/Second-Order reliability method (FORM/SORM). Structural safety, 21(2):95–112.

[Zhou et al., 2020] Zhou, Y., Lu, Z., and Yun, W. (2020). Active sparse polynomial chaos expansion for system reliability analysis. Reliability Engineering & System Safety, 202:107025.

[Zuhal et al., 2021] Zuhal, L. R., Faza, G. A., Palar, P. S., and Liem, R. P. (2021). On dimensionality reduction via partial least squares for kriging-based reliability analysis with active learning. Reliability Engineering & System Safety, page 107848.

[Zwick et al., 2014] Zwick, D., Schafhirt, S., Brommundt, M., Muskulus, M., Narasimhan, S., Mechineau, J., and Haugsøen, P. (2014). Comparison of different approaches to load calculation for the OWEC Quattropod jacket support structure.